

N 68 33 164

R-7548

NASA CR 96447

# CASE FILE COPY

## SPACECRAFT ROCKET ENGINE CHAMBER INSULATION MATERIALS

*(Second Interim Report)*

**ROCKETDYNE**

A DIVISION OF NORTH AMERICAN ROCKWELL CORPORATION  
6633 CANOGA AVENUE, CANOGA PARK, CALIFORNIA 91304

# ROCKETDYNE

A DIVISION OF NORTH AMERICAN ROCKWELL CORPORATION  
6633 CANOGA AVENUE, CANOGA PARK, CALIFORNIA 91304

R-7548

32

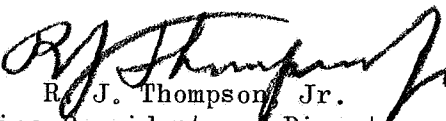
SPACECRAFT ROCKET ENGINE CHAMBER  
INSULATION MATERIALS  
(Second Interim Report)

Contract NAS7-474

## PREPARED BY

L. W. Carlson  
H. Carpenter  
A. L. Huebner  
L. Manson  
E. Talmor

## APPROVED BY

  
R. J. Thompson, Jr.  
Vice President and Director  
Research Division

NO. OF PAGES 218 & xvi

## REVISIONS

DATE 30 July 1968

DATE	REV. BY	PAGES AFFECTED	REMARKS



#### APPROVAL

The draft of this report, dated 30 July 1968,  
was approved for formal printing by JPL TWX of  
9 August 1968, signed by Robert W. Riebling,  
Technical Manager.

## FOREWORD

The effort described in this report was performed under G.O. 08842 from 1 July 1967 through 30 June 1968 and was technically managed by the Jet Propulsion Laboratory for the National Aeronautics and Space Administration under Contract No. NAS7-474. The Rocketdyne number assigned to this report is R-7548.

The vital help in data handling and reduction provided by Mr. J. Sabol is gratefully acknowledged. Mr. E. Rudolph provided valuable assistance in test section construction and instrumentation; his considerable careful effort during testing merits special recognition.

## ABSTRACT

Three insulation systems were evaluated in an extensive experimental program: multilayers of silica fabric/molybdenum foil, carbon fabric/tantalum foil and fine tungsten powder dispersed in a matrix of hollow zirconia microspheres.

At temperatures below 2000 F, molybdenum/silica is clearly the superior insulation. Above 2000 F, tantalum/carbon is clearly superior. The tungsten/zirconia insulation system has an order of magnitude higher conductivity than the other material systems at the low temperatures, but is only 30 percent higher at the higher temperature. Means of maintaining tungsten/zirconia homogeneity under vibration have to be provided.

Measurements of effective thermal conductivity and thermal stability tests were conducted at temperatures up to and exceeding 3500 F. Compatibility studies were conducted with B-66 (a columbium alloy), Ta-10W, Mo-1/2 Ti, and Haynes 25 vs molybdenum and tantalum foils, and with Haynes 25 vs silica fabric. While no compatibility problems were encountered at 2000 F, diffusion barriers may be required to keep the materials from welding at temperatures exceeding 2000 F.

The details of all phases of work are fully discussed in a four-section report: (1) Selection of Materials, (2) Thermal Properties, (3) Thermal Stability and Compatibility, and (4) Applications Analysis. The latter includes four design examples of insulation systems for "buried" rocket chambers having arbitrary duty cycles, geometrical features, propellants and thrust. Insulation temperature profiles for each case are graphically presented.

## CONTENTS

Foreword . . . . .	iii
Abstract . . . . .	v
Introduction . . . . .	1
Summary and Conclusions . . . . .	5
Materials Selection . . . . .	9
Silica Fabric/Molybdenum Foil System . . . . .	9
Zirconia Matrix-Dispersed Tungsten Powder System . . . . .	10
Thermal Properties . . . . .	13
Apparatus . . . . .	13
Test Procedures . . . . .	34
Error Analysis . . . . .	43
Results and Discussion . . . . .	46
Data Comparisons . . . . .	77
Thermal Stability and Compatibility . . . . .	87
Procedure . . . . .	89
Conditions . . . . .	92
Results and Discussion . . . . .	92
Applications Analysis . . . . .	115
Heat Transfer in an Insulated Space Engine:	
General Design Criteria . . . . .	115
Thermal Properties of Insulations . . . . .	116
Electric Analog of the Heat Transfer	
in a Buried Insulated Engine . . . . .	119
Preliminary Calculations for the Computer Input . . . . .	123
Format of Data Input for TAP II . . . . .	125
Examples of Application of Analytical Model . . . . .	126
References . . . . .	165
Nomenclature . . . . .	167
<u>Appendix A</u>	
Selection of a Silica Fabric . . . . .	169

Appendix B

Selection of a Materials System for

Detailed Investigation . . . . . 177

Appendix C

Curve Fitting Molybdenum/Silica Effective Thermal Conductivity

Results for Argon Pressurization of 1-, 400-, 800-,  
and 1600 Microns . . . . . 187

Appendix D

Typical TAP II Data Input and Results Output Listing for the

Graphite Chamber, Insulation Thickness Equals 1.5 Inches  
of Tantalum/Carbon, Firing Time Equals 600 Seconds,  
Soakback Equals 10,000 Seconds . . . . . 189

Appendix E

Distribution List . . . . . 211

## ILLUSTRATIONS

1. Schematic of Vacuum System Used for Testing . . . . .	15
2. Vacuum System . . . . .	17
3. Winding Machine . . . . .	20
4. Schematic of Typical Cylindrical Test Section . . . . .	25
5. Test Setup for Cylindrical Section . . . . .	28
6. Cylindrical Section Installed in Vacuum Chamber Well . . . . .	29
7. Schematic of Typical Planar Test Section . . . . .	32
8. Planar Test Section Installed in Vacuum Chamber Well . . . . .	33
9. Molybdenum Foil Specimens . . . . .	35
10. Silica Cloth Specimens . . . . .	36
11. Tantalum Foil Specimens . . . . .	37
12. Carbon Cloth Specimens . . . . .	38
13. 2-Percent Tungsten/98-Percent Zirconia Specimens . . . . .	39
14. Effective Thermal Conductivity as a Function of Temperature and Time (First Heating Cycle), 1 December 1967, Molybdenum/Silica No. 1 . . . . .	49
15. Variation of Effective Thermal Conductivity With Argon Pressure, 1 and 4 December 1967, Molybdenum/Silica Number 1 . . . . .	50
16. Effective Thermal Conductivity as a Function of Temperature and Time (First Heating Cycle), 11 December 1967, Molybdenum/Silica No. 2 . . . . .	51
17. Midplane Temperature Histories . . . . .	52
18. Effective Thermal Conductivity as a Function of Temperature and Time (First Heating Cycle), 25 December 1967, Molybdenum/Silica Number 3 . . . . .	54
19. Effective Thermal Conductivity as a Function of Temperature and Time (Second Heating Cycle), 27 December 1967, Molybdenum/Silica Number 3 . . . . .	55
20. Effective Thermal Conductivity as a Function of Temperature and Time (First Heating Cycle), 7 February 1968, Molybdenum/Silica Number 5 . . . . .	56

21.	Effective Thermal Conductivity, 7, 9, and 12 February 1967, Molybdenum/Silica Number 5 . . . . .	57
22.	Effective Thermal Conductivity, 15 to 16 September 1968, Molybdenum/Silica Number 6 . . . . .	59
23.	Effective Thermal Conductivity as a Function of Temperature and Time (Second Heating Cycle), 15 March 1968, Molybdenum/Silica Number 8 . . . . .	60
24.	Effective Thermal Conductivity, 13 and 15 March 1968, Molybdenum/Silica Number 8 . . . . .	61
25.	Effective Thermal Conductivity as a Function of Temperature and Time (First Heating Cycle), 21 March 1968, Tantalum/Carbon Number 1 . . . . .	63
26.	Effective Thermal Conductivity as a Function of Temperature and Time (Second Heating Cycle), 22 March 1968, Tantalum/Carbon Number 1 . . . . .	64
27.	Effective Thermal Conductivity, 21 March 1968, Tantalum/Carbon No. 1 . . . . .	65
28.	Midplane Temperature Decay, Tantalum/Carbon No. 2, 8 April 1968 . . . . .	66
29.	Variation of Effective Thermal Conductivity With Argon Pressure, 17 April 1968, Tantalum/Carbon Number 3 . . . . .	68
30.	Effective Thermal Conductivity as a Function of Temperature and Time (First Heating Cycle), 26 April 1968, Carbon Number 1 . . . . .	69
31.	Effective Thermal Conductivity as a Function of Temperature and Time (Second Heating Cycle), 29 April 1968, Carbon No. 1 . . . . .	70
32.	Effective Thermal Conductivity as a Function of Temperature and Time (First Heating Cycle), 16 May 1968, Tungsten/Zirconia Number 1 . . . . .	71
33.	Effective Thermal Conductivity as a Function of Temperature and Time (Second Heating Cycle), 20 May 1968, Tungsten/Zirconia No. 1 . . . . .	72

34.	Effective Thermal Conductivity as a Function of Temperature and Time (First Heating Cycle), 28 May 1968, Tungsten/Zirconia Number 2 . . . . .	74
35.	Effective Thermal Conductivity as a Function of Temperature and Time (Second Heating Cycle), 3 June 1968, Tungsten/Zirconia Number 2 . . . . .	75
36.	Molybdenum/Silica No. 9 (Planar) 13, 17, and 18 June 1968, Ratio of Effective Thermal Conductivity as a Function of Temperature and Loading Pressure . . . . .	76
37.	Tantalum/Carbon No. 4 (Planar) 24, 25, and 26 June 1968, Ratio of Effective Thermal Conductivity as a Function of Temperature and Loading Pressure . . . . .	78
38.	Comparison of Effective Thermal Conductivities of all Cylindrical Molybdenum-Silica Test Sections . . . . .	79
39.	Comparison of Effective Thermal Conductivities of Carbon and Tantalum/Carbon Test Sections . . . . .	81
40.	Comparison of Effective Thermal Conductivities of Two Tungsten/Zirconia Test Sections . . . . .	82
41.	Comparison of Effective Thermal Conductivities of all Material Combinations Studied . . . . .	83
42.	Comparison of Temperature Dependence of Experimental Effective Thermal Conductivity Values With Theoretical Radiation Model . . . . .	85
43.	Multilayer Insulation Specimen . . . . .	90
44.	Effect of Time and Loading Pressure on Silica Fabric Annealed (Vacuum at 2000 F) . . . . .	94
45.	Cross-Section of Silica Fabric Loaded Under 1/2 psi Pressure and Annealed in Vacuum for 1 Hour at 2000 F (50X and 150X Magnification) . . . . .	95
46.	Effect of Loading Pressure on "As-Received" Silica Fabric and Paper . . . . .	97
47.	Change in Thickness of Carbon Fabric Used in Multilayer System as a Function of Time and Loading Pressure at 3500 F . . . . .	99



48.	Effect of Loading Pressure on "As-Received"	
	Carbon Fabric . . . . .	101
49.	Zirconia Insulation Material in the As-Received Condition	
	With (a) 0 Percent and (b) 10 Percent by Weight Tungsten	
	Powder. . . . .	103
50.	Zirconia Insulation Material Containing 10 Percent by	
	Weight Tungsten Powder Annealed at 3000 F in a Vacuum	
51.	Cross Sections of Thrust Chamber Material/Insulation	
	Material Compatibility Specimens . . . . .	108
52.	Hardness Across Molybdenum/B-66 and Tantalum/B-66	
	Interfaces . . . . .	111
53.	Hardness Across Molybdenum/Ta-10W Interfaces . . . . .	112
54.	Hardness Across Molybdenum/Mo-1/2 Ti and Tantalum/Mo-1/2	
	Ti Interfaces . . . . .	113
55.	Heat Capacity of the Molybdenum-Silica and the	
	Tantalum-Carbon Insulation . . . . .	117
56.	Thermal Conductivity of the Molybdenum-Silica and the	
	Tantalum-Carbon Insulation as Used for	
	Application Analysis . . . . .	118
57.	Typical Analog Network . . . . .	121
58.	Thermal Analysis of the RS-14 Engine for a	
	196-Second Firing . . . . .	128
59.	Analog Network for the RS-14 Beryllium Engine . . . . .	130
60.	Steel Shell Temperature and Heat Flux to Spacecraft,	
	Soakback (RS-14 Engine, 100-Second Firing,	
	Beryllium Engine) . . . . .	132
61.	Steel Shell Temperature and Heat Flux to Spacecraft	
	(RS-14 Engine, 1000-Second Firing)	
	(Beryllium Engine) . . . . .	133
62.	Temperature Profiles in the Nozzle Insulation	
	After a 100-Second Firing (RS-14 Engine)	
	(Beryllium Engine) . . . . .	134
63.	Temperature Profiles in the Nozzle Insulation Firing	
	Duration: 1000 Seconds (Beryllium Engine) . . . . .	135

64.	Analog Network for Heat Transfer in the Columbium Engine . . . . .	137
65.	Steel Shell Temperatures for the Columbium Engine (Tantalum-Carbon Insulation) . . . . .	139
66.	Heat Flux and Total Heat Received by Spacecraft Columbium Engine . . . . .	140
67.	Temperature-Time Variations in the Nozzle Insulation of a Columbium Engine . . . . .	141
68.	Temperature Distribution in the Nozzle Insulation of a Columbium Engine . . . . .	142
69.	Mariner 69 Engine . . . . .	144
70.	Analog Network for the Mariner Engine . . . . .	146
71.	Steel Shell Temperatures at Various Insulation Thicknesses (Mariner Engine) . . . . .	148
72.	Mariner Engine Heat Flux and Total Heat Load to Spacecraft . . . . .	149
73.	Temperatures in the Chamber Insulation During Soakback (Mariner Engine) . . . . .	150
74.	Temperature in the Nozzle Insulation During Soakback (Mariner Engine) . . . . .	151
75.	Schematic of Graphite Chamber Assembly . . . . .	153
76.	Analog Network for the Graphite Engine . . . . .	155
77.	Analog Network for the Graphite Engine, Including a Radiation Shield in the Gap Between Engine Wall and Inlet . . . . .	155
78.	Steel Shell Temperatures for Varying Insulation Thickness (Graphite Engine) . . . . .	157
79.	Heat Flux and Total Heat to Spacecraft (L = 1.0, 1.5, and 2.0 Inch) (Graphite Engine) . . . . .	158
80.	Heat Flux and Total Heat Input to Spacecraft (L = 1.5 and 2.0 Inch) (Graphite Engine) . . . . .	160
81.	Temperature Profiles in the Insulation; L = 1.0 (Graphite Engine) . . . . .	161

82.	Temperature Distribution in the Insulation; $L = 1.5$ Inch;	
	Chamber Section (Graphite Engine) . . . . .	162
83.	Temperature Distribution in the Insulation; $L = 1.5$ Inch;	
	Nozzle Section (Graphite Engine) . . . . .	163
A-1.	Refrasil Paper and Fabrics . . . . .	170
A-2.	Astrosil Fabrics . . . . .	171

## TABLES

1. Test Section Description . . . . .	24
2. Variations of Test Section Parameters . . . . .	47
A-1. Comparison of Silica Fabrics . . . . .	173
B-1. List of Candidate Materials Systems . . . . .	180
B-2. Summary of Test Results . . . . .	183
B-3. Summary of Test Data on Zirconia Mixtures . . . . .	184

## INTRODUCTION

Extended space missions have led to the need for high-performance attitude control and orbital maneuver rocket engines capable of extended-operating durations with completely arbitrary duty cycles. In some cases, the engines may be installed within the structure of the spacecraft to minimize the thermal management problem which might be encountered because of variations in spacecraft orientation. The so-called "buried" installation imposes a requirement of low skin temperature (approximately 400 to 600 F) upon the external surface of the rocket engine, both during firing and thermal soakback, to preclude excessive heating of surrounding supporting structure.

A program entitled Spacecraft Rocket Engine Chamber Insulation Materials was initiated by the Rocketdyne Research Division on 1 June 1966. The objective of this program was to generate information concerning the thermal properties, thermal stability, chemical compatibility, and contact resistance of high-temperature insulation materials. Major emphasis was placed on experimental studies. However, a limited analytical study was required to discern which modes of heat transfer would be encountered in testing. Thus, design of experiments was accomplished.

Four insulation systems were selected from a large number of candidate systems by a screening procedure which evaluated thermal stability and chemical compatibility with rocket engine materials. The four insulation systems selected were molybdenum foil/silica (Refrasil) paper multilayer, molybdenum foil/zirconia paper multilayer, tantalum foil/carbon cloth multilayer, and a 25-percent theoretical density foamed zirconia composite. Hollow cylindrical and planer (flat) test sections were formed from these material systems and instrumented to determine their effective thermal conductivity as a function of temperature, gas pressure, and mechanical loading pressure.

The effective thermal conductivity ( $k_e$ ) results showed that radiation heat transfer is the dominating mechanism at higher temperatures. The

in-vacuum  $k_e$  values for the multilayer materials were a factor of 10 below ordinary "good" (foamed ceramic brick) insulators at equivalent temperatures. However, the foamed zirconia composite only equalled average good insulators in insulative value.

Two problem areas were encountered in the first year's program: severe outgassing of binder materials in the silica and zirconia papers and carbon cloth, and thermal degradation of the paper materials. Thermal cycling of the insulation prior to its being sealed within an engine package would be necessary to preclude pressurization, loss of insulative effectiveness, and a possible burst hazard. The thermal weakening of spacer materials would require further study to ensure applicability in strong vibration environments.

A follow-on effort was initiated on 1 July 1967 to continue generation of engineering information on the cited properties of insulations. Two auxiliary goals were the selection of several of the insulation systems as prime candidates for possible future spacecraft engines, and the establishment of engineering design criteria governing their use in such applications. To these ends, additional data on some of the more promising materials already studied were collected. A new material was examined, and those problem areas which developed during the first year were examined more closely. Whereas effort during the first year was limited primarily to a single cylindrical geometry, testing of other cylindrical configurations was accomplished. A wider variation of test section thickness was investigated; in addition, the length of the cylindrical test sections was varied to determine end heat-loss effects more accurately. The foil-to-spacer thickness ratio was also varied to determine the associated effect upon the effective thermal properties.

Three materials systems were tested in the follow-on program: (1) molybdenum foil/silica (Refrasil) cloth multilayer, (2) tantalum foil/carbon cloth multilayer, and (3) tungsten powder/zirconia microsphere powder mixtures. Though the two multilayer material systems had been tested

in the previous effort, additional effort was required to reduce outgassing, and to obtain sufficient, accurate data.

Refrasil cloth was substituted for Refrasil paper to alleviate the outgassing problem associated with binder decomposition, and to provide a separator having higher pre- and post-use strength. The tantalum/carbon multilayer system had shown such promise as high temperature insulation that it was advisable to obtain more precise data for this material system. The tungsten/zirconia materials system was chosen for evaluation of the opacified powder-insulation concept which promised isotropic, spacially-distributed properties.

The following sections of this report will summarize the effort and results of the follow-on program, provide a description of apparatus and test procedures, present data and error analysis, and present and discuss the experiment results of the testing program.

The report is subdivided into four major parts corresponding to the program tasks: Materials Selection, Thermal Properties, Thermal Stability and Compatibility, and Applications Analysis. The purpose of the Applications Analysis is to provide examples of designing insulation packages for buried rocket chambers having arbitrary duty cycles, geometrical features, propellants, and thrust. Criteria for evaluation of insulation effectiveness are suggested.

## SUMMARY AND CONCLUSIONS

An experimental program was conducted to evaluate the thermal properties, stability, and compatibility of three insulation systems as a function of temperature, time, gas pressure, mechanical loading pressure and geometrical features. The three insulation test materials were: molybdenum foil/silica (Refrasil) cloth multilayer; tantalum foil/carbon cloth multilayer; and tungsten powder/zirconia microspheres powder. Temperatures from ambient to 2200 F were obtained in testing the molybdenum/silica system; temperatures from ambient to approximately 3500 F were obtained with the two other insulation systems. Both transient and steady-state data were obtained utilizing electrically-heated hollow-cylindrical and planar test sections under moderate vacuum ( $10^{-4}$  torr) conditions.

The effective thermal conductivity results strongly depend upon temperature; a lower order dependence is evident at low temperature, but it approaches a cubic relationship with temperature at higher temperatures, as predicted by a theoretical radiation heat transfer model. The absolute value of the effective thermal conductivity for the two multilayer insulation systems is an order of magnitude below common (porous brick ceramics) high-temperature insulation materials at equivalent temperatures; the powder-type insulation is only somewhat better than ordinary insulation.

The lower conductivity of the molybdenum/silica system at lower temperatures favors its use below 2000 F. The time dependence of the effective thermal conductivities is presumed to be associated with the outgassing exhibited by each materials system. Bakeout of gasifying materials resulted in subsequently smaller transient effects upon heating.

Intentional pressurization of test materials with argon gas resulted in regular increases in effective thermal conductivity with increasing gas pressure in the range (from 1 to 1600 microns) investigated. Transient effective thermal conductivity values always closely approached the independently determined steady-state values for the given materials system. No anomalous effect of geometry upon the effective thermal conductivity was noted in any of the data.



Increased mechanical loading of the two multilayer systems resulted in increased effective thermal conductivity. However, the increase varied with temperature in a different manner for the two insulations. Both multilayers are considered to be structurally adequate while segregation of the tungsten powder within the zirconia matrix in a vibration environment would pose a problem unless preventative measures are taken. A partial sintering of the bed by exposure to approximately 3500 F temperatures could alleviate the segregation problem. However, increased values of effective thermal conductivity at low temperatures would ensue.

The results of thermal stability studies indicate that silica fabric is preferable to silica paper in a multilayer insulation system for use to 2000 F. The fabric is stronger, does not tear during use and does not contain a binder material that decomposes in the hot region and then condenses as a viscous liquid in cooler regions.

Carbon fabric did not undergo changes when annealed at temperatures exceeding 3500 F. Tantalum foils in a multilayer system carburize when annealed in contact with the carbon fabric, but the carbon fabric supported and cushioned the embrittled tantalum carbide radiation shields.

Compatibility between insulation and thrust chamber materials at 2000 F did not constitute a problem. Above 2000 F, diffusion barriers may be needed to keep the materials from welding. Molybdenum versus tungsten was the only combination of materials that did not weld together at 3500 F.

Stable insulation systems of refractory oxides containing a well dispersed phase with high reflectance are yet to be developed and tested. Promising systems are zirconia microspheres or fused thoria powder coated with a tungsten or iridium film and graphite particles coated with a film of iridium. Perhaps, half of the ceramic particles should be coated so that the metal film will not form a continuous phase. This film can be deposited by vapor deposition or by decomposition from an organic solvent.

Applications Analysis has been conducted with the help of an electric analog using the thermal property data generated in the program. The propulsion systems considered included: NT0/MMH-beryllium chamber with molybdenum/silica multilayer insulation, NT0/MMH-columbium chamber with tantalum/carbon insulation, monopropellant hydrazine-Haynes-25 alloy chamber with molybdenum/silica insulation and  $\text{OF}_2/\text{B}_2\text{H}_6$ -pyrolytic graphite chamber with tantalum/carbon insulation. Insulation temperature profiles are given for each case at various times.

## MATERIALS SELECTION

### SILICA FABRIC/MOLYBDENUM FOIL SYSTEM

In previous efforts, silica paper was used in combination with molybdenum foil. The paper was dimensionally and chemically stable to acceptable limits at and below 2000 F for 5 hours. It did not react significantly with the highly reflective molybdenum substrate, and did not shrink enough to appreciably change the thermal conductance properties of the multilayer system.

The silica paper had some shortcomings that did not limit its usefulness as an insulator. Being very weak, cylindrical multilayer insulation systems had to be rolled very carefully. Although the paper shrank only about 6 percent parallel to the plane of the molybdenum metal foils, the paper tore as it shrank during annealing. This did not affect the conductance appreciably because: (1) only a relatively small area of molybdenum was exposed, (2) tears in different layers did not necessarily occur directly over each other so that radiation short circuits were not formed, and (3) tear were narrow so that the adjacent layers of molybdenum foils did not touch each other to form a metal-to-metal thermal short circuit.

It was generally agreed that tearing of the insulating spacer layer in the multilayer system should be eliminated if possible. Another shortcoming of the paper was outgassing of the organic binder during the initial heating period. The gaseous products condensed in the cooler layers as a syrupy liquid which was undesirable from a contamination point of view.

To improve the multilayer system involved, a high-purity silica fabric (Refrasil Fabric Type C-100-48, H. I. Thompson Co.) was substituted for the silica paper. The fabric was selected on the basis of screening tests described in Appendix A. It contained less than 1 percent by weight impurities; did not contain a binder; was strong, economical, and available in a variety of weaves and thicknesses (Fig. 1 and 2 in Appendix A).

## ZIRCONIA MATRIX-DISPERSED TUNGSTEN POWDER SYSTEM

This new insulation material system was selected on the basis of screening tests conducted during the early part of the program (Appendix B). The system consisted of dispersed tungsten powder suspended in a matrix of zirconia insulation material\*. Specimens containing 2 and 10 percent by weight tungsten powder were prepared and tested in molybdenum cans.

A combination of a zirconia matrix and tungsten powder was selected because: (1) it is representative of the basic concept of a highly reflective dispersed phase in a low-density insulative matrix, (2) the materials are stable at 3500 F, (3) the raw materials are readily available and reasonably inexpensive, and (4) the system can be easily prepared without a developmental effort. Screening tests at 3500 F showed this materials system to be better than all other candidate systems. It shrank 5 percent or less and did not outgas or react with the molybdenum can.

Requirements of the new materials system also included those of existing systems, viz.: a low effective thermal conductivity and thermal diffusivity, chemical and physical stability for at least 1 hour at 3500 F at a pressure of  $10^{-4}$  torr or less, availability in the desired form (material development and fabrication were beyond the scope of this effort), low cost, and lightweight. It was desirable that it constituted an improvement relative to present systems so as to afford wider flexibility in design and fabrication.

Reflective surfaces within a matrix are required to reduce conduction due to radiation because the radiation heat transfer mode is dominant at the higher temperatures, particularly above 2000 F. Several basic methods can be used to introduce reflective surfaces. For example, a reflective

---

\*Tungsten powder: -200 mesh particle size, Grade G, 99.9-percent purity, Firth Sterling, Inc.  
Zirconia powder: -36, +100 mesh size hollow microspheres, Norton Type I

compound can be vapor-deposited on the surface of the ceramic particles. It can be painted on or dispersed within the matrix in powder form. Although the latter method would not yield the best insulative system for rocket applications, it was nonetheless satisfactory for producing prototype test specimens at minimum cost. Thus, the new insulation system consisted of a matrix of loosely packed, hollow zirconia microspheres containing a small amount of a dispersed tungsten powder.

Two large batches of material were prepared so that the thermal properties of this materials system could be measured. A sufficient amount of material for each batch, more than 1500 grams, was prepared to fill a thermal conductivity test container 16 inches long by 6 inches OD and 4 inches ID. The zirconia and tungsten powders were mixed for 1/2 hour in a twin-shell-type blender. One batch consisted of 90 percent by weight  $ZrO_2$  microspheres plus 10-percent tungsten powder while the other was 98 and 2 percent, respectively. The  $ZrO_2$  was -36, +100 mesh hollow microspheres (Zirnorite I, Norton Co.). Although the  $ZrO_2$  material was purchased as -36, +100 mesh material it contained 19 percent by weight -100 mesh fines. These fines, which were probably fragments of hollow spheres that were broken during handling and shipping, were removed before the tungsten powder was added. Tungsten powder, -200 mesh, was used in the as-received condition.

One problem with using this material is segregation of the fine, heavy tungsten powder. A uniform dispersion was somewhat more difficult to obtain when using a newer batch of raw materials. This might have been due to the drier atmosphere at the time of mixing the large batch of this material. A more humid atmosphere would cause the fine tungsten powder to cling to the larger grains of  $ZrO_2$ . Thus, to overcome this problem, the  $ZrO_2$  raw material was stored before use in an enclosed glove box which contained humid air. The amount of absorbed water is estimated to be less than 1 percent by weight.

The tungsten powder was not stored in a humid atmosphere to avoid difficulties in dispersion within the  $ZrO_2$  matrix. The tungsten powder, being much finer, would tend to agglomerate. Such a condition would reduce its effectiveness in dispersing radiation.

Bulk density of the  $ZrO_2$ , tungsten, and 90-percent  $ZrO_2$  + 10 percent by weight mixture were determined. A 10-cc graduated cylinder was filled with the powder and weighed. Volume of the powder was also measured after 10 minutes of constant low-amplitude vibration. These bulk density data are listed below; bulk density is reported in gm/cc.

	<u>As-Poured</u>	<u>Vibrated</u>
Tungsten Powder	4.9	5.2
$ZrO_2$ Microspheres	2.6	2.6
90 Percent by Weight $ZrO_2$ and 10 Percent by Weight	2.7	2.8

Several other combinations of materials are potentially useful for eventual use, in one form or another, in rocket engine applications. The ceramic matrix can be zirconia, thoria, carbon, or graphite, whereas the reflective powder can be tungsten, tantalum, columbium, molybdenum, rhenium, iridium, or ruthenium. Use of precious metals should not be excluded, because these metals can be painted or deposited as very thin layers so that only a relatively small amount of material would actually be required. If this thermal insulation concept shows merit, improvement of the materials systems appears possible in several respects. Matrix materials can be made more stable by using higher purity raw materials in the form of coarse, fused grains that would not sinter (and hence shrink), or it can be made lighter in weight by using hollow microspheres. Bulk density of the system would also be lower if the reflective surfaces were in the form of thin coatings rather than particles.

## THERMAL PROPERTIES

This section presents a detailed discussion of the experimental work conducted to determine the local effective thermal conductivity of the candidate insulation materials over a range of temperatures under steady-state and transient conditions. The tests were conducted with hollow cylindrical and planar insulation configurations under high-vacuum conditions.

### APPARATUS

The apparatus used to measure effective thermal conductivities consisted of a vacuum system, auxiliary equipment, instrumentation and the test sections which were placed within the vacuum chamber. Before describing the apparatus, the characteristic problems with the insulation systems under consideration are described.

Extreme cleanliness is usually axiomatic in high-vacuum work. Care should be taken to remove all unnecessary gas sources to allow maintenance of high vacuum while using reasonable sized pumps. In the present application, a large amount (on the order of 5 to 10 pounds) of material which is a natural source of gas, is placed within the vacuum system as the material under test. It has been possible to achieve sufficient vacuums ( $10^{-4}$  torr range) in a reasonably sized chamber while heating these gas-containing materials to temperatures as high as 3750 F within time periods less than an hour. Vacuum in the  $10^{-4}$  torr range was sufficient to preclude significant gas conduction contribution to the effective thermal conductivities of superinsulation materials. This vacuum range was consistently achieved in the first and second year effort. Because of the successful operation experienced during the first year, little change in the vacuum system was necessary. Some auxiliary equipment was replaced and augmented as described below.

Because the vacuum system had been in continual operation during the latter portion of the first years testing program, no maintenance had been possible.

Therefore, a first effort of the second-year program was to disassemble, inspect, clean and reassemble all vacuum system components. During this overhaul, a brown sticky varnish coating was observed on all interior surfaces. This varnish apparently resulted from the binder decomposition products of the materials of the first testing program. The varnish responded well to rubbing with trichlorethylene and acetone washes. Steel wool was required to remove baked on deposits on the diffusion pump chimney structure. Deposits nowhere were sufficient to cause blockage. However, these deposits had probably limited vacuum performance.

Upon reassembly, the vacuum system was checked out to an ultimate vacuum of  $10^{-6}$  torr after only a few hours of pumping. The inspection of components during overhaul and the improved vacuum after reassembly afforded confidence that the present testing program could be accomplished with little trouble.

#### Vacuum System

The vacuum system consisted of various commercially-available vacuum devices as shown schematically in Fig. 1. Two Model 1397 Welch roughing pumps were used in conjunction with a 6-inch-diameter, CVC, oil-type diffusion pump and an intervening liquid-nitrogen-cooled cold trap. The Pyrex bell jar was 17 inches in diameter by 30 inches high. Nominal 2-inch plumbing provided a bypass line between the chamber and the roughing system, and connected the outlet of the diffusion pump to the roughing system. The 2-inch foreline valve and the 6-inch high vacuum valve were solenoid-controlled and pneumatically actuated. The bypass line was closed with a hand valve. Two cold traps, both water-cooled in the present application, were interposed between the diffusion pump and the high-vacuum valve. The vacuum chamber had a well-type base plate in which 12 shear-seal ports of 3/4-inch diameter were incorporated to accommodate the various vacuum lead-throughs.



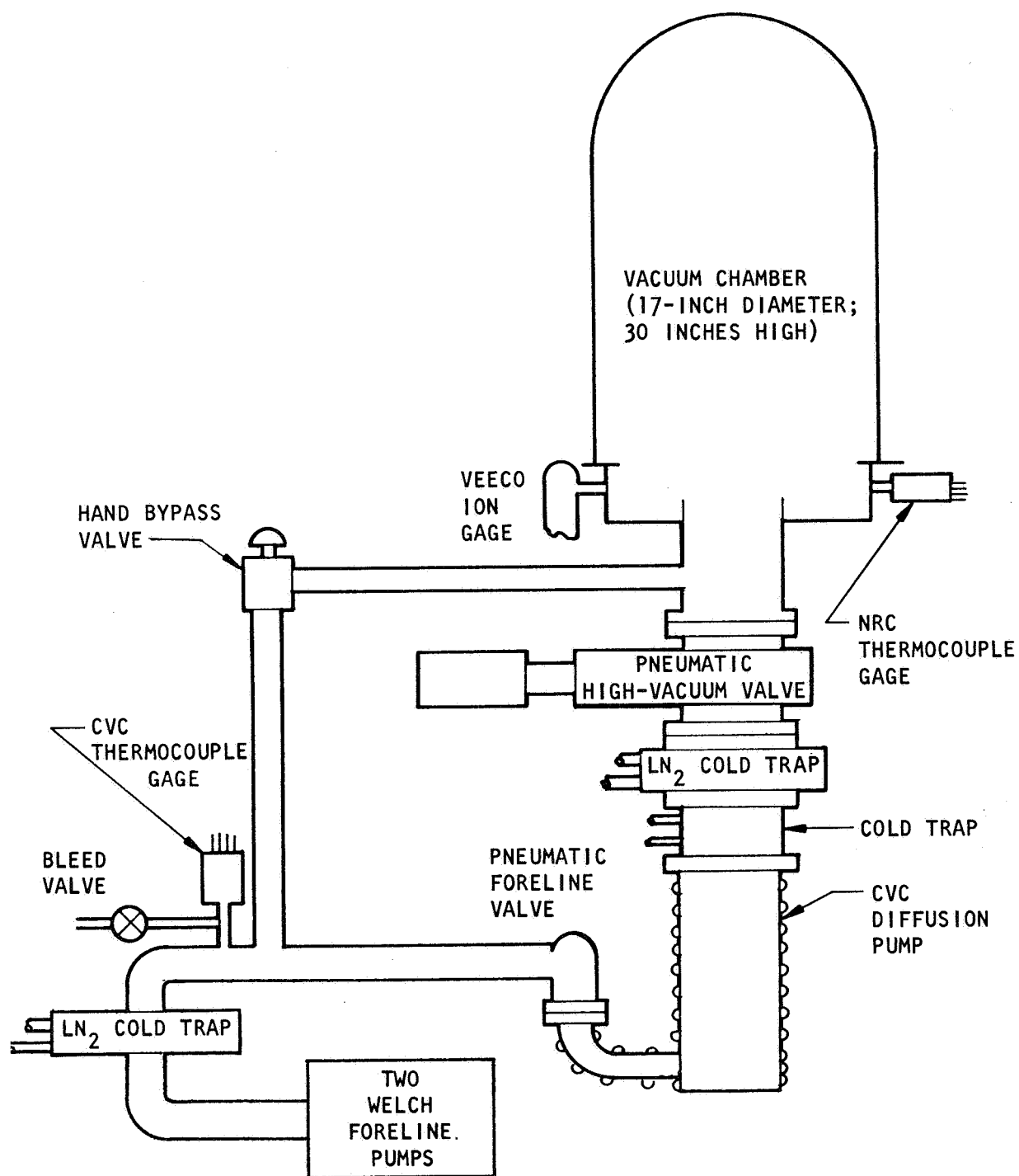


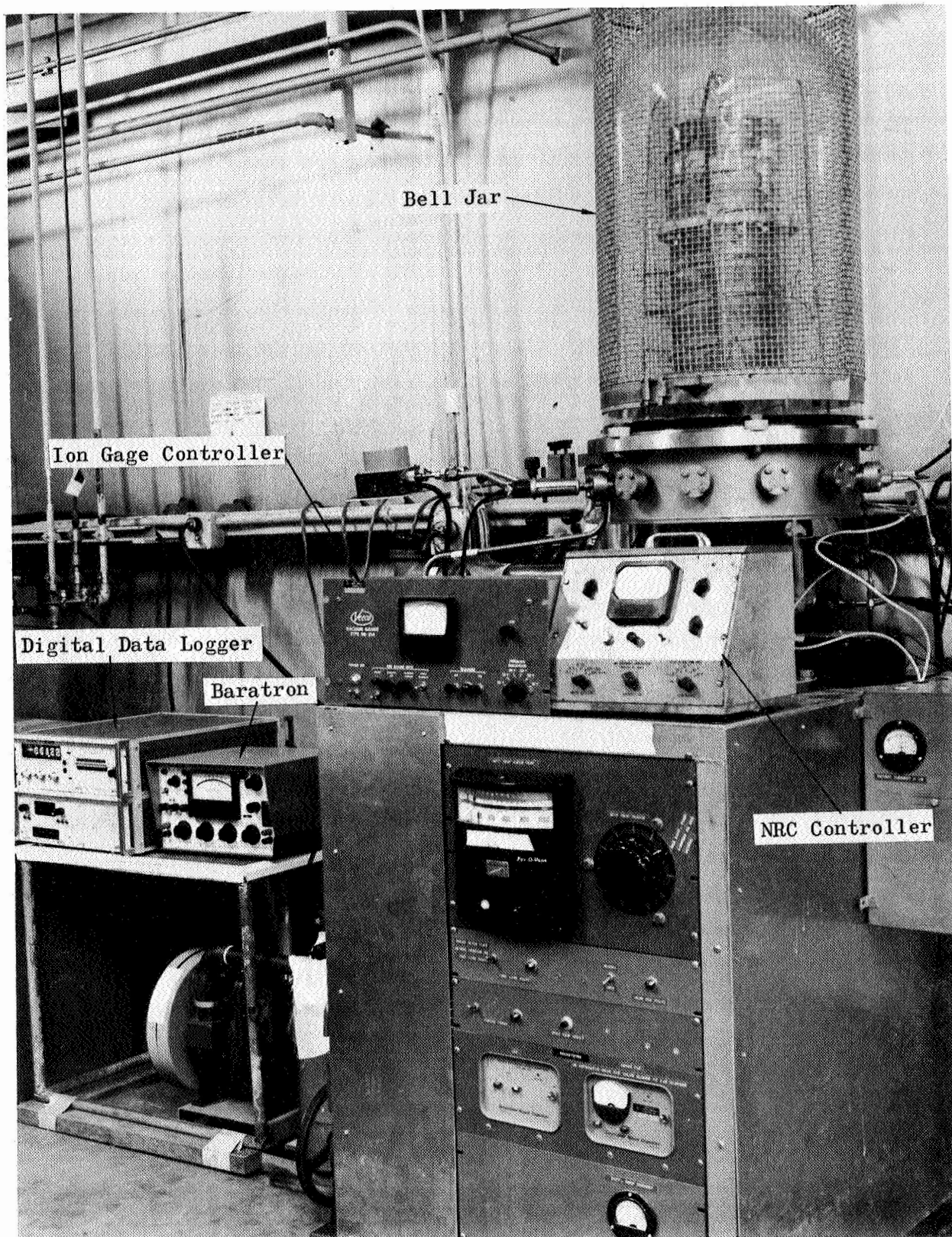
Figure 1. Schematic of Vacuum System Used for Testing

A CVC (model GTC-004) thermocouple gauge was located at the inlet to the liquid-nitrogen-cooled cold trap. An NRC thermocouple gauge (model 501) was located in one of the access ports in the base plate of the vacuum chamber. A Veeco ion gauge (model RG-75K) was located in another access port of the base plate. Variable electrical heating power to the diffusion pump was supplied by a 20-amp Variac transformer. A Honeywell Pyr-O-Vane temperature limiter was used to shut off the diffusion pump electrical power in the event of overtemperature. The CVC thermocouple gauge controller automatically closed the high vacuum valve in the event of overpressurization in the foreline. Separate water circuits were provided for the diffusion pump and first cold trap, the liquid nitrogen cold trap, and the quench coil on the diffusion pump. The complete vacuum system test setup is shown pictorially in Fig. 2.

#### Auxiliary Equipment

Additional equipment which was necessary for operation of the vacuum system is described below.

Water Supply. Six water supply circuits were incorporated into a manifold to supply soft, filtered water to the vacuum system and test apparatus. Commercially-softened water was filtered in a  $40\mu$  filter cartridge. Three of these water circuits were utilized in the vacuum system as described above. Essentially, on-off control was provided by  $1/4$ -inch Grove hand valves. The three other water circuits supplied the test section. The copper power leads to the test section heater were water-cooled in a series arrangement of electrically-insulated, concentric, tubular bus bars. Heated water was supplied to the guards of the calorimeter. The calorimeter was supplied with a constant flowrate of coolant water in a separate circuit; the constant flowrate was obtained by supplying an excess flowrate of water to a constant-head tank, allowing the excess to overflow through a spill line, and utilizing a gravity head and a finely-tapered, hand needle valve for establishing the calorimeter flow.



5AH23-1/23/68-S1

Figure 2. Vacuum System

Guard Water Heater. The water which was supplied to the various guards of any particular test section was heated so that an arbitrarily small temperature difference could be maintained between these guards and the calorimeter. In this way, superfluous heat leaks between guard surfaces and calorimeter were minimized. A 1500-watt "Cal-Rod" electric resistance heater was soft-soldered to a 3-foot length of 1/4-inch copper tubing to form the guard water heater. The water through the guard system was supplied at a relatively high flowrate compared to the calorimeter flow so that heat gains from the test section resulted in only a small temperature rise within the guards.

Test-Section Electrical Power Supply. The test section electrical heaters, whether carbon rod or metal foil, required a high-current, low-voltage power source. Two such power supplies were utilized in the present program. The first power supply, which was used with molybdenum/silica test sections numbered 1 through 5, consisted of an 8-gauge, copper-wire secondary winding on a 220-volt toroidal transformer coil. It had 1.2-kw power capacity. This transformer was forced-air cooled.

An ammeter and portable voltmeter in the secondary circuit were used to indicate heating power input. Voltage taps were located on the carbon adapter pieces into which the heater rod was fastened. A second power supply of 12-kw capacity was constructed and utilized for the last heating cycle of molybdenum/silica test section No. 5 and all tests thereafter. It consisted of a single-phase 12-kva (40 volt/300 ampere output, 50 ampere/240 volt input) secondary transformer coupled to a 50 ampere/240 volt variable transformer (Superior Electric). Voltage taps on the test section were utilized as previously stated; current was measured on the input to the secondary transformer. Knowing the turns ratio of the secondary transformer permitted calculation of the test section heating power. Voltage and current measurements were utilized to establish and monitor heating power levels, and check on the heat balance. The heat balance check was used for evaluation of the system performance during test.

The electrical power leads to the test section heater consisted of water-cooled copper tubing. Two concentric tubes, the outer 1/4-inch OD and the inner 1/8-inch OD, were connected in a Tee at one end, with the larger tube blocked at the test section end. The water flowed in through the 1/8-inch tube and out through the annulus between the tubes. The two power leads were connected in series for the water flow. Micarta insulators isolated each electrical lead, the water inlet, and outlet.

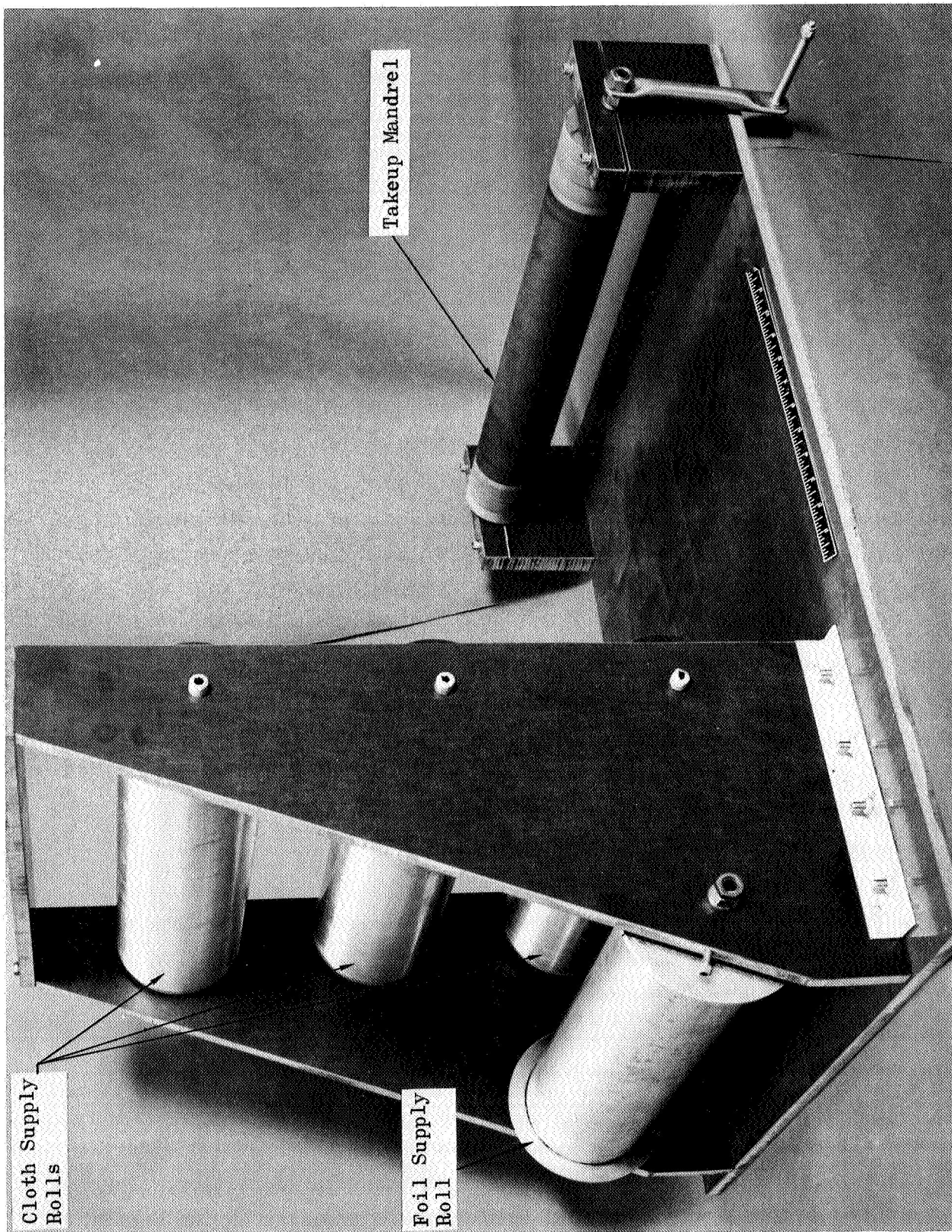
Cylindrical-Test-Section Winding Machine. The winding machine, which was used in constructing all of the cylindrical test sections, is shown in Fig. 3. Three cloth supply rolls, a foil supply roll and the takeup roll are pictured. The dark center portion of the takeup roll remains within the test section as the inner stiffening cylinder. Two modifications were made to the winding machine subsequent to this picture (Fig. 3). The end flanges on the foil supply were machined flush with the roll to eliminate a transverse wiping action upon the edge of the foil that interfered with accurate winding. The second modification was the addition of another foil supply roll situated above the one pictured.

Sixteen-inch-wide foil is not available commercially. Therefore, two parallel strips of foil (one 6 inches wide, one 10 inches wide) were wound together to make 16-inch-long cylinders.

### Instrumentation

Thermocouples. Two types of thermocouple wire were utilized in the testing program; chromel-alumel, and tungsten-5 percent rhenium/tungsten-26 percent rhenium. Chromel-alumel thermocouples were used in the temperature range from ambient to 2200 F. The tungsten-rhenium thermocouples were used up to temperatures of 3750 F. The 0.005-inch-diameter chromel-alumel wire was encased in a 321 stainless-steel sheath of 0.040 inch OD and was insulated with magnesia. The 0.005-inch-diameter tungsten-rhenium wire was encased in 0.040-inch-OD tantalum sheath with magnesia insulation. Thermocouple junctions were fusion-welded bare wire not grounded to the sheath.





5AH81-10/5/67-S1

Figure 3. Winding Machine

Thermocouple leads were soft soldered to gold-plated brass pins, 1/16 inch diameter by 1/2 inch long, which were mounted in micarta blocks with epoxy cement. The male and female pins mated with similar pins which terminated a permanent thermocouple harness. The micarta blocks provided an adequate thermal shunt between each of a pair of leads to minimize formation of extraneous electrical potential. These pinned junctions were located in ambient temperature regions, out of sight of high-temperature radiation sources.

Thermopiles. Ten-element thermopiles were fabricated by connecting 0.010-inch-diameter, chromel-alumel, duplex fiberglass-insulated premium-grade thermocouple wire. Thus, an order of magnitude increase in sensitivity was gained in measuring differential water temperatures. Thermopile junctions were electrically isolated from, yet thermally mated to water inlet and outlet tubing using epoxy cement. The epoxy was built up behind the junctions for approximately 3/8 inch to minimize error from heat conduction down the wire. Two thermopiles were utilized with the calorimeter, and one each with the guard water supply and electrical power leads. Two thermopiles had chromel leads and two had alumel leads. Four regular thermocouple lead-outs in the thermocouple harness were rewired for the thermopile signals.

Thermocouple Harness. Thermocouples and thermopile leads from each test section mated with a permanent thermocouple harness. Twenty eight chromel-alumel and 12 tungsten-5 percent rhenium/tungsten-26 percent rhenium thermocouples were accommodated. The chromel-alumel part of the harness was made of duplex fiberglass-insulated premium-grade thermocouple wire. Hoskins lead wire was used to match the tungsten-5 percent rhenium tungsten-26 percent rhenium electromotive force characteristics at low temperatures (less than 300 F); this wire was insulated with fiberglass spaghetti-type insulation.

The harness wire was led out of the bell jar through a drilled plexiglass plate. Epoxy cement sealed the leadthrough holes in the plexiglas. The

lead wire was continuous from the thermocouple connection into an ice bath. The double, cold-junction termination of the thermocouple lead wire within the ice bath allowed all-copper leads from the ice bath to the recorder. The possibility of spurious thermocouple junctions in the thermocouple harness was thereby avoided.

Ice Bath. The thermocouple harness cold junctions were contained within a 2-inch-diameter by 16-inch-long, oil-filled test tube. This oil-filled test tube was centered within a 6-inch-ID stainless-steel dewar flask. A mixture of water and crushed ice ( $\sim 1/4$  inch pieces) filled in the annular space between the test tube and dewar. A micarta disk covered the top of the dewar and held the tube in position.

Water Flowrate. The water flowrates through the calorimeter, the guard system, and the power leads were determined by collecting the efflux from each system in graduate cylinders over timed intervals. Four graduate cylinders of 50-, 100-, 500-, and 1000-milliliter capacities were available. Flows were collected for 60 seconds using a 12-inch-dial electric clock with sweep second hand as a timer.

Millivolt Recorders. Both transient and steady-state millivolt thermocouple signals were recorded using digital data logger equipment built by Non-Linear Systems, Inc. The majority of the data were obtained with a 40-channel data logger featuring an X-2 model voltmeter, a series 2300 scanner, a model 2504 printer, and an expandable switching network. This device operated at two samples per second and was accurate within  $\pm 0.01$  millivolt in the 100 millivolt range. The X-2 voltmeter malfunctioned midway in the testing program so that it was necessary to build a backup recording system. A manually operated thermocouple switch was wired to mate with the thermocouple harness and an X-1 digital voltmeter. Data were recorded by hand at an average rate of 1 sample per 5 seconds. The X-1 voltmeter can discern  $\pm 1$  microvolt in the 100-millivolt range. Approximately  $\pm 3$  microvolt noise was experienced in the thermocouple recording system. Though the sampling rate with the backup system was reduced by a factor of 10, accuracy of transient or steady-state temperature data were not compromised because of the long time intervals (40 minutes) allowed between sets of data.



Pressure Transducers. Pressure within the vacuum chamber was measured with either an NRC type 501 thermocouple gauge, a Veeco ion gauge (model RG-75K) or an MKS Systems Baratron gauge (model 77H-30) depending upon the pressure level. The thermocouple gauge was used to indicate pressure level during pumpdown as an indicator for determining when the diffusion pump could be operated. The ion gauge was used to indicate the working vacuum during test. The Baratron gauge measured pressure levels during the argon pressurization tests and had a sensitivity of 1 micron in the operational mode utilized.

### Test Sections

Test sections were designed to accommodate the full temperature range from ambient to maximum in a single heating cycle. This required multiple thermocouple capability and rather large dimensions, to accomplish the goal of obtaining thermal conductivity data at a number (~5 to 10) of discrete temperatures throughout the temperature range imposed. An optimization was required in test section design so that a sufficient number of temperatures, representative of macroscopic properties, could be measured. Multilayer materials have highly-anisotropic, variable properties on the microscale. Thus, care and judgement were required in thermocouple placement to minimize measurement error.

Test sections of cylindrical and planar geometry were employed in the thermal properties testing program. Fourteen cylindrical and two planar test sections were constructed. Of the cylindrical test sections, 12 were multilayer and 2 were powdered insulation. Both planar test sections were of multilayer construction. The material, geometry and other design details of each test section are presented in Table 1.

Cylindrical Multilayer Type. These test sections were constructed by continuously winding a wrap of foil and cloth around a hollow, cylindrical carbon mandrel until the desired total thickness of insulation was obtained. A schematic drawing of a typical cylindrical test section is shown in cross section in Fig. 4. In this way, layers of foil and cloth alternated in

TABLE 1

## TEST SECTION DESCRIPTION

Test Section	Inside Diameter, inch	Outside Diameter, inch	Total Length, inch	Length of Each End Guard, inch	Length of Calorimeter, inch	Number of Wraps of Insulation	Number of Thermocouple Stations Through Insulation	Spacer-to-Foil Thickness Ratio	Notes
Molybdenum/Silica No. 1	4.0	7	16	5	8	45.0	10	31.6/1	
Molybdenum/Silica No. 2	4.0	7	16	5	8	43.0	10	33.9/1	
Molybdenum/Silica No. 3	3.0	7	16	5	8	54.0	10	32.9/1	
Molybdenum/Silica No. 5	4.0	6	16	5	8	34.0	7	28.4/1	
Molybdenum/Silica No. 6	4.0	6	16	5	8	11.5	7	85.9/1	3 layers of cloth per layer of foil
Molybdenum/Silica No. 7	4.0	6	16	5	8	11.33	7	87.2/1	3 layers of cloth per layer of foil
Molybdenum/Silica No. 8	4.0	6	10	2	8	33.0	7	29.2/1	2 layers of cloth per layer of foil
Tantalum/Carbon No. 1	4.0	6	16	5	8	23.0	6	42.5/1	2 layers of cloth per layer of foil
Tantalum/Carbon No. 2	4.0	6	16	5	8	22.0	6	44.4/1	2 layers of cloth per layer of foil
Tantalum/Carbon No. 3	4.0	6	16	5	8	22.0	6	44.4/1	2 layers of cloth per layer of foil
Carbon Cloth No. 1	4.0	6	16	5	8	44.0	6	No foil	1 layer of cloth equals 1 wrap
Tungsten/Zirconia No. 1	4.25	6	16	5	8	—	8	No layers	10 w/o tungsten 90 w/o ZrO <sub>2</sub>
Tungsten/Zirconia No. 2	4.25	6	16	5	8	—	8	No layers	2 w/o tungsten 98 w/o ZrO <sub>2</sub>
Molybdenum/Silica No. 9 (Planar)	Square test sections: foil 8-inch square; spacer 12-inch square. Thickness varies with 3 different loading pressures					25 layers	6	Total thickness, inch ① 0.85 ② 0.77 ③ 0.73	Loading Pressure, psi ① 0.05 ② 0.5 ③ 1.8
Tantalum/Carbon No. 4 (Planar)						20 layers	5	Total thickness, inch ① 0.8906 ② 0.750 ③ 0.6875	

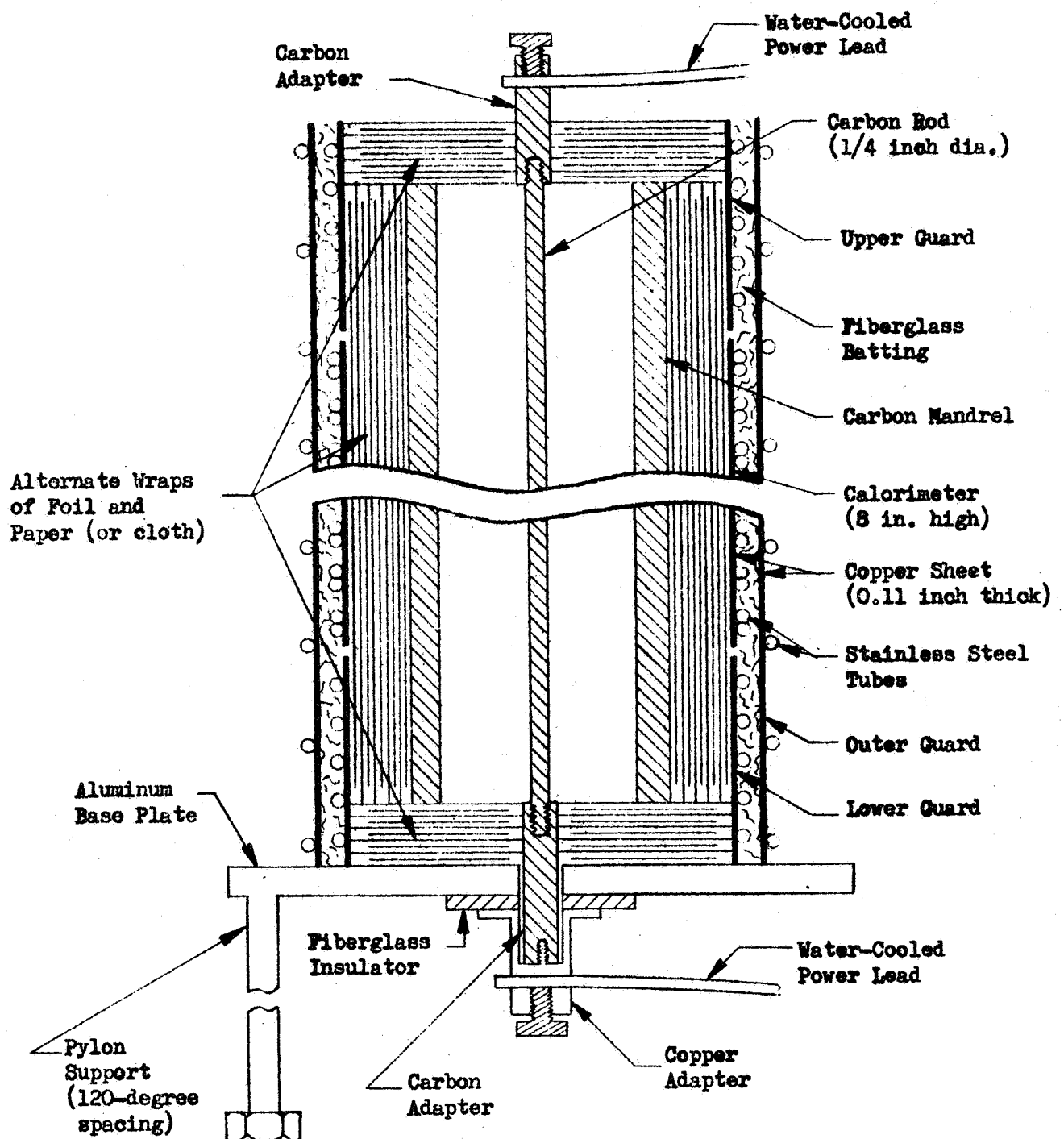


Figure 4. Schematic of Typical Cylindrical Test Section

the radial direction throughout the thickness of insulation. A nominally small amount (~5 pounds) of tension was applied to the foil during the wrapping process to keep the insulation bundle tightly wrapped. Carbon mandrel diameters of 3 and 4 inches were used. Insulation thickness of 1, 1-1/2 or 2 inches resulted in overall insulation outside diameters of 6 or 7 inches. The length of the cylindrical test section was nominally 16 inches except for molybdenum/silica No. 8 (length equals 10 inches).

Metal sheathed thermocouples were positioned at regular radial intervals throughout the insulation with junctions placed in the center plane of the test section and in a parallel plane a few inches from the end of the test section. The thermocouple positions were indexed circumferentially to avoid radial bulging at any location. With this thermocouple placement technique, both radial temperature gradients and axial temperature gradients were measured so that heat loss corrections could be made to the calculated values of the effective thermal conductivity.

Each end of a cylindrical test section was insulated with a number of planar layers of the same type of material as under test. These end stacks of insulation consisted of circular disks of cloth having the same outside diameter as the test section, and a center hole for the heater power posts to come through. The intervening metal foil disks had an OD equal to the carbon mandrel.

The test section heater was a 1/4-inch-diameter carbon rod. The heater rod threaded into a 1/2-inch-diameter carbon rod at each end of the test section. The larger carbon pieces degrade the heater temperature and permit connection to water-cooled copper power leads.

The cylindrical test section and end stacks of insulation are encased within a water-cooled calorimeter and end guards. The calorimeter (6 or 7 inches diameter and 8 inches long) consisted of a thin (0.011 inch thick) copper sheet rolled into a cylinder with a double helical wrap of 3/16-inch OD stainless-steel tubing, soft soldered to the outside surface at approximately 1-inch axial intervals. The double helix of tubing maintained the

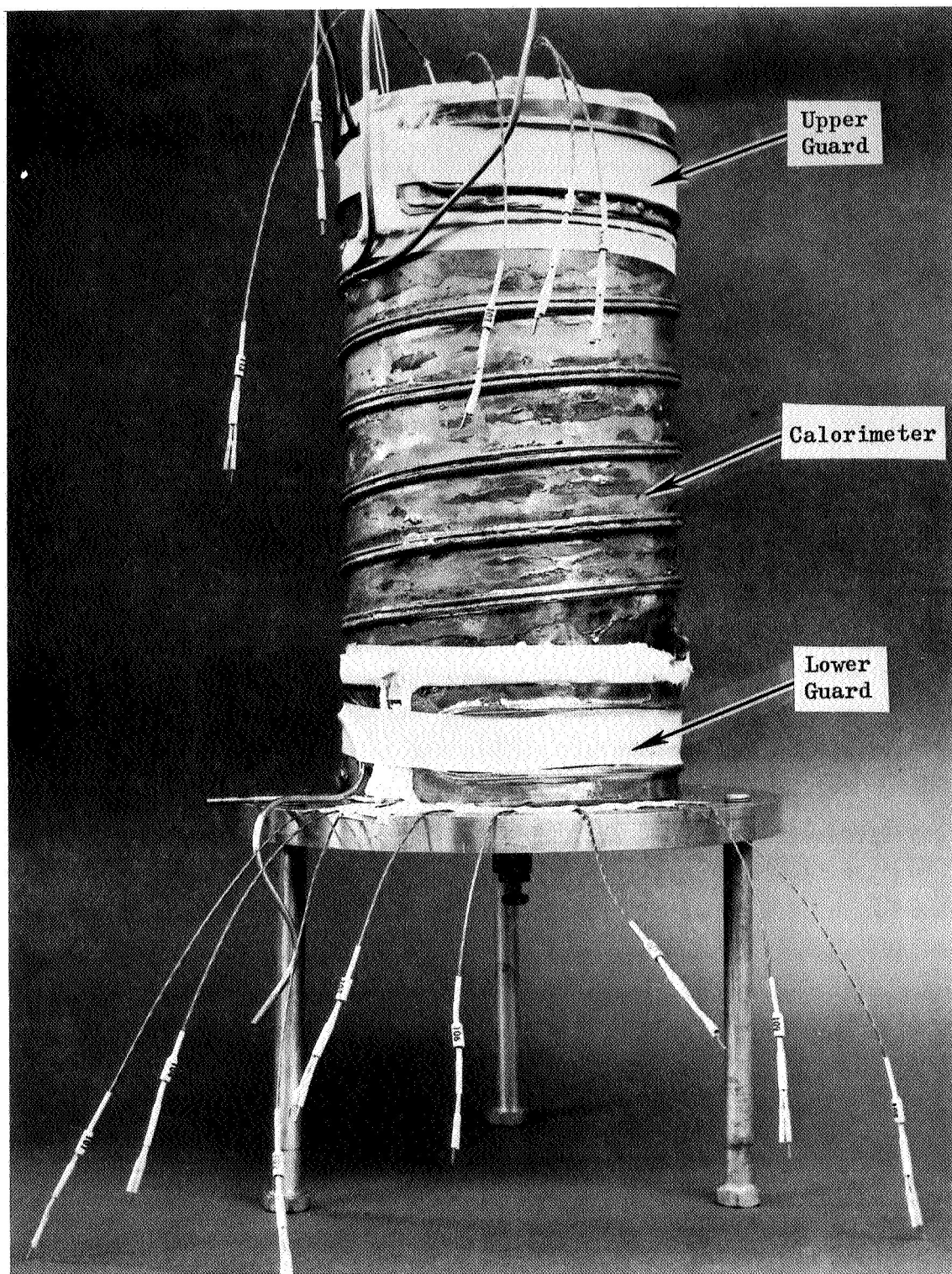
whole calorimeter surface at a relatively constant temperature because the average coolant water temperature was the same at any location. The cylindrical end guards (6 or 7 inches diameter and 2 or 5 inches long) also were made of 0.011-inch-thick copper with 3/16-inch OD stainless-steel tubing soft soldered to them. A typical test section with the calorimeter and end guards installed is shown in Fig. 5.

As pictured, the test section assembly is vertical, free standing upon an aluminum base plate which mounts within the vacuum chamber.

An outer guard cylinder of 0.011-inch-thick copper sheet was positioned around the calorimeter and end guards. Fiberglass mat was placed in the intervening annular space. The outer guard cylinder was water-cooled with the same water as the end guards. Thermocouples mounted on the calorimeter and end guards indicated the copper surface temperatures. It was possible to maintain the calorimeter temperature between the guard temperatures by controlling the inlet temperature of the water flowing through the guard coolant circuit. All water-cooled line joints were soft soldered within sleeves for vacuum tight seals. A typical cylindrical test section is shown installed within the vacuum system in Fig. 6.

Cylindrical Powder Type. In addition to the cylindrical multilayer type of test section, two cylindrical test sections were constructed using powder type of insulation. The construction techniques had to be considerably modified for this type of insulation. However, many of the components from the multilayer type test sections were utilized.

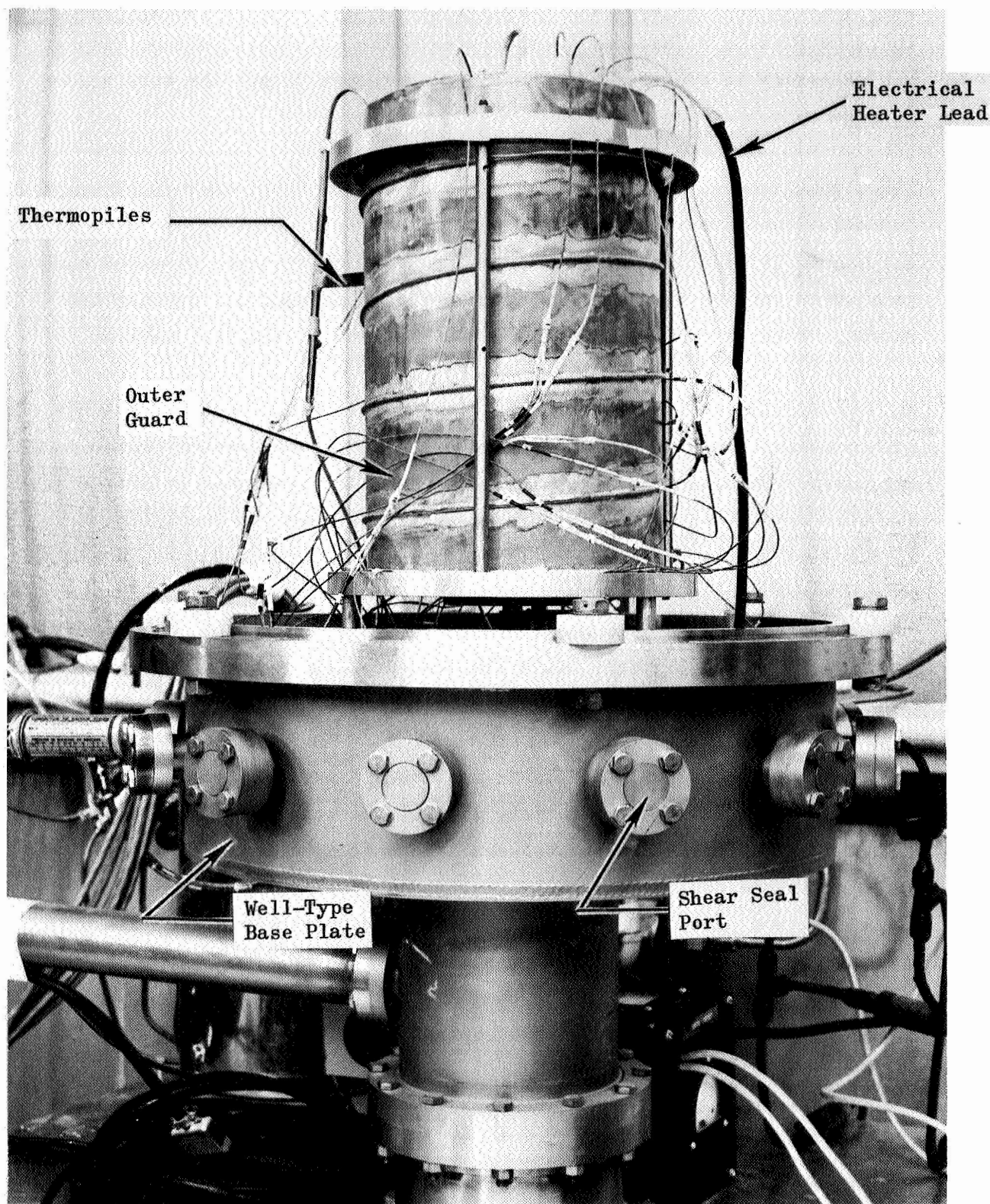
The first modification was to soft solder the calorimeter and end guard cylinders together using intervening stainless-steel shim stock (0.010 inch thick) as thermally resistive tie strip. Tantalum sheathed thermocouples were placed with junctions at regular radial spacing but at different circumferential spacing around the inside of the calorimeter at the midplane. Another set of thermocouples was similarly placed in a parallel plane near the end of the test section. The thermocouples were bent so



5AE33-11/23/66-S1

Figure 5. Test Setup for Cylindrical Section





5AG36-1/9/67-S1B

Figure 6. Cylindrical Section Installed in Vacuum Chamber Well

that approximately 1-1/2 inches next to the junction was parallel to the test section axis to minimize error by conduction down the wire. The thermocouples were fastened to the calorimeter with soft solder. It was necessary to nickel plate the tantalum sheath to get the soft solder to adhere.

The carbon mandrel was wrapped with six layers of 0.001-inch-thick molybdenum foil and inserted within the calorimeter-guards assembly. The mandrel was spaced within this assembly by using 1/4-inch-diameter threaded carbon rods which screwed into the carbon mandrel and pressed out against the guards. Three spacer rods were used at each end of the test section.

End insulation consisted of foamed zirconia blocks, 1 inch thick by 4 inches diameter having 3/4 inch diameter holes for the carbon heater lead-out posts. The electrical heating power was also generated by a 1/4-inch-diameter carbon rod. The outer guard and fiberglass mat insulation were utilized as in the previous multilayer test sections. The test section assembly was sealed to the base plate and mounted in the vacuum chamber. Powdered premixed insulation was poured into the annular space between the mandrel and calorimeter while the test section was in place in the vacuum chamber.

Planar Multilayer Type. The planar test sections consisted of alternate layers of metal foil and refractory fabric, stacked upon a flat base plate with thermocouples interposed between layers at specific intervals. The holding fixture for the planar test sections consisted of two 1/2-inch-thick aluminum plates 14 inches square with corners rounded to a 16.5 inch circumscribed diameter. The bottom plate was mounted rigidly on three pylons bolted to an inner vacuum chamber flange. A top plate was bolted to the bottom plate with a 14-inch separation distance by four additional pylons mounted at the corners. A third 1/2-inch thick aluminum plate 14 inches by 12 inches had clearance holes drilled for the four pylons so it could move freely in the vertical direction. The stacks of insulation and calorimeters were positioned between the bottom plate and the



movable plate. The loading force on the test sections was supplied by piling lead bricks on the movable plate. A side view schematic drawing of a planar test section is shown in Fig. 7. Figure 8 shows a typical planar test section installed in the vacuum well.

Two test sections comprised an assembly. A dummy test section, usually of construction identical to the active test section but without instrumentation, was placed on the bottom water-cooled guard and bottom plate. A metal foil heater separated the two test sections. The water-cooled planar calorimeter, 8 inches square and a guard ring 2 inches wide covered the top of the active test section. A number of layers of fabric insulation separated the calorimeter-guard ring assembly from a water-cooled top guard surface. The movable plate of 1/2-inch-thick aluminum supported the load of lead bricks and distributed this load across the test section. The test section cloth layers were 12.5 inches square. The metal foil pieces were 8 inches square centered on the cloth pieces.

A 2-1/2 inch thickness of cloth insulation was left at the edges to reduce edge conduction losses. Thermocouples were placed under the calorimeter, ring guard, and top guard so that temperatures could be monitored and guard water inlet temperatures adjusted to minimize heat losses to or from the calorimeter. The thermopile was close-connected to the inlet and outlet of the calorimeter. All tubing connections between the floating top surface of the test sections and the rigidly mounted bottom surface were provided with flexible tubing to minimize vertical forces.

A number of thermocouples were incorporated into each measurement section at edge and center positions so that edge heat losses could be determined for correction of effective thermal conductivity values. Total insulation thickness for each loading was determined by measuring the distance between the top edges of two thin, stiff metal shims inserted next to the heater and the calorimeter at each of the four corners.

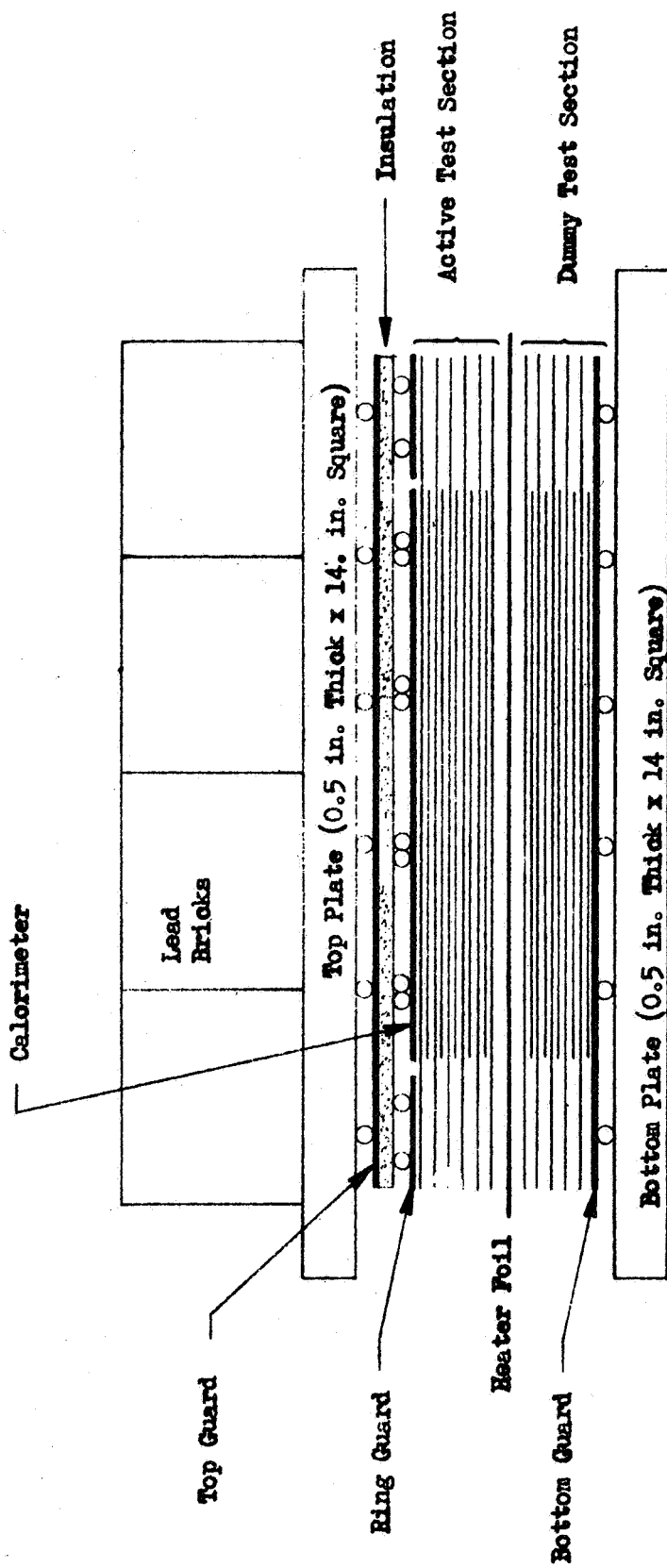
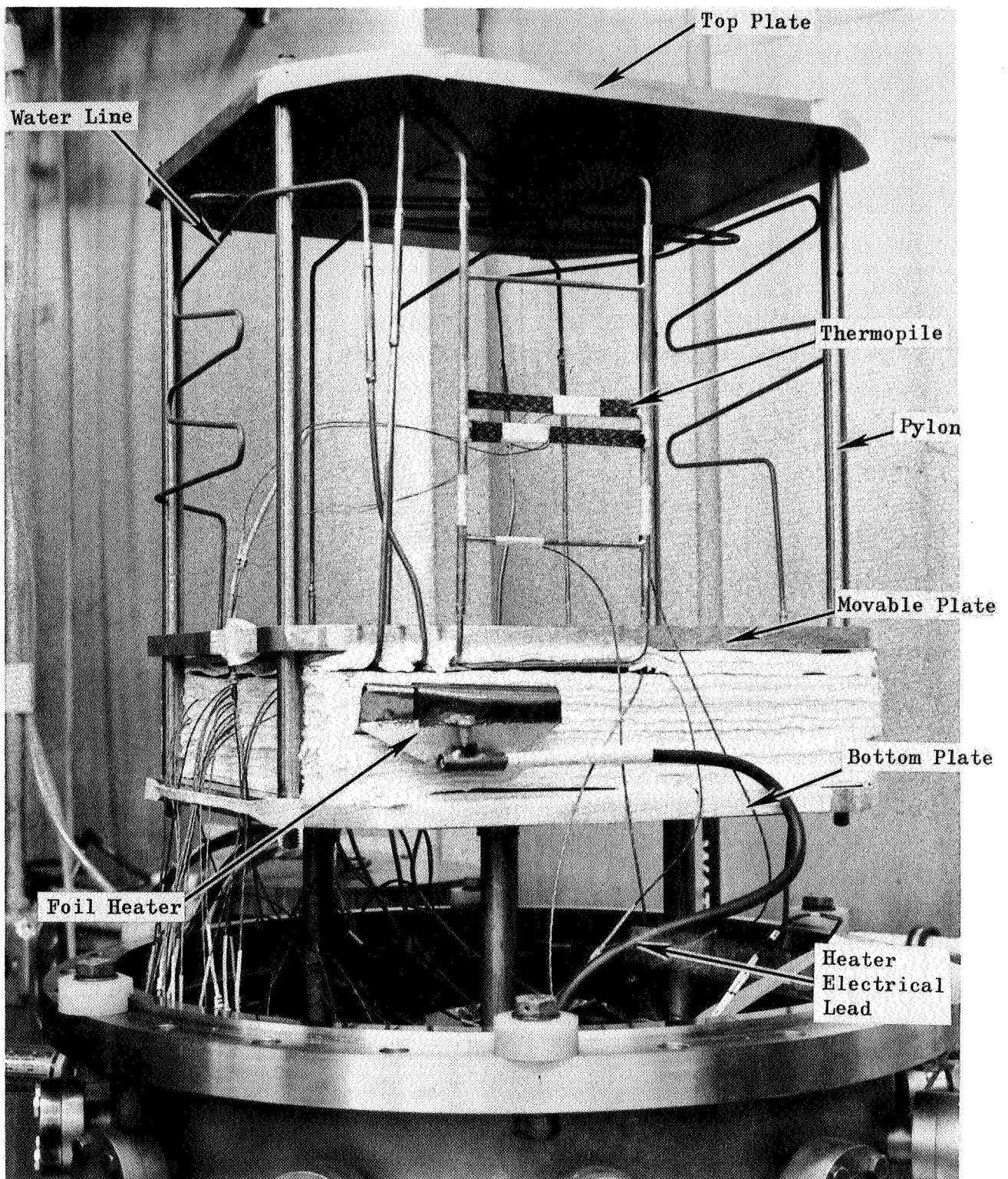


Figure 7. Schematic of Typical Planar Test Section



5AE23-1/25/67-S1

Figure 8. Planar Test Section Installed in Vacuum Chamber Well

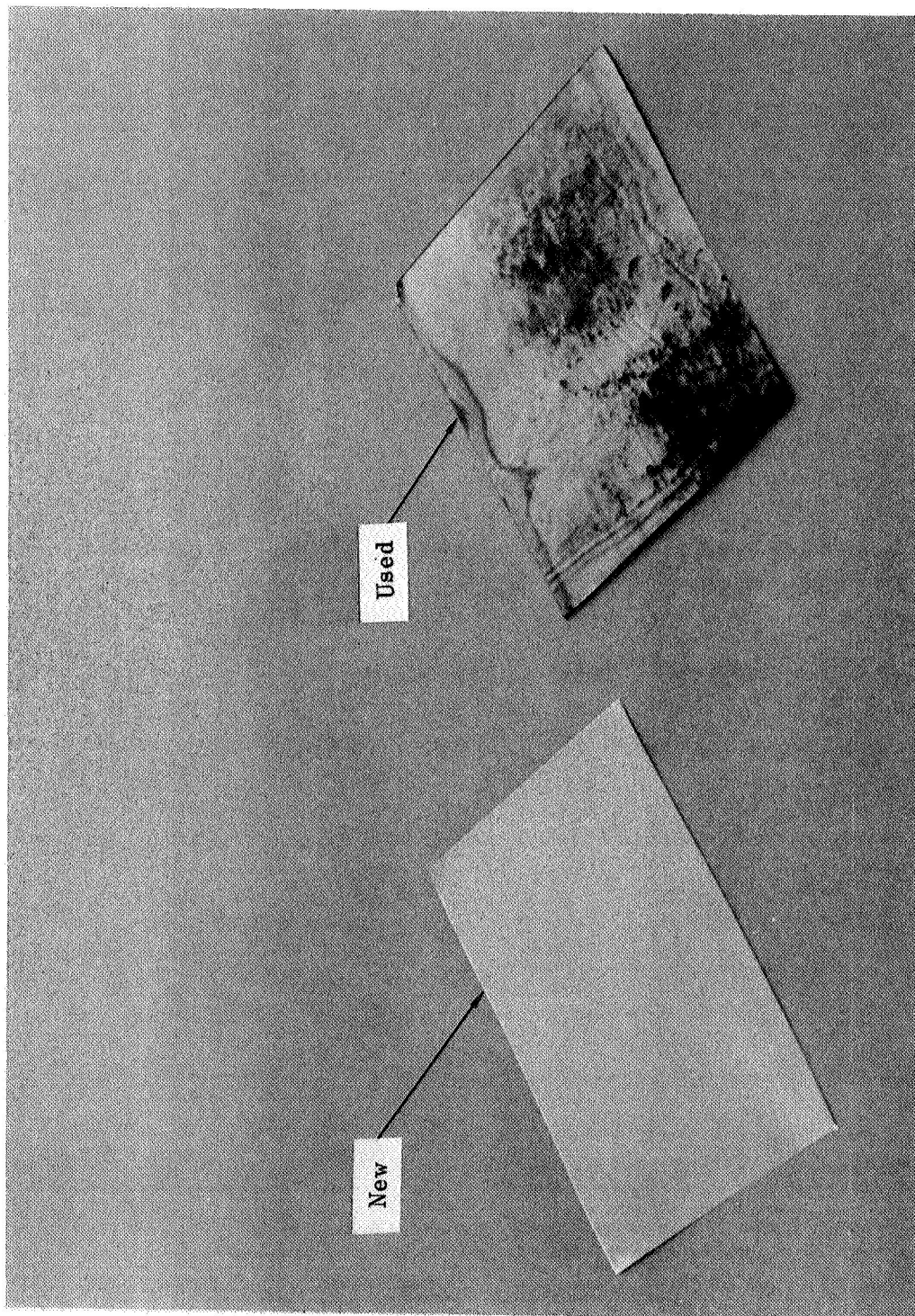
Photographs were taken of samples of test section materials before and after exposure to their maximum temperature conditions. Molybdenum foil is shown in Fig. 9, silica (Refrasil) cloth in Fig. 10, tantalum foil in Fig. 11, carbon cloth in Fig. 12, and 2-percent tungsten/zirconia in Fig. 13. The molybdenum foil as received has a bright mirror finish. The used molybdenum foil often had a somewhat wrinkled purple and grey colored surface. The new silica cloth is rather soft and looks like a loose woven fabric. The used silica cloth is stiff and breaks when flexed.

The new tantalum foil is soft and mirror bright. The tantalum is converted to gold colored brittle tantalum carbide at high temperatures, when in contact with carbon. The carbon cloth weave impressions are clearly visible in the photograph. The new carbon is a soft coarse-woven lustrous-black cloth. Used carbon cloth loses its luster and gains a slight permanent set. However, used carbon fabric can be flexed repeatedly without tearing or fracture. The unused mixture of tungsten/zirconia powder has a light cream color with small black spots. The used tungsten/zirconia is a single sintered black mass that has very little compressive strength. The crumbled sintered material resembles a mixture of salt and pepper.

## TEST PROCEDURES

### Equipment Operation

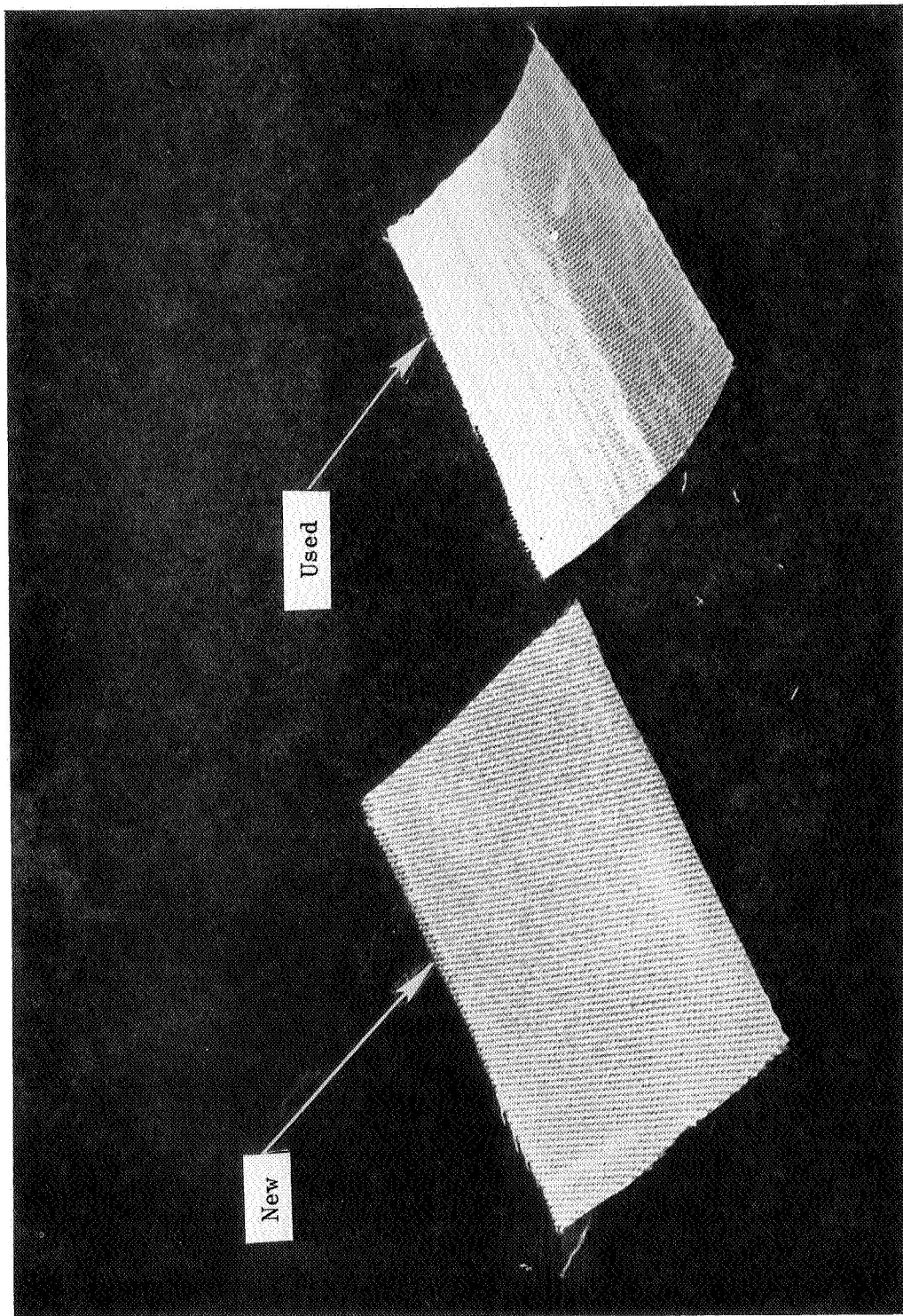
After a test section was installed in the vacuum chamber, heater leads and thermocouples were connected and checked for continuity and resistance to ground. The bell jar was then put in place and the system roughed down slowly as a precaution to prevent the insulation from billowing. The diffusion pump was activated after system pressure reached the  $100\mu$  range. Outgassing at ambient temperature with the five pumps usually took approximately 30 minutes to 2 hours before the diffusion pump could be activated. The diffusion pump was usually operated overnight before the first heating cycle was initiated. Prior to testing, the ice bath and  $\text{LN}_2$  cold trap



1HZ94-6/25/68-S1D

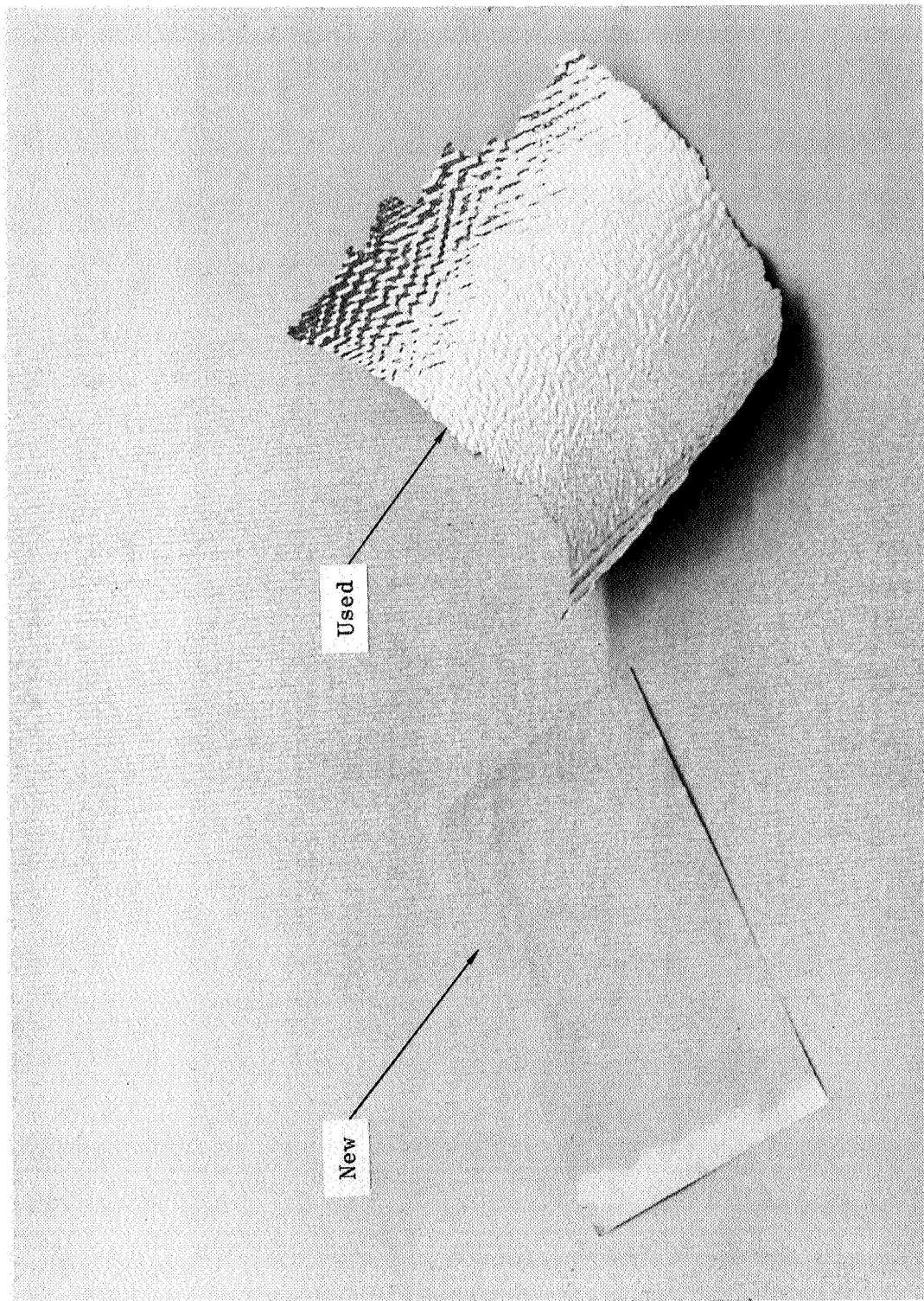
Figure 9. Molybdenum Foil Specimens





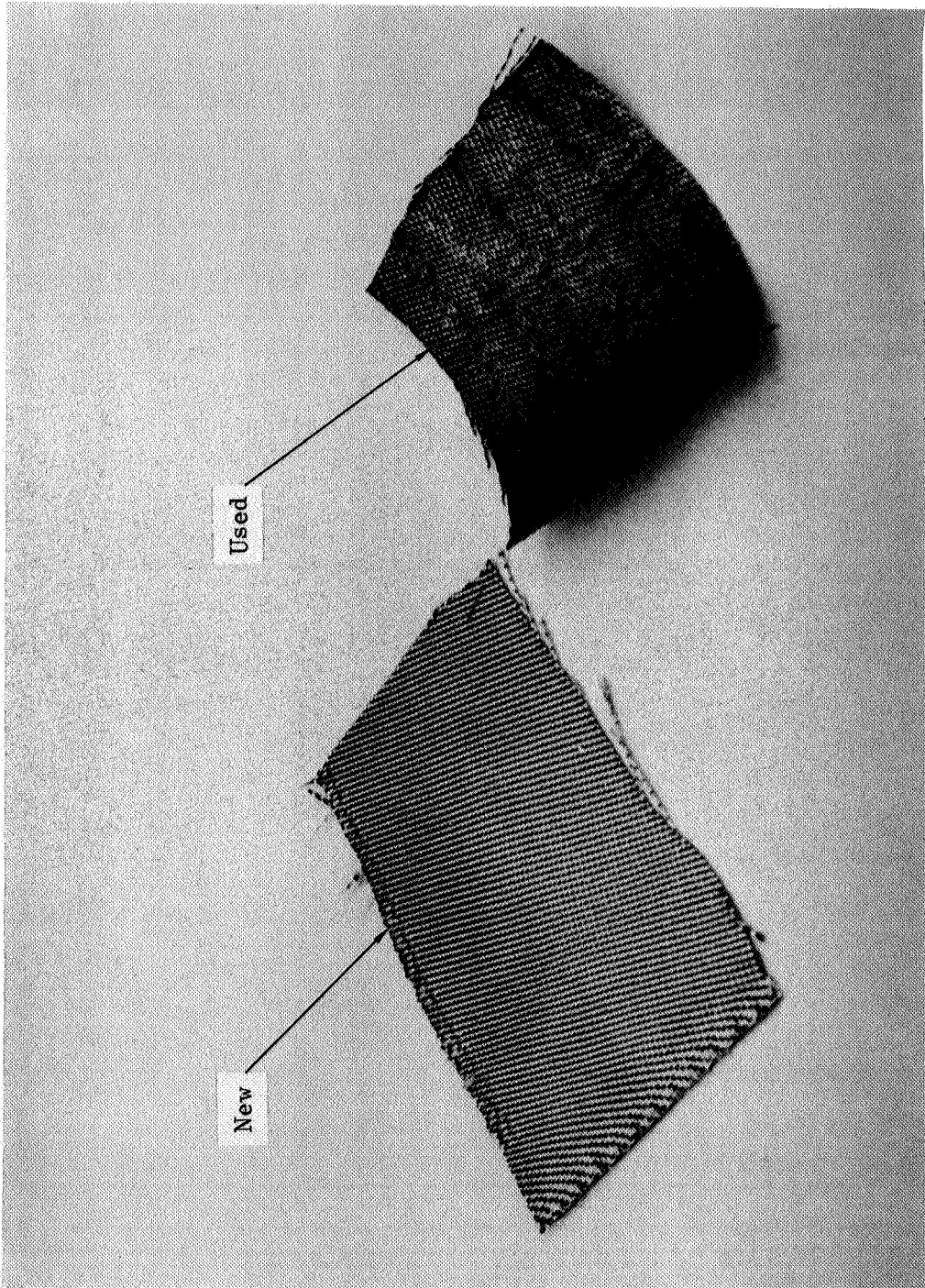
1HZ94-6/25/68-S1B

Figure 10. Silica Cloth Specimens



LHZ94-6/25/68-SLE

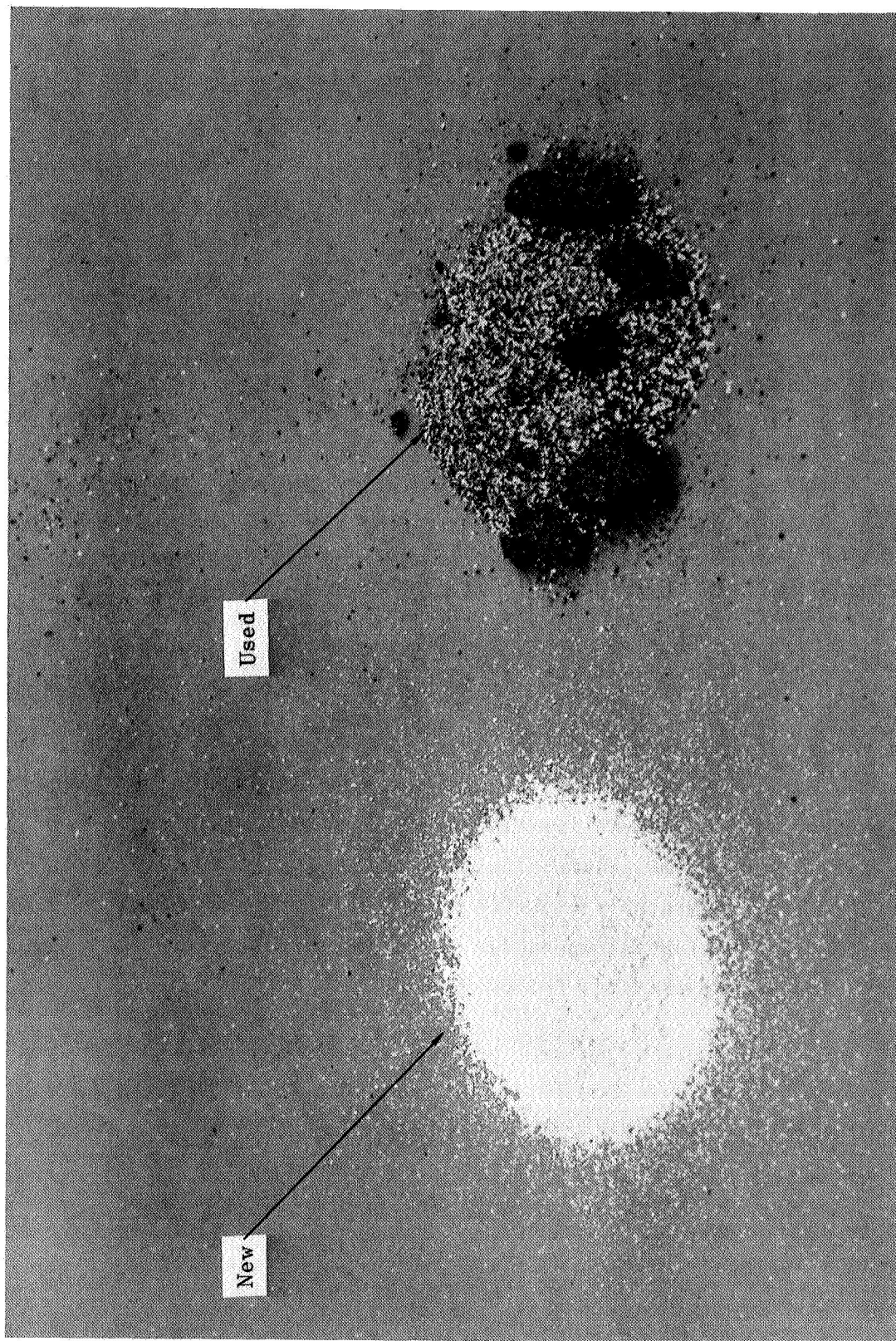
Figure 11. Tantalum Foil Specimens



1HZ94-6/25/68-S1C

Figure 12. Carbon Cloth Specimens





1HZ94-6/25/68-S1A

Figure 13. 2-Percent Tungsten/98-Percent Zirconia Specimens

were filled, and the calibration of the millivolt recorder was checked at zero and 50 millivolts. The recorder zero and span were adjusted within less than  $\pm 0.01$  millivolts.

The ice bath was allowed to come to equilibrium (15 minutes). Power initially was applied to the test section at the maximum rate available or at a rate which was limited by the outgassing characteristics of the test section and the pumping speed of the vacuum system. After the test section inside temperature reached a desired value, heating power was reduced manually to maintain this temperature level for the remainder of the heating cycle. The maximum applied power level and the observed outgassing level are discussed in conjunction with the results for each test section.

Each test section was subjected to two or more transient heating cycles for the purpose of obtaining additional data on the effect of outgassing on effective thermal conductivity as a function of time. The molybdenum/silica test sections were usually operated at equal power levels for each heating cycle because the chromel-alumel thermocouples could tolerate the maximum exposure temperatures. The first heating cycle for each tantalum/carbon or tungsten/zirconia test section was intentionally limited to a maximum temperature of approximately 2100 F to obtain additional low temperature data. The chromel-alumel thermocouples burned out in these test sections as the temperatures exceeded 2400 F in the second heating cycle. The tungsten-rhenium thermocouples had limited useful life (2 hours) at the highest temperatures ( $\sim 3500$  F).

#### Transient Data Recording

Transient data sets were taken at regular time intervals as power was applied to each test section. A transient data set consisted of millivolt values of all operative thermocouples along with identifying channel number; millivolt values of thermopiles and channel identification; water flowrates through the calorimeter, guards, and power leads; vacuum

pressure readings; heating current and voltage; time and date. A complete data set constituted a run and was given a four digit run number. The first two digits were test section identification. The last two digits were run numbers sequenced by time.

Steady-State Data Recording. Steady-state data sets were obtained when temperatures throughout a test section approached a constant value at each location. Consecutive data sets were compared point by point until steady state was deemed to exist.

#### Data Analysis

Two stages were required in analyzing the recorded data. The first step was to scale millivolt values into temperature units. The second step was to select temperatures to be used in calculating effective conductivities.

Millivolt values were scaled into temperature units using two computer programs written in Basic Language for a General Electric time sharing computer. One program scaled chromel-alumel data referenced to 32 F in the temperature range from ambient to 2500 F. The 0- to 55-millivolt range was subdivided into eleven 5-millivolt ranges each of which was fitted with a second order polynomial equation. This scaling program was accurate to within  $\pm 0.3$  F of the NBS Circular No. 561 data over the entire temperature range.

A second scaling program was written (in Basic Language) for the tungsten-5 percent rhenium/tungsten-26 percent rhenium thermocouple system with 32 F as reference. Two-millivolt subintervals were fitted with second order polynomials for the temperature range from ambient to 3800 F; accuracy was within  $\pm 0.2$  F of published Hoskins Co. data. Three-hundred and eighty four millivolt data sets were reduced to yield 8278 temperature points in the first stage of the data reduction program.

Temperature values are selected from the scaled data as input to both steady-state data and transient data computer programs which calculate effective thermal conductivities. Two or more thermocouple junctions were often placed in the same location in a test section for redundancy in temperature measurements. When calculated temperatures were nearly the same, a simple average was usually taken. If a disparity in temperatures existed, graphs of temperature versus time or position were used as an aid in selecting the most reasonable temperature value.

### Steady-State Heat Transfer

A computer program was written in Basic Language for the General Electric time sharing computer to reduce steady-state data sets into effective thermal conductivities as a function of temperature. This program solves the finite difference form of the linear conduction equation taking into account variable average conduction area at each position in a test section, and axial heat losses as a function of position. The equation is of the form:

$$k_e = \frac{\Delta R}{\bar{A}_c \Delta T} (q_c + q_{\text{loss}}) \quad (1)$$

where the symbols are defined in the nomenclature. Both the cylindrical and planar test section data sets could be accommodated using this program because of its incorporation of the heat loss determination.

### Transient Heat Transfer

Another computer program was written in Fortran II language for the General Electric time sharing computer to solve the finite difference form of the integrated cylindrical transient conduction equation including the effects

of axial heat losses. This equation is of the form:

$$k_e(R, \theta) = \frac{1}{2\pi LR \left(\frac{\Delta T}{\Delta R}\right)_{R_i}} \left[ q(R_N, \theta) + \sum_{R_N}^{R_1} \rho_e c_{pe}(T) \left(\frac{\Delta T}{\Delta \theta}\right)_{R_i, \theta} 2\pi LR \Delta R_i + \sum_{R_N}^{R_1} \frac{K_{loss}(T) 2A_{loss, R_i} \Delta T_{loss, R_i}}{\Delta Y} \right] \quad (2)$$

The transient data computer program output is effective thermal conductivity as a function of temperature and time. The effect of pressure can be inferred through the time dependence which is recorded in the data set.

A simple and general technique had to be adopted for determining the space and time derivatives in the above equation. Various curve-fitting procedures were attempted for temperature data sets consisting of all radial positions at a given time or vice-versa. It was not possible to generalize the curve-fitting procedure and obtain stable derivative functions for an entire set of data. Therefore, a "floating second-order polynomial" curve fit was adopted for all interior points of a data matrix. This amounts to taking double differences and yields accuracy on the order of cubic terms. Instability in the end point derivative determinations prompted use of simple differences for all exterior points of the temperature data matrix.

Thermal property values for input to the transient computer program were obtained from Ref. 1. Appropriate averages of composite properties were computed by the program.

#### ERROR ANALYSIS

A logarithmic differentiation of the linear steady-state heat conduction equation results in the expression that the percentage error in the effective thermal conductivity is less than or at most equal to the sum

of the absolute values of the percentage errors in the heat flux, the conduction area, the conduction distance and the temperature difference. The heat flux and conduction area have constituent errors associated with their determination. These will be discussed below under the sub-headings of the error factors listed.

### Heat Flow

A number of factors enter into determination of total heat flow at a given location in a test section. The first breakdown of heat flow is into calorimeter heat load and heat losses. The calorimeter heat load is determined by measuring a water flowrate and a temperature difference. Water flowrate is measured with a graduate cylinder in conjunction with a sweep second hand on a large electric clock. Temperature difference is measured using 10-element thermopiles. The determination of weight of water collected is assumed to be within 1/2 percent because of calibration accuracy and scale readability on the graduate cylinders. Collection time can be controlled within 1/2 second out of 60 seconds or approximately 1 percent. Temperature difference is known within 1 percent because of  $\pm 0.02$  millivolt uncertainty in recording a 2-millivolt (average) signal; thermopile accuracy is believed to be well below 1 percent in the temperature range utilized. The two thermopiles showed excellent agreement. Calorimeter heat load accuracy is believed to be within 3-1/2 percent.

Heat loss in two areas can be considered: calorimeter heat loss, and test section axial heat loss. The calorimeter-guard system was built to minimize these losses by using heated guard water to match temperatures and prevent extraneous heat transfer. In an intentional temperature difference of 30 F between guards and calorimeter, thermopile output changed 4 percent. Therefore, a calorimeter heat loss of 1/2 percent is assumed for the usual temperature difference of 4 or 5 F.

Test section axial heat losses are accounted for in the calculation of effective thermal conductivities. Axial heat losses of up to 10 percent are believed to be corrected to within 10 percent resulting in an additional uncertainty of 1 percent. Heat loss uncertainty adds up to 1-1/2 percent, and total steady-state heat flow uncertainty is 5 percent.

#### Conduction Area

Because the linear heat conduction equation is utilized in a cylindrical geometry, another error is introduced, in addition to measurement errors. The maximum magnitude of this error (Appendix B, Ref. 2) is always less than 1 percent for the test sections of the present study. Calorimeter length is known within  $\pm 1/32$  inch of 8 inches or 1/2 percent. The average diameter associated with the conduction area is known within  $\pm 1/32$  inch of 4 inches or 1 percent. Therefore, the conduction area is known within 2-1/2 percent.

#### Conduction Distance

The distance between thermocouple stations is well defined in multilayer insulation systems because the total insulation thickness essentially is subdivided into multiples of an integer based fraction. Therefore, the percentage error in conduction distance amounts to the percentage error in the insulation thickness. A thickness of 1 inch was known within  $\pm 1/64$  inch or 1-1/2 percent.

#### Temperature Differences

The temperature difference accuracy depends upon recorder and thermocouple accuracy. Recorder accuracy is  $\pm 0.01$  millivolt considering differential values only which corresponds to  $\pm 0.5$  F for chromel-alumel or 1.0 F for tungsten-5 percent rhenium/tungsten-26 percent rhenium. Premium grade wire was utilized throughout this study. Guaranteed accuracy for premium wire is 3/8 percent. This would amount to 8 F uncertainty in absolute temperature at 2000 F. However, experience has shown that premium thermocouple

wire is usually accurate within 2 to 5 F of the laboratory standard platinum-platinum/10-percent rhodium thermocouples calibrated by N.B.S. (No. 162069 A and B). Inplace comparison of the chromel-alumel and tungsten rhenium thermocouples showed agreement many times within 2 F and most of the time within 5 F. Temperature differences between thermocouples range from 100 to 800 F. Therefore, percent error in temperature differences could range between 2 and 10 percent with an average of 6 percent.

Taking the sum of the absolute values of the listed errors, an expected maximum error range of 12 to 20 percent is obtained. However, some of the stated errors can be expected to mutually cancel each other. Therefore, an actual error somewhat less than the above numbers would be expected (on the order of 10 percent).

Heat balances were performed for random data sets of a number of test sections; values ranged near 90 percent of the input power.

## RESULTS AND DISCUSSION

The experimental thermal property results which were obtained from 15 of 16 test sections will be presented and discussed in this section. Results from molybdenum/silica test section No. 4 were not processed as its instrumentation had failed during test because of overtemperature. Molybdenum/silica No. 5 was constructed to duplicate No. 4.

A systematic variation in geometrical factors and materials was followed in establishing the testing matrix. Table 2 lists test section identification, the run series designation, and the sequence of variation in parameters.

Results are presented following the parametric change accorded each test section. In some cases, duplication of parameter change could not be avoided. After discussions of results per test section, a cross comparison is made by grouping test sections and material combinations.



TABLE 2

## VARIATIONS OF TEST SECTION PARAMETERS

Test Section	Run Series	Change of Parameter
Molybdenum/Silica (Cylindrical)		
No. 1	0100	Base case (plus argon tests)
No. 2	0200	Different purchase lot of material
No. 3	0300	Small ID (greatest thickness)
No. 4	0400	(Not used for data)
No. 5	0500	Small OD (least thickness)
No. 6	0600	Larger spacer to foil ratio
No. 7	0700	Duplicate No. 6
No. 8	0800	Shorter test section length
Tantalum/Carbon (Cylindrical)		
No. 1	0900	Base case
No. 2	1000	Duplicate No. 1
No. 3	1100	Duplicate No. 1 (plus argon tests)
Carbon (Cylindrical)		
No. 1	1200	Eliminate tantalum foil
Tungsten/Zirconia		
No. 1	1300	10 w/o tungsten
No. 2	1400	2 w/o tungsten
Molybdenum/Silica		
No. 9	1500	Planar, three loading pressures
Tantalum/Carbon		
No. 4	1600	Planar, three loading pressures

### Molybdenum/Silica No. 1

Transient effective thermal conductivity ( $k_e$ ) values as a function of temperature are presented in Fig. 14 for the first heating cycle of this test section. Note the progressive decrease in conductivity in the lower temperature range with time. Steady-state values of  $k_e$  for argon pressure levels of 0, 400, 800, and 1600 microns are given in Fig. 15. Note the regular increase in effective thermal conductivity with pressure over the entire temperature range. Comparison of Fig. 14 and 15 strongly suggests that the transient (time) effect on  $k_e$  in Fig. 14 is really a pressure effect. Gas pressure within the vacuum chamber during the first heating cycle was less than 6 microns within the time interval represented in Fig. 14. However, the gas pressure within the test section was undoubtedly much higher initially and decreased with time, as evidenced by the factor of 15 change in chamber pressure during this time interval. For design convenience, a curve fit of the results presented in Fig. 15 is included as Appendix C of this report.

### Molybdenum/Silica No. 2

This test section was made to be identical to the first test section except for having different purchased lots of material. The transient data for the first heating cycle and the steady-state data at various argon pressure levels are essentially identical to the corresponding data presented in Fig. 14 and 15. Figure 16 depicting transient data, is to be compared with Fig. 14.

### Molybdenum/Silica No. 3

The third test section had a smaller inside diameter (and thicker insulation) than the two previous test sections, to determine thickness scaling effects. A set of transient temperature data is given in Fig. 17 to show the change in temperature profile with time. The temperature profiles which start concave upward change through S-shaped curves to convex upward

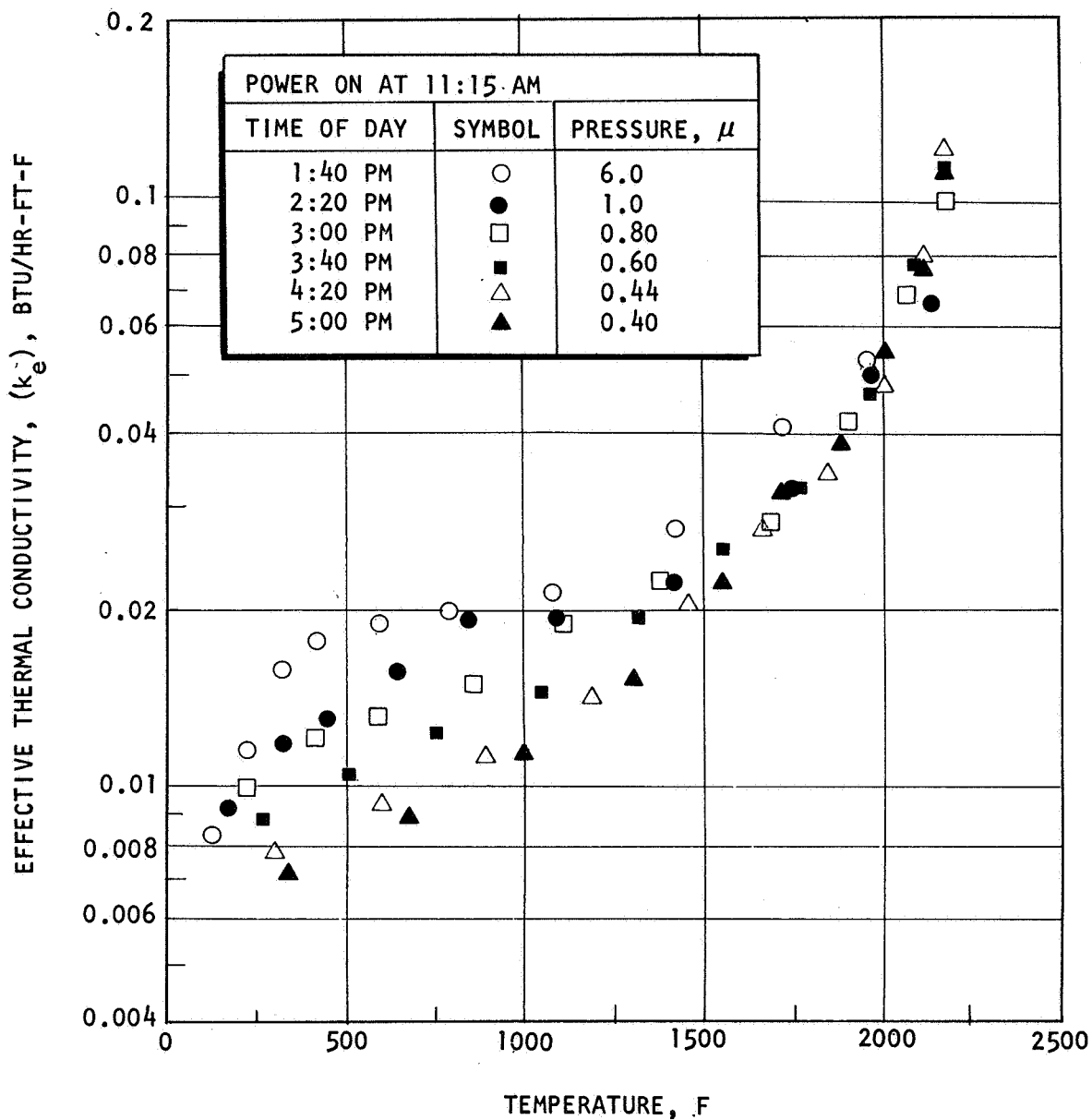


Figure 14. Effective Thermal Conductivity as a Function of Temperature and Time (First Heating Cycle), 1 December 1967, Molybdenum/Silica No. 1

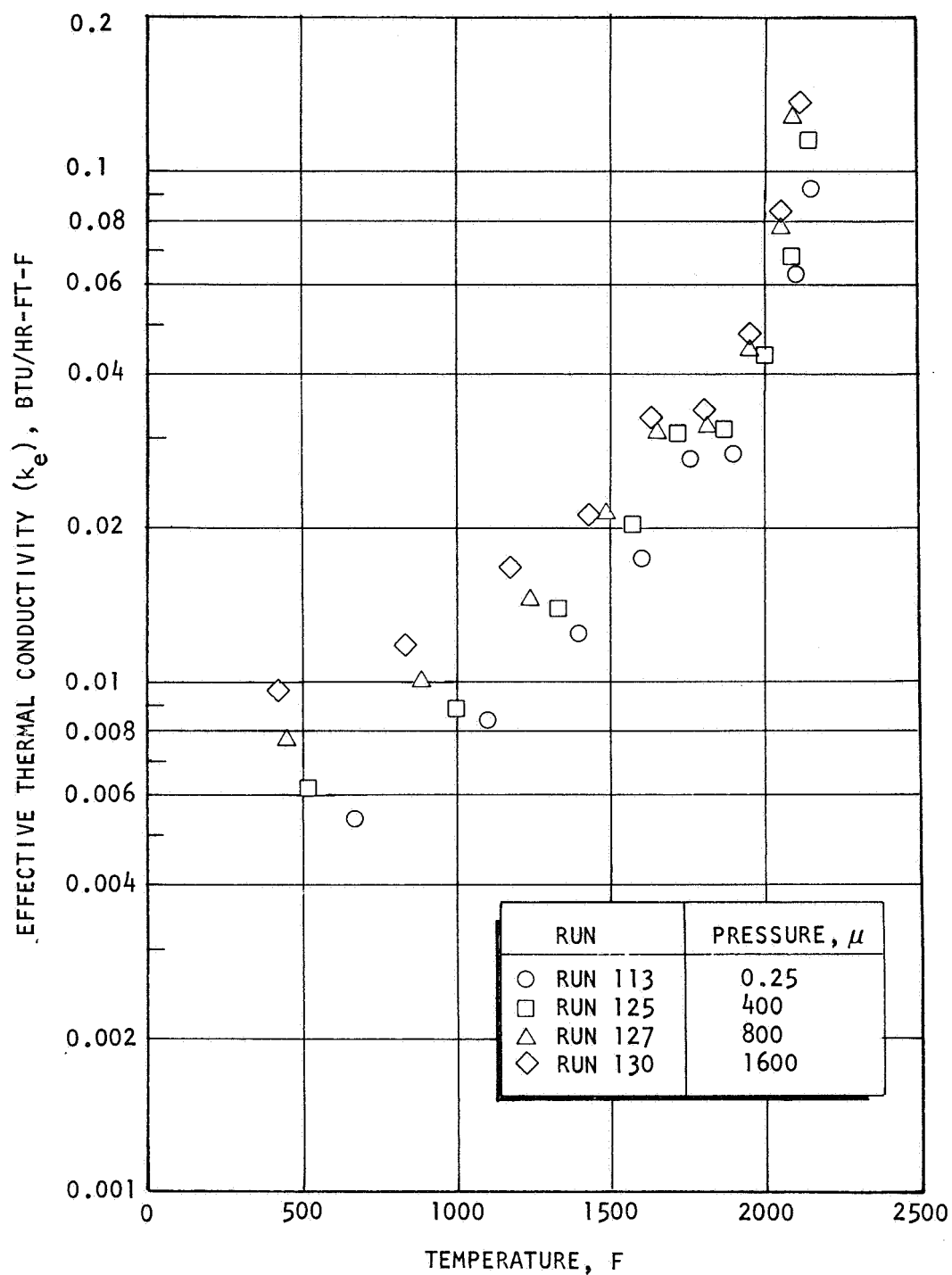


Figure 15. Variation of Effective Thermal Conductivity With Argon Pressure, 1 and 4 December 1967, Molybdenum/Silica Number 1 (Steady State)

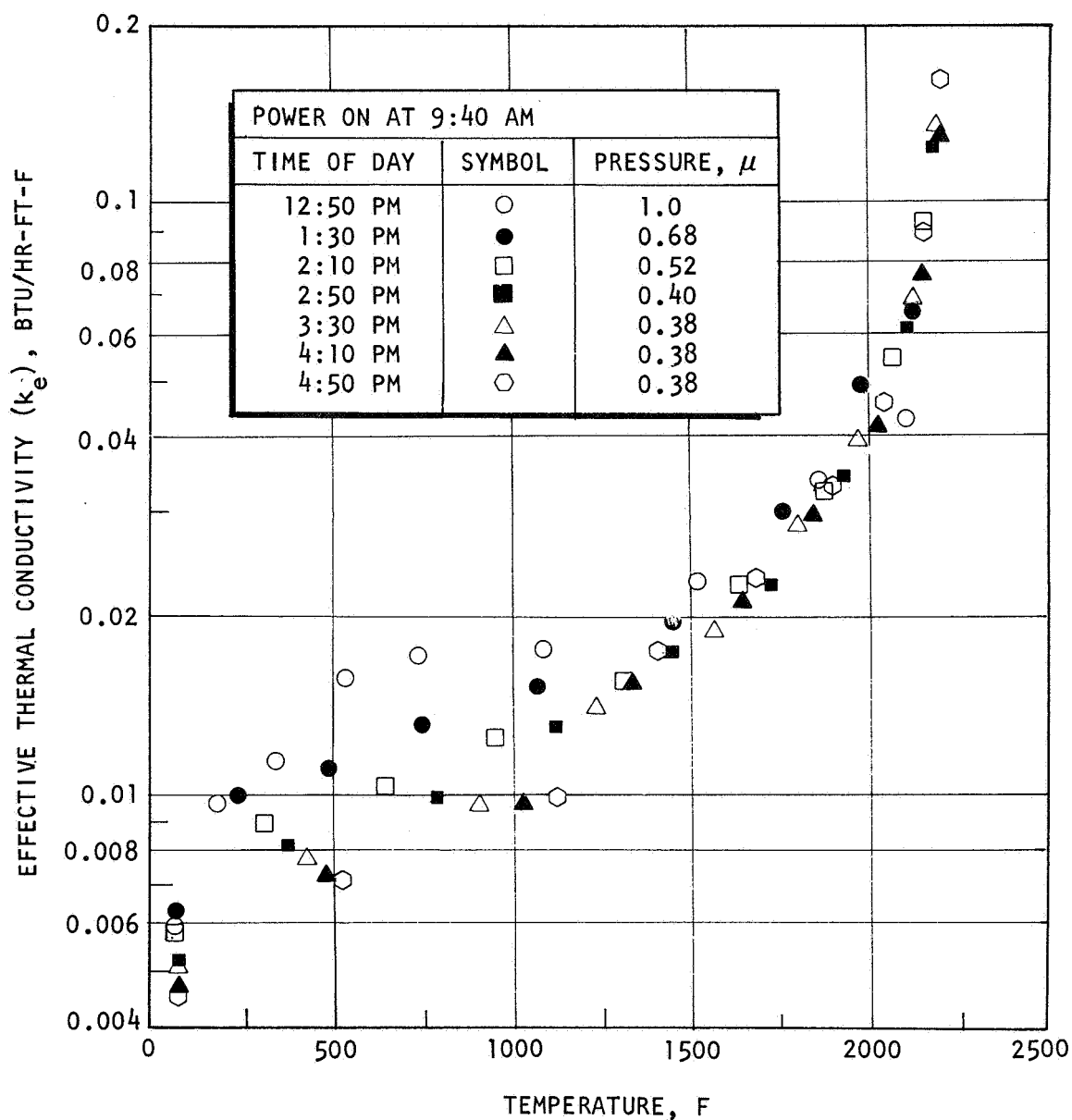


Figure 16. Effective Thermal Conductivity as a Function of Temperature and Time (First Heating Cycle), 11 December 1967, Molybdenum/Silica No. 2

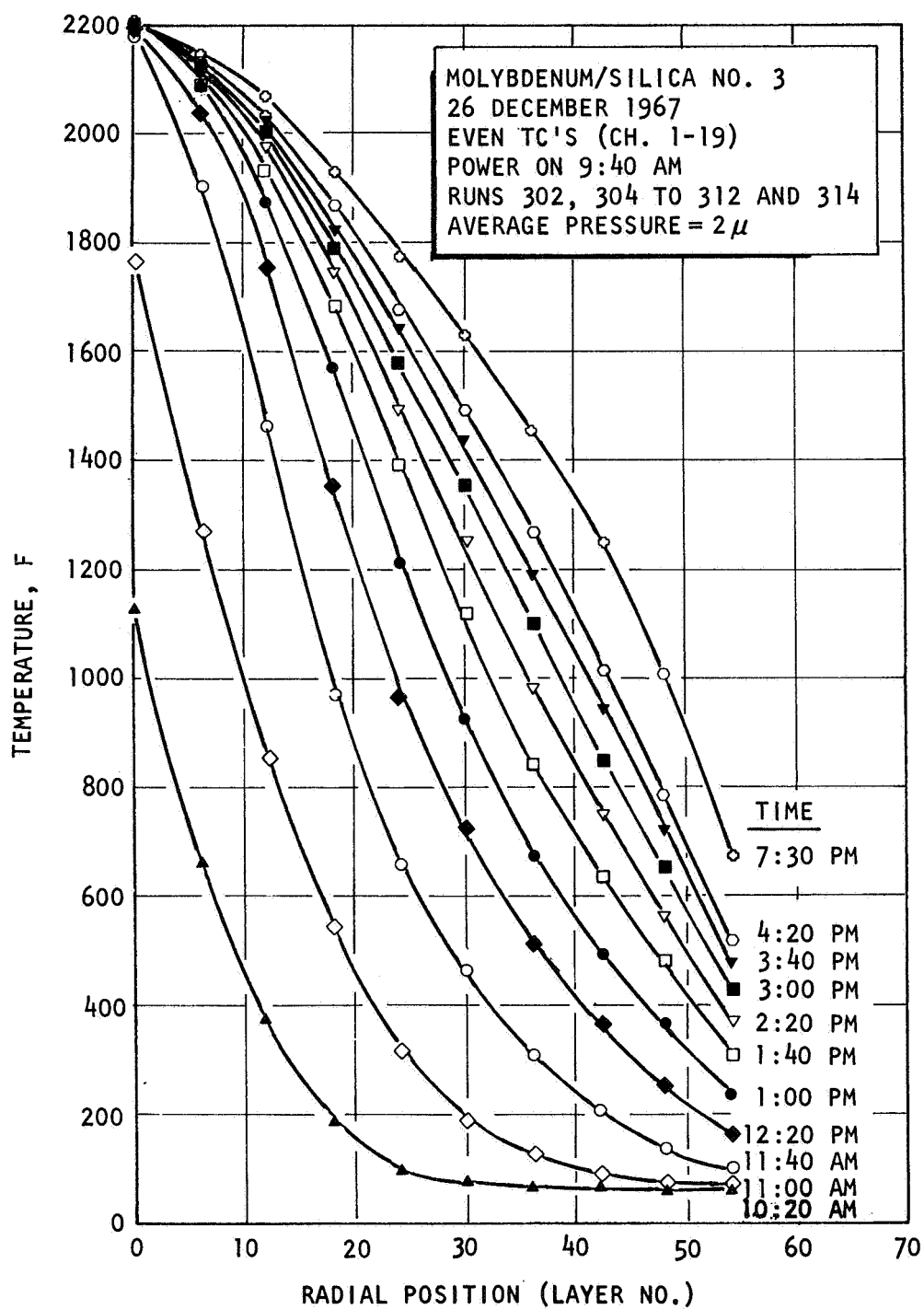


Figure 17. Midplane Temperature Histories

shapes. This behavior is characteristic of materials which have increasing conductivity with increasing temperature. Transient values of  $k_e$  derived from the temperature data of Fig. 17 are shown in Fig. 18. Comparable bell jar gas pressures were maintained throughout the first heating cycle with this test section as with the first test section.

Excellent agreement is evident when the results of Fig. 18 are compared to those of Fig. 14. Transient effective thermal conductivity values are depicted for the second heating cycle of this test section in Fig. 19; a much smaller spread in time dependence is noted for the second heating cycle than for the first. With increasing time of exposure to temperature, transient results approached more closely steady-state results.

#### Molybdenum/Silica No. 4

A malfunctioning recorder resulted in overtemperature and loss of instrumentation, therefore data were not reduced.

#### Molybdenum/Silica No. 5

This test section was a duplicate of No. 4 and had a maximum inside diameter and minimum outside diameter (or thinnest insulation). Transient results are presented in Fig. 20 for the first heating cycle during which time low (less than 1 micron) vacuum was maintained. The results exhibit the characteristics similar to those of other test sections; i.e., decreasing values of  $k_e$  with time and close approach to steady-state values.

Steady-state values are presented in Fig. 21 for six runs taken at the end of three heating cycles. Excellent agreement is evident between the latter transient results and the steady-state results. Excellent agreement is also exhibited by the data of Fig. 20 and the latter time values of Fig. 21. This shows that no radius ratio or thickness effect upon  $k_e$  is of consequence for the extremes of the cases tested.

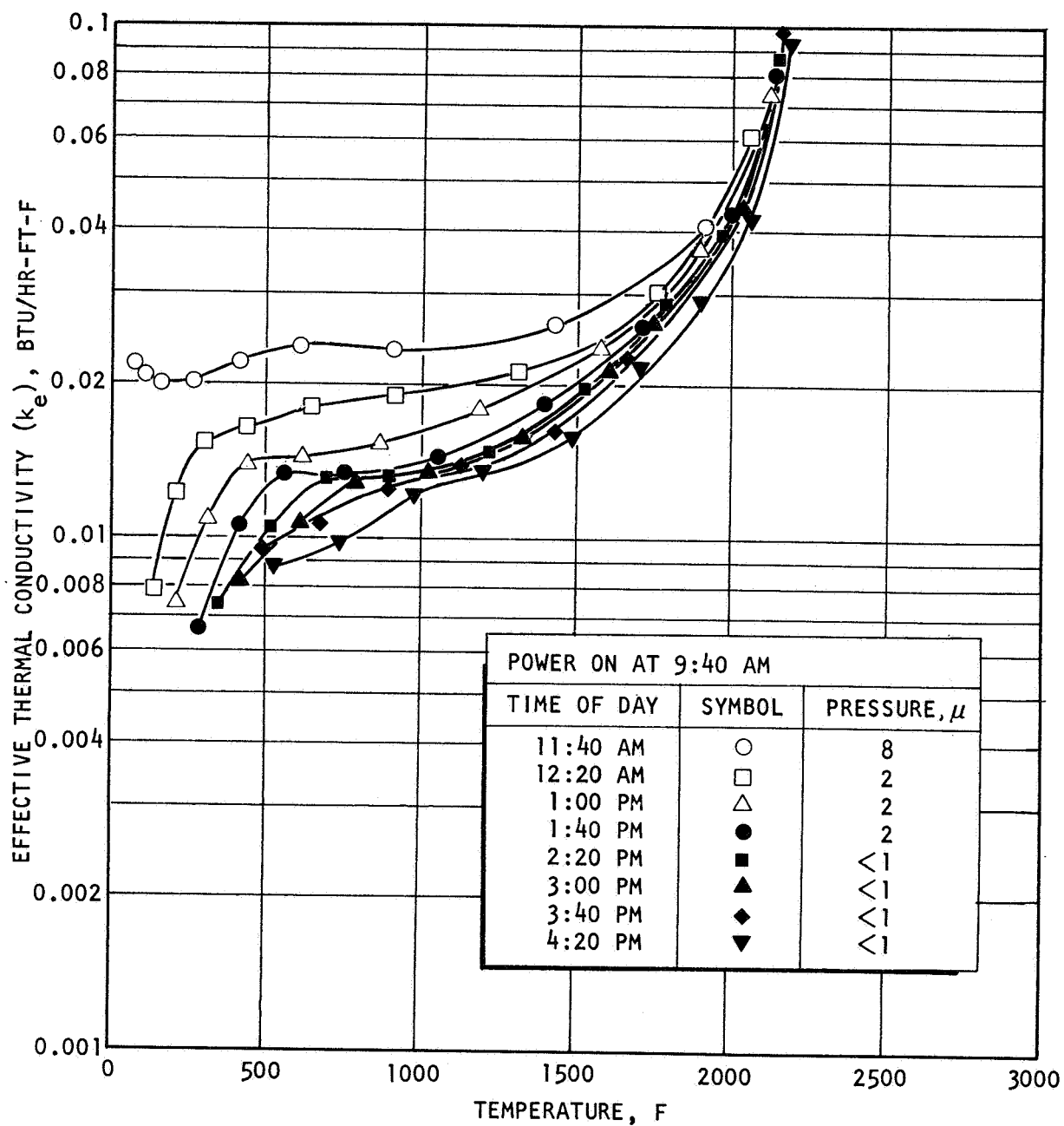


Figure 18. Effective Thermal Conductivity as a Function of Temperature and Time (First Heating Cycle), 25 December 1967, Molybdenum/Silica Number 3



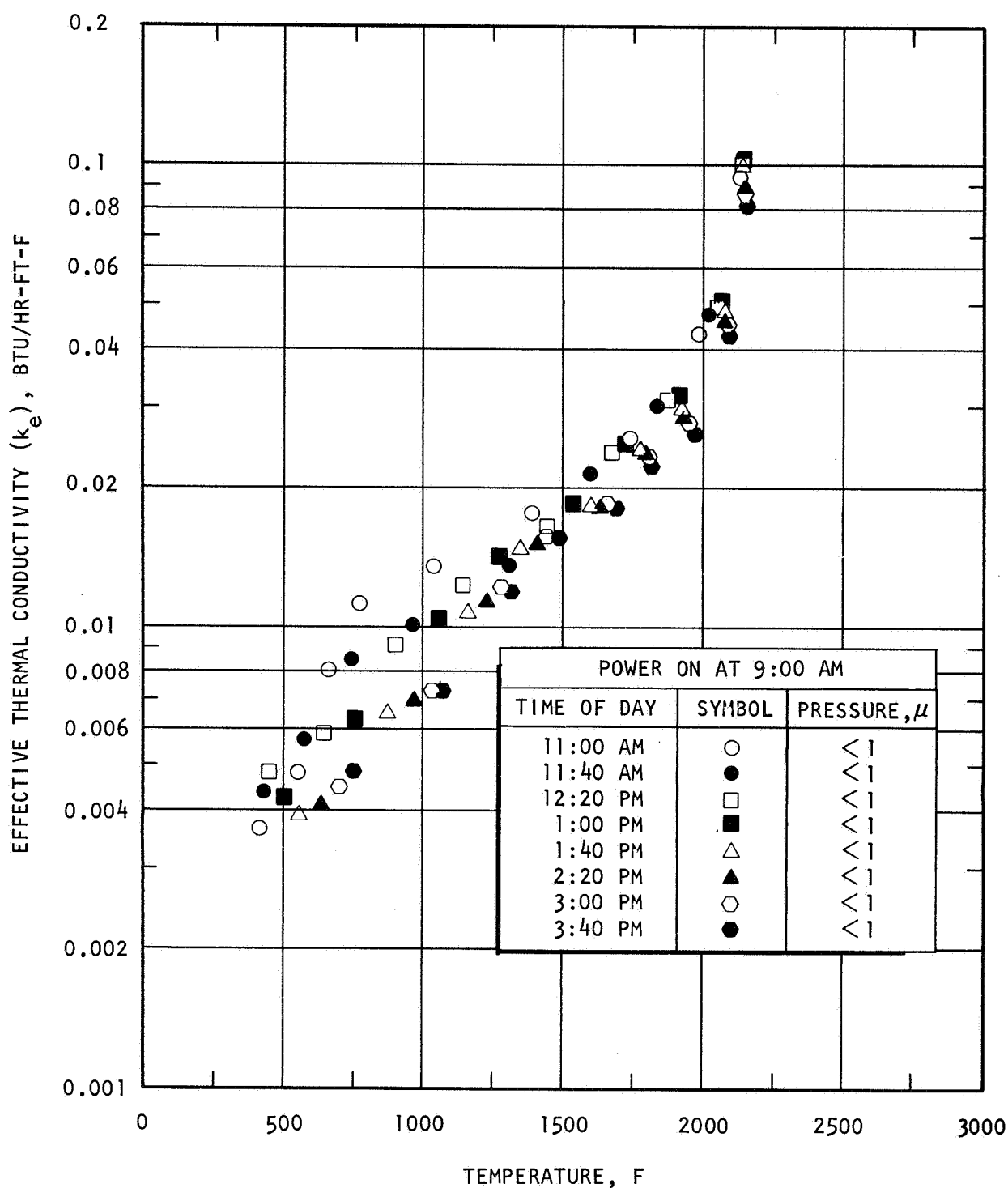


Figure 19. Effective Thermal Conductivity as a Function of Temperature and Time (Second Heating Cycle), 27 December 1967, Molybdenum/Silica Number 3

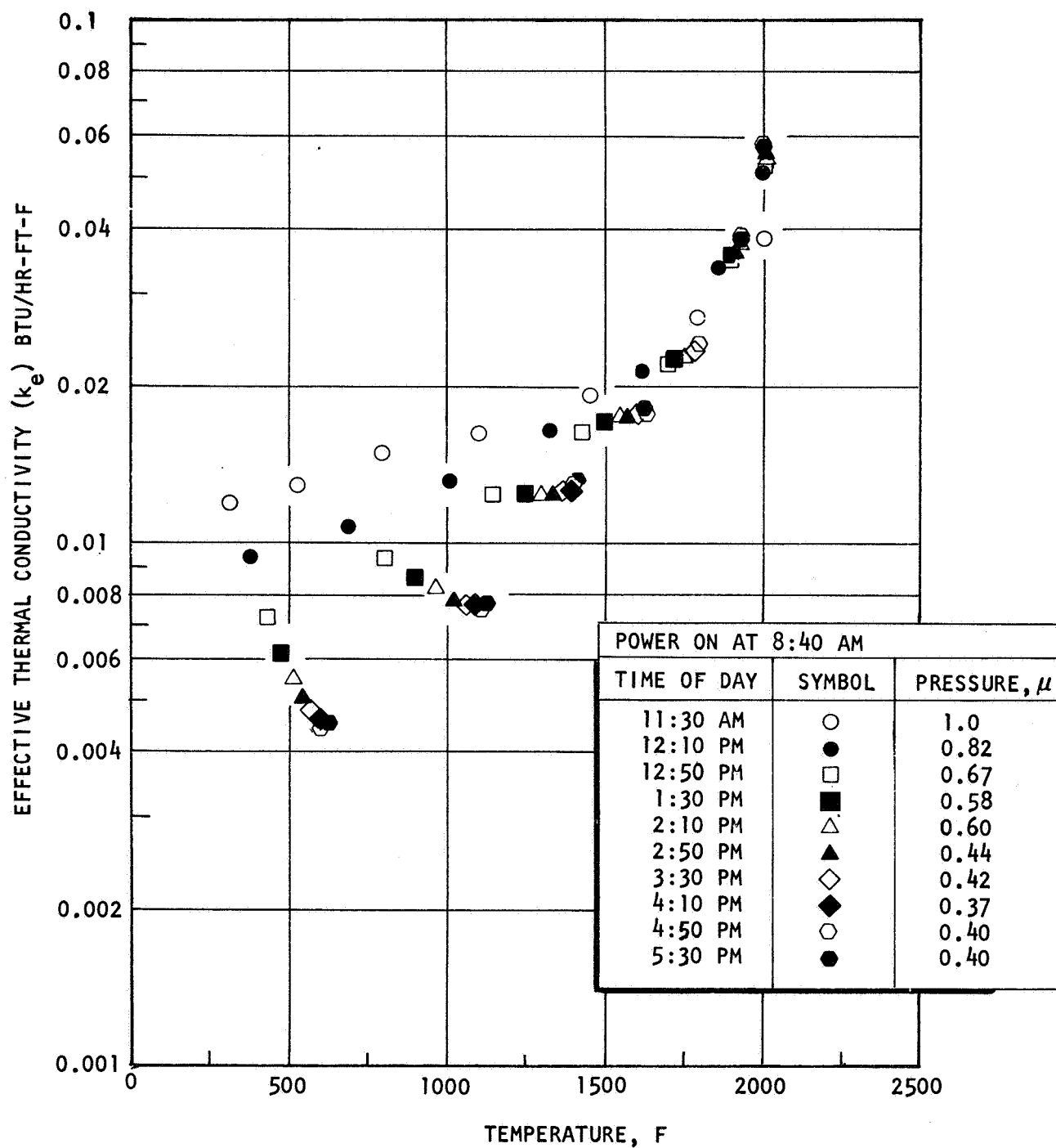


Figure 20. Effective Thermal Conductivity as a Function of Temperature and Time (First Heating Cycle), 7 February 1968, Molybdenum/Silica Number 5

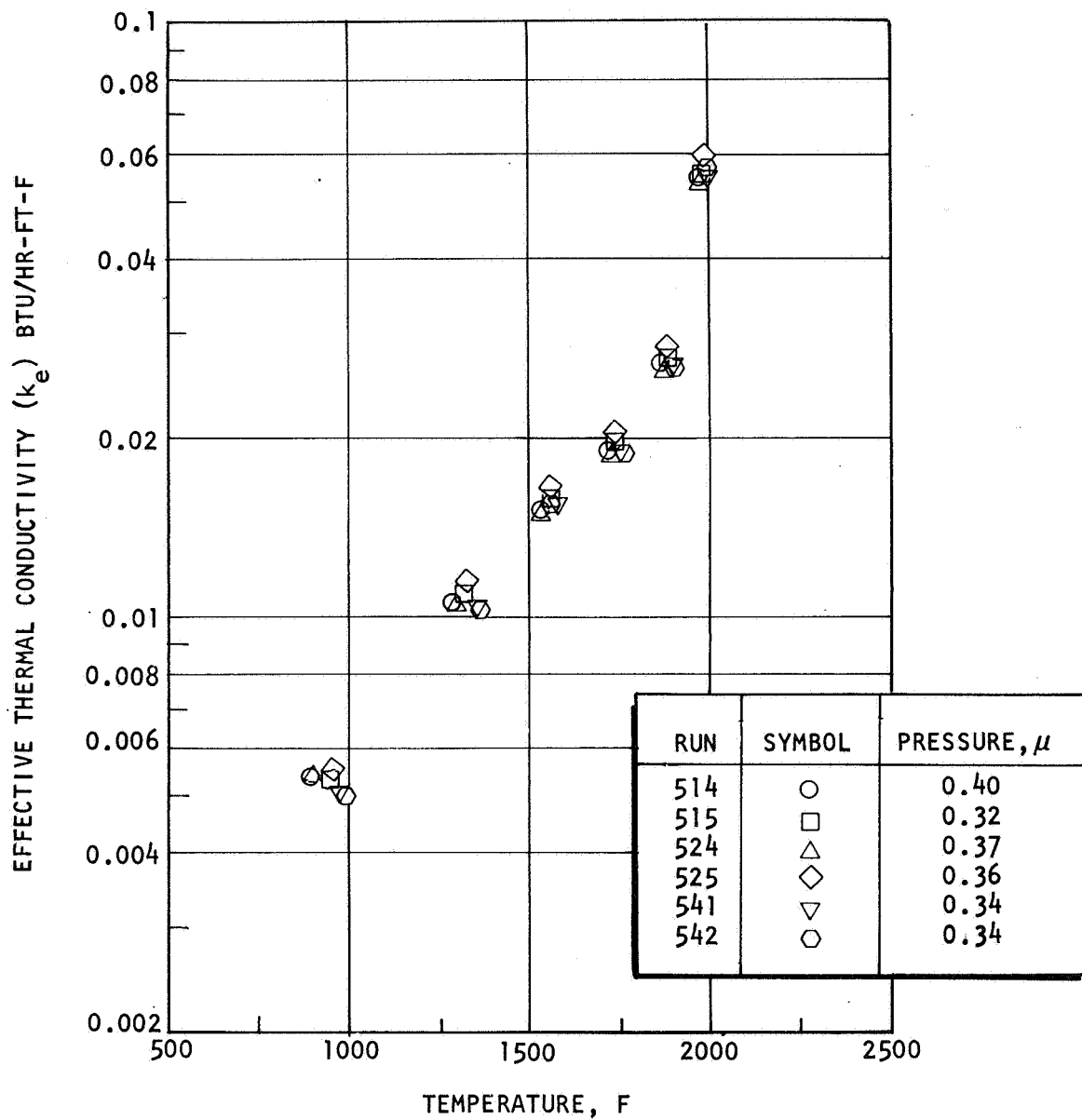


Figure 21. Effective Thermal Conductivity, 7, 9, and 12 February 1967, Molybdenum/Silica Number 5 (Steady State)

Transient data which were taken also in the second and third heating cycles show limited spread with time. In the third heating cycle, the larger power supply was used, and transient temperature data were taken at 10- and 40-minute intervals. Little difference in results is revealed by the two data sets except that small temperature differences at the low temperature range in the 10-minute interval result in much more data scatter, as would be expected.

#### Molybdenum/Silica No. 6

The spacer-to-foil thickness ratio was increased by a factor of three over the preceding test sections by wrapping three layers of cloth per layer of foil. Steady-state values of  $k_e$  obtained at the end of two heating cycles are presented in Fig. 22 for low gas pressure conditions. These values are approximately 35 percent higher than the corresponding values for multilayer molybdenum/silica test sections having one layer of cloth per layer of foil. Transient  $k_e$  values obtained from the two heating cycles also have correspondingly higher values.

#### Molybdenum/Silica No. 7

This test section was a duplicate of No. 6. Both the steady-state  $k_e$  values and transient  $k_e$  values are essentially identical to corresponding values for test section molybdenum/silica No. 6.

#### Molybdenum/Silica No. 8

The length of this test section was 10 inches compared to the 16 inch length of all previous test sections. Because 8-inch-long calorimeters were used for all test sections, No. 8 had only 1 inch of edge insulation compared to 4 inches for the others. Therefore, test section No. 8 could be expected to have larger end effects. The transient results of the second heating cycle (Fig. 23 ) agree well with the preponderance of the previous data. Steady-state results shown in Fig. 24 are 10 percent high

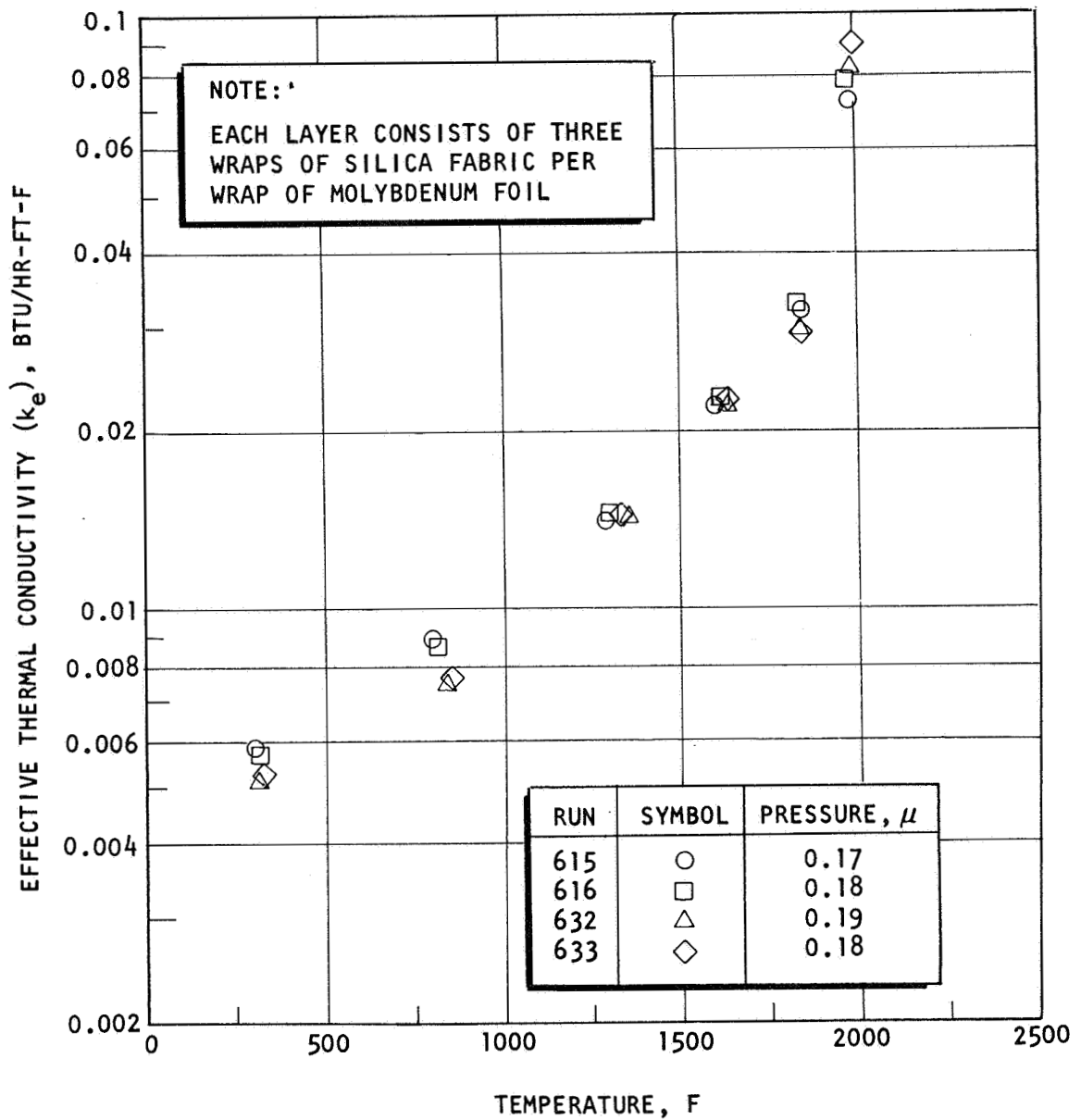


Figure 22. Effective Thermal Conductivity, 15 to 16 September 1968, Molybdenum/Silica Number 6 (Steady State)

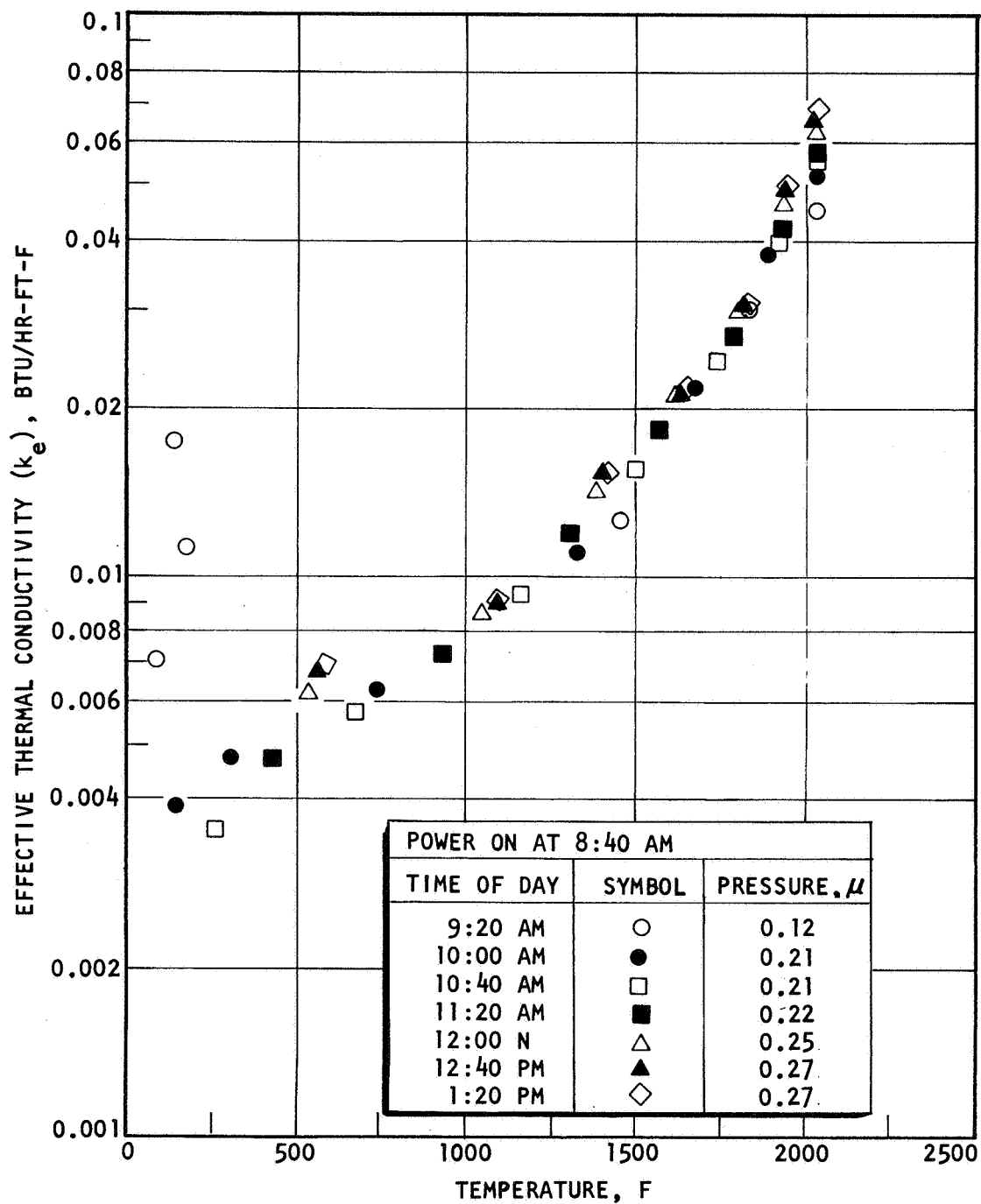


Figure 23. Effective Thermal Conductivity as a Function of Temperature and Time (Second Heating Cycle), 15 March 1968, Molybdenum/Silica Number 8

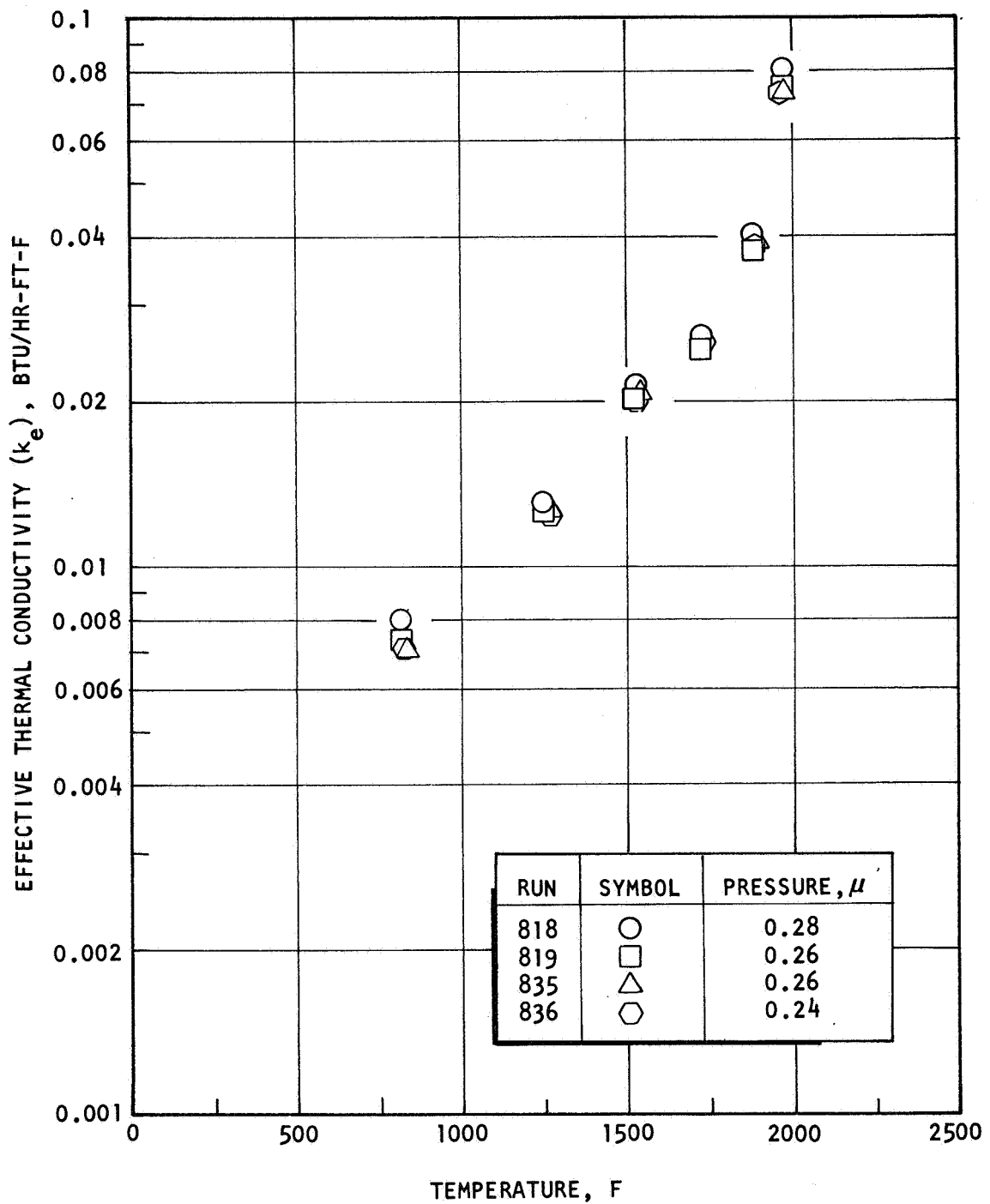


Figure 24. Effective Thermal Conductivity, 13 and 15 March 1968, Molybdenum/Silica Number 8 (Steady State)

throughout the temperature range. Because of this generally good agreement, test section length is not considered to be significant in affecting  $k_e$  values.

#### Tantalum/Carbon No. 1

Transient effective thermal conductivity values are shown in Fig. 25 and 26 for the first (low temperature) and second (high temperature) heating cycles. The results from the first heating cycle are slightly lower (10 percent) than results at corresponding temperature from the second heating cycle. The transient effect upon  $k_e$  has the same trend as with molybdenum/silica, namely a decrease in  $k_e$  with time. The latter time transient results of Fig. 25 agree very well with the steady-state results of Fig. 27.

#### Tantalum/Carbon No. 2

This test section was a duplicate of tantalum/carbon No. 1; both transient and steady-state results were identical to those reported for tantalum/carbon No. 1. No detailed  $k_e$  values are presented for this test section. However, it is interesting to note that a set of temperature decay curves presented in Fig. 28 for this test section match in concept hypothesized decay curves in the fifth quarterly report (Ref. 3 ).

#### Tantalum/Carbon No. 3

This test section also duplicated tantalum/carbon No. 1 for the purpose of providing additional data on this important materials systems. As with the second test section, a very close match of transient and steady-state results was obtained in comparison to the results of tantalum/carbon No. 1. For the sake of brevity, these data will not be presented in detail; though, best curve fits of all steady-state data are presented for a later comparison.



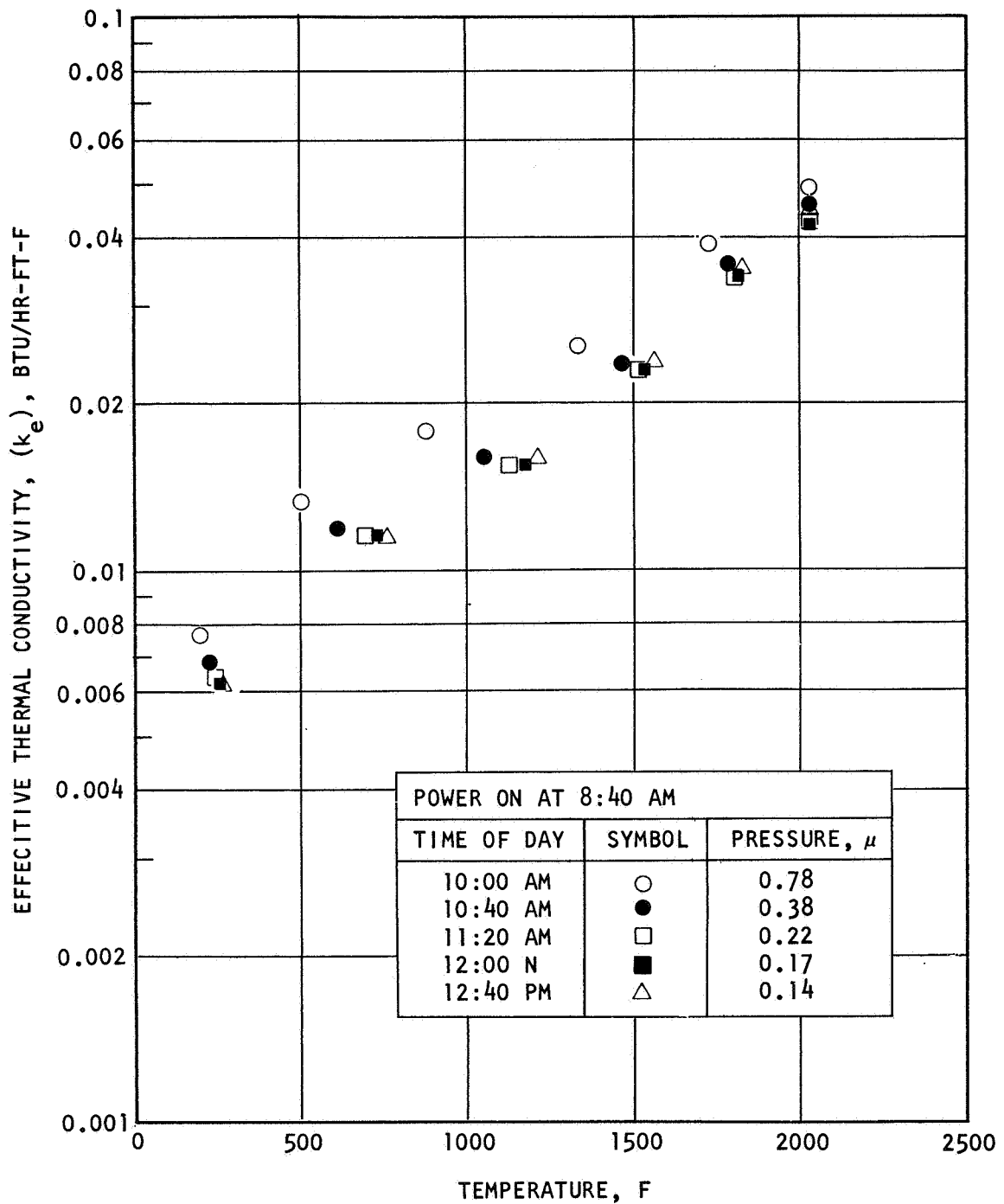


Figure 25. Effective Thermal Conductivity as a Function of Temperature and Time (First Heating Cycle), 21 March 1968, Tantalum/Carbon Number 1

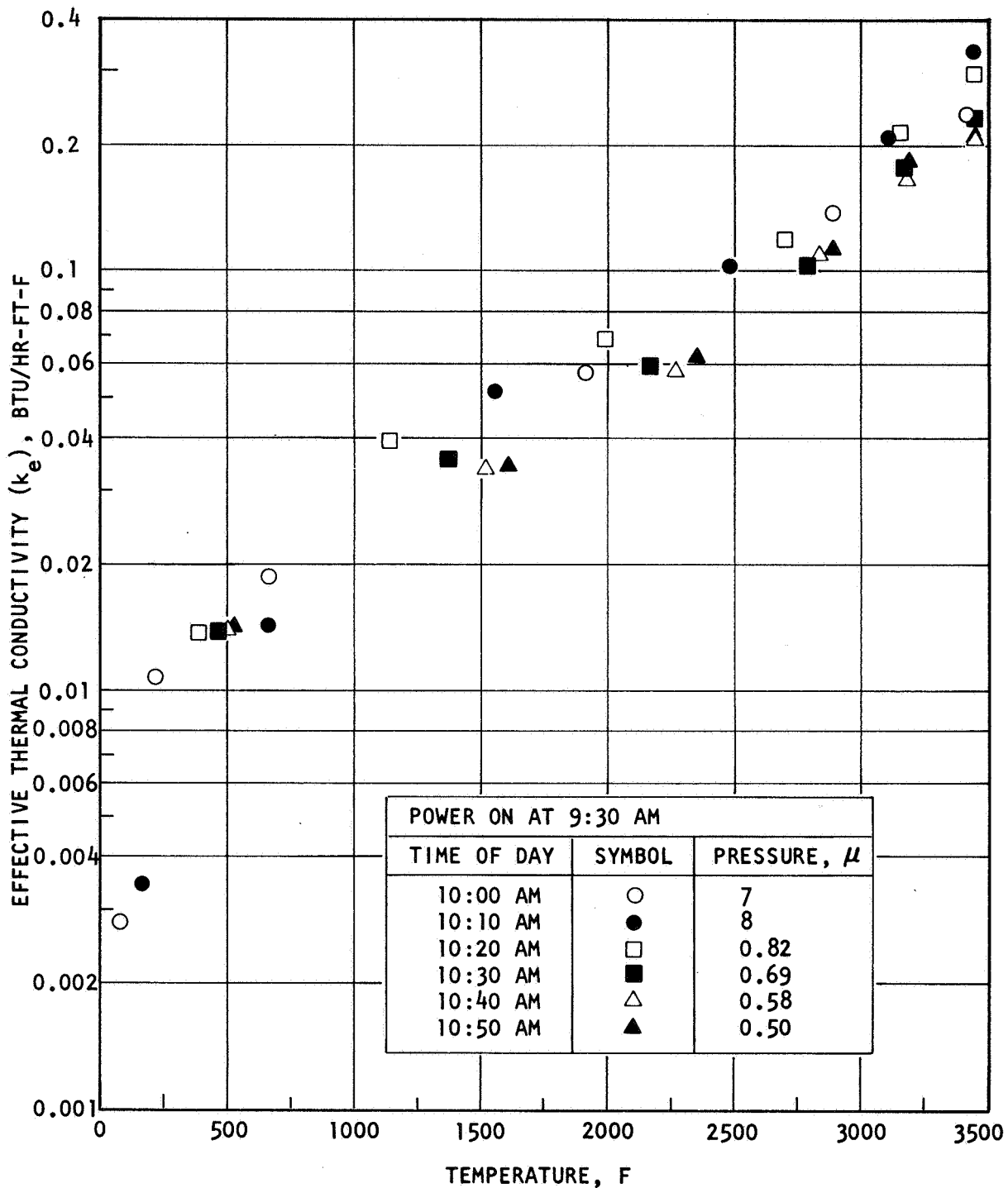


Figure 26. Effective Thermal Conductivity as a Function of Temperature and Time (Second Heating Cycle), 22 March 1968, Tantalum/Carbon Number 1

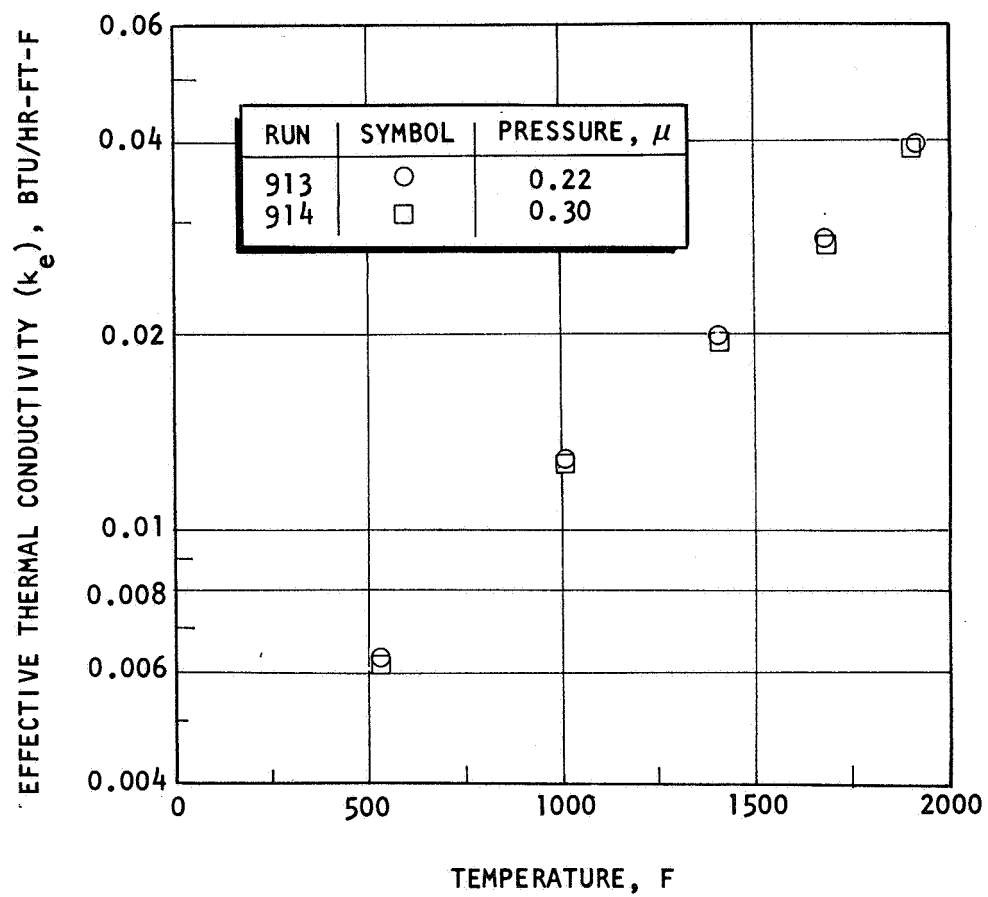


Figure 27. Effective Thermal Conductivity, 21 March 1968, Tantalum/Carbon No. 1 (Steady State)

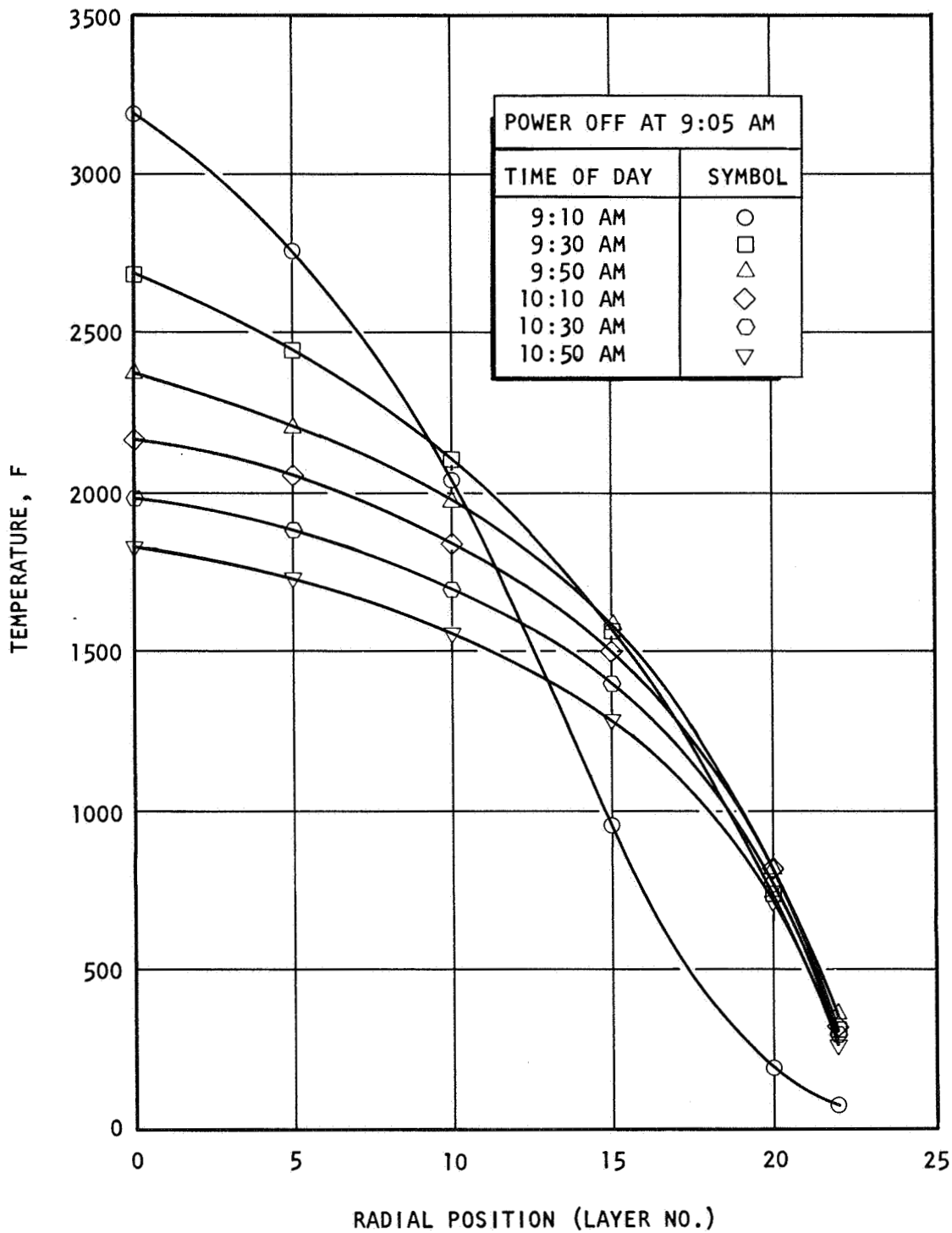


Figure 28. Midplane Temperature Decay, Tantalum/Carbon No. 2,  
8 April 1968

Argon pressurization tests at ~1, 400, 800, and 1600 $\mu$  were performed with this test section at a maximum temperature of 2000 F. The results of these tests are shown in Fig. 29. A regular increase in  $k_e$  with increasing pressure is noted over the temperature range just as occurred with the molybdenum/silica test sections (Fig. 15). Though the values are somewhat displaced in absolute magnitude because of different materials, comparison of Fig. 15 and 29 indicates that the magnitude of the effect of gas pressure is equivalent for both material systems.

#### Carbon No. 1

An extreme case of a high spacer-to-foil thickness ratio, i.e., no foil, was imposed, to determine the total contribution of tantalum in establishing the insulation effectiveness of the tantalum/carbon material system. Transient  $k_e$  values, showing very little time dependence, are presented in Fig. 30 and 31 for a low- and high-temperature heating cycle. The match between the curves is excellent except for a single group of data in each figure representative of a single common measurement station. The carbon test section  $k_e$  values are approximately 50 percent higher than the tantalum/carbon values at low temperature (500 F) but approach within 5 percent at high temperature (3500 F).

#### Tungsten/Zirconia No. 1

A low- and high-temperature heating cycle were imposed upon this test section. The transient effective thermal conductivity values for these two heating cycles are presented in Fig. 32 and 33. It is apparent in comparing the two sets of results that a gross change in  $k_e$  occurred between the two heating cycles. Upon disassembly of this test section, it was observed that gross sintering had occurred to form a weak crusty structure throughout the insulation. Before the second heating cycle, this test section had been subjected to vibration from the forepumps for approximately 120 hours at a frequency of about 5 cycles per second. Gross segregation of the tungsten was noted as reported in a subsequent section of this report.

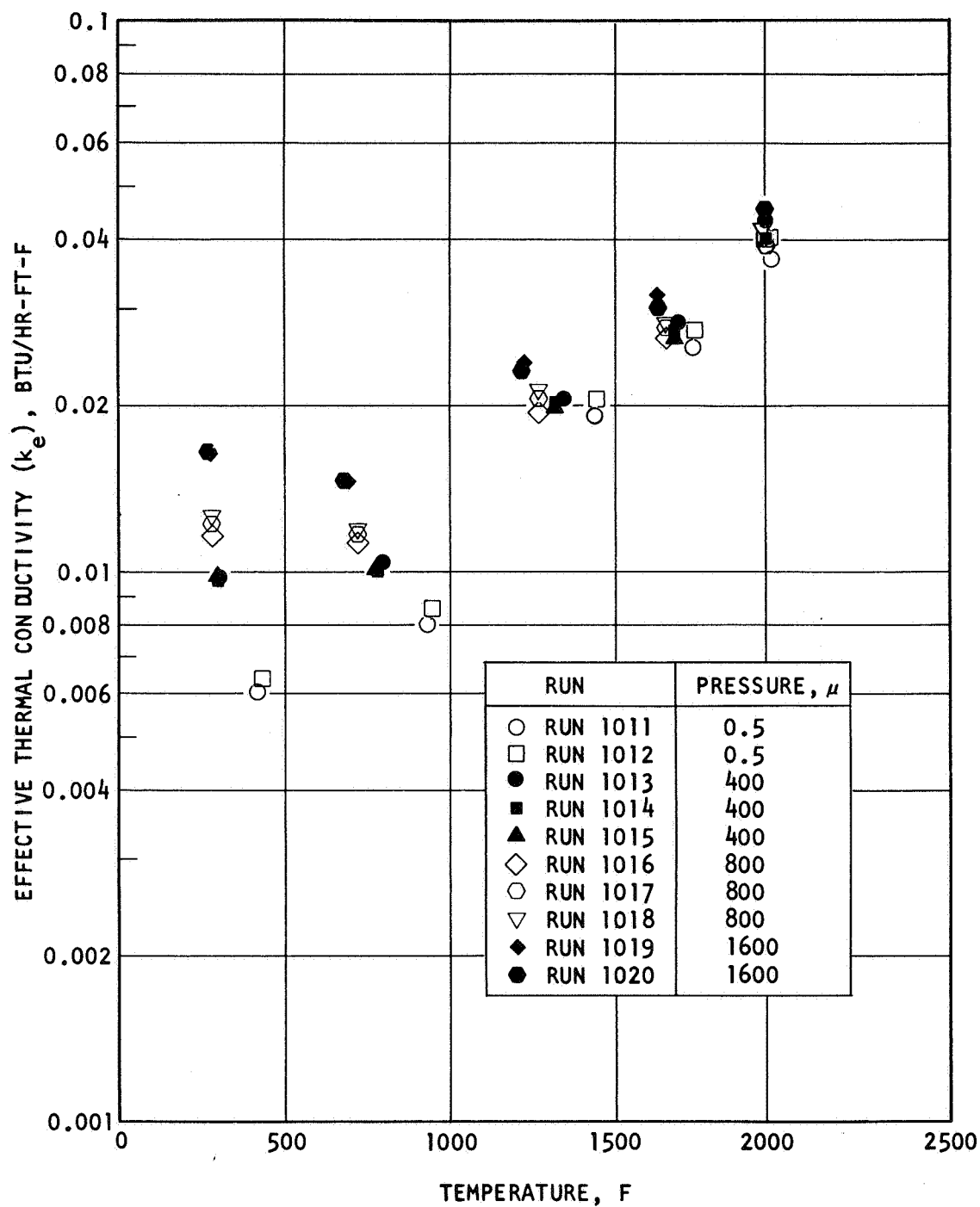


Figure 29. Variation of Effective Thermal Conductivity With Argon Pressure, 17 April 1968, Tantalum/Carbon Number 3 (Steady State)

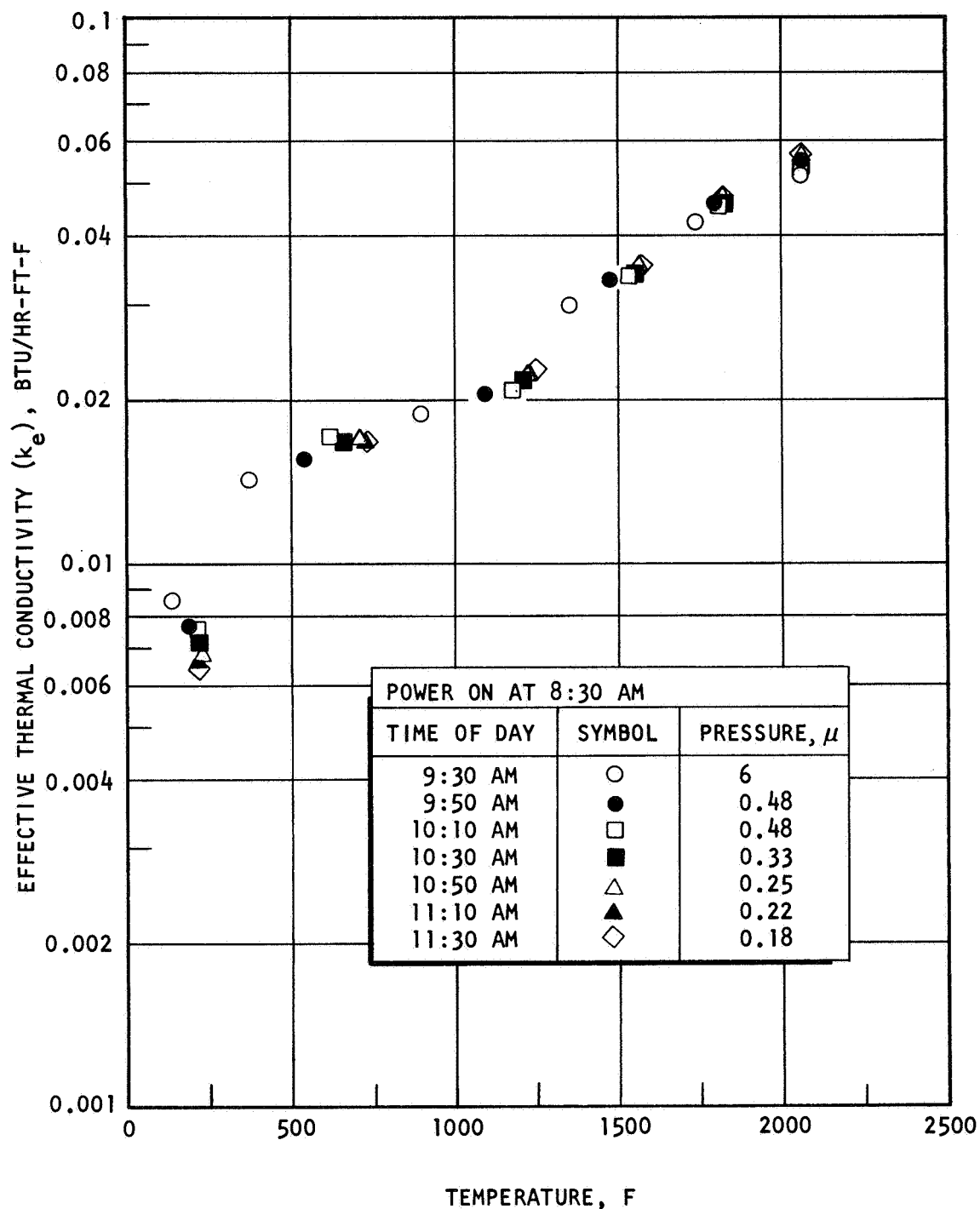


Figure 30. Effective Thermal Conductivity as a Function of Temperature and Time (First Heating Cycle), 26 April 1968, Carbon Number 1

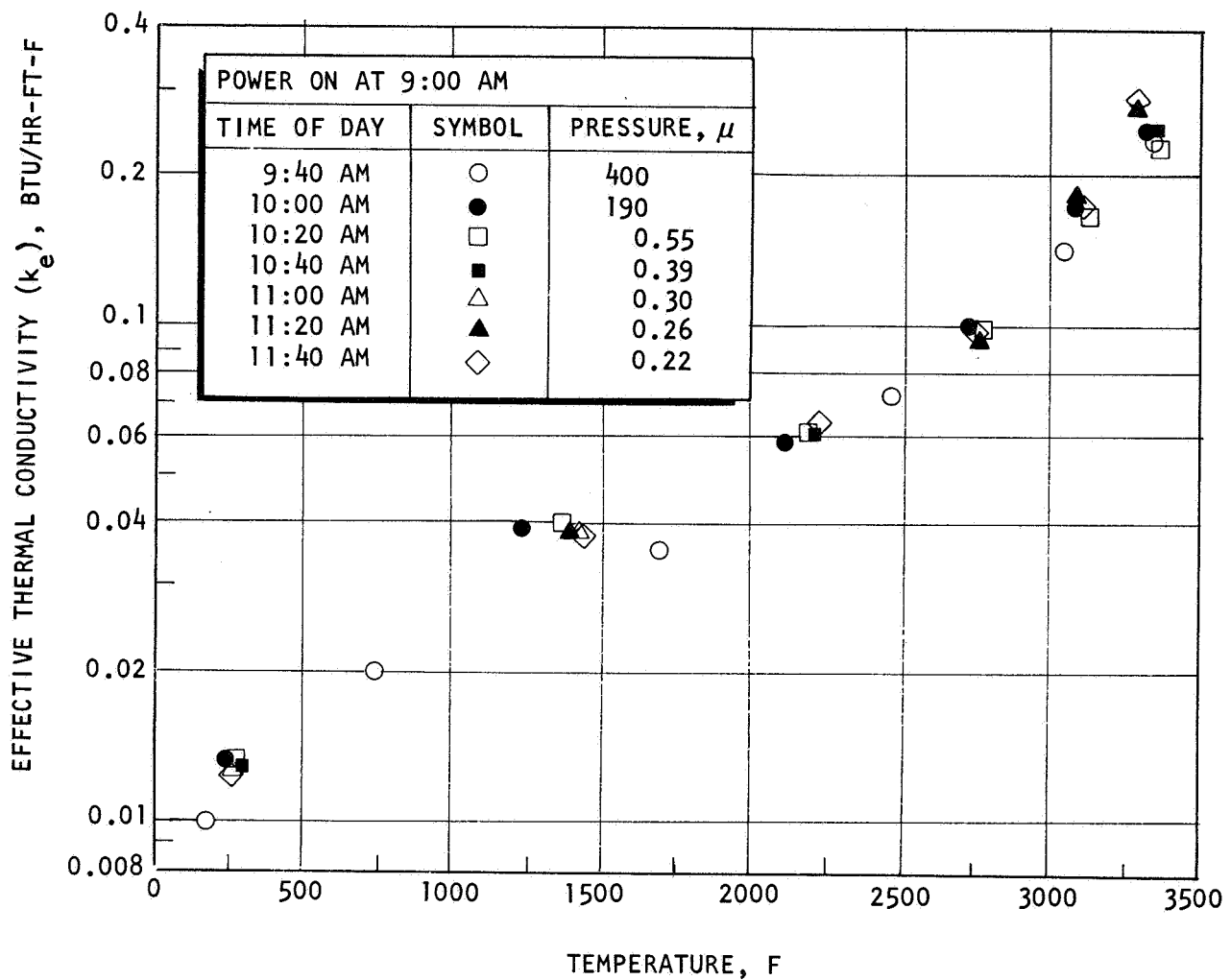


Figure 31. Effective Thermal Conductivity as a Function of Temperature and Time (Second Heating Cycle), 29 April 1968, Carbon No. 1



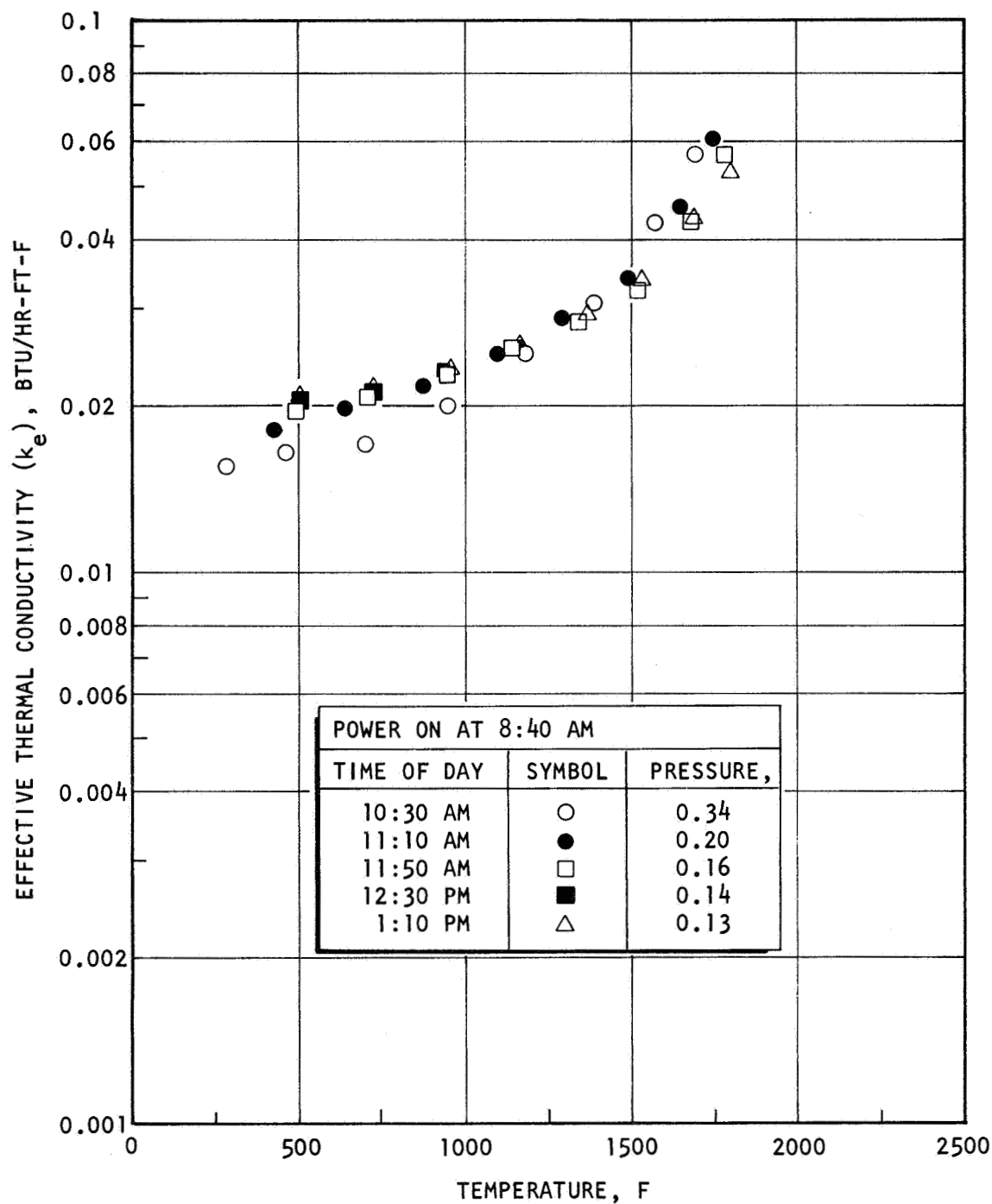


Figure 32. Effective Thermal Conductivity as a Function of Temperature and Time (First Heating Cycle), 16 May 1968, Tungsten/Zirconia Number 1

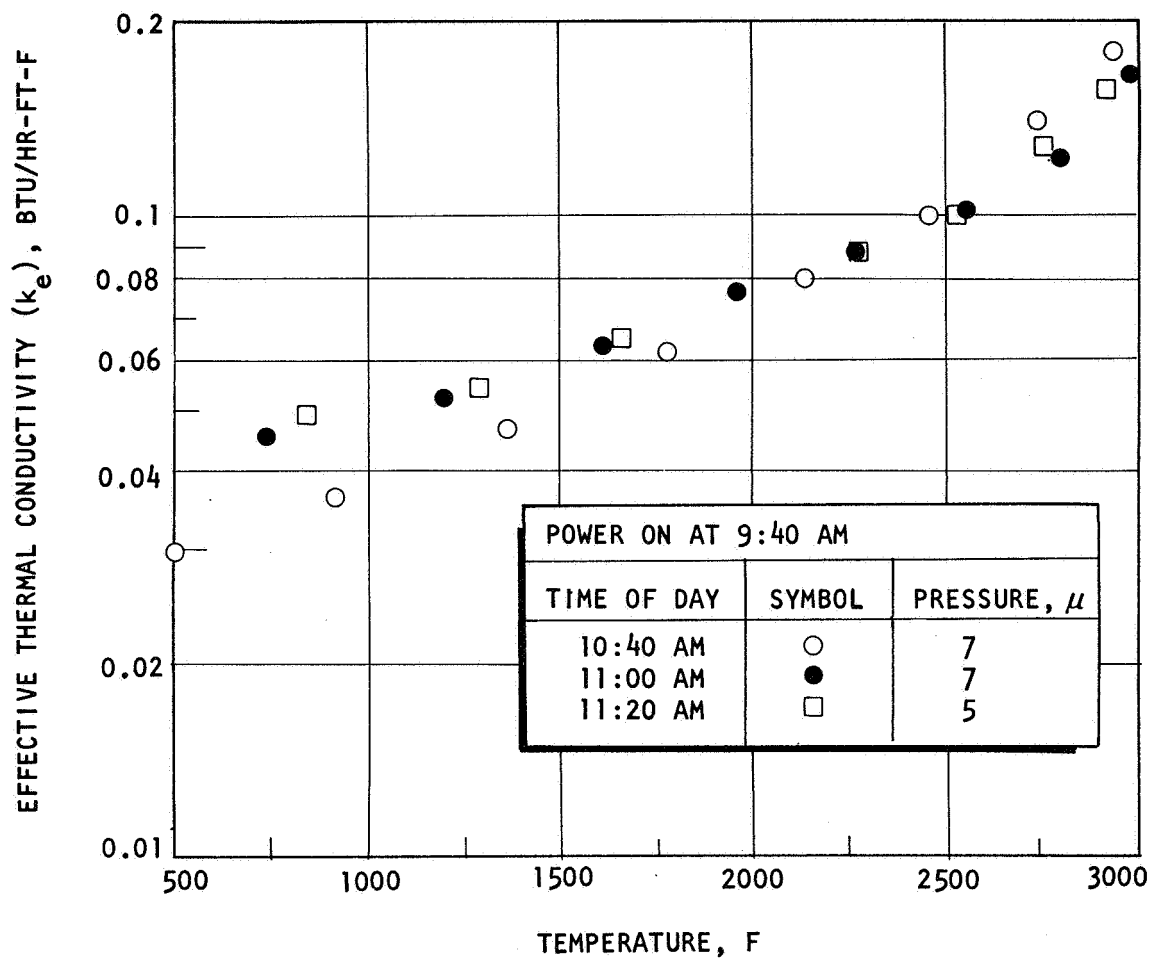


Figure 33. Effective Thermal Conductivity as a Function of Temperature and Time (Second Heating Cycle), 20 May 1968, Tungsten/Zirconia No. 1

#### Tungsten/Zirconia No. 2

The weight percentage of tungsten was decreased from 10 percent in the first test section to 2 percent in the second one. Again, low- and high-temperature heating cycles were imposed. The  $k_e$  values obtained are presented in Fig. 34 and 35. The low-temperature heating cycle values of Fig. 34 appear roughly equivalent to those of Fig. 32 of the previous test section. However, a significant change in magnitude of  $k_e$  is apparent in the high-temperature heating cycle values depicted in Fig. 35 compared to Fig. 33. By decreasing the tungsten content, the low-temperature values of  $k_e$  increased by as much as 50 percent and the high-temperature values increased by approximately 20 percent.

#### Molybdenum/Silica No. 9 (Planar)

This test section was constructed and tested to determine the effect of mechanical loading pressure upon the effective thermal conductivity. Three sets of steady-state runs were conducted at loading pressures of 0.05, 0.5, and 1.8 psi. The values of thermal conductivity at the two highest loading pressures were ratioed to the value at the lowest loading pressure. The ratios are presented as a function of temperature in Fig. 36, where higher loading pressure results in higher values of  $k_e$ .

The increase in conductivity with pressure is due to compression of the materials and reduced contact resistance; the increase with temperature might be due to increased sintering of fibers. It is recommended that the steady-state thermal conductivity derived from the cylindrical test sections be used as the base values.

#### Tantalum/Carbon No. 4 (Planar)

The effect of loading pressure was studied with this materials system by conducting three sets of steady-state tests at the loading pressures of 0.05, 0.5, and 1.8 psi. Temperatures were limited so that thermocouple

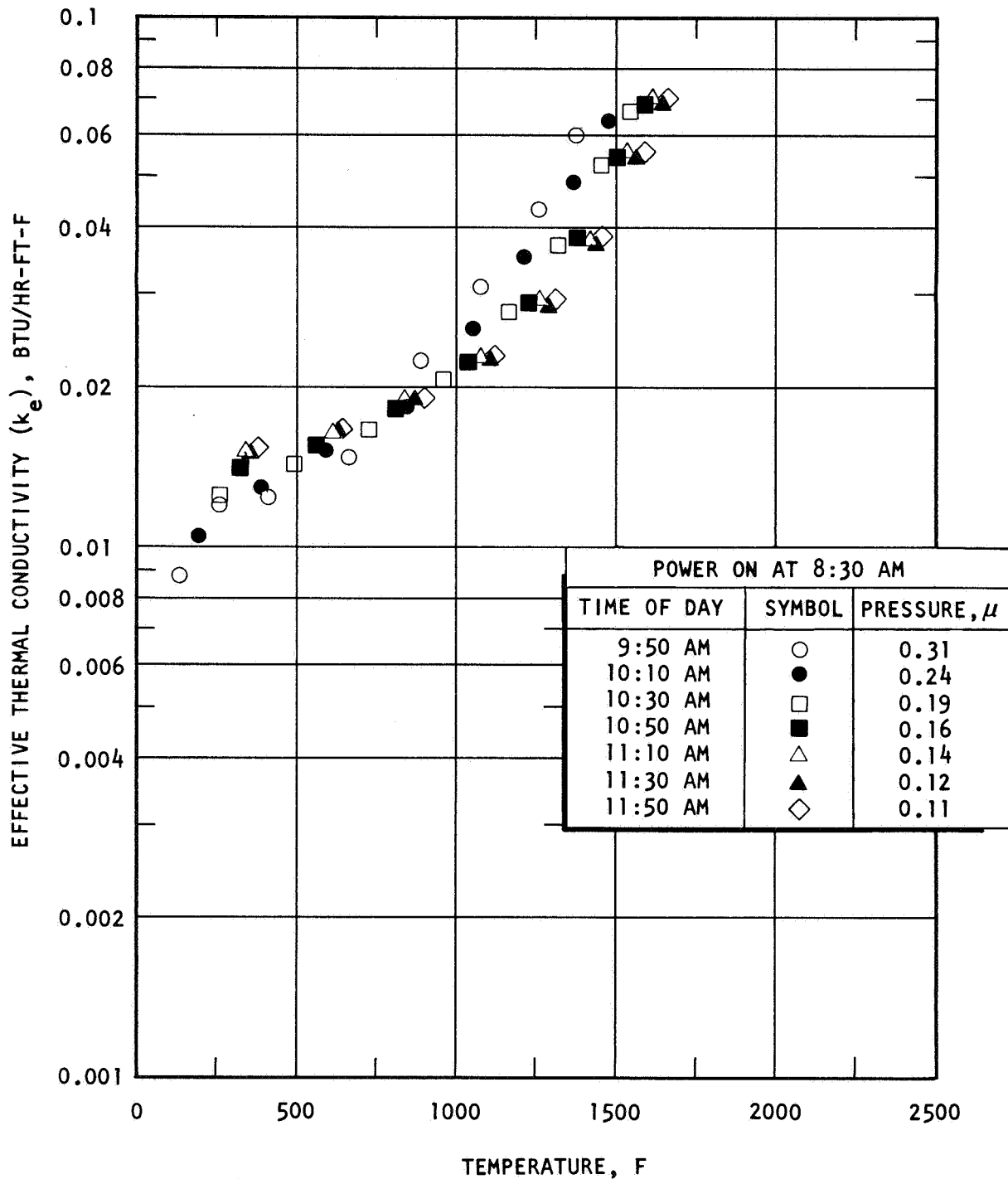


Figure 34. Effective Thermal Conductivity as a Function of Temperature and Time (First Heating Cycle), 28 May 1968, Tungsten/Zirconia Number 2

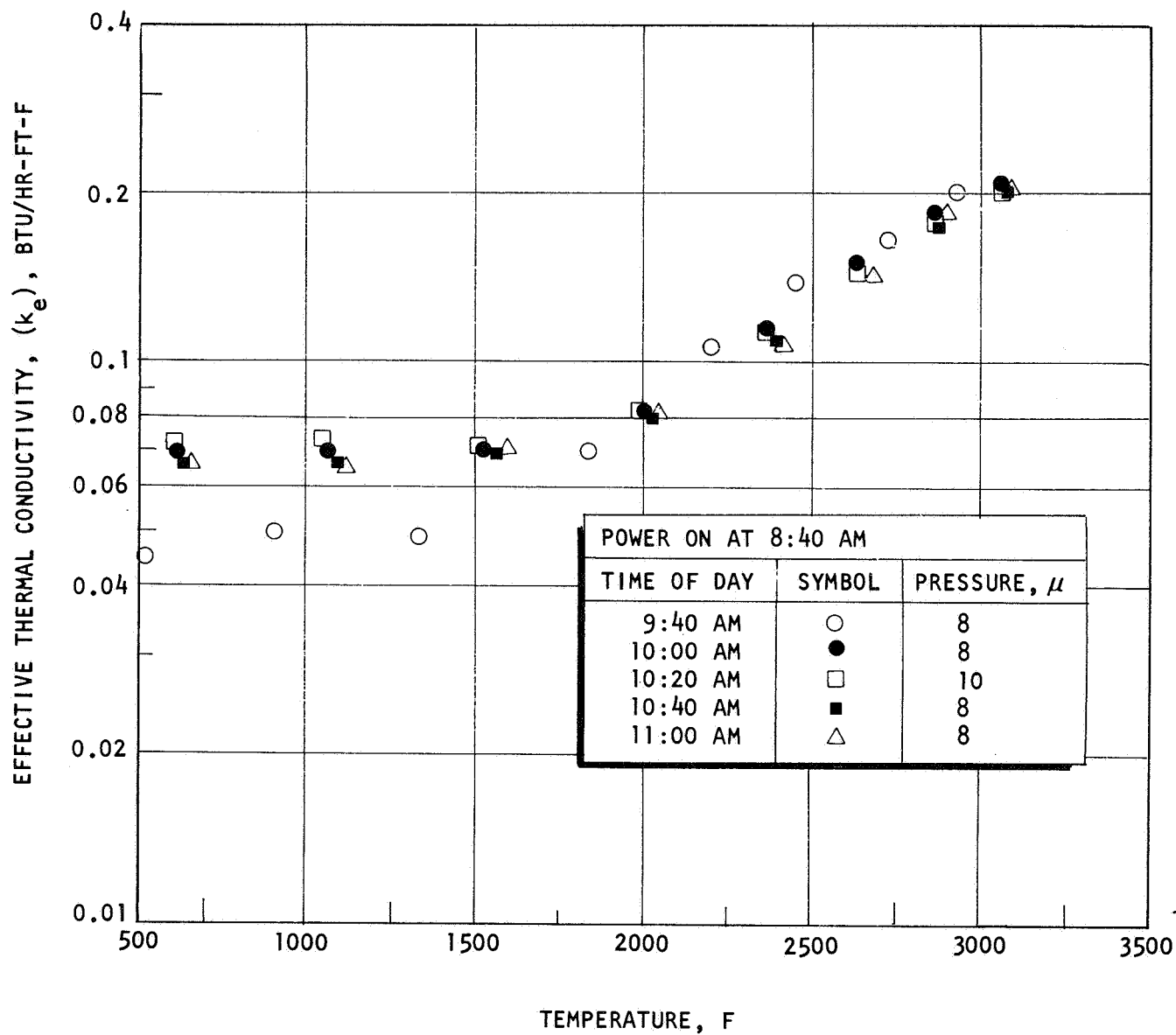


Figure 35. Effective Thermal Conductivity as a Function of Temperature and Time (Second Heating Cycle), 3 June 1968, Tungsten/Zirconia Number 2

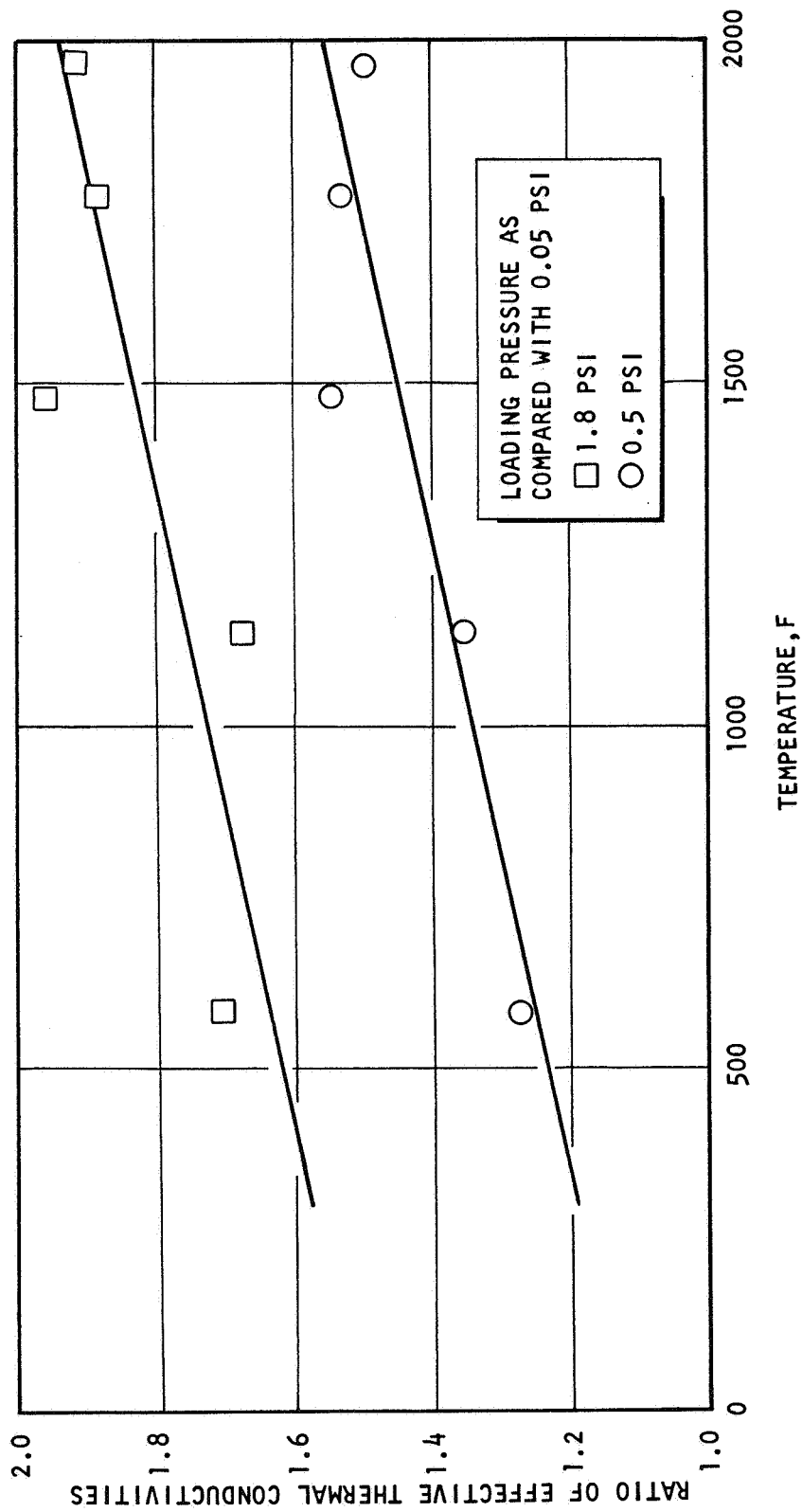


Figure 36. Molybdenum/Silica No. 9 (Planar) 13, 17, and 18 June 1968, Ratio of Effective Thermal Conductivity as a Function of Temperature and Loading Pressure

accuracy would not be affected by temperature-induced degradation. The results are presented in Fig. 37 as ratios of effective thermal conductivity based upon the value obtained at the lowest (0.05 psi) loading pressure. The data of Fig. 37 indicate a decreasing dependence of the ratio of conductivities with increasing temperature. Thus, the apparent asymptotic approach of the ratio toward unity was fortuitous in that higher temperature data were not necessary.

The noted increase in the conductivity ratio with pressure follows the trend exhibited by molybdenum/silica. However, the decrease with temperature is not adequately explained by lack of sintering. A possible explanation might be a decrease in the relative effect of lattice conduction with increasing temperature.

#### DATA COMPARISONS

In this section of the report, graphs are presented comparing curve fits of steady-state values of effective thermal conductivities versus temperature for each materials combination. Average curve fits having comparable conditions are superimposed on a single graph for comparison. Finally, the average tantalum/carbon and molybdenum/silica data are compared to a radiation model with respect to the dependence  $k_e$  upon temperature.

##### Molybdenum/Silica

The curve fits of steady-state results from the seven useful test sections are given in Fig. 38. It is apparent that there are two groupings of results. One group comprises test sections 1 through 5 which have the lower spacer-to-foil thickness ratio. The second group comprises test sections 6, 7, and 8. Test sections 6 and 7 had the larger (by a factor of three) spacer-to-foil thickness ratio.

Generally, agreement among comparable data is within  $\pm 10$  percent. The limited steady-state results of test section 8 were previously noted to be higher than extensive transient results, and may therefore be discarded.

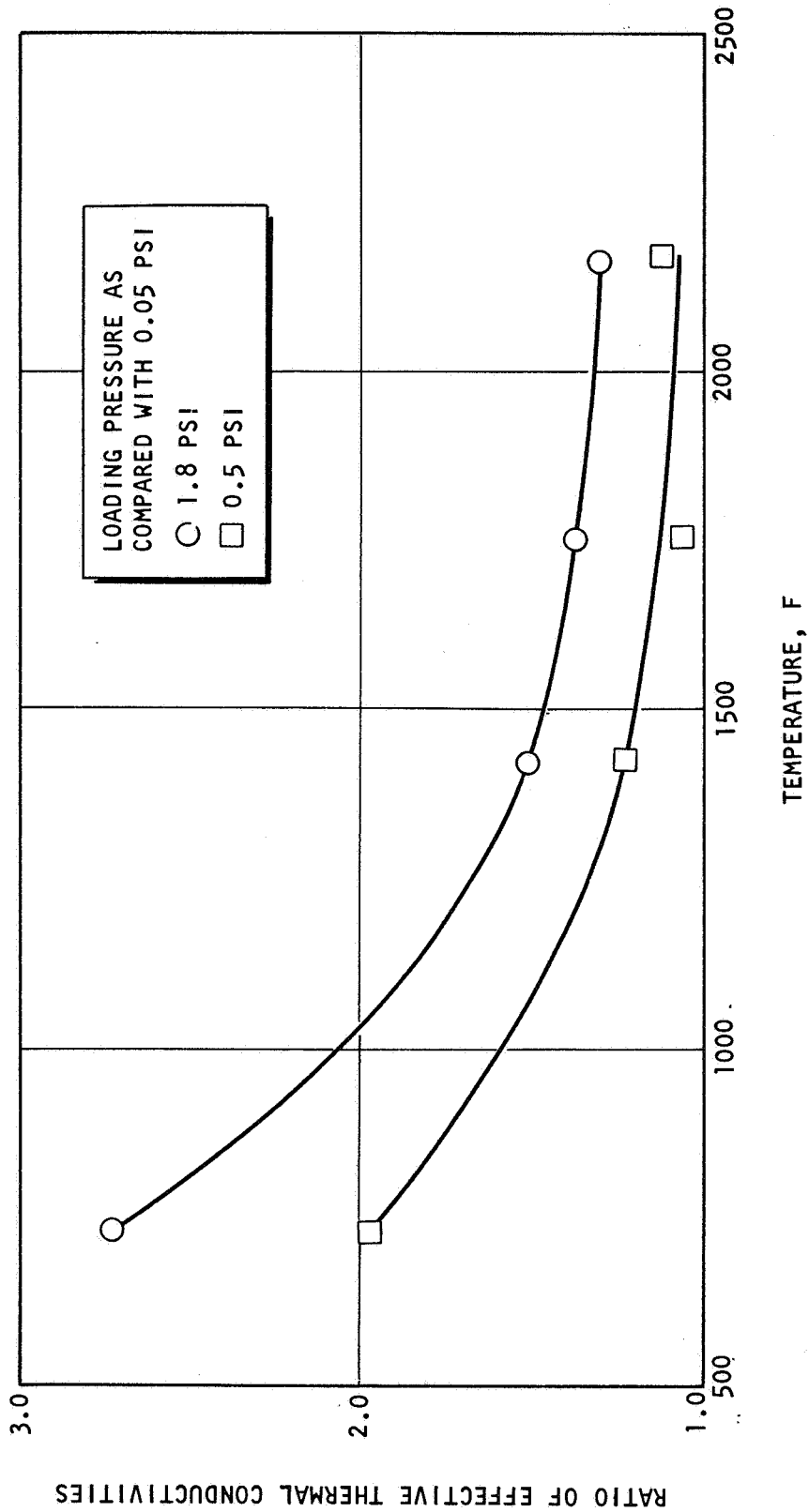


Figure 37. Tantalum/Carbon No. 4 (Planar) 24, 25, and 26 June 1968, Ratio of Effective Thermal Conductivity as a Function of Temperature and Loading Pressure



SYMBOL	TEST SECTION	SPACER TO FOIL THICKNESS RATIO
—————	MOLYBDENUM/SILICA NO. 1	31.6/1
.....	" " NO. 2	33.9/1
-----	" " NO. 3	32.9/1
—————	" " NO. 5	28.4/1
—————	" " NO. 6	85.9/1
—————	" " NO. 7	87.2/1
—————	" " NO. 8	29.2/1

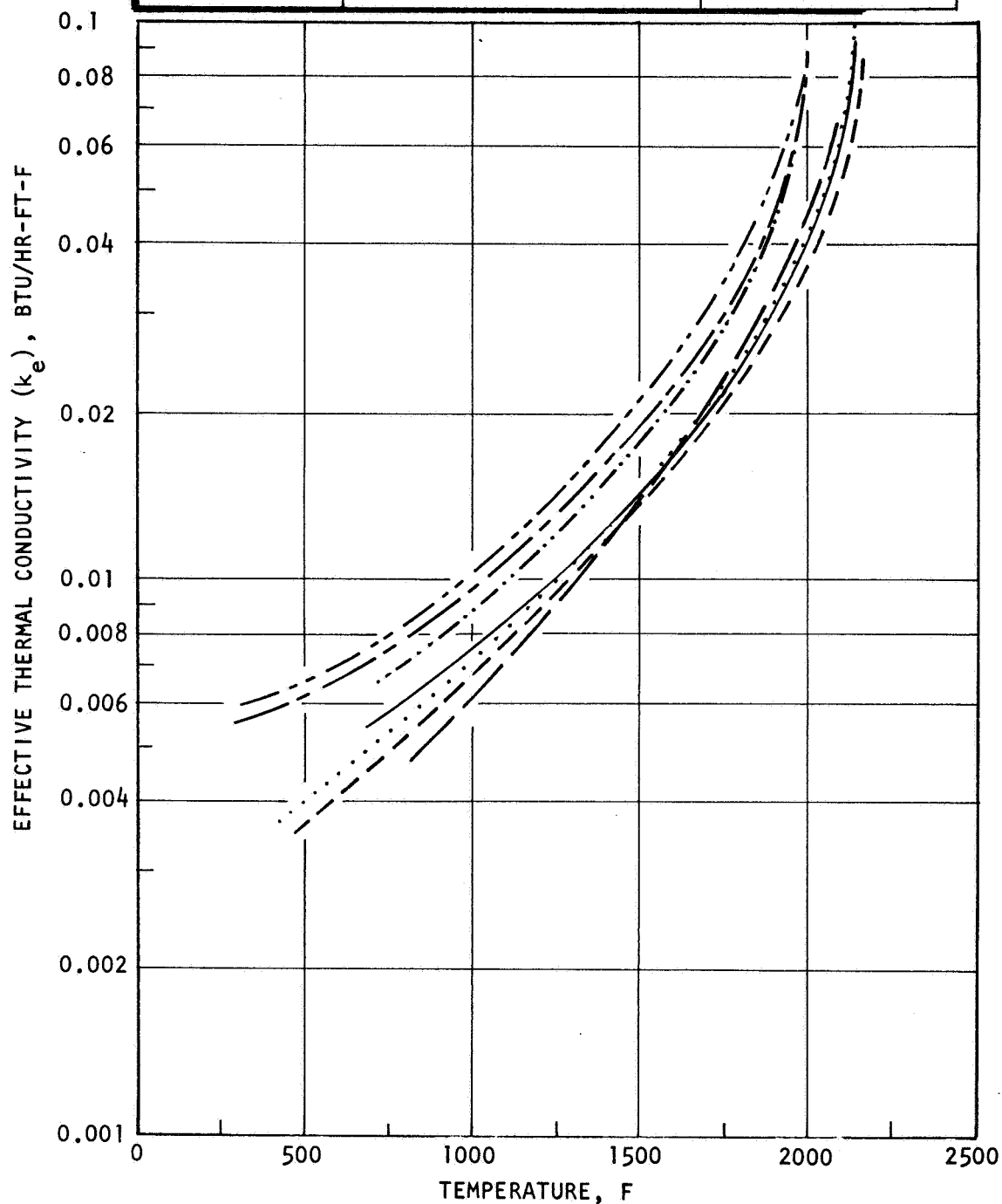


Figure 38. Comparison of Effective Thermal Conductivities of all Cylindrical Molybdenum-Silica Test Sections

The higher conductivity at the higher spacer-to-foil thickness ratio suggests the existence of an optimum in terms of weight and cost in designing an insulation system using these materials.

#### Tantalum/Carbon-Carbon

The curve fits of steady-state results from the three tantalum/carbon and the one carbon test sections are given in Fig. 39. Excellent agreement throughout the entire temperature range is exhibited by the tantalum carbon results. The higher conductivity of the carbon test section also suggests optimization for insulation system design.

#### Tungsten/Zirconia

The curve fits of the higher temperature heating cycles for the two tungsten zirconia test sections are presented in Fig. 40. The results of the lower temperature heating cycle were disregarded because thermal conditioning precluded the initial state of the insulation.

#### Cross Comparison of Material Systems

Averaged curve fits are presented in Fig. 41 for the molybdenum/silica multilayer insulation system at two spacer-to-foil thickness ratios (32/1 and 90/1), for the tantalum/carbon multilayer insulation system including the case of no foil, and for the tungsten/zirconia powder insulation system. At temperatures below 2000 F, molybdenum/silica is clearly the superior insulation. Above 2000 F, tantalum/carbon is clearly superior. The tungsten/zirconia insulation system has an order of magnitude higher conductivity than the other materials at the low temperatures but is only slightly higher (30 percent) at the highest temperatures.

#### Comparison of Theory and Experiment

A theoretical analysis (Ref. 2) established that radiation is the dominant heat transfer mode through multilayer insulation systems at the higher

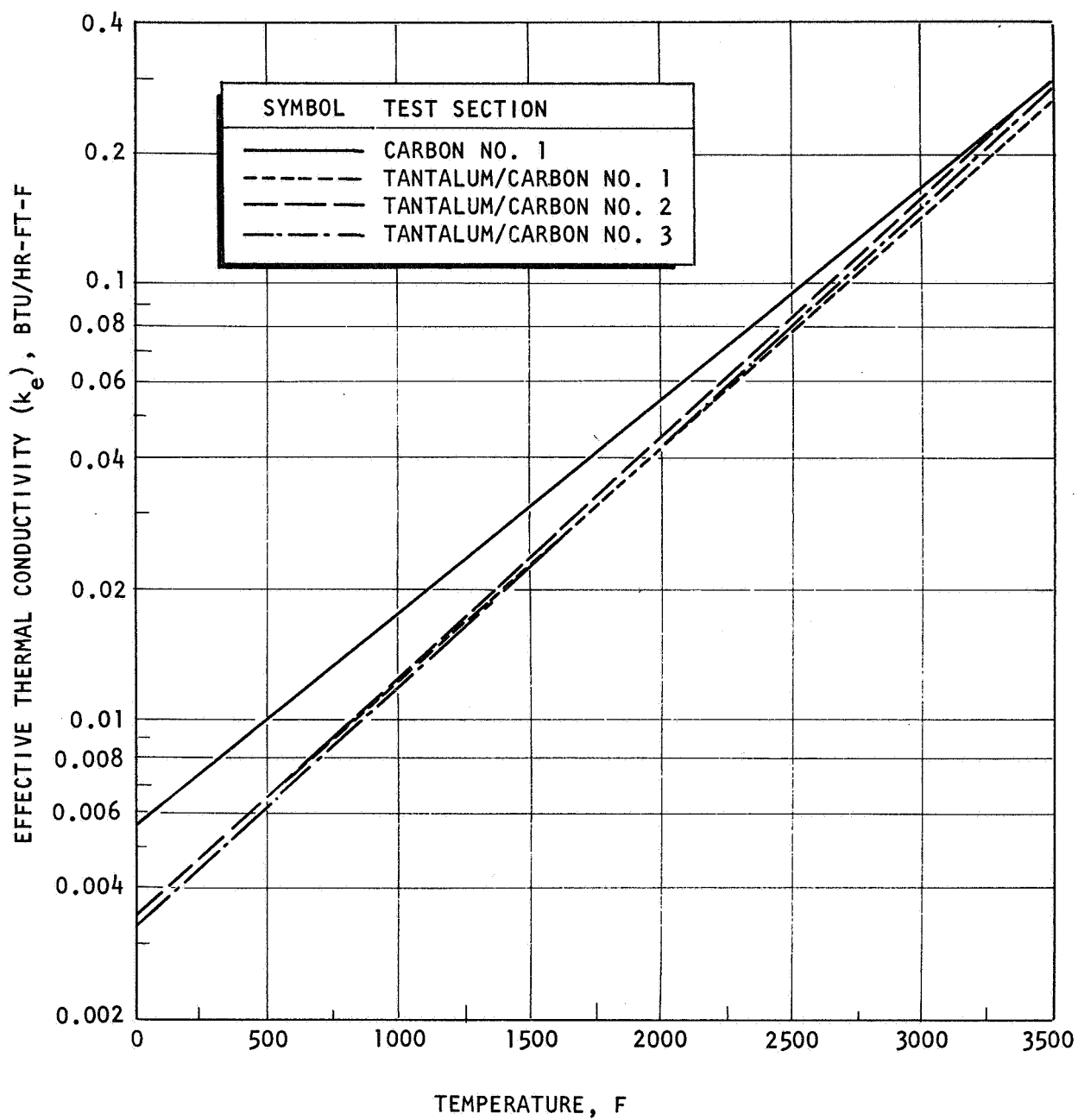


Figure 39. Comparison of Effective Thermal Conductivities of Carbon and Tantalum/Carbon Test Sections

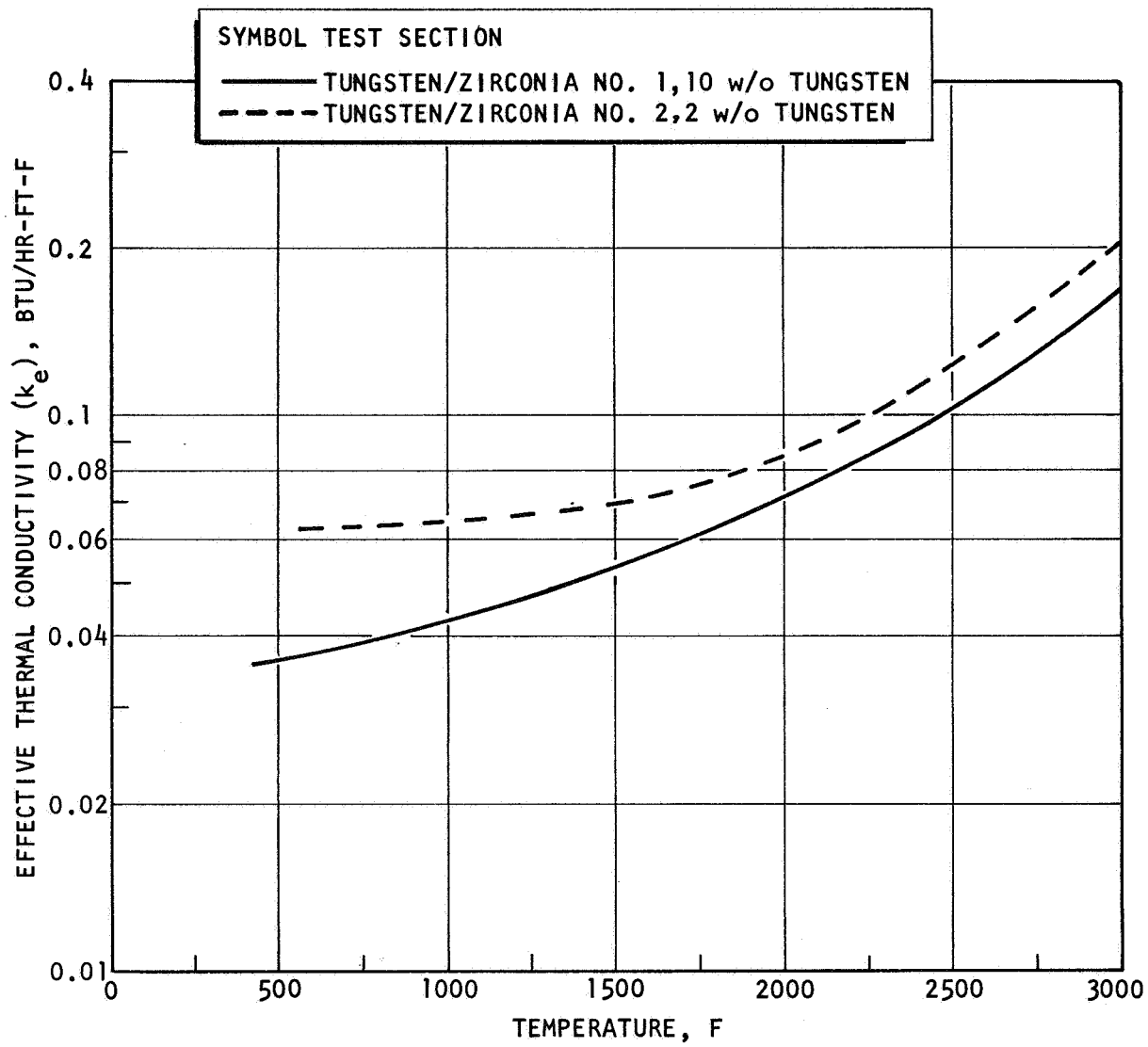


Figure 40. Comparison of Effective Thermal Conductivities of Two Tungsten/Zirconia Test Sections

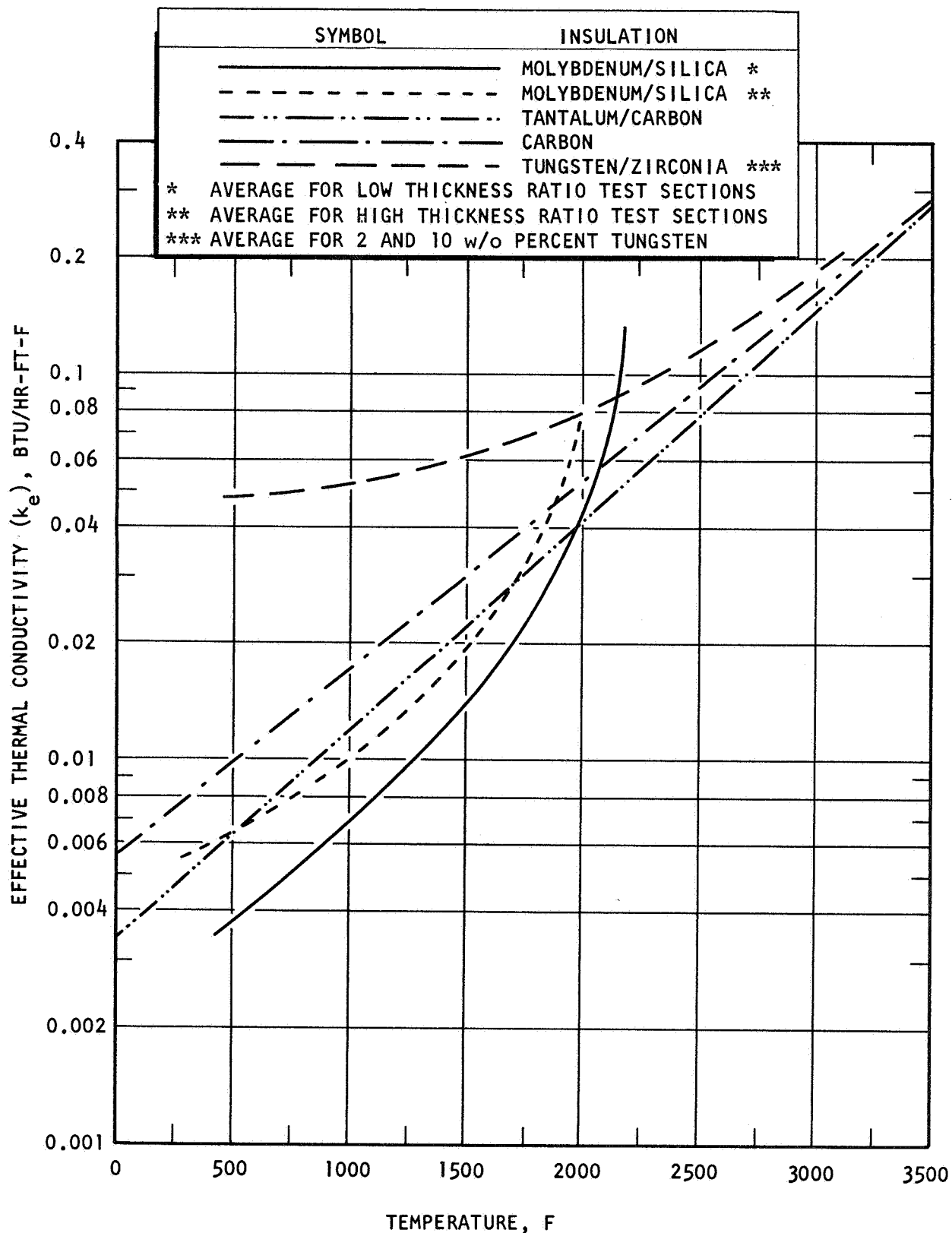


Figure 41. Comparison of Effective Thermal Conductivities of all Material Combinations Studied

temperatures and predicted that the effective thermal conductivity is proportional to the cube of the temperature. The average curve fits of the tantalum/carbon and molybdenum/silica results from Fig. 41 are replotted in Fig. 42 as the logarithm of  $k_e$  versus the logarithm of temperature. A line with a slope of 3 is arbitrarily positioned on Fig. 42 for comparison.

The tantalum/carbon results at the highest temperature seem to establish the predicted slope. However, the molybdenum/silica results have a slope greater than 3 above 1700 F. This is believed to be due to the observed sintering of silica fibers.

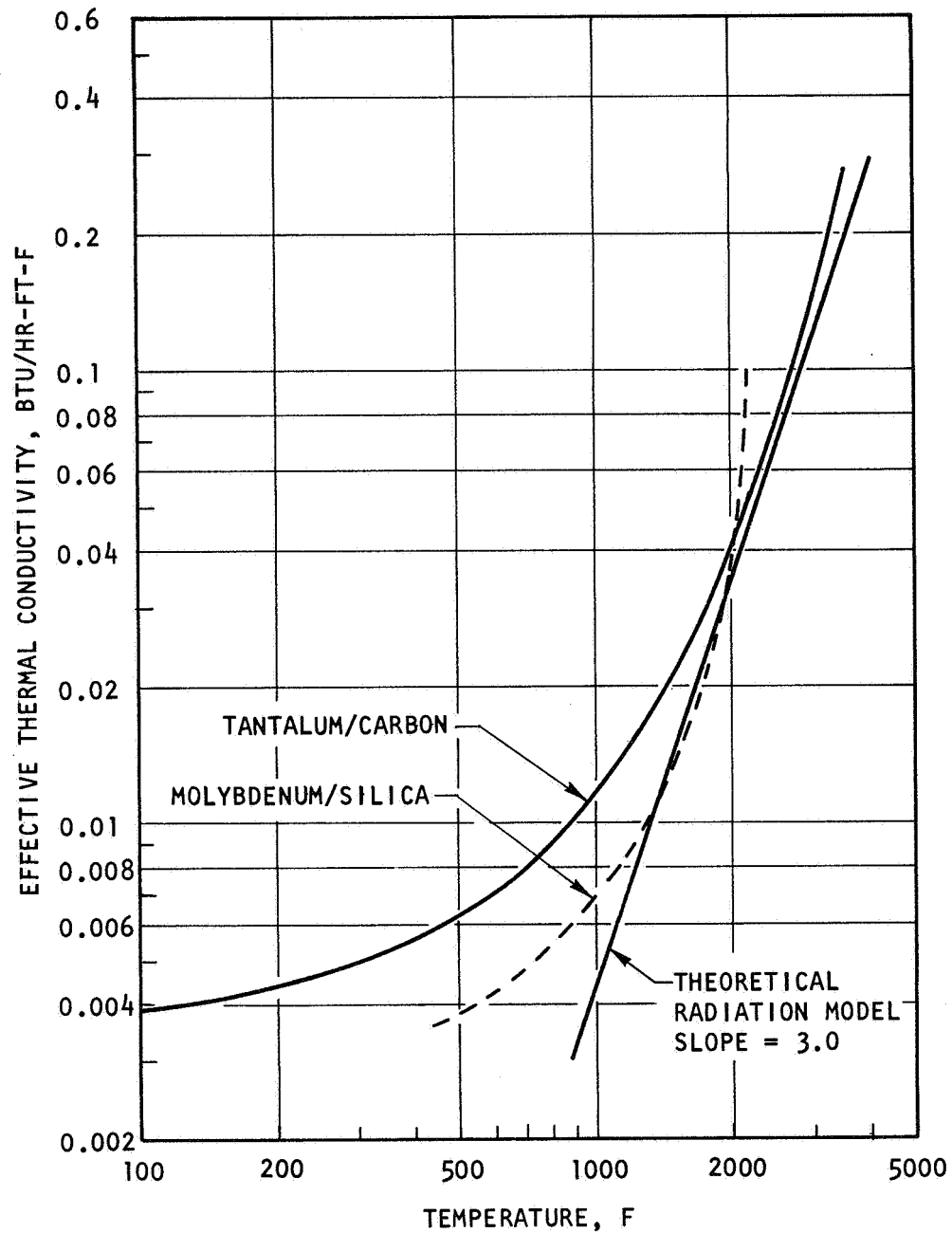


Figure 42. Comparison of Temperature Dependence of Experimental Effective Thermal Conductivity Values With Theoretical Radiation Model

## THERMAL STABILITY AND COMPATIBILITY

Present insulation systems are not totally stable at temperatures associated with buried spacecraft rocket engines. Efficient materials that provide a barrier to heat flow at high temperatures necessarily must have a very low bulk density to minimize solid conduction and a means of scattering radiation. Even though these materials are ordinarily considered to be stable, density and reflectance values can change enough to affect thermal properties under service conditions. Materials with high porosity densify, and contacting particles (grains or fibers) bond due to sintering. Reflective surfaces of metals (foils or particles) tarnish and even roughen by reacting with gases or adjacent solids. As a result, the effective thermal conductivity and thermal diffusivity of the materials system change as the properties change. Thus, the behavior of the materials must be known so that performance can be predicted and improved under various service conditions.

Changes in important properties of the insulation materials systems that affect thermal properties and integrity and hence, reliability were studied under a range of service conditions. Most of the study, however, was concentrated on the most severe combinations of expected service conditions. Changes under less harsh conditions were generally not apparent and were relatively unimportant. Variables that were considered most important were temperature, time, loading pressure, and environmental pressure (vacuum). Small, essentially identical specimens were systematically annealed and studied under selected conditions. Specimens that were used for measurement of thermal properties were not appropriate for thermal stability studies, because test specimens and parameters were not designed for these studies, and test parameters could not be controlled in the required manner.

Another task was to determine the compatibility of the insulation materials systems with potential advanced state-of-the-art thrust chamber materials.



Interaction between insulation and chamber materials can be important from the standpoint of the effect on thrust chamber performance. Surface reaction or surface contamination of a refractory metal thrust chamber could impair its strength, ductility, and thermal fatigue properties. Refractory metals are very sensitive to impurities. An increase of only a few ppm of oxygen, for example, can embrittle molybdenum. For this reason, interaction and interdiffusion between the refractory metal chamber and the insulation materials should be prevented by a diffusion barrier.

Surface effects on superalloys, such as Haynes 25, would be less detrimental to performance of the thrust chamber. A surface reaction on a graphite or carbon thrust chamber would not significantly impair performance. These materials are less sensitive to surface flaws than refractory metals. Moreover, molten eutectic compositions are not likely to form. The lowest melting eutectic temperature in the molybdenum-carbon system is 4000 F, and in the tantalum-carbon system it is 5750 F. Many combinations of refractory materials were tested for compatibility during a previous phase of the program to find a material that would form a good diffusion barrier for any given combination of chamber and insulation material. Compatibility studies this year focused on two new thrust chamber materials, Haynes 25 and a columbium alloy B-66, and on a more detailed evaluation of refractory metals.

Compatibility, from the standpoint of insulation material, is minor. Even a reaction that would destroy the inner layer of insulative material would not impair the effective thermal conductivity or integrity of the system. Alteration or even destruction of one layer out of many layers of a multilayer system would have a proportionately small effect on overall properties. The same reasoning would be true of a refractory ceramic matrix insulation system, such as low-density zirconia. One possible disadvantage of the insulation system, should it react with the thrust chamber, would be difficulty in removal after use. But even this prospect seems unimportant for most applications.

Compatibility studies were conducted with B-66 (a columbium alloy), Ta-10W, Mo-1/2 Ti, and Haynes 25 vs molybdenum and tantalum foils, and with Haynes 25 vs silica fabric. Compatibility was also evaluated between molybdenum foil and a zirconia-tungsten system. Molybdenum foil containers were used to house the zirconia-tungsten material during measurement of thermal properties.

## PROCEDURE

### Thermal Stability Studies

Test specimens simulating multilayer insulation systems resembled small sandwiches. Each specimen consisted of three layers of the appropriate fabric, each separated by at least one layer of refractory metal foil, and protected on top and bottom by at least one layer of the same refractory metal foil (Fig. 43). When tantalum foil was used, at least two sheets were used and these were protected from the tungsten weights on top and from the tungsten base plate by one sheet of molybdenum foil.

All sheets were 1-inch square. Materials were obtained from the same batches that were used in measuring thermal properties, except as noted below. Four stacks, or sandwiches, of each insulation system were used in each test, and each of three stacks were weighted to a loading pressure of approximately 0, 1/2, and 1 psi. The fourth stack, which was loaded at 1/2 psi, contained fabric from a different batch of material. Rigid 1-inch square tungsten plates were placed on top to provide the appropriate loading pressure and to uniformly distribute the load. Each tungsten plate weighed 13 gms, so that loading of the 1/2- and 1-psi-loaded specimens was within 0.035 psi of the correct pressure to yield 1/2 or 1 psi. One plate was used on the "zero" psi-loaded specimen to hold the foils in place. This resulted in an actual loading pressure of 0.035 psi.

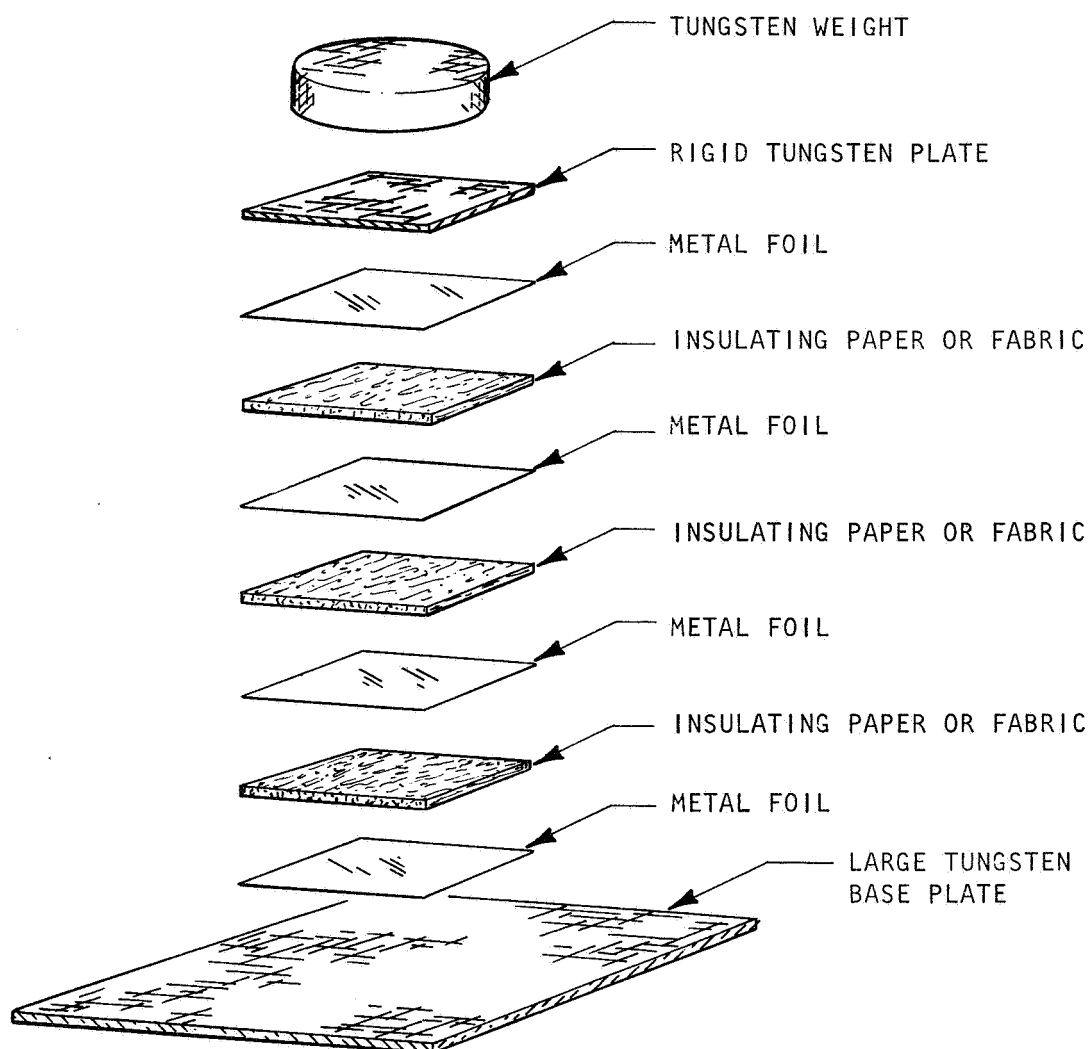


Figure 43. Multilayer Insulation Specimen

The thickness of each fabric was determined by measuring the total thickness of the stack, subtracting the thickness of the foils, and dividing by three, which was the number of pieces of fabric. Measurements were made optically with a cathetometer so that handling of the specimen was unnecessary. This procedure was mandatory because annealed specimens, especially carbon fabric/tantalum foil specimens, could not be handled without their breaking apart. The optical measurements were accurate and efficient. The length and width of fabrics could not be accurately or reproducibly measured because of the nature of small pieces of loosely-woven fabrics.

Specimens were visually observed with the unaided eye and with a 50-power stereomicroscope. Certain specimens were also observed microscopically at high magnification. Fabrics were mounted for microscopic study by compressing them with the appropriate loading pressure and vacuum infiltrating them with a low-viscosity, cold-setting epoxy. Specimens were then remounted perpendicular to the plane of the fabrics and polished by standard ceramographic procedures.

#### Compatibility Studies

Compatibility specimens of the refractory metal alloys were 1/2-inch squares of as-received sheet stock. Thickness was 65 mils for the B-66 alloy, 40 mils for the Ta-10W alloy, and 30 mils for the Mo-1/2 Ti alloy. Haynes 25 specimens were 1/2-inch cubes cut from 1/2-inch stock. The as-received surface was used. Tantalum and molybdenum foils were obtained from the same stock used in the entire program. All specimens were cleaned in acetone and rinsed in ethanol. A loading pressure of 1/2 psi was always used. Annealed specimens were mounted perpendicular to the plane of viewing and polished by standard metallographic procedures. Interfaces between metals were observed before and after etching. Microhardness was obtained with a Miniload (Zeitz) microhardness tester. Loading weight was 25 grams.

Since tantalum foil bonded to all metals at 3500 F, it was protected by a second sheet of tantalum foil and a sheet of molybdenum foil. The molybdenum foil did not react with the tungsten weights on top of the tungsten base plate.

## CONDITIONS

Specimens were heated in a tungsten, resistance-heated vacuum furnace. Heating and cooling cycles were not considered in determining total time at temperature because they were rapid. Heating and cooling rate at upper temperatures was about 50 F/min. Pressure in the furnace chamber was generally  $2 \times 10^{-4}$  torr during heating due to furnace wall and specimen outgassing. Pressure decreased to about  $5 \times 10^{-5}$  torr at test temperature.

Testing parameters were selected based on the most severe conditions expected for buried rocket engine chambers during spacecraft operation. Testing temperature was 2000 F for the silica fabric/molybdenum foil system and 3500 F for the carbon fabric/tantalum and zirconia-tungsten systems. Duration was 1 hour or less. Compatibility and thermal stability specimens were annealed simultaneously when appropriate.

## RESULTS AND DISCUSSION

### Thermal Stability

Silica Fabric/Molybdenum Foil System. Silica fabric was not affected significantly by annealing at 2000 F. Appearance, flexibility, and strength of the fabric did not perceptibly change. The fabric only reacted slightly with the contacting molybdenum foil enough to tarnish locally. The slight shrinkage that occurred with loading at high temperature was permanent.

Reaction of the silica fibers with the foil was random; it did not occur in all specimens nor all over a single specimen. Moreover, the tarnish

was only visible where high spots of the fabric touched the metal. Conversely, silica paper tested last year sintered slightly, never had any appreciable strength, and slightly tarnished the entire surface of the molybdenum foil due to the higher contact area of the paper.

Shrinkage of the silica fabric is shown in Fig. 44. Shrinkage was 5 percent with a 1/2-psi loading pressure, and 12 percent with a 1-psi loading pressure. Zero-psi data for annealed specimens were not plotted because the scatter was too large. The scatter was due to insufficient loading pressure to keep the molybdenum foils flat. An estimated curve was drawn in Fig. 44 with the same slope as the 1/2-psi and 1-psi curves.

A cross section of the silica fabric under high magnification is given in Fig. 45. The loading pressure was 1/2 psi, and the specimen was annealed for 1 hour in vacuum at 2000 F. No change was observed as a result of annealing. The small fibers show no sign of sintering or of changing shape.

Data for silica paper are also presented for comparison. Higher shrinkage for the paper compared to the fabric is evident. Percent shrinkage is listed below:

<u>Silica Fabric</u>	<u>Shrinkage After 1 Hour, percent</u>
1/2 psi	5
1 psi	12
<u>Silica Paper</u>	
1/2 psi	33
1 psi	32

Shrinkage for a fabric from a different lot of material was 9 percent compared to 5 percent for the reference lot. Loading pressure was 1/2 psi.

○, △, □ DATA WERE  
INTERPOLATED FROM DATA  
THAT WERE TAKEN AT 0,  
1/2, AND 5 HOURS, RESPECTIVELY

○ 0 PSI LOADING PRESSURE  
△ 1/2 PSI LOADING PRESSURE  
□ 1 PSI LOADING PRESSURE

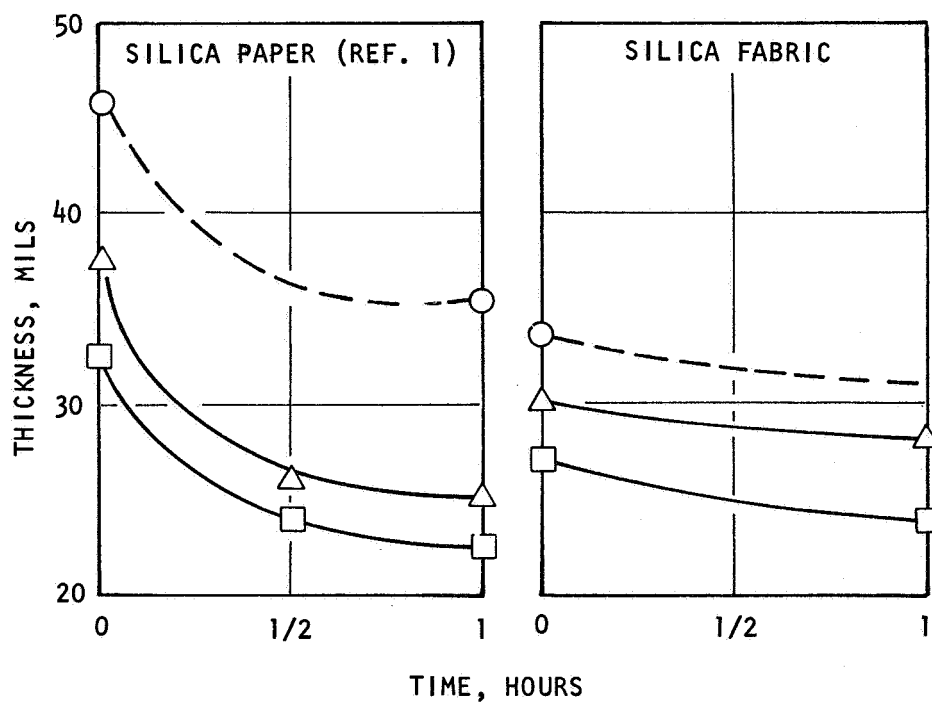
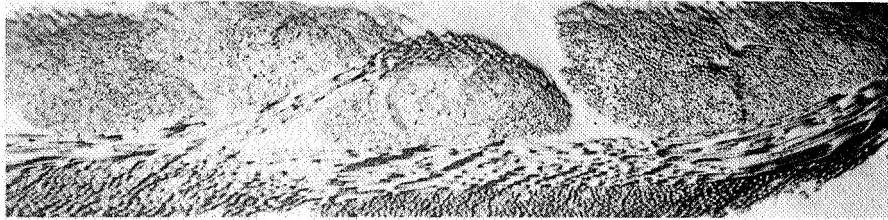
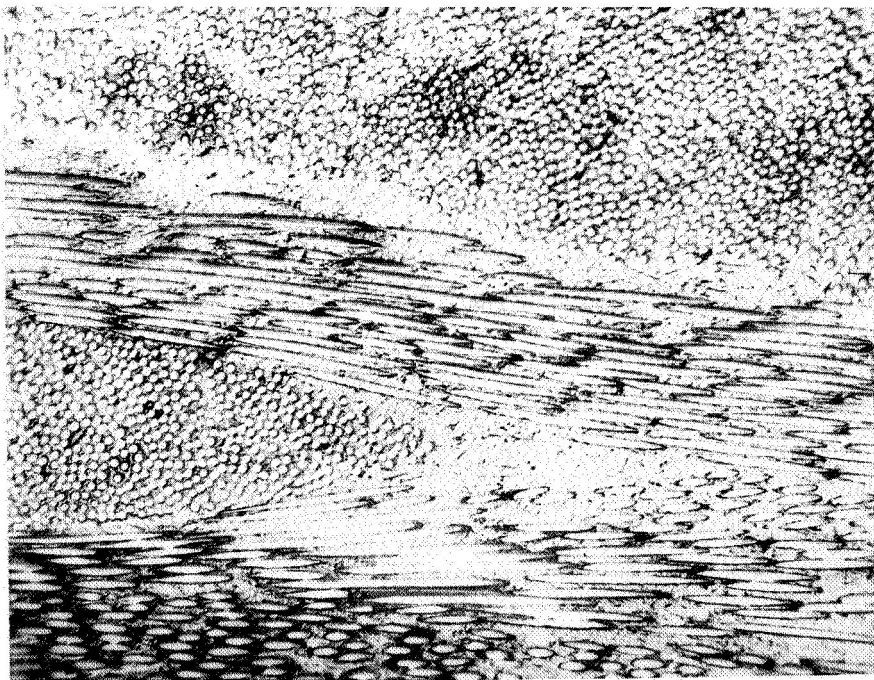


Figure 44. Effect of Time and Loading Pressure on Silica Fabric Annealed (Vacuum at 2000 F)



50X



150X

Figure 45. Cross-Section of Silica Fabric Loaded Under  $1/2$  psi Pressure and Annealed in Vacuum for 1 Hour at 2000 F (50X and 150X Magnification)



The difference is significant, indicating that some differences can be expected between different lots of material, but 9 percent shrinkage is still not excessive.

The effect of loading pressure on the thickness of silica fabric at room temperature is shown in Fig. 46. Data for silica paper are included. Silica fabric was compressed 18 percent by a load of 1 psi, whereas the paper was compressed 27 percent.

Weight-loss data for silica fabric were obtained by heating specimens in both air and vacuum furnaces. The purpose of measuring weight loss in air was to determine whether volatiles could be driven off at low temperatures, and whether the fabric would readily re-absorb the gases.

Weight loss of silica fabric from both lots of material after annealing 1 hour at 2000 F in a vacuum was 2.4 and 3.1 percent. Weight-loss data obtained by heating in air for material from both lots were 2.5 percent at 1500 F and 3.3 percent at 2000 F. Weight gain after exposure to air for eight days was 0.1 percent.

Initially these specimens were heated to 500 F, where the weight loss was 2.5 percent. After exposure to ambient conditions, these specimens regained 2.5 percent in weight. Apparently, the extent of gas absorption on unannealed silica fabric depends on ambient conditions, particularly humidity.

Carbon Fabric/Tantalum Foil System. Multilayers of carbon fabric/tantalum foil were previously found to be a very good insulation materials system (Ref. 2). Effective thermal conductivity at elevated temperatures was as low or lower than all other material systems, and it was an order of magnitude lower than that of the low-density zirconia, the latter having the lowest thermal conductivity of all pure materials. Moreover, carbon

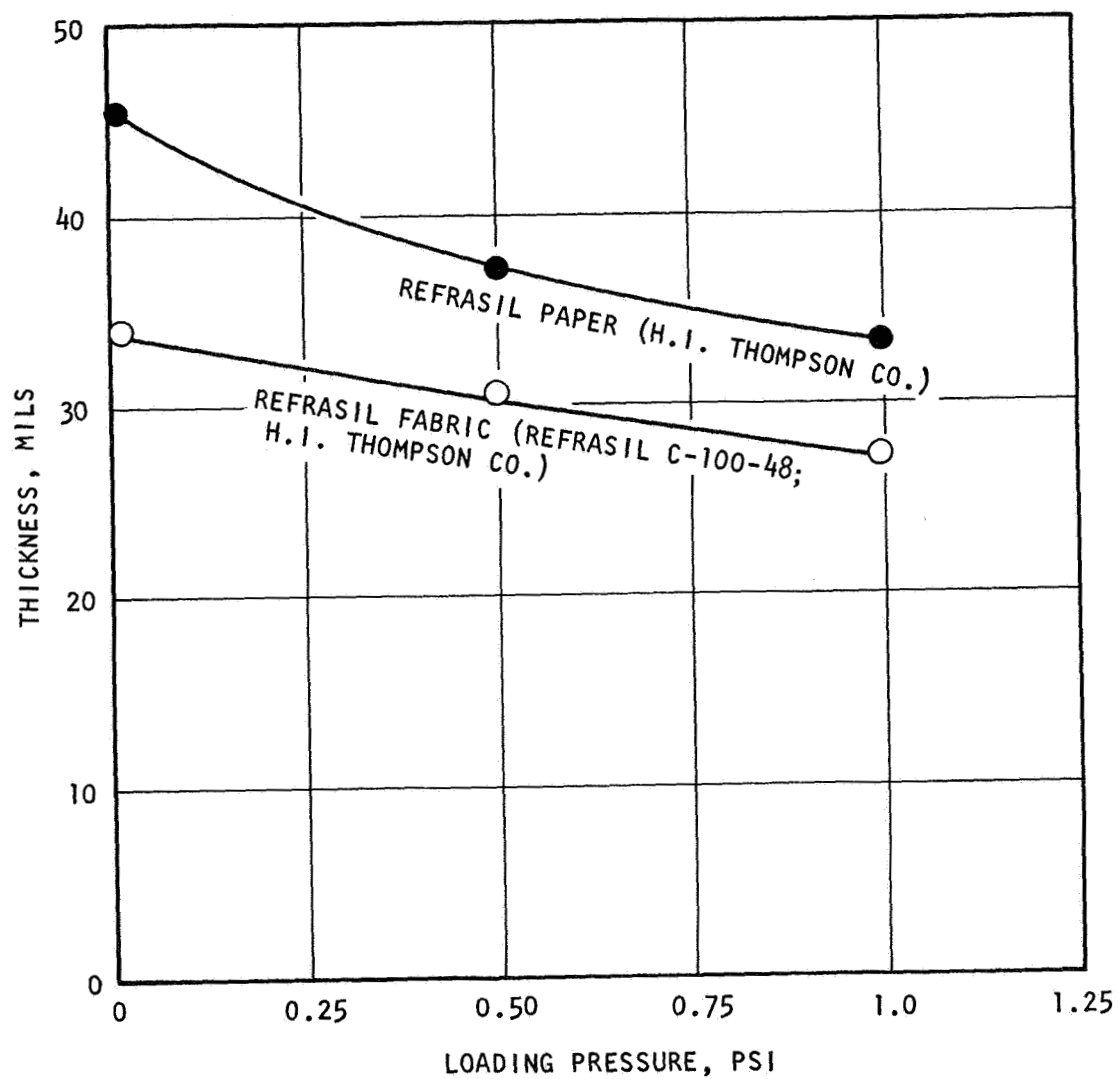


Figure 46. Effect of Loading Pressure on "As-Received" Silica Fabric and Paper

fabric did not change significantly during annealing to 4500 F, and the flexibility and strength of the fabric were not affected by environmental testing.

Measured weight loss was unexpectedly high, but this was apparently due to loss of the container material that reacted with adjacent metal supports. The fabric weight-loss specimen was wrapped in tantalum foil which, as expected, carburized during annealing. The tantalum carbide in turn welded to the small tungsten supports. Reaction was slight, but could have accounted for considerable error in calculating weight loss of the carbon fabric. Although the radiation shields of tantalum foil in the multilayer system carburized rapidly during testing at 3500 F, the effective thermal conductivity of the system was not impaired. However, embrittlement was encountered. Embrittlement is not necessarily harmful because the carbon fabric protects and holds the tantalum carbide radiation shields in place. Since this system was the best one tested (Ref. 2), no changes in the materials were made in the continued evaluations reported herein.

Appearance and properties of annealed carbon fabric/tantalum foil specimens were the same as previously reported (Ref. 2). The carbon fabric was unaffected by heating or by contact with tantalum; and the tantalum foil carburized, becoming very brittle.

The effect of loading pressure and time on shrinkage of carbon fabric/tantalum foil multilayer systems at 3500 F is shown in Fig. 47. The data include results of all tests run at 3500 F. The amount of shrinkage seems to be independent of loading pressure. This may be due to the insensitivity of the carbon fabric to low loading pressures and to the fact that much of the apparent shrinkage is due to the deformation of the tantalum foil by the fabric which results in more efficient stacking of adjacent layers of the carbon fabric. In other words, the foil, as a result

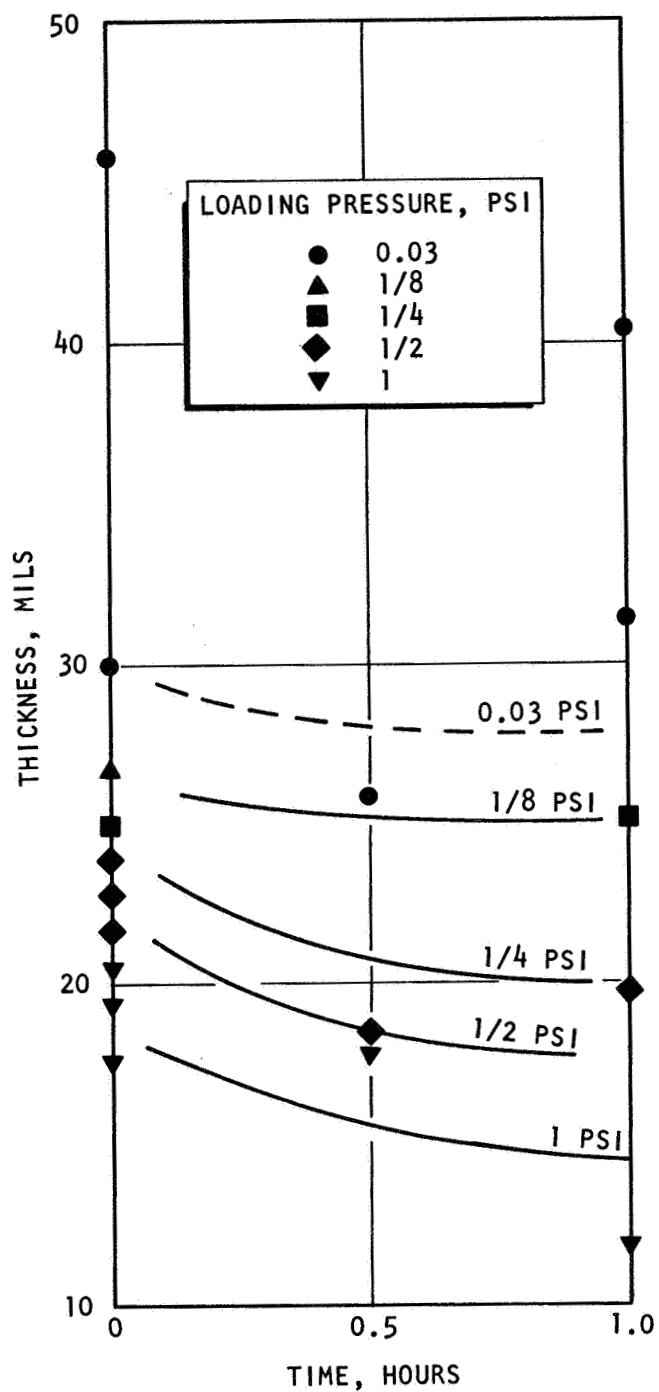


Figure 47. Change in Thickness of Carbon Fabric Used in Multilayer System as a Function of Time and Loading Pressure at 3500 F

of heat and pressure, conforms to the texture of the carbon fabric. Because the foil is no longer a flat surface, it allows adjacent layers of fabric to pack more efficiently. The foil deformation is permanent.

Drawing a meaningful curve through the data obtained at a negligible loading pressure (0.03 psi) is not possible because of the large scatter of data. The scatter is due to inadequate loading pressure to straighten out the bowed sheets of tantalum foil. The dashed curve representing a loading pressure of 0.03 psi was drawn parallel to the other curves and through the intercept of 30 mils on the ordinate. Thirty mils is an accurate measurement of the thickness of single sheet of carbon fabric under 0 psi loading pressure.

Shrinkage data from multilayer specimens in which the carbon fabric was obtained from different lots of material from the vendor were also obtained. The loading pressure was 1/2 psi at a temperature of 3500 F, and a test duration of 1 hour. The difference in shrinkage was nominal and within the range of experimental error.

Weight-loss of the carbon fabric was 5.1 percent. This figure is considered more accurate than that reported previously (Ref. 2).

The effect of loading pressure at room temperature on as-received carbon fabric is shown in Fig. 48. This information is important for designing insulation systems for a specific use.

#### Zirconia-Tungsten System.

Sampling. Thermal stability studies on the zirconia-tungsten system (other than those performed in the screening tests described in Appendix B) were performed on samples taken from the large thermal conductivity specimens. Samples of about 80 grams of the composite were removed from the

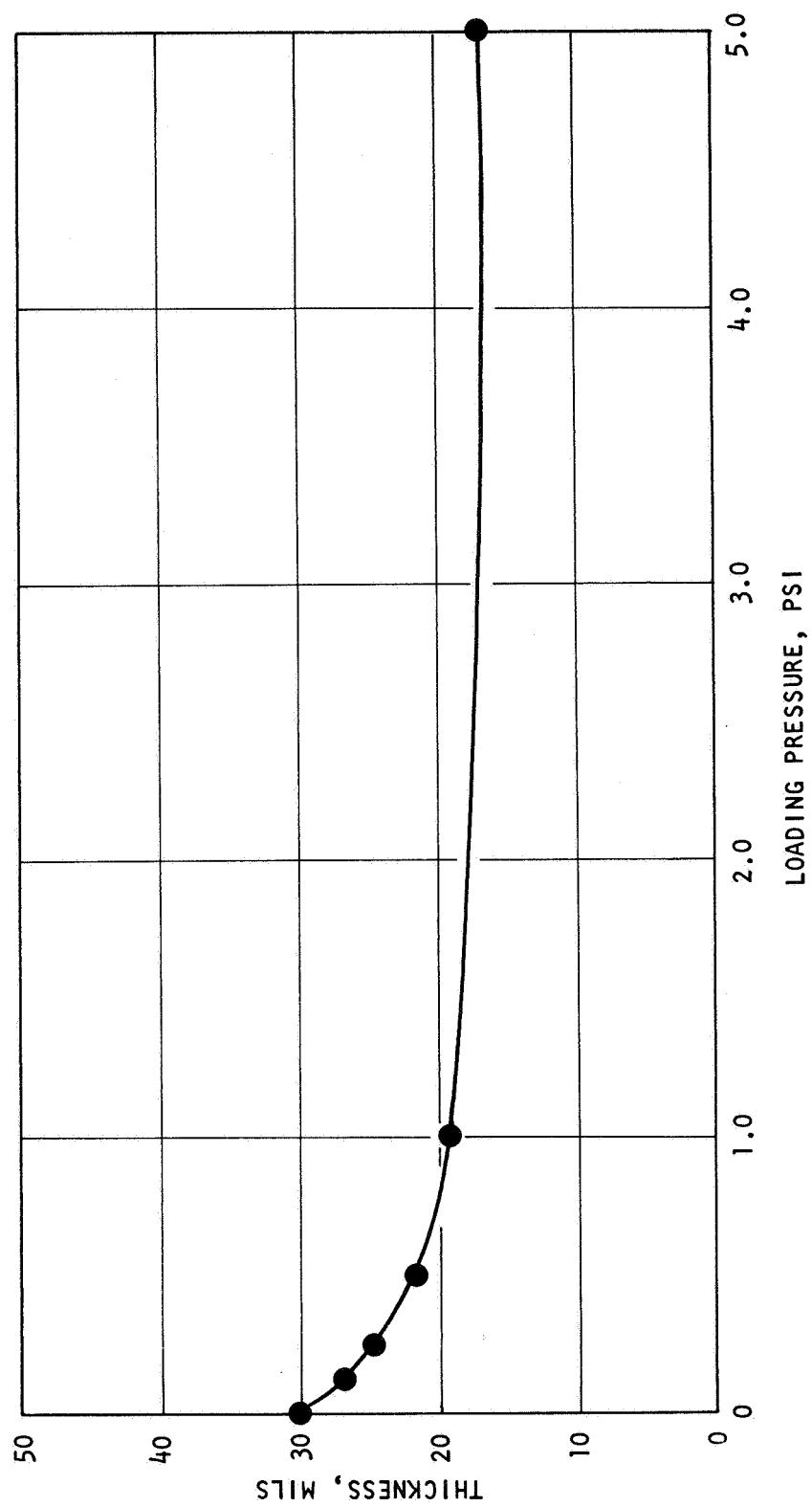


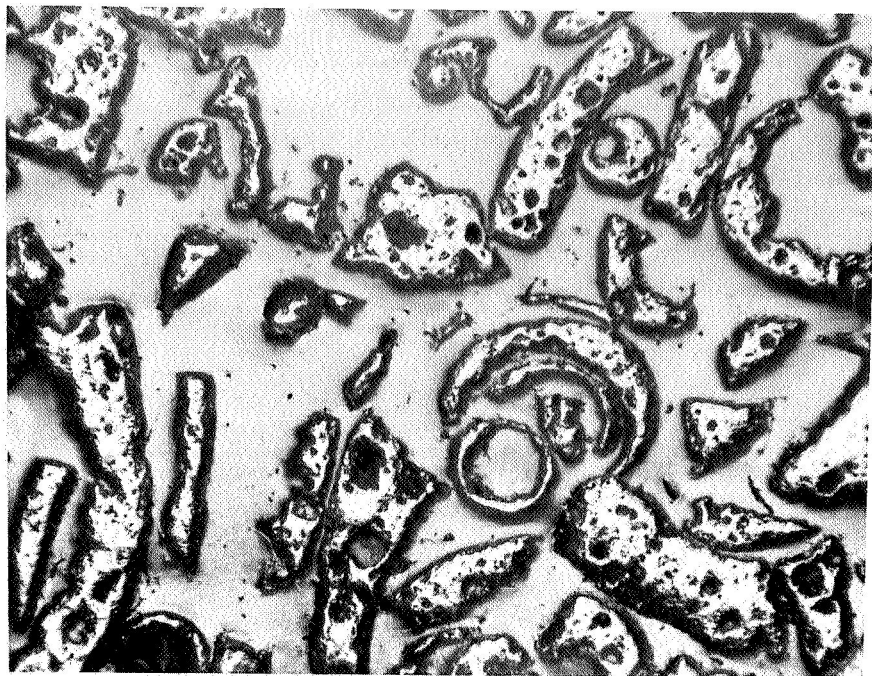
Figure 48. Effect of Loading Pressure on "As-Received" Carbon Fabric

hottest sections of the thermal conductivity specimen in the top, middle, and bottom layers. Maximum temperature for the 90 percent  $ZrO_2$ -10 percent W composite was 3000 F, and for the 98 percent  $ZrO_2$ -2 percent W composite, was 3380 F.

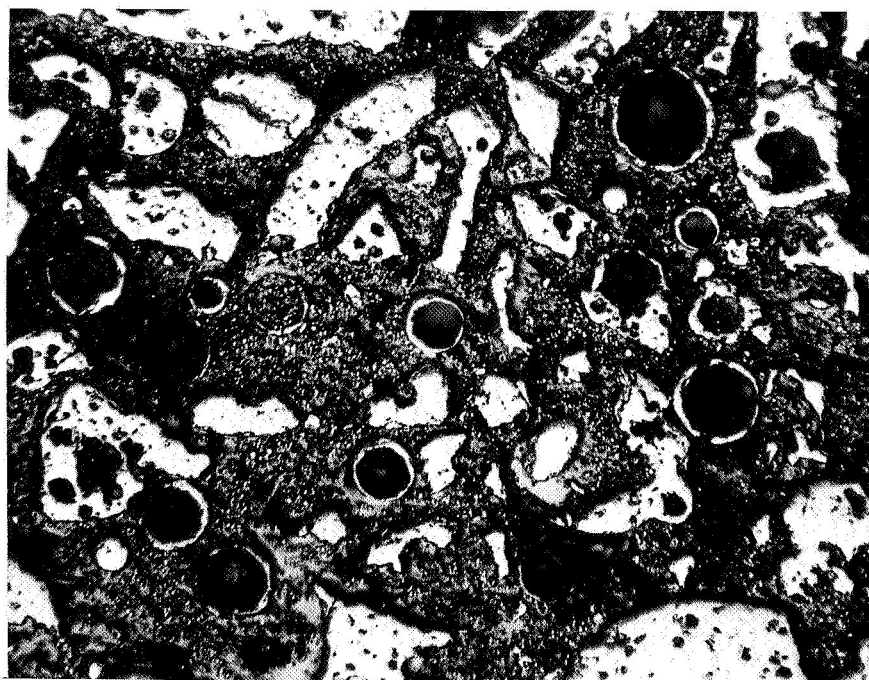
Segregation. Segregation of tungsten in the zirconia matrix in the 90-10 mixture was evident by visual examination. Segregation was observed to some extent in each sample, top, middle, and bottom, but it was most pronounced between the top and bottom samples. The dark tungsten powder sifted through the coarse, beige zirconia matrix, making the bottom sample much darker and the top sample lighter than they were initially.

A microscopic examination of polished samples that were infiltrated with epoxy was made (Fig. 49 and 50). Figure 49a shows the zirconia insulation material alone and Fig. 49b shows the 10 weight percent tungsten sample before testing. Samples taken from the thermal conductivity specimen after testing are shown in Fig. 50. Very little tungsten powder is visible in the top sample except where the tungsten is trapped inside hollow microspheres. A medium amount of dispersed tungsten is visible in the middle sample, whereas excessive tungsten powder is visible in the bottom sample. Tungsten distribution in the bottom sample was not uniform and, whereas the photomicrograph is of a highly concentrated area of tungsten powder, such a high concentration was not uncommon. Caution must be used in evaluation of the results of the microscopic examination because of two factors. First, each sample was selected randomly; therefore, each mount represents material from only one small area of a large non-homogeneous section. Secondly, the mounting compound could have dispersed, or agglomerated, the fine tungsten powder during impregnation.

Segregation of tungsten powder in the 98-2 mixture was visually masked because the zirconia phase turned dark grey during testing. The dark color of the zirconia can be explained by an ion-deficient structure that results from annealing zirconia in a vacuum (or a reducing environment) above 3000 F. This material was not mounted and examined under the microscope.



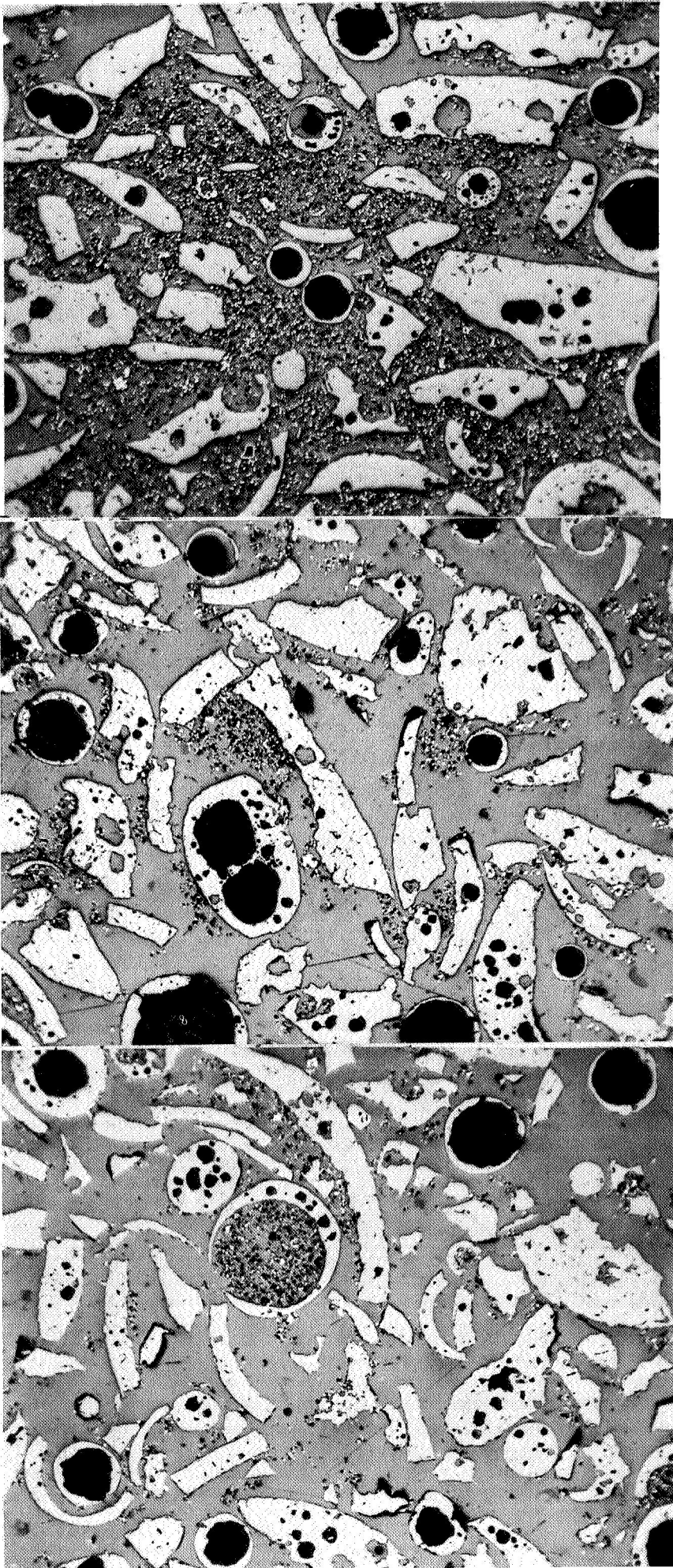
(a)



(b)

Figure 49. Zirconia Insulation Material in the As-Received Condition With (a) 0 Percent and (b) 10 Percent by Weight Tungsten Powder. (50X Magnification)





(a) (b) (c)

Figure 50. Zirconia Insulation Material Containing 10 Percent By Weight Tungsten Powder Annealed at 3000 F in a Vacuum. Samples Were Taken From (a) Top, (b) Middle, and (c) Bottom Sections of the Thermal Conductivity Specimen. (50X Magnification)

Segregation was measured quantitatively by separating the tungsten powder from the zirconia matrix and weighing it. The tungsten powder was removed by vigorously shaking (on an automatic machine) the composite through a 200 mesh sieve. Results were:

<u>Mixture</u>	<u>Section of Thermal Property Specimen</u>	<u>Weight Percent Through A 200-mesh Sieve</u>	
{ 90 percent ZrO <sub>2</sub> 10 percent W	Top	7.0	} average 9.9
	Middle	10.1	
	Bottom	12.6	
{ 98 percent ZrO <sub>2</sub> 2 percent W	Top	1.3	} average 1.6
	Middle	1.4	
	Bottom	2.2	

Whether most of the segregation occurred before or during testing could not be determined. Although precautions were taken, the heavier, finer, tungsten powder no doubt segregated to some degree when the mixture was poured into the thermal property test container. Further segregation could have occurred during testing due to the vibration caused by the vacuum pump.

Bulk density of samples taken from the top, middle, and bottom sections of the 90-10 mixture specimen also indicated the degree of segregation of the two components. Exactly 10 cc of composite material was poured into a graduated cylinder and weighed. The graduated cylinder was placed on a vibration table to obtain a more reproducible measurement of volume. The results listed below also indicate that tungsten concentration decreased with height in the thermal property specimen.

<u>Section of Thermal Property Specimen</u>	<u>As-Poured Density gm/cc</u>	<u>Vibrated Density gm/cc</u>
Top	2.67	2.88
Middle	2.65	2.99
Bottom	2.67	3.03

Chemical Reactions. Signs of chemical reaction between the tungsten and zirconia were not apparent. Tungsten particles did not adhere to the zirconia particles, and no observable physical changes in either material were apparent.

Sintering. No sintering of either zirconia or tungsten was observed by microscopic examination. However, some particles in the hottest sections of the thermal conductivity specimens bonded together very slightly. Lumps of aggregate about 1/2 inch across were found after annealing above 3000 F, but these agglomerates had a crushing strength estimated at less than 1 psi.

#### Compatibility

Haynes 25 Alloy. Haynes 25 alloy was tested in contact with tantalum foil, molybdenum foil, silica fabric, and silica paper at 2000 F for 1 hour in a vacuum. The loading pressure was 1/2 psi. Haynes 25 did not react or bond to either molybdenum or tantalum foil, with one exception. It did bond to molybdenum in one proportionally small area, but the remaining area was unaffected. The local bonding encountered is not considered typical because it was most likely due to an unusual condition, such as an inclusion or impurity on one of the surfaces.

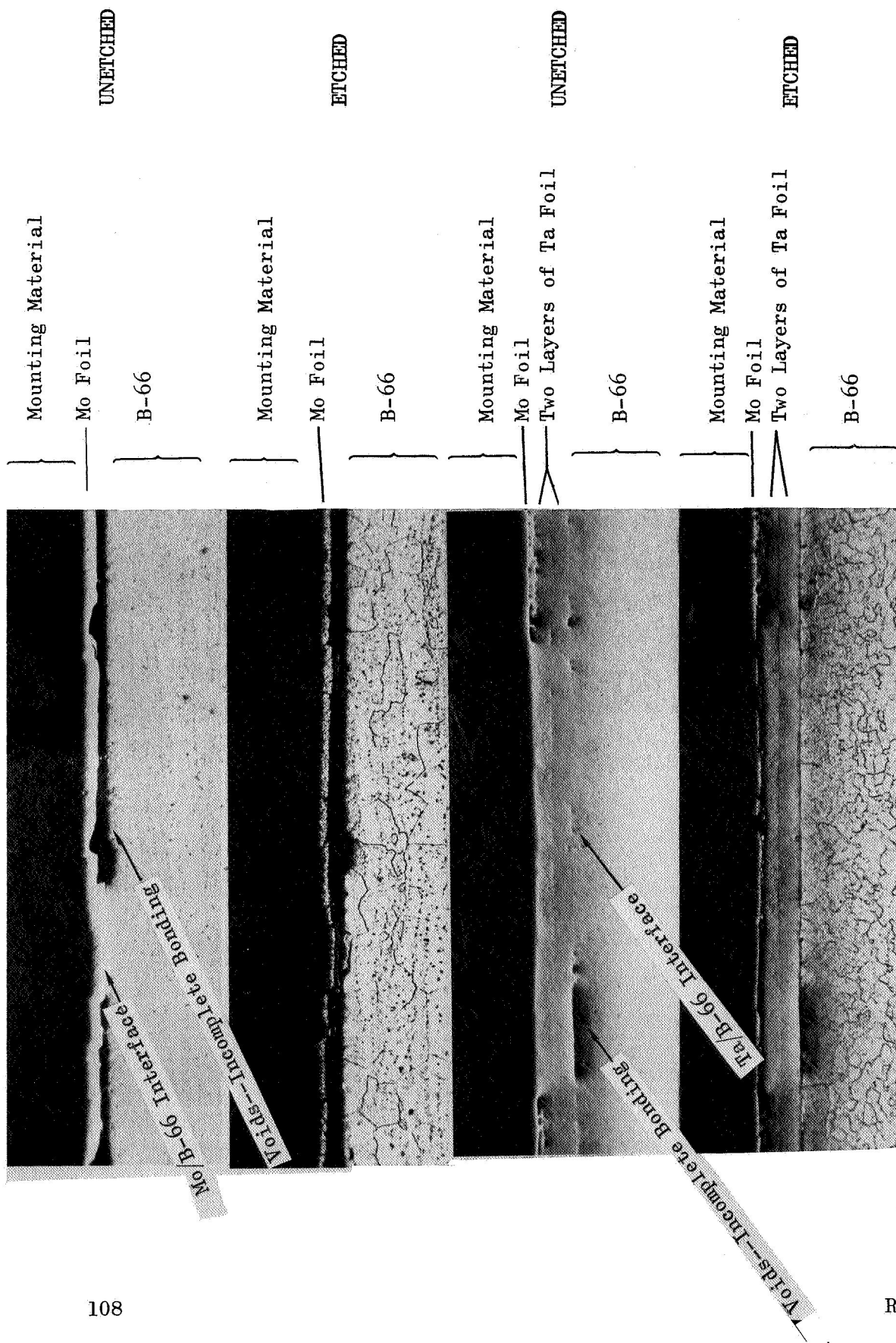
The silica paper that contacted the Haynes 25 alloy turned dull green-yellow and the alloy surface tarnished. Although these materials reacted, they did not adhere to each other. The same reaction was observed in the case of silica fabric in contact with Haynes 25 alloy but contact area was limited to the high spots of the fabric weave. Therefore, reaction area between the fabric and the metal was proportionately smaller. A compatibility problem does not exist in this system as long as the silica is separated from the Haynes 25 chamber by a layer of molybdenum foil.

Refractory Metals. Compatibility specimens were potential thrust chamber alloys: B-66 (a columbium-based alloy), Mo-1/2 Ti, and Ta-10W against the insulation systems materials tantalum and molybdenum foils. Couples of each combination of chamber and insulation metals were weighted with a 1/2 psi loading pressure and annealed at 3500 F for 1 hour in a vacuum.

All combinations bonded together as a result of diffusion and could not be separated. Microscopic observation, however, showed that bonding was not uniform and was intermittent along the interface on all specimens. The photomicrographs in Fig. 51a, b, and c show the extent of bonding between each pair of materials.

Microhardness measurements were made across the interface of each pair of materials to determine the depth of the thrust chamber alloy that was affected. The results are given in Fig. 52 through 54.

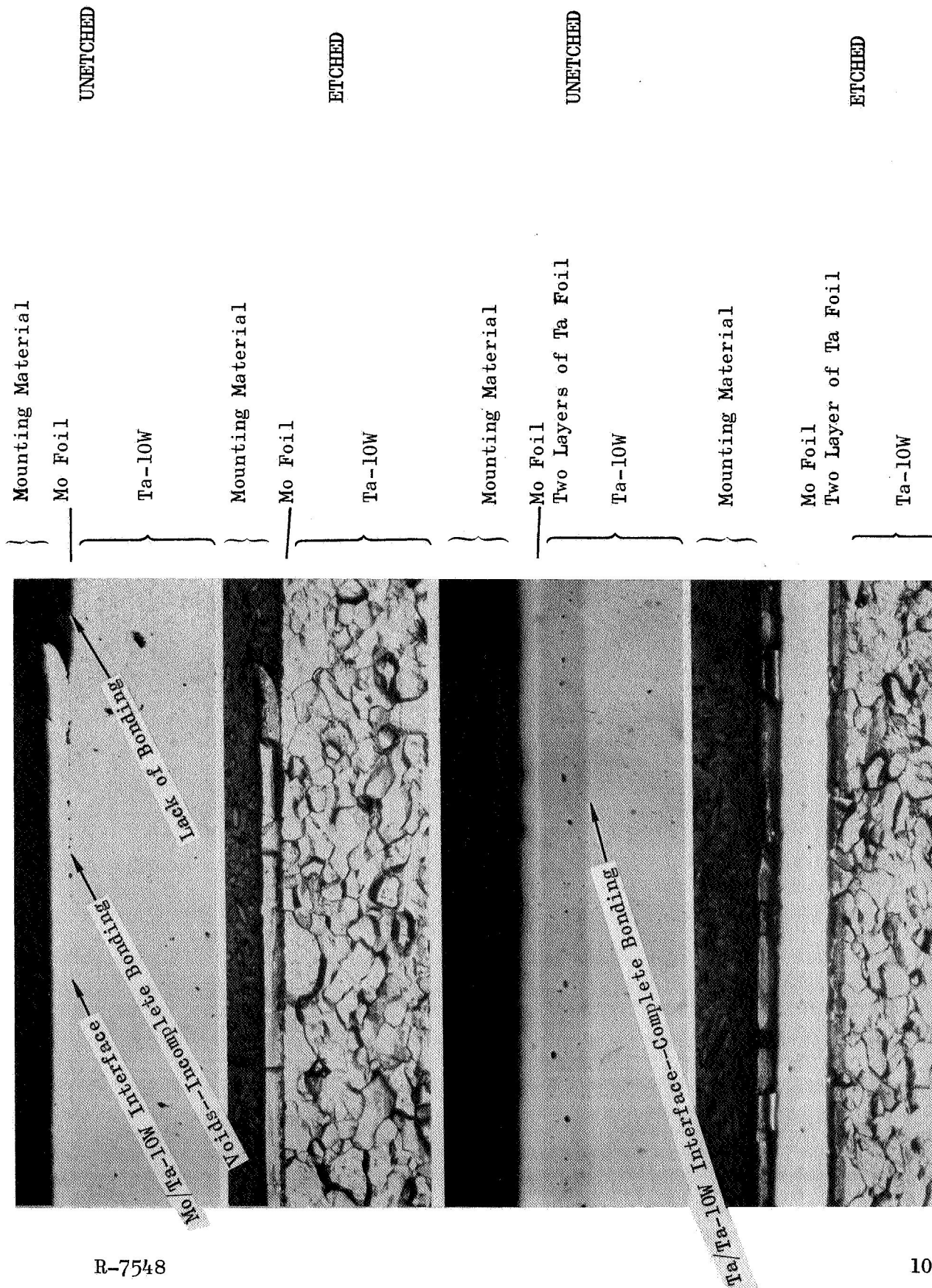
As shown, interdiffusion between B-66 and tantalum, and between Mo-1/2 Ti and molybdenum resulted in a significant change in hardness of the base alloys. The depth of the affected area was approximately 3 mils. It seems that a diffusion barrier, such as a thin layer of tungsten, should be interposed between the metals to alleviate the diffusion problem.



(a) Columbium Alloy

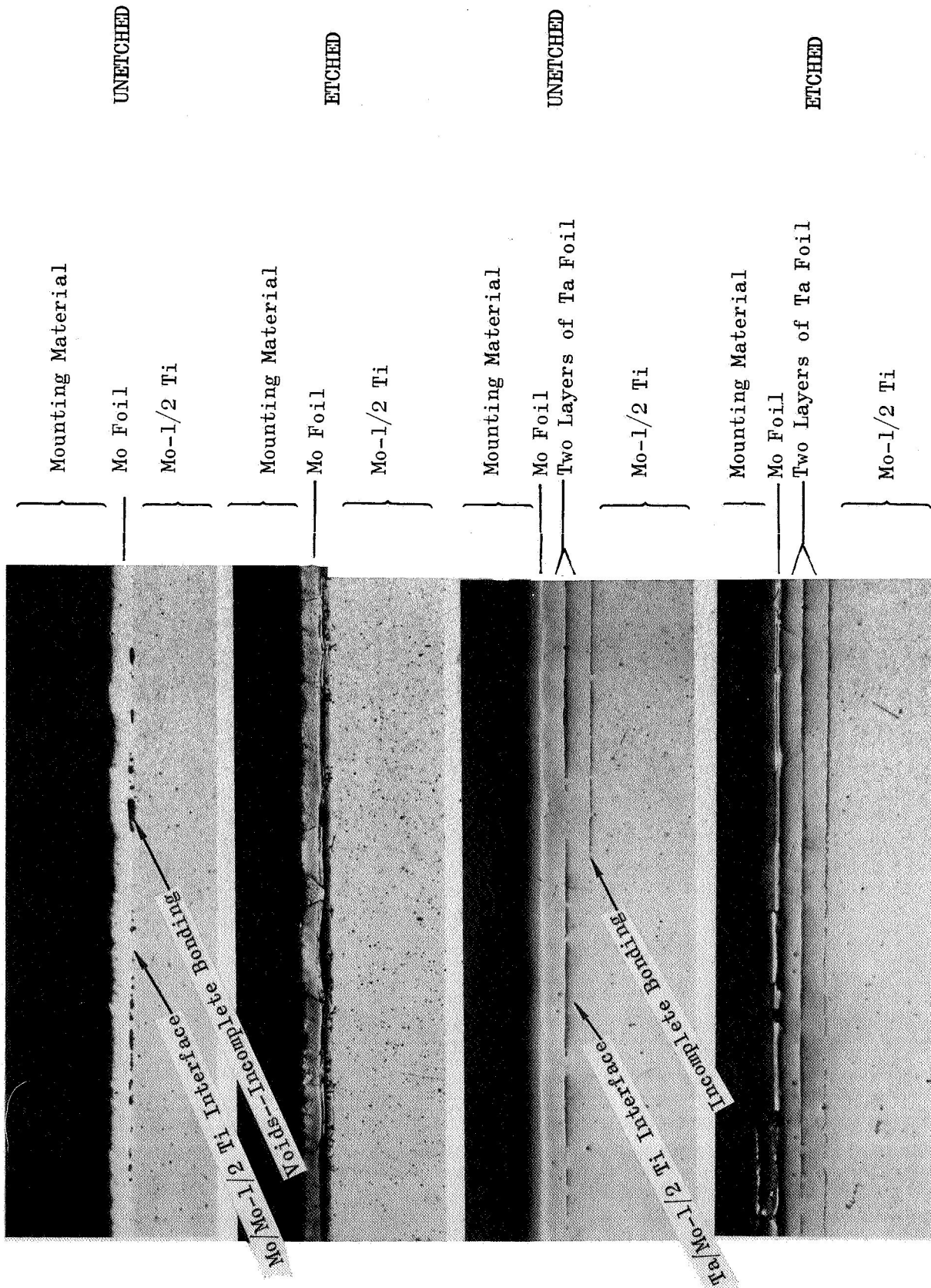
Figure 51 . Cross Sections of Thrust Chamber Material/Insulation Material Compatibility Specimens. Specimens were Annealed for 1-Hour in a Vacuum at 3500 F. (100X Magnification.) Etchant = 5 parts HF, 10 parts  $\text{HNO}_3$ , 10 parts lactic acid, parts by volume.





(b) Tantalum Alloy

Figure 51. (Continued)



(c) Molybdenum Alloy

Figure 51. Concluded

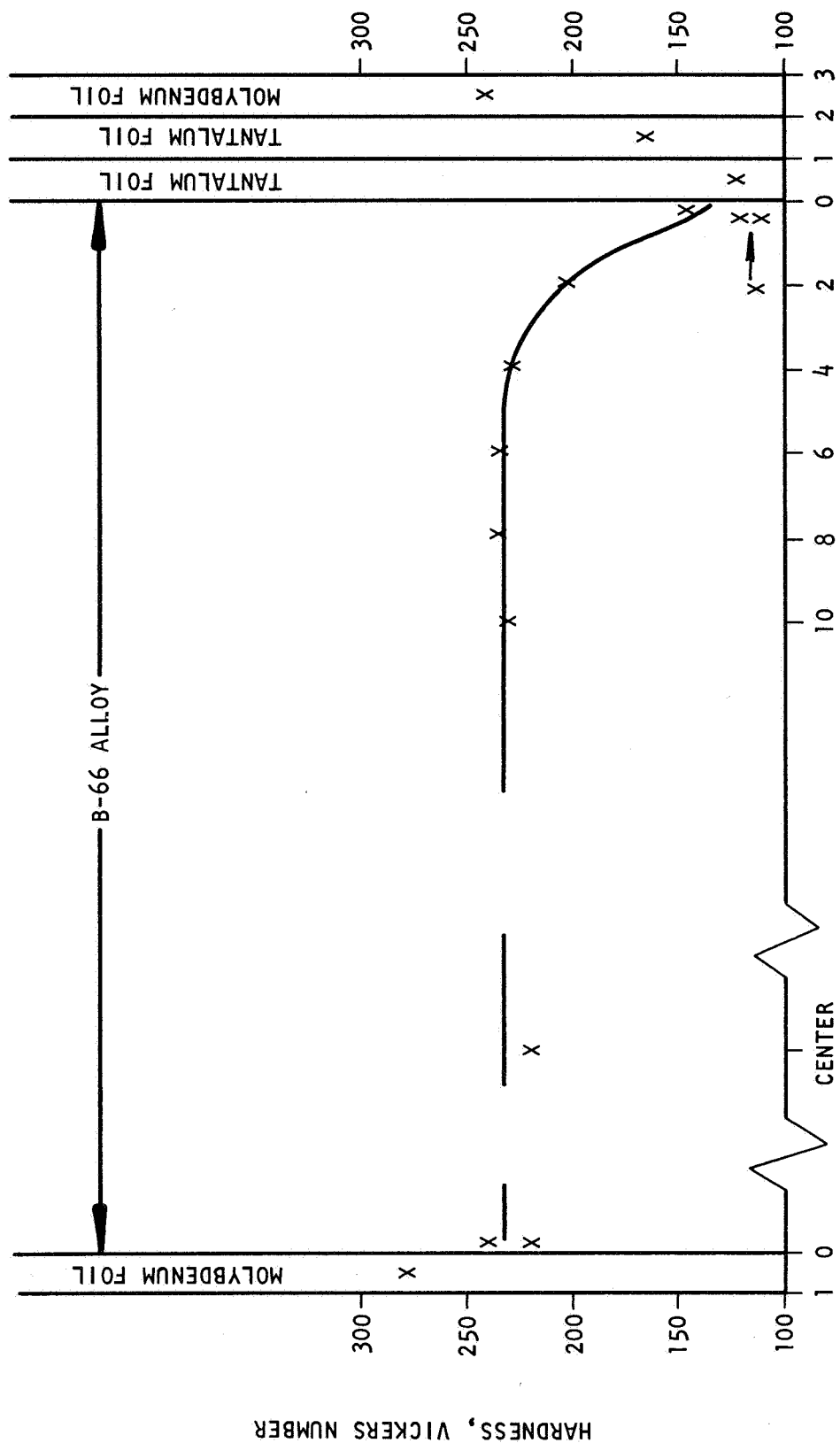


Figure 52. Hardness Across Molybdenum/B-66 and Tantalum/B-66 Interfaces  
(25-gm Loading Pressure)



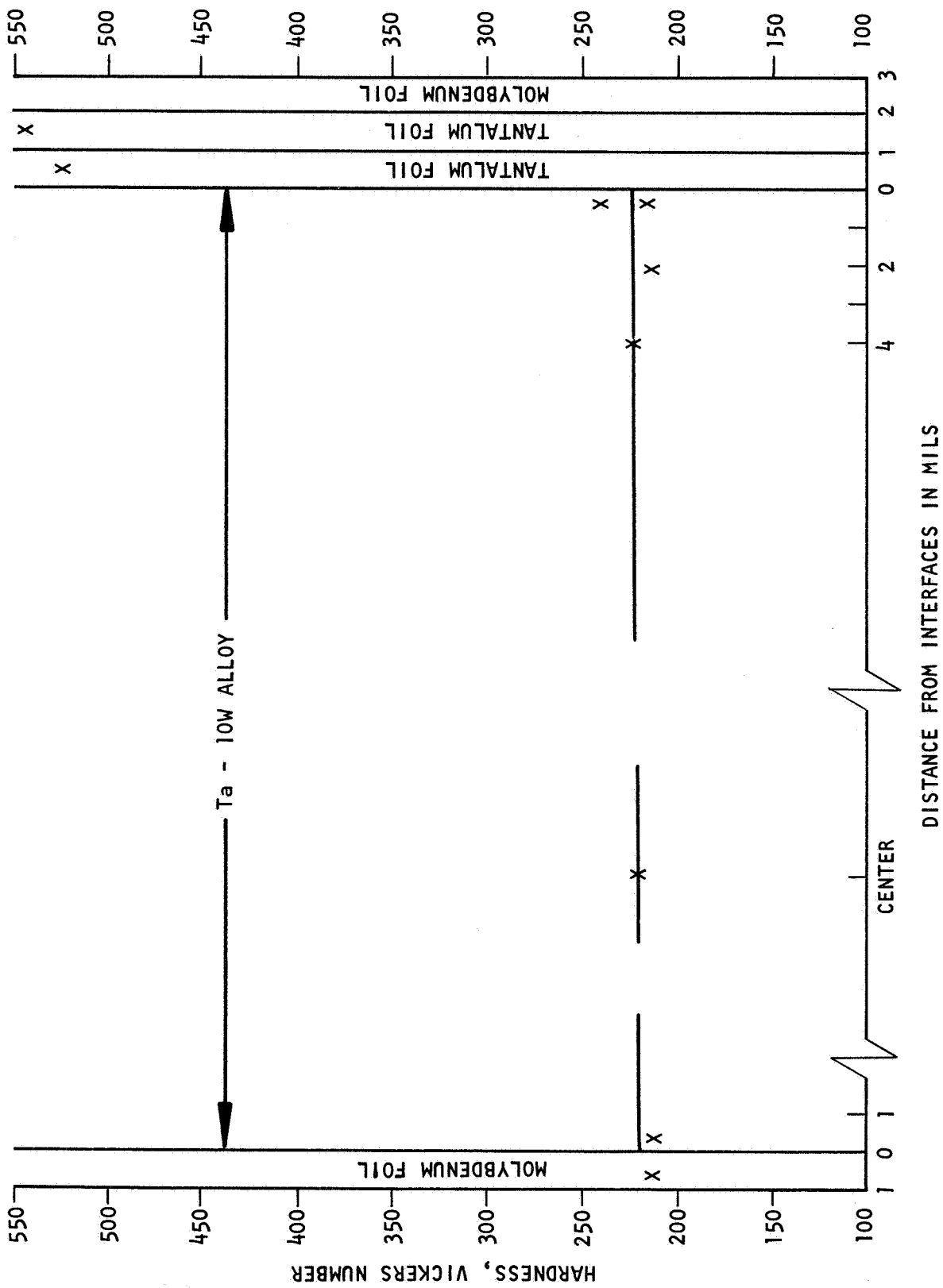
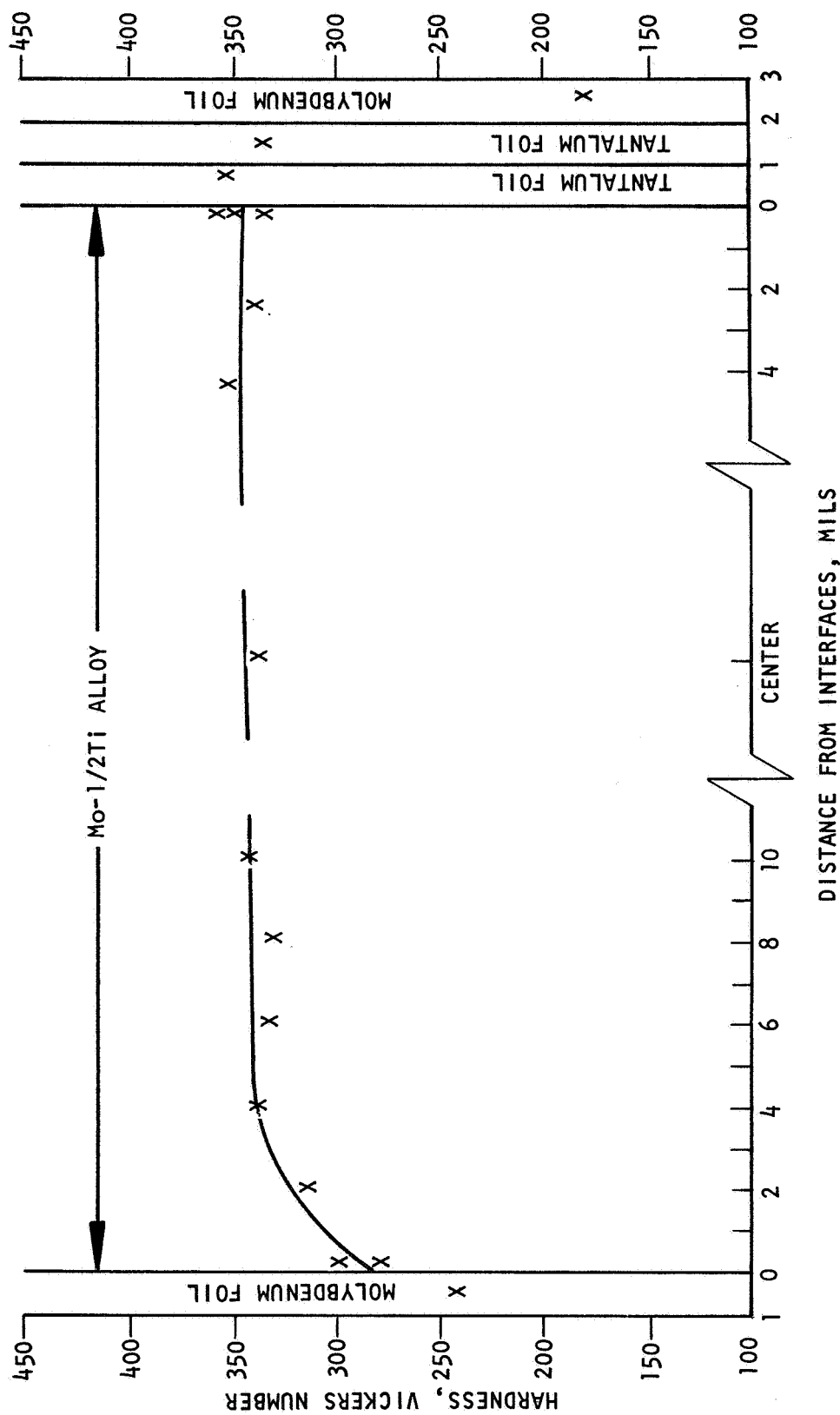


Figure 53. Hardness Across Molybdenum/Ta-10W and Tantalum/Ta-10W Interfaces (25-gm Loading Pressure)



## APPLICATIONS ANALYSIS

The capability of a spacecraft to accept heat loads is strictly limited, because available electronic equipment demands an essentially constant temperature environment. Thus all excess heat must be rejected to space by radiation. The limiting factor may be the maximum acceptable heat flux or the total heat load per firing, depending on the heat storage capability of the spacecraft. In general, there is a trade-off between the weight of engine insulation needed to limit the heat transmitted to the spacecraft by the buried engines and the weight of space radiators necessary to dispose of additional heat loads. The trade-off factors depend on the specific spacecraft design and mission, so such overall optimization calculations were not possible in this program. However an analytical model for calculating the heat flux from engine to spacecraft during firing and during the heat soakback period following the firing was developed. This information can, in turn, be used in system optimization calculations. The following paragraphs discuss the analytical model, and give examples of its application to insulation system design for typical spacecraft engines.

### HEAT TRANSFER IN AN INSULATED SPACE ENGINE:

#### GENERAL DESIGN CRITERIA

Evaluation of heat loads as a function of insulation properties and thickness should be conducted with a simplified model of the heat transfer to permit evaluation of a large number of designs. Selected optional designs can subsequently be analyzed in more detail. The total effort and the computer time spent to obtain the necessary information can thus be minimized.

The transient behavior of a multi-component system with temperature-dependent thermal properties cannot be treated by closed analytical methods. A thermal analyzer program of the type described in Ref. 5, which is known by the acronym TAP II, was used for the calculations. Two heat transfer regimes, firing and soakback, must be analyzed for each engine and each

firing cycle. During firing the chamber walls receive heat from the combustion gases; the chamber wall temperature increases, and heat is conducted into the insulation. During the soakback period which follows the firing, no additional heat is received by the system, but the heat stored in the engine walls and in the insulation is lost by radiation from nozzle walls to space and from the steel shell enclosing the insulation to the spacecraft walls, while temperatures tend to equalize throughout the system.

#### THERMAL PROPERTIES OF INSULATIONS

The first requirement imposed upon the insulation is that it must withstand the maximum temperature encountered at any time. In most cases, this temperature is the highest engine backwall temperature at the end of firing, though with a thick-wall intergen or film-cooled engine a higher backwall temperature may occur after the firing. The insulation characteristics have little influence on this peak temperature. The choice of insulation materials is therefore dictated by engine operation rather than by spacecraft heat load requirements.

The two best performing insulations developed during the present research program, a molybdenum-silica multilayer system and a tantalum-carbon multilayer system, will be considered here. The molybdenum-silica insulation will be used when the maximum temperature does not exceed 2000 F, while the tantalum-carbon insulation must be chosen for all higher temperature applications.

The thermal properties of the insulation of interest in the transient heat flow analysis are the effective thermal conductivity,  $k_e$ , and the heat capacity per unit volume,  $\rho C$ . The conductivities of the insulations, were obtained experimentally (see Thermal Properties section), while the heat capacities (Fig. 55) were calculated from weighted component properties (Ref. 1). The smoothed values of thermal conductivity used for analysis application are reproduced in Fig. 56 for convenience.

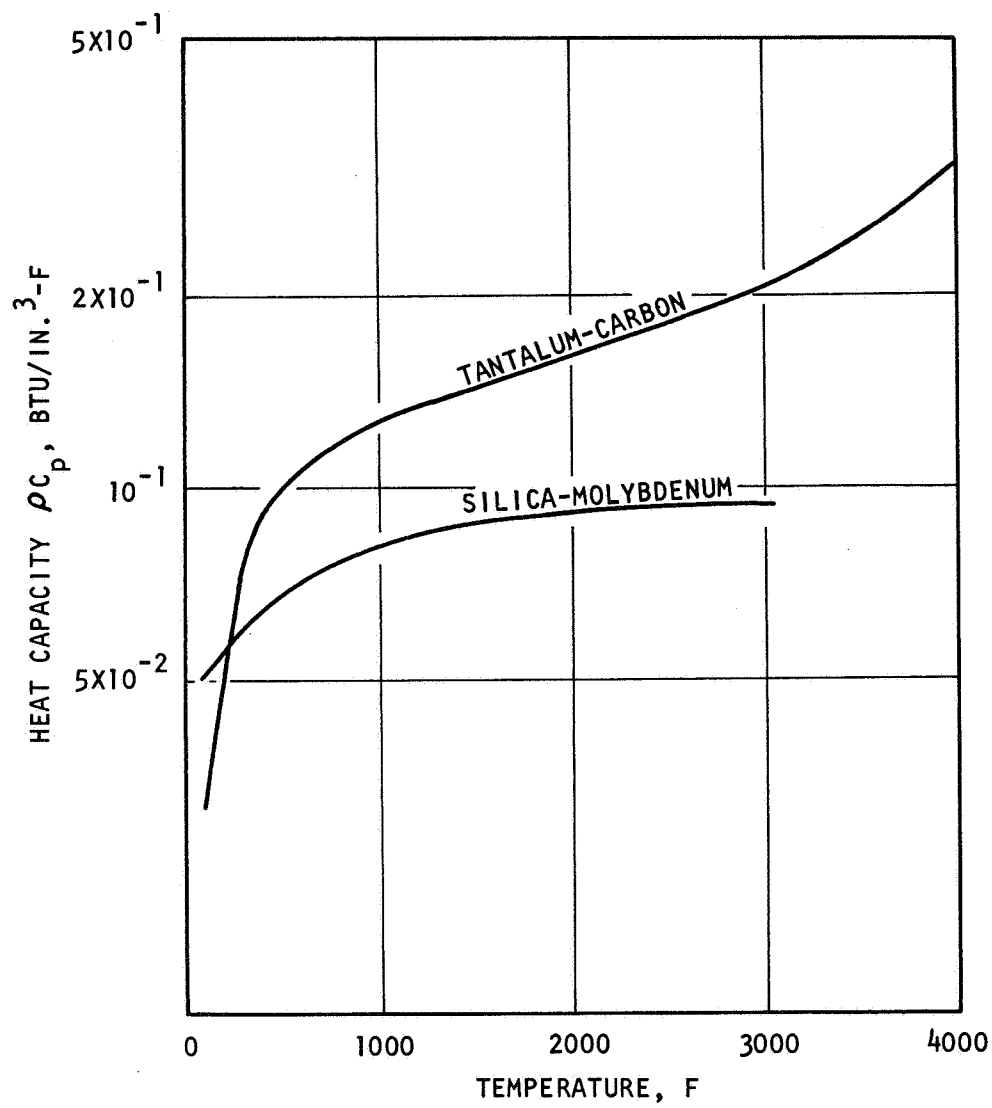


Figure 55. Heat Capacity of the Molybdenum-Silica and the Tantalum-Carbon Insulation

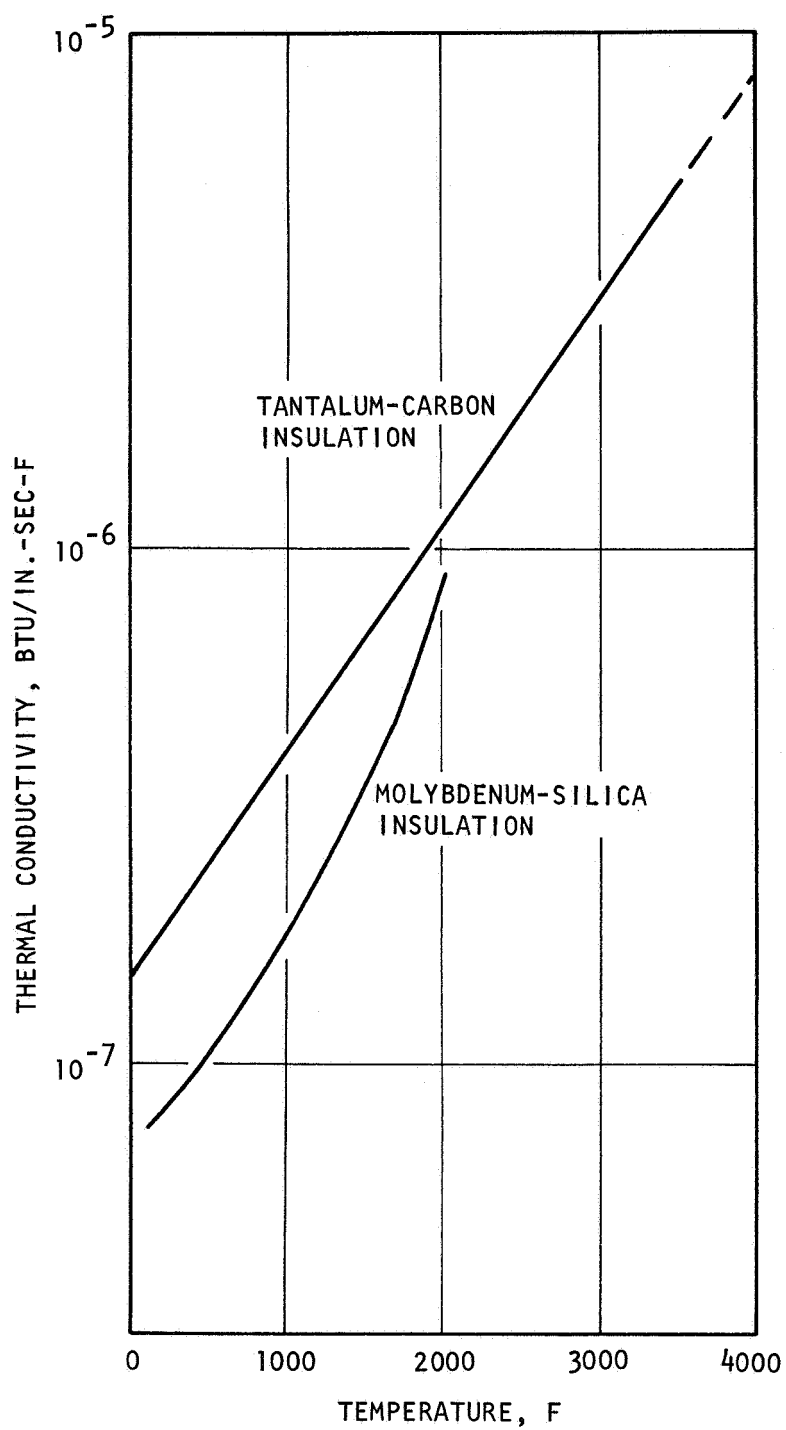


Figure 56. Thermal Conductivity of the Molybdenum-Silica and the Tantalum-Carbon Insulation as Used For Application Analysis

## ELECTRIC ANALOG OF THE HEAT TRANSFER IN A BURIED INSULATED ENGINE

The Thermal Analyzer Program (TAP II) solves transient heat transfer problems by computing temperatures of an analog network of lumped heat capacity nodes ( $C = V\rho C_p$ ) connected by conductors  $K = (A/d)k$  where

$V$  = volume concentrated in the node

$\rho$  = density

$C_p$  = specific heat

$A$  = cross sectional heat flow area

$d$  = distance between two nodes

$k$  = thermal conductivity

The theoretical basis for analog solutions of transient heat conduction problems can be found in Ref. 4. A TAP program description and input instructions are given in Ref. 5.

The model of the heat transfer in the system must comprise a sufficient number of nodes to yield a reasonably accurate solution without entailing an unreasonable expenditure of hand and computer calculation time. The time step used in the computer calculations is determined by the smallest characteristic response time ( $\theta_{\min} = V\rho C_p/k$ ) of any of the nodes. It is therefore important to make sure that the model includes no unnecessary fast-response elements. For instance, a thin engine wall subjected to intense convective heating during firing will heat rapidly. It may be expeditious to represent the wall as a steady-state node kept at the equilibrium temperature for the whole duration of the firing, rather than to include the starting transient of the engine wall. The error in the heat flow in the insulation due to this simplification was found to be negligible, while a very sizeable reduction in computer time was thus achieved. Of course, such an approach assumes that the engine wall equilibrium temperatures are known, either from experiment or from a more rigorous analysis of the engine operation during firing.

Four propulsion systems were considered.

1. NTO-MMH - Beryllium Chamber (Rocketdyne's RS-14)  
Chamber pressure 125 psia; thrust 300 pounds  
Interegen cooling. Firing duration 10, 100, and 1000 seconds
2. NTO-MMH - ColumbiuM Chamber  
Chamber pressure 100 psia; thrust 500 pounds  
Firing duration 600 seconds
3. Monopropellant Hydrazine - Haynes 25 Alloy Chamber  
Chamber pressure 200 psia; thrust 50 pounds  
Firing duration 600 seconds
4.  $\text{OF}_2/\text{B}_2\text{H}_6$  - Pyrolytic Graphite Chamber  
Chamber pressure 150 psia; thrust 2000 pounds,  $L^* = 20$   
Firing duration 600 seconds

The electric analog was somewhat different for every engine, and each case will be discussed in more detail under the appropriate heading, while only the general approach is given here. For each engine, the liner was broken into three sections: nozzle, chamber, and throat; or into two sections: nozzle and chamber, with the chamber section including the throat. Three sections are needed for interegen-cooled thick-walled engines. Two sections suffice for thin-walled engines.

An example of the analog network modelling the heat flow is shown in Fig. 57. Nodes 1 and 2 represent the engine walls. The heat capacity of the chamber walls and of the nozzle walls are lumped into these two nodes; they are connected by a conductor ( $K_1$ ) corresponding to axial heat conduction in the wall. If the temperatures in the liner during firing are known, nodes 1 and 2 are constrained to stay at given temperatures during firing by assigning the proper value to the initial temperature and an exaggerated value to the heat capacity (say  $10^{10}$  times the correct  $V\rho C_p$ ). The correct value of heat capacity is restored in the calculations of heat transfer during soakback. If liner temperatures are not known, or if the starting temperature transient in the liners occupies a





significant portion (or the totality) of the firing period, heat convection from combustion gas is simulated by introducing constant temperature nodes representing the combustion gas (nodes 3 and 40 of Fig. 57) and connectors (K30) and (K40) representing the convective term  $hA$ . The connectors are disconnected (multiplied by  $10^{-10}$ ) during the soakback period.

Whether convectively heated, or maintained at a given temperature, the engine walls lose heat by conduction to the insulation at all times. The insulation of thickness  $L$  was divided into five nodes and assumed to be enclosed in a 0.010-inch-thick steel case. The steel case was assumed to be separated from the spacecraft walls by a gap and to lose heat by radiation alone. The nozzle also lost heat by radiation to space (conductor K2).

Geometrically similar nozzles of expansion ratio of 40 and 80-percent optimum bell shape, were used with all four engines. The view factor from nozzle to space was obtained from a specialized computer program for Rocketdyne's RS-14 engine, and the product of the nozzle area and the local value of the view factor was averaged over the nozzle length. The average value of the radiation area times the view factor was then derived for the other engines by geometric scaling. In most cases the temperature dependence of the emissivity of the nozzle was not known, and a constant value was used. However, a temperature-dependent emissivity was used for the beryllium engine.

The radiation from the steel-encased insulation to the spacecraft walls was calculated assuming a view factor  $F = [1/\epsilon_1 + 1/\epsilon_2 - 1]^{-1} = 0.145$  corresponding to steel case and the spacecraft wall emissivities of 0.2 and 0.5, respectively. The spacecraft wall temperature was assumed to remain at 70 F. In all cases but one (columbia engine for which convective heating was simulated) the engine wall nodes were maintained at constant temperature during the firing period, while all the other temperatures increased from an initial value of 70 F; the temperature distribution

obtained at the end of the firing period became the initial temperature distribution for the soakback period. During the soakback, the engine wall nodes were free to cool by conduction to each other and the insulation, and by radiation, to space (K2). The specific heat value of each node was always calculated by the computer using the value of specific heat  $C_p$  at the temperature of the node, while the conductivity of the material in a conductor was computed for the arithmetic mean value of the temperatures of the nodes connected by the conductor. These computations were made possible by entering tables of the thermal property values vs temperature into the computer input data.

#### PRELIMINARY CALCULATIONS FOR THE COMPUTER INPUT

Input data for the TAP II program includes the thermophysical properties of the component materials, ( $\rho C$ ,  $k$  and  $\epsilon$ ) and geometric factor, viz., the volume attributed to each node, the area/distance ratio for each conductor, and the areas exposed to convection and/or radiation. The specific heat values and the thermal conductivities are entered in tables giving their temperature dependence. The geometric factors are calculated from engine dimensions. Use of the "arbitrary functions" section of the TAP II program permits the program to calculate the capacitances and conductances from the geometric factor and the tabulated values of the properties.

Calculation of the volumes of nodes representing the engine wall is straight foreword. Several ways of calculating the volume of the nodes are possible. For simplification, equal volumes are attributed to the  $N$  insulation nodes, so that:

$$V_i = (\pi \bar{D} l) (L/N) \quad (3)$$

where

$\bar{D}$  = mean insulation diameter = chamber or nozzle outer diameter +  $L$

$L$  = insulation thickness

$l$  = axial length of chamber or nozzle

Since calculations are usually conducted for several values of insulation thickness,  $L$ , it is convenient to introduce  $V_i/L$  instead of the volume in the geometric factor section, and tabulate  $\rho C_p L$  rather than  $\rho C_p$ . Thus, the geometric factor sections of the program input do not have to be changed when  $L$  is varied, only the tables are changed. Moreover, this arrangement permits compensation for the use of the mean diameter ( $\bar{D}$ ) value when  $L$  is changed. A correction factor can be introduced into the table of  $\rho C_p L$  if  $L/\bar{D}$  is sufficiently large to warrant the use of such a correction.

Similarly, the conductances in the insulation are entered as a geometric factor ( $\pi \bar{D} L N$ ) and a tabulated factor ( $k/L$ ), with a correction for the mean diameter increase introduced, when needed, in the tabulated values of ( $k/L$ ).

The steel shell volume was calculated for one value of  $L$ :  $\pi(\bar{D} + 2L) \times 1 \times 0.01$  and its variation with  $L$  was neglected. The heat content of a 0.01-inch-thick steel case is usually small compared to that of the insulation and its temperature increase is relatively small, so that the approximation does not introduce an appreciable error.

Convective conductances, (K30) and (K40) of Fig. 57, represent the heat input ( $h \times A$ ). The heat transfer coefficient  $h$  must be obtained from predictive equations, or from experimental data. The convection area is calculated from engine dimensions. The conductance  $hA$  may be entered as a gain into an appropriate section of the TAP II program (function 7 section) and multiplied by a time-dependent factor entered as a table. This factor is unity for the duration of the firing, and made very small, say  $10^{-10}$ , one second after firing ends. Convective heat input from the combustion gas is thus effectively suppressed during the soakback period.

Radiative heat transfer is handled by the TAP program through a specific function which calculates an approximate equivalent conductance between two nodes,  $i$  and  $j$ , which exchange heat by radiation.

$$K_{i,j} = R_{i,j} \left[ (T_i + 460)^2 + (T_j + 460)^2 \right] (T_i + T_j + 920)$$

where  $R_{i,j}$  must be obtained by hand calculation:

$$R_{i,j} = \sigma A_i F_{i,j}$$

$\sigma$  is the Stefan-Boltzman constant

$$(0.335 \times 10^{-14} \text{ Btu/in.}^2\text{-sec-F}^4)$$

$A_i$  is the radiative area of node  $i$ , and  $F_{i,j}$  the view factor from  $i$  to  $j$ .

The radiation from the steel case to the spacecraft wall is adequately represented by the parallel plate formula

$$A_i F_{ij} = A_i \left[ \frac{1}{\epsilon_i} + \frac{1}{\epsilon_j} - 1 \right]^{-1}$$

The view factors from the nozzle inner surface to space were obtained by use of a computer program as applied to the RS-14 engine. Since all the engines analyzed were assumed to have geometrically similar nozzles, geometric scaling of the area yielded the AF values for all nozzles.

#### FORMAT OF DATA INPUT FOR TAP II

There are many ways of arranging the computerized calculations, and the ones adopted here are not necessarily the best for all cases. On the basis of previous experience, arbitrary functions and tabulated properties for all capacitances and all conductances were used. The only exceptions were the radiative conductances, for which the radiation function was used.

The conductances and capacitances are entered uniformly as having a value of 1 in the first two blocks of the program. Nodes remaining at a constant temperature (space and spacecraft wall) are given a negative capacitance. After that the geometric factor for all conductances except the radiative ones, and all nodes other than the constant temperature ones, are entered in the arbitrary functions block. The gain assigned to each node represents the geometric factor. The appropriate multiplying thermal property ( $\rho C_p, k$ ) or time dependence factor (for convective heating) is entered as a table, and is referenced by its number. The numbered tables form the last block of the program. The program prints out, at specified time intervals, the temperature of any node and the value of any conductance, as requested. The heat received by the spacecraft from the engine can be calculated from the value of the conductances representing radiation from the stainless steel insulation shell to the spacecraft wall, and the shell temperatures.

A slightly different approach was used for every engine analyzed, in an effort to adapt the procedure to the problem at hand.

## EXAMPLES OF APPLICATION OF ANALYTICAL MODEL

### Beryllium Engine Description

Propellants:  $N_2O_4$ -MMH

Thrust: 300 pounds

Dimensions:

Chamber pressure: 125 psia

Throat diameter: 1.354 inches

Chamber diameter: 3.000 inches

Nozzle: expansion ratio: 40, 80-percent  
optimum bell shape

Interegen cooled chamber walls

Firing duration: 10, 100, and 1000 seconds

## Engine Operation

A complete thermal analysis based on experimental data and using a 400-node network was available for a 196-second firing followed by soakback. At the end of firing the liner temperatures were still rising rapidly. Some of the results are shown graphically in Fig. 58, others were given in printout form only. During the tests, the engine insulation consisted of a 1/2-inch thick layer of Min-K; heat penetration into the insulation during the first 100 seconds of the firing was minimal. It was negligible in the first 10 seconds; at the end of 10 seconds the engine wall temperature did not reach 600 F at any location, nor did it reach 250 F at the backwall surface. Clearly, the insulation requirements for 10-second firings are trivial. For the 100-second firing cycle, the initial temperature distribution for the soakback period was taken from the detailed firing analysis, and the firing portion was not included in the insulation analysis.

No experimental data were available for a 1000-second firing duration, and substantial heat penetration into the insulation during the lengthy firing was to be expected. Extrapolation of the temperature-time curves from 196 seconds to 1000 seconds was not advisable. Such an extrapolation would show higher than acceptable engine wall temperatures. The engine operation, i.e. mixture ratio and/or injector design, will have to be modified to permit long firings. Therefore, to analyze the insulation requirements for the long-firing engine, it was assumed that the engine wall temperatures stabilized at acceptable values; viz: 400 F at the interegen cooled chamber wall, 2000 F at the throat, and 1600 F on the nozzle. The alternative scheme of simulating convective heating, was not used because of the difficulty of properly simulating interegen cooling in a network with only three nodes representing the thick engine walls.

05/22/68

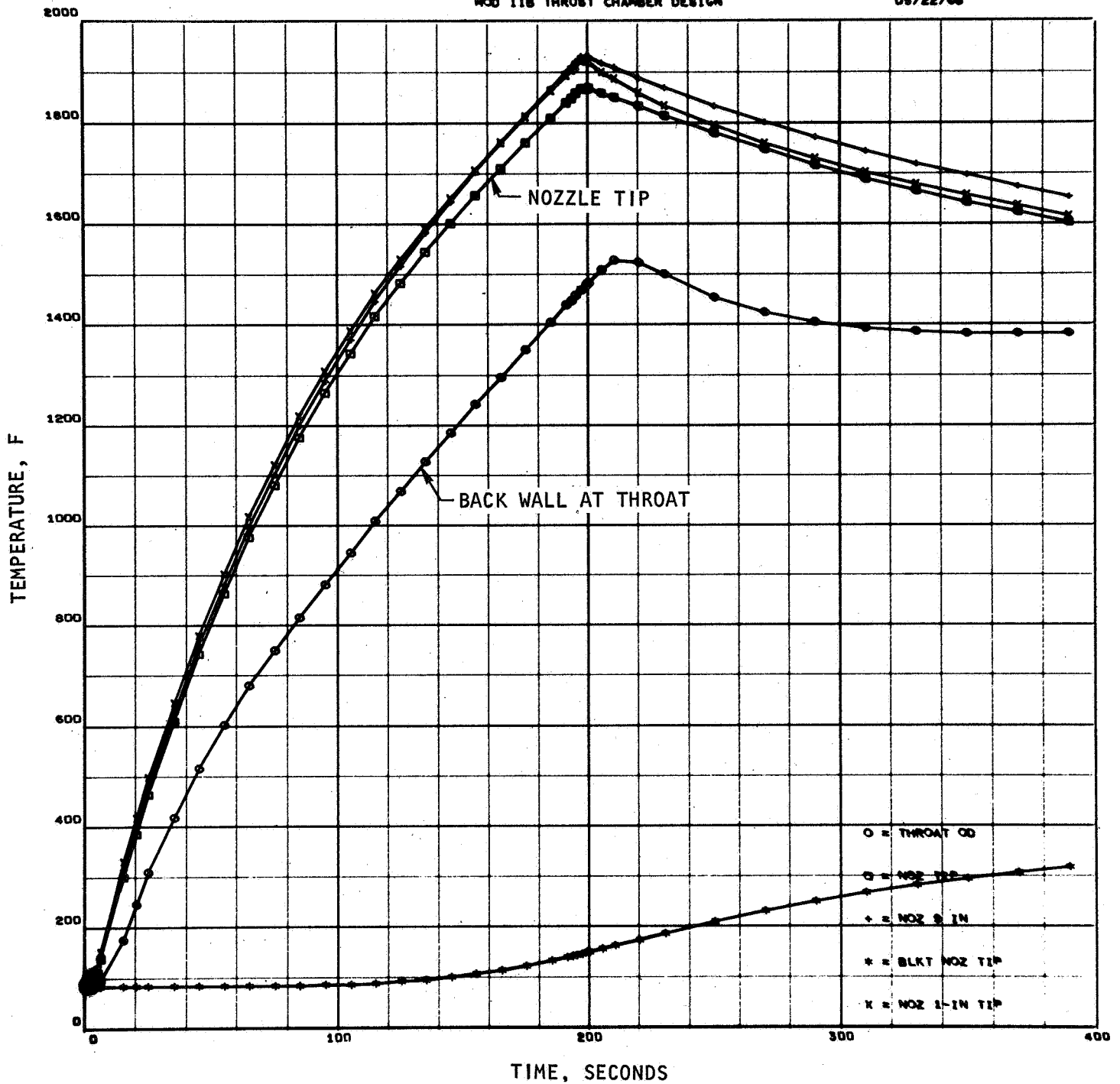


Figure 58. Thermal Analysis of the RS-14 Engine for a 196-Second Firing



## Insulation

The molybdenum-silica multilayer insulation was chosen for the beryllium engine; it was assumed that backwall temperatures never exceed 2000 F.

## Analog Network and Data Input

The analog network shown in Fig. 59 was used for both the 100-second and the 1000-second firing duration cycles. For the 100-second firing cycle, the calculations began at the end of firing with an initial temperature distribution obtained from an engine performance analysis. For the 1000-second firing, the calculations were made for the firing duration (case 1) followed by soakback (case 2). In case 1, the weights of the engine wall nodes were multiplied by a factor of  $10^9$  to impose a constant temperature upon them. This factor was removed for the soakback period.

Several features distinguish the approach taken for the RS-14 engine.

1. A weight analysis was available. Therefore, weights rather than values of nodes were used and  $C_p$  (not  $\rho C_p$ ) entered into the tables. The engine walls were represented by three nodes (chamber, throat, and nozzle) to take into account the low chamber wall temperatures characteristic of intergen cooling, and the high heat capacity of the much hotter throat section.
2. The thermal analysis of the RS-14 engine for a 196-second firing included a table of beryllium emissivity vs temperature. The variation was quite large,  $\epsilon = 0.1$  for -100 F,  $\epsilon = 0.5$  for 2800 F. A correct value of  $K4 = \sigma A_3 F_3 (T_3 + 460)^4$  is obtained by tabulating  $\epsilon (T_3 + 460)^3$  versus  $\bar{T} = 1/2 (T_3 + 460)$  and entering  $(A_3 F_{3,4})$  as the geometric factor in the arbitrary functions section.
3. Axial conduction in the steel shell was included (K8 and K9 of Fig. 59). This refinement was not really needed since the temperature gradients in the steel shell were not large.

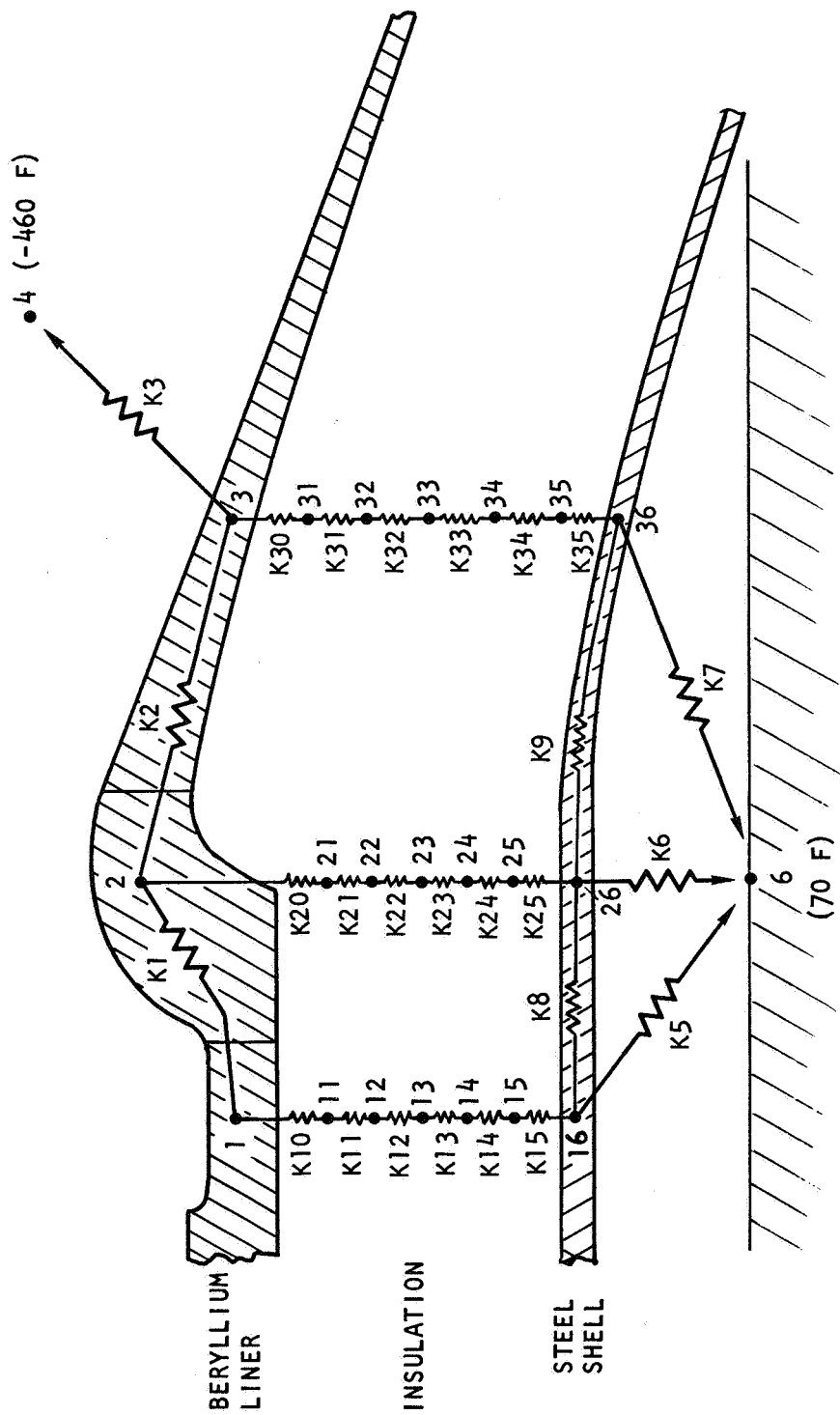


Figure 59. Analog Network for the RS-14 Beryllium Engine

4. For the 100-second firing, only the soakback period was analyzed.
5. Comparison of heat transfer for varying insulation thicknesses was not made. A 3/8-inch insulation thickness for the 100-second firing, and a 1-inch thickness for the 1000-second firing were chosen to conserve machine time.

#### Results of Computations

Figures 60 and 61 show the temperatures of the steel shell and the heat flux from engine to spacecraft for the two firing durations. Temperature distribution profiles in the nozzle insulation at various soakback times are given in Fig. 62 and 63. Radiation to space from the nozzle surface is small compared to the amount of heat stored in the thick beryllium engine walls. A long time is required for cooling; hence the computations must be run for a long time. Therefore the soakback was not extended to the time when heat flux or total heat load maximums occurred.

#### Columbium Engine Description

Propellants:  $N_2O_4$  - MMH

Thrust: 500 lb<sub>f</sub>; Chamber pressure: 100 psia

Firing duration: 600 seconds

In the absence of a developed engine design, it was decided to analyze an engine design geometrically similar to the RS-14 engine, scaled to produce 500 lb<sub>f</sub> thrust at 100 psia instead of 300 lb<sub>f</sub> thrust at 125 psia. The scaling factor found by prorating the throat area to account for the lower chamber pressure and the higher thrust was 1.5. The engine dimensions thus obtained were:

Throat diameter: 2 inches

Chamber diameter: 4.5 inches

Nozzle expansion ratio: 40; 80 percent optimum bell shape

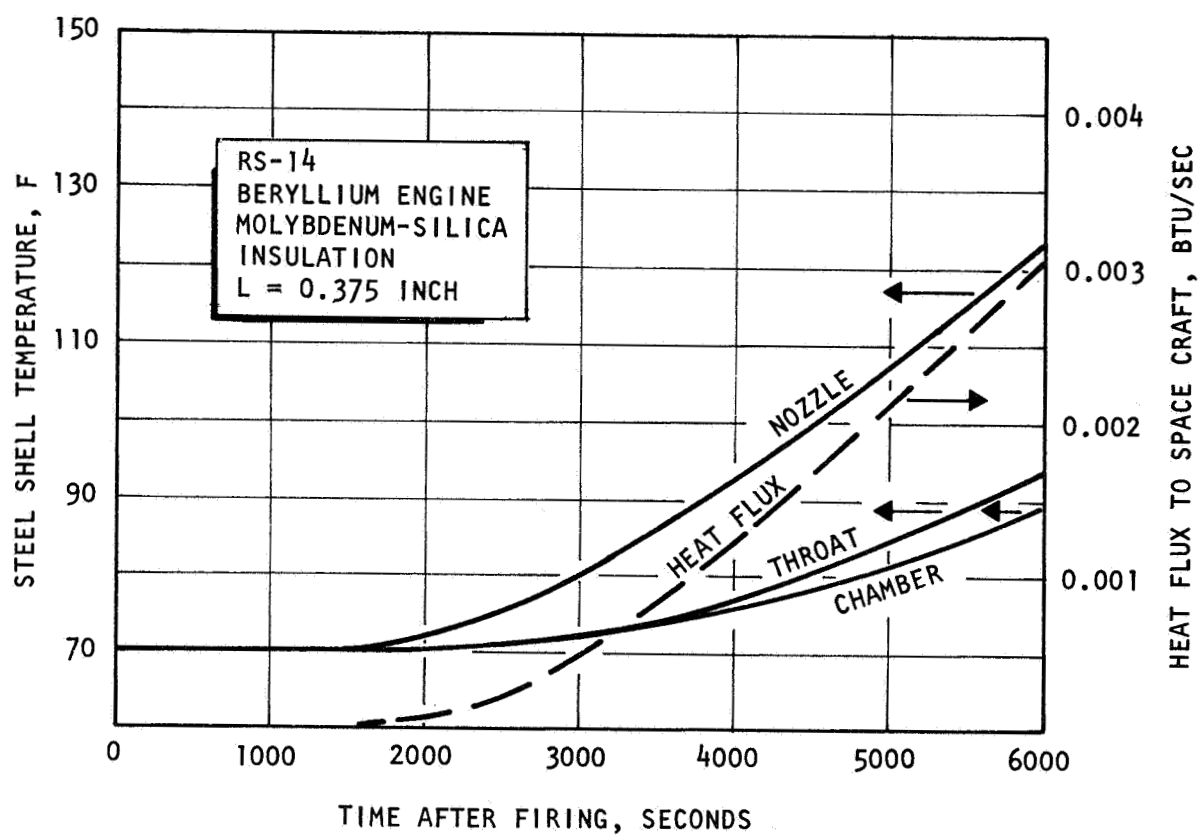


Figure 60. Steel Shell Temperature and Heat Flux to Spacecraft Soakback (RS-14 Engine, 100-Second Firing) (Beryllium Engine)

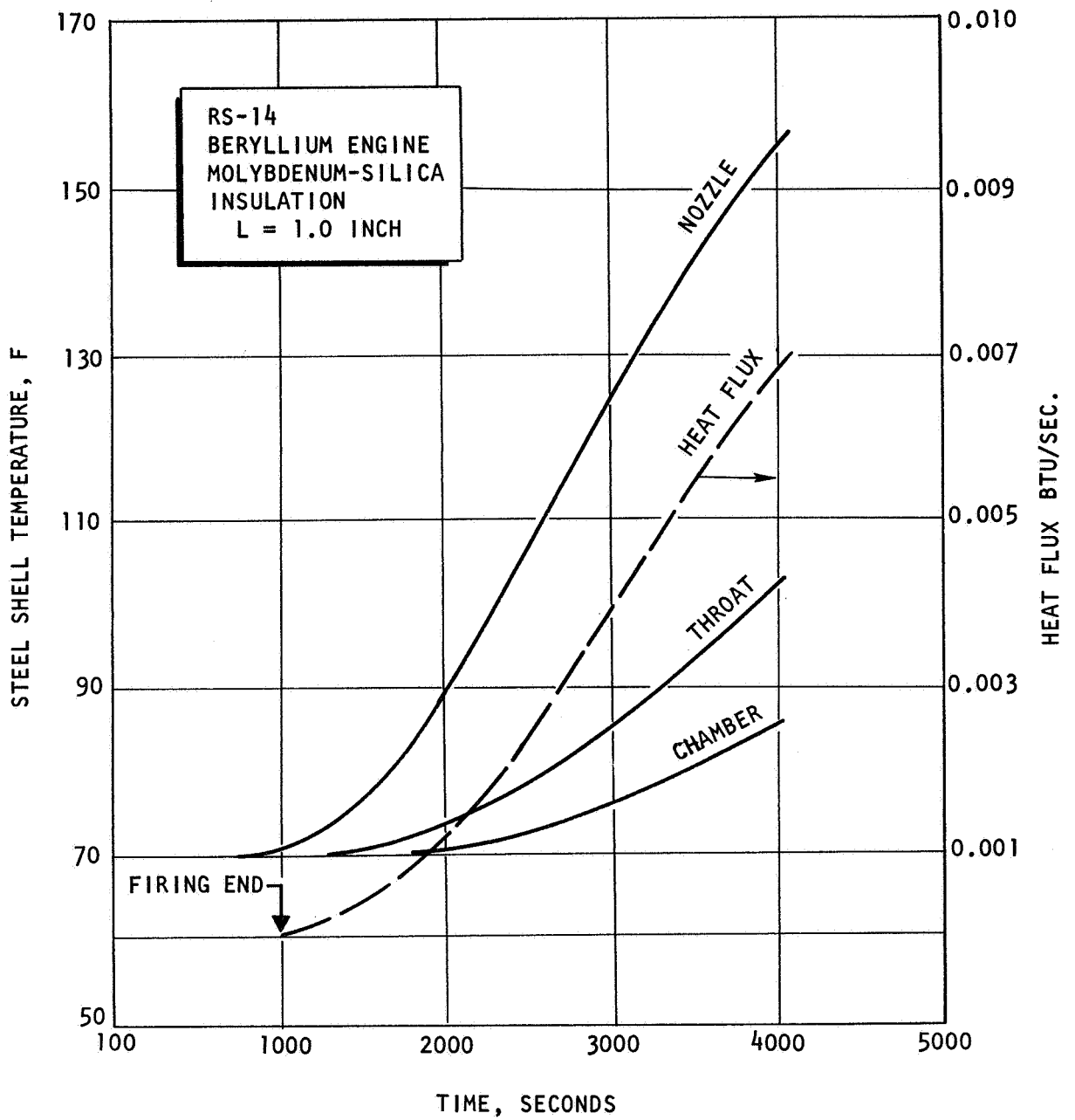


Figure 61. Steel Shell Temperature and Heat Flux to Spacecraft  
(RS-14 Engine, 1000-Second Firing)  
(Beryllium Engine)

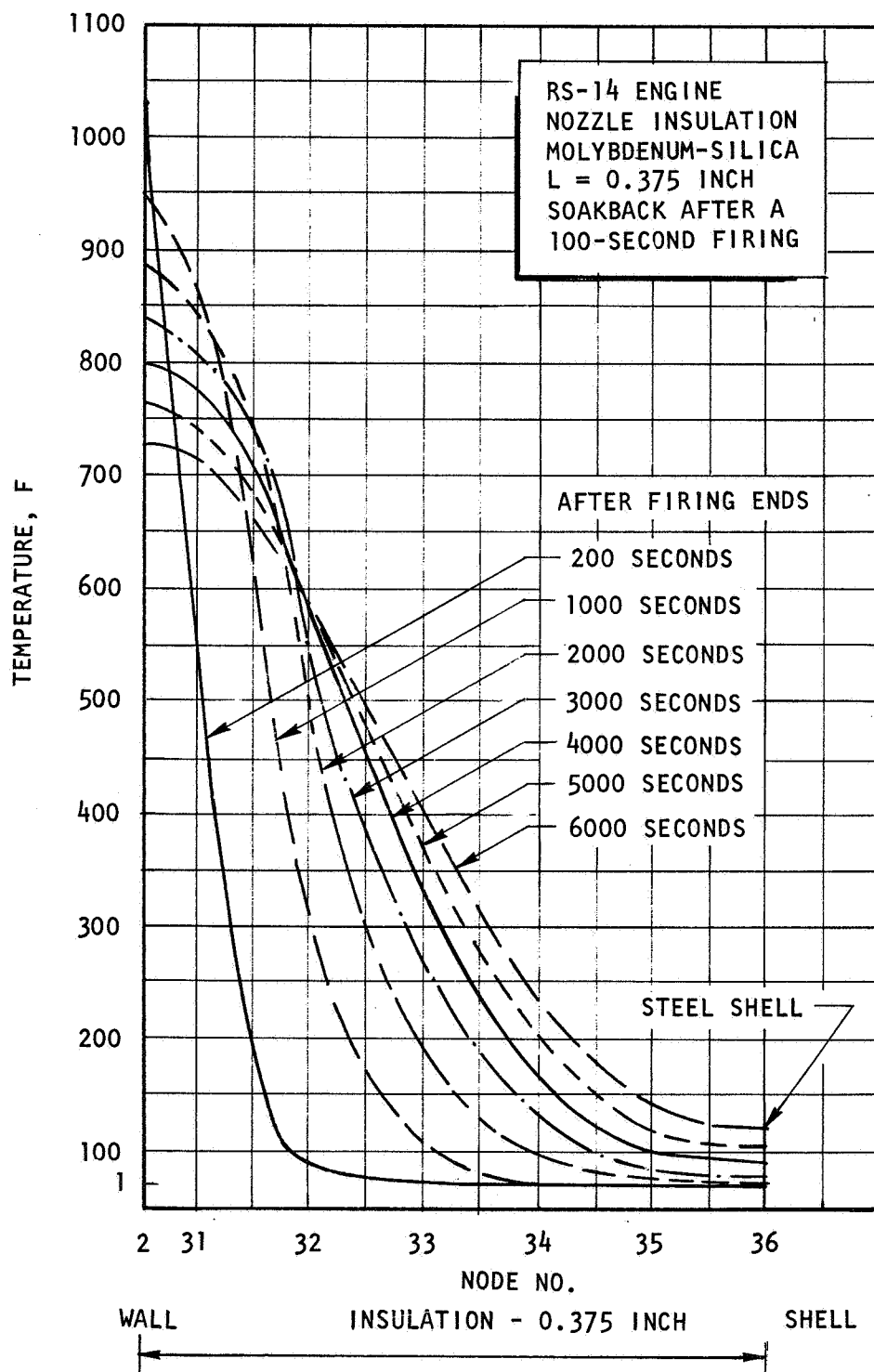


Figure 62. Temperature Profiles in the Nozzle Insulation  
After a 100-Second Firing (RS-14 Engine)  
(Beryllium Engine)

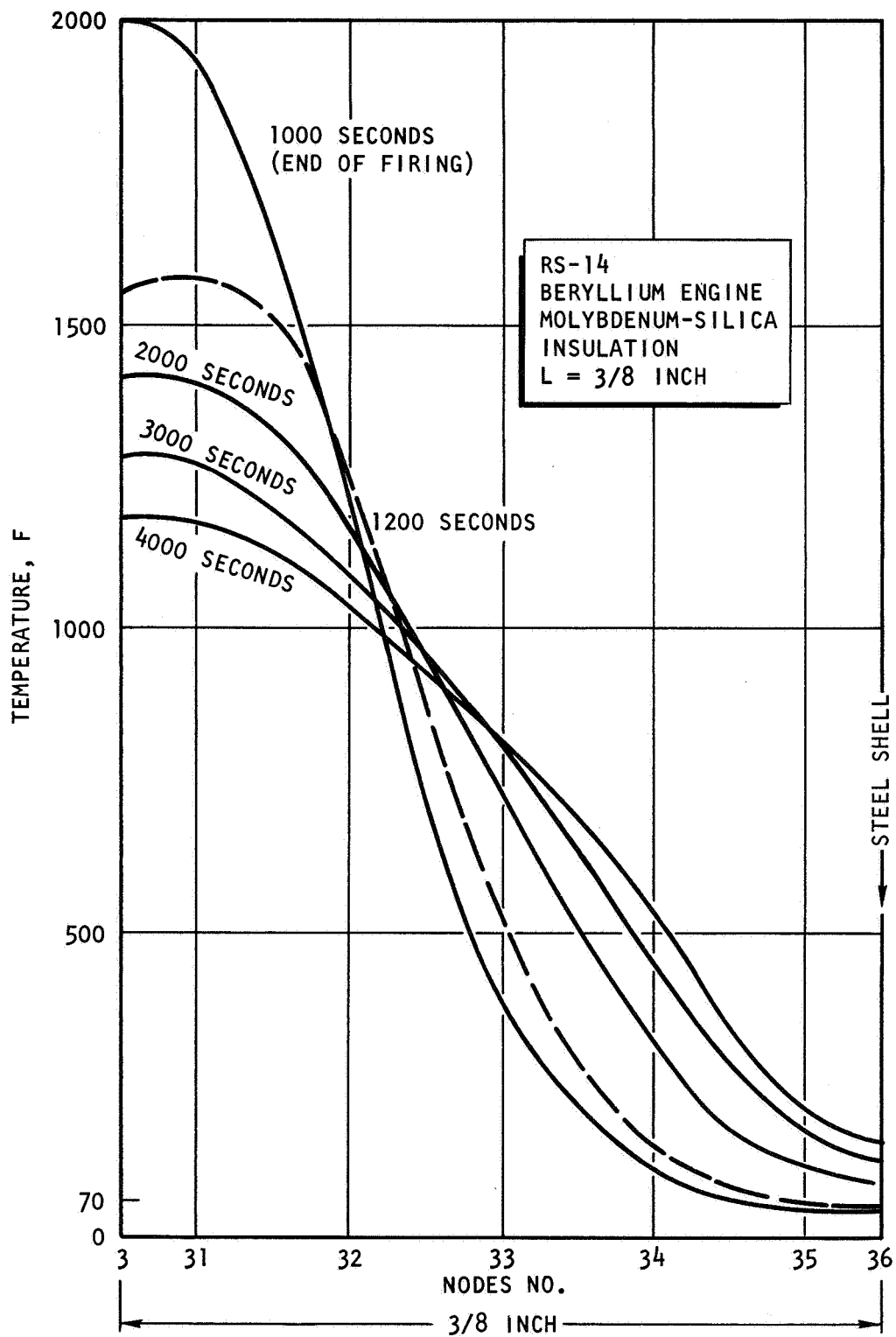


Figure 63. Temperature Profiles in the Nozzle Insulation  
Firing Duration: 1000 Seconds  
(Beryllium Engine)

### Engine Operation

Columbium is limited to operation below 3000 F by creep stresses in the nozzle. Thin walls can be used if the creep-limited temperature is not exceeded, since columbium is a high-strength material.

An average wall thickness of 0.4 inch for the combustion chamber and throat section, and 0.15 inch for the nozzle are acceptable realistic values. Film cooling of chamber walls was assumed to maintain the chamber wall temperature at 400 F during firing, while the nozzle was at 3000 F.

### Insulation

The tantalum-carbon insulation can withstand 3000 F and was therefore chosen.

### Analog Network and Data Input

The analog network is shown in Fig. 64. Nodes 1 and 2 represent the lumped heat capacity of the chamber and throat walls, and of the nozzle, respectively. Conductor K1 is the axial conductance of the walls. Convective heating during firing is represented by the constant temperature nodes 5 and 6 and the conductors K5 and K6. Node 5 is held at 400 F and the conductance K5 is large, so as to simulate the high heat conductance between the engine wall and the fuel which is wetting the wall in film cooling. After the firing, the conductance K5 is divided by a factor  $10^{10}$  to effectively eliminate convective heat exchange.



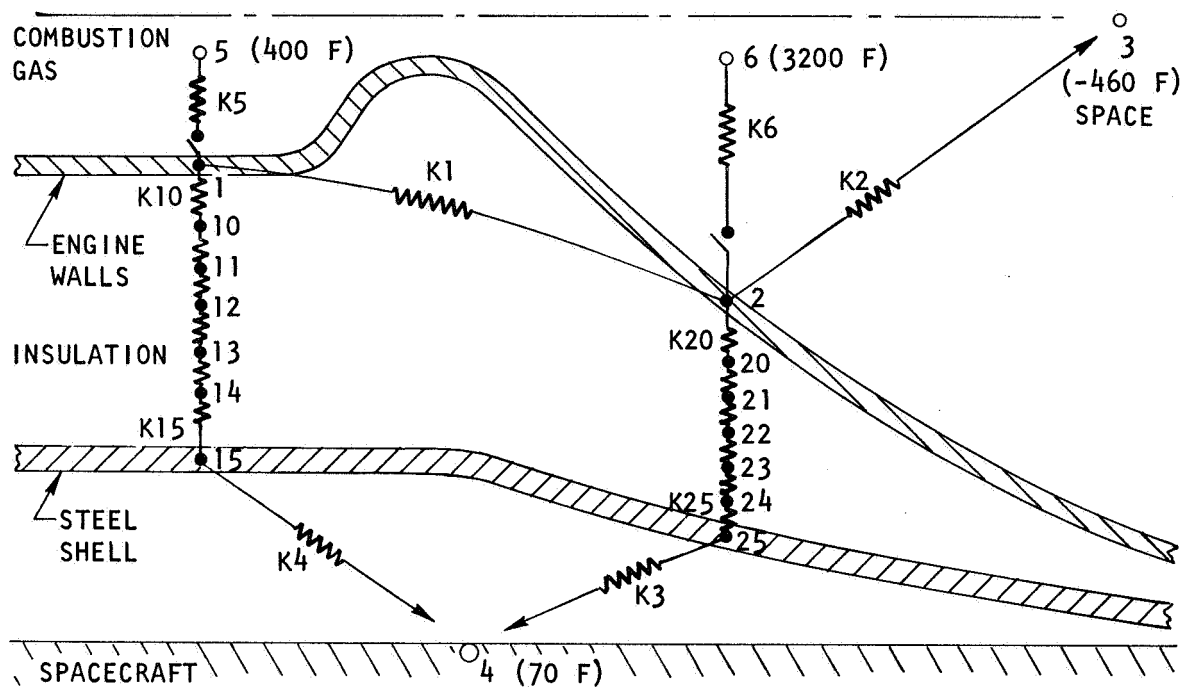


Figure 64. Analog Network for Heat Transfer in the Columbiu Engine

Similarly, the constant temperature of node 6 is set to 3200 F and the convective conductance  $K_6$  is chosen so as to yield a temperature of 3000 F in the nozzle during firing. After firing, the conductance  $K_6$  is divided by  $10^{10}$  to effectively remove convective heat transfer. The columbium emissivity was assumed to be 0.6, and the radiation function allowed to calculate  $K_2$ .

Except for the introduction of the convective heat transfer with time-dependent convective conductances, the data input does not differ from the RS-14 engine data. The use of convective heating with a switch-off at the end of firing makes it possible to examine firing and soakback as one case. Three cases were examined corresponding to insulation thicknesses of 1 inch, 1/4 inch and 1/8 inch.

The steel shell heat content was calculated for  $L = 1.0$  and not corrected for the smaller values of  $L$ . Axial conduction in the steel shell was neglected.

## Results

The temperature rise in the steel shell enclosing the insulation is given in Fig. 65. Clearly, a 1-inch insulation is too thick. The choice between 1/4 and 1/8 inch thickness must be made on the basis of heat flux to the spacecraft (Fig. 66). An increase of insulation thickness from 1/8 to 1/4 inch decreases the maximum heat flux by nearly an order of magnitude and the total heat load by a factor of approximately 3.

Temperature variation with time and temperature profiles in the nozzle insulation at different times for a 1/4-inch insulation thickness are given in Fig. 67 and 68, respectively. Since the heat stored in the thin engine walls is not large, radiation to space quickly cools the nozzle walls, while the heat stored in the insulation leaks out more slowly.

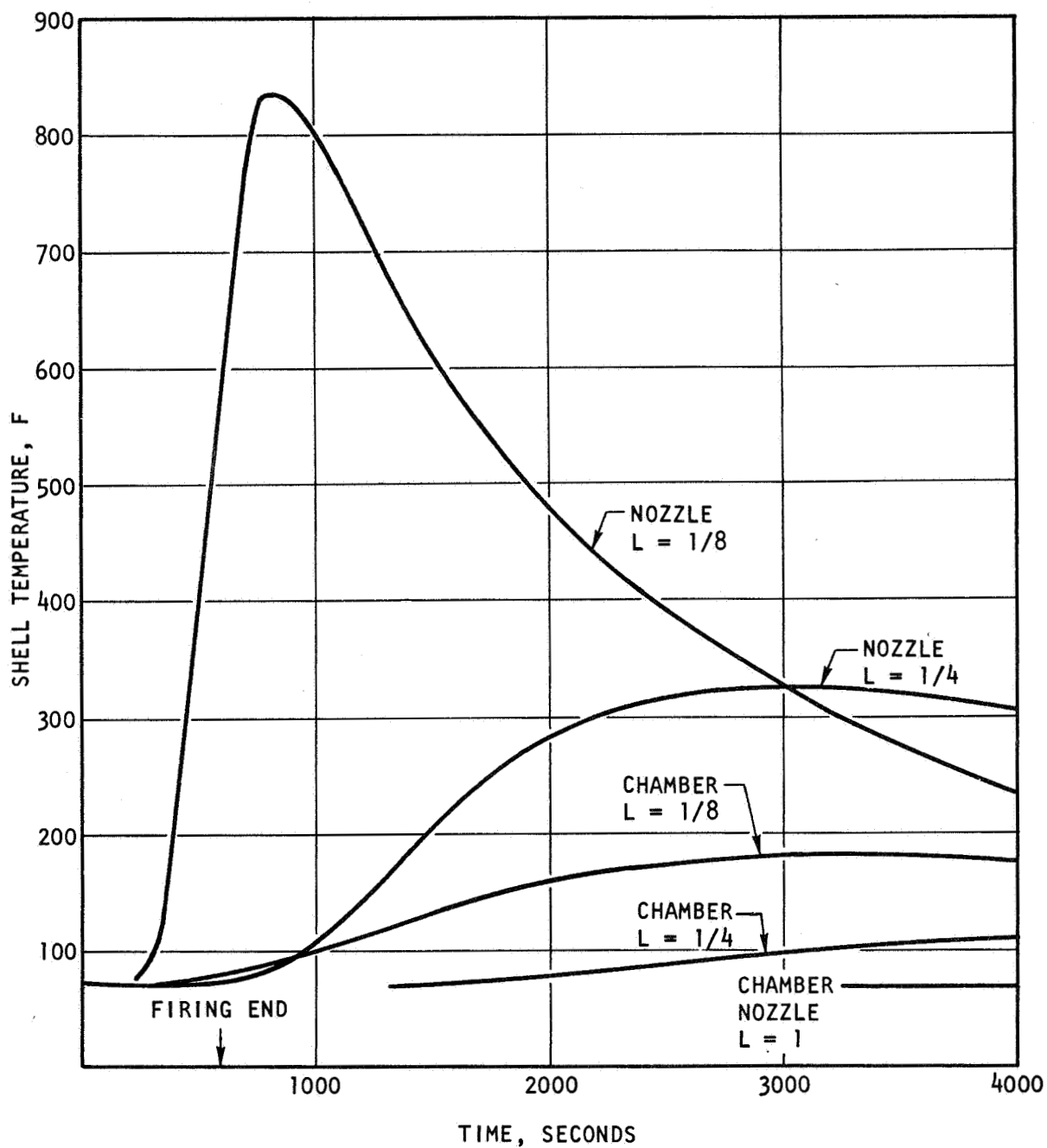


Figure 65. Steel Shell Temperatures for the Columbum Engine (Tantalum-Carbon Insulation)

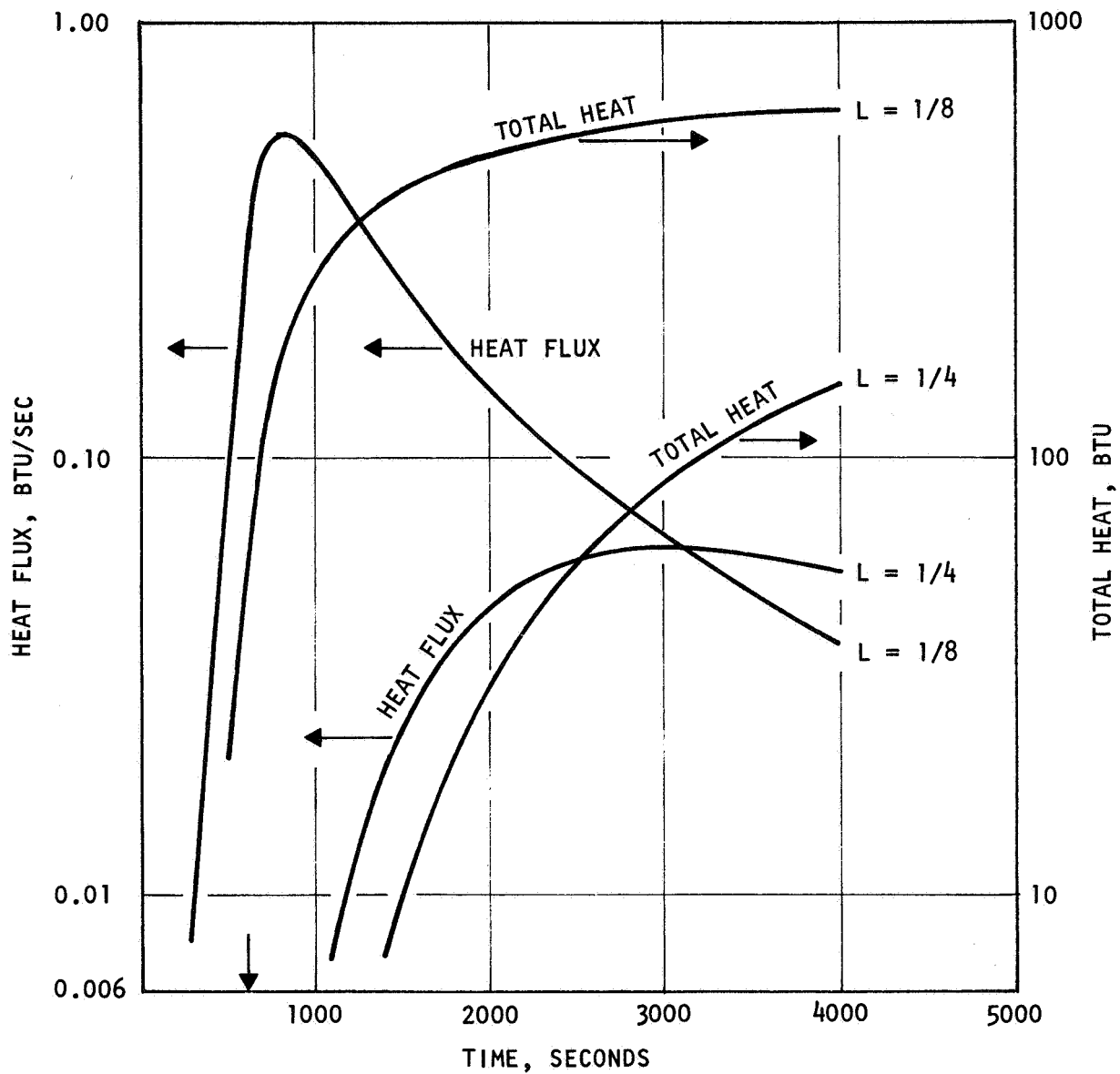


Figure 66. Heat Flux and Total Heat Received by Spacecraft Columbum Engine

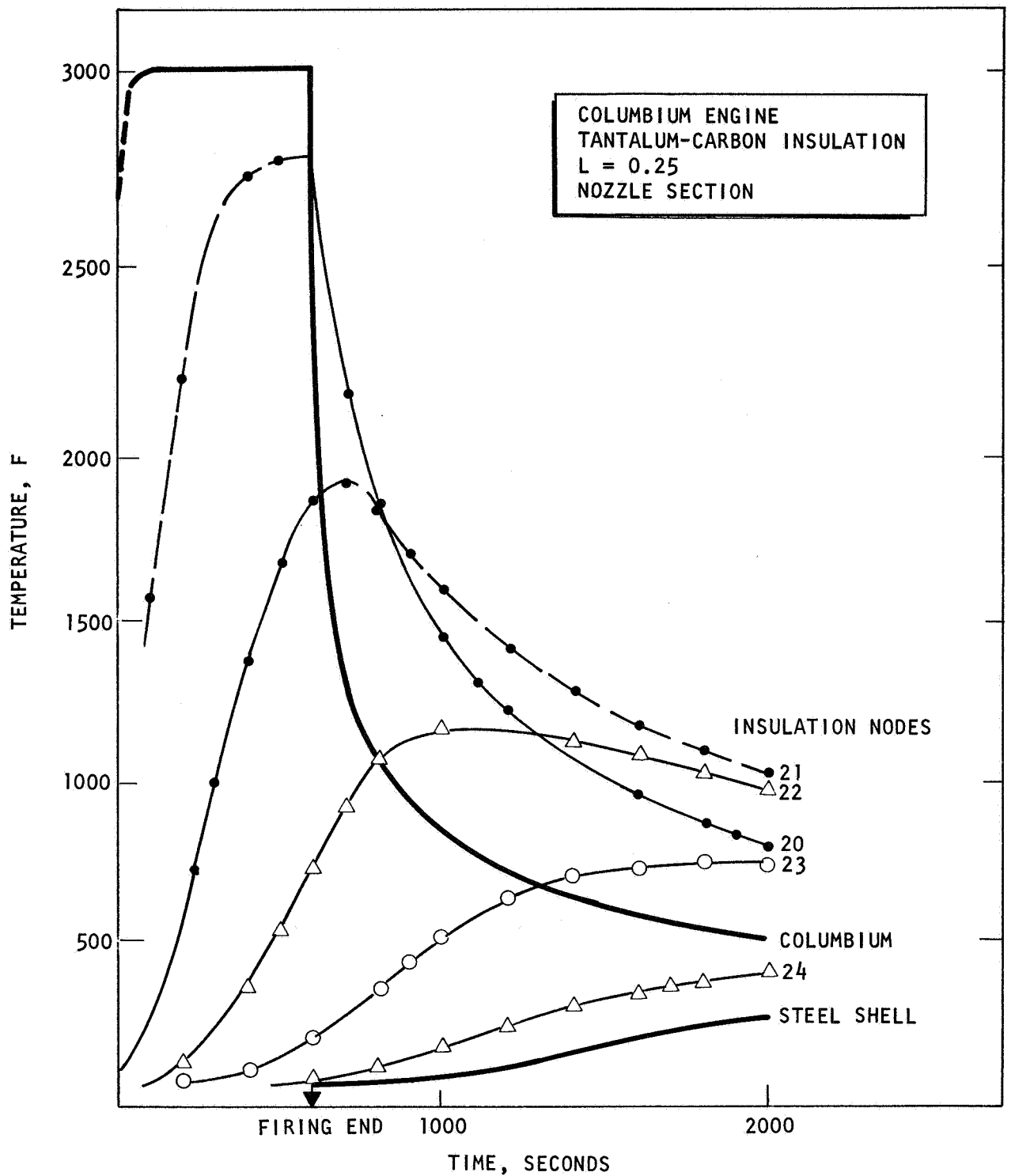


Figure 67. Temperature-Time Variations in the Nozzle Insulation of a Columbiu Engine

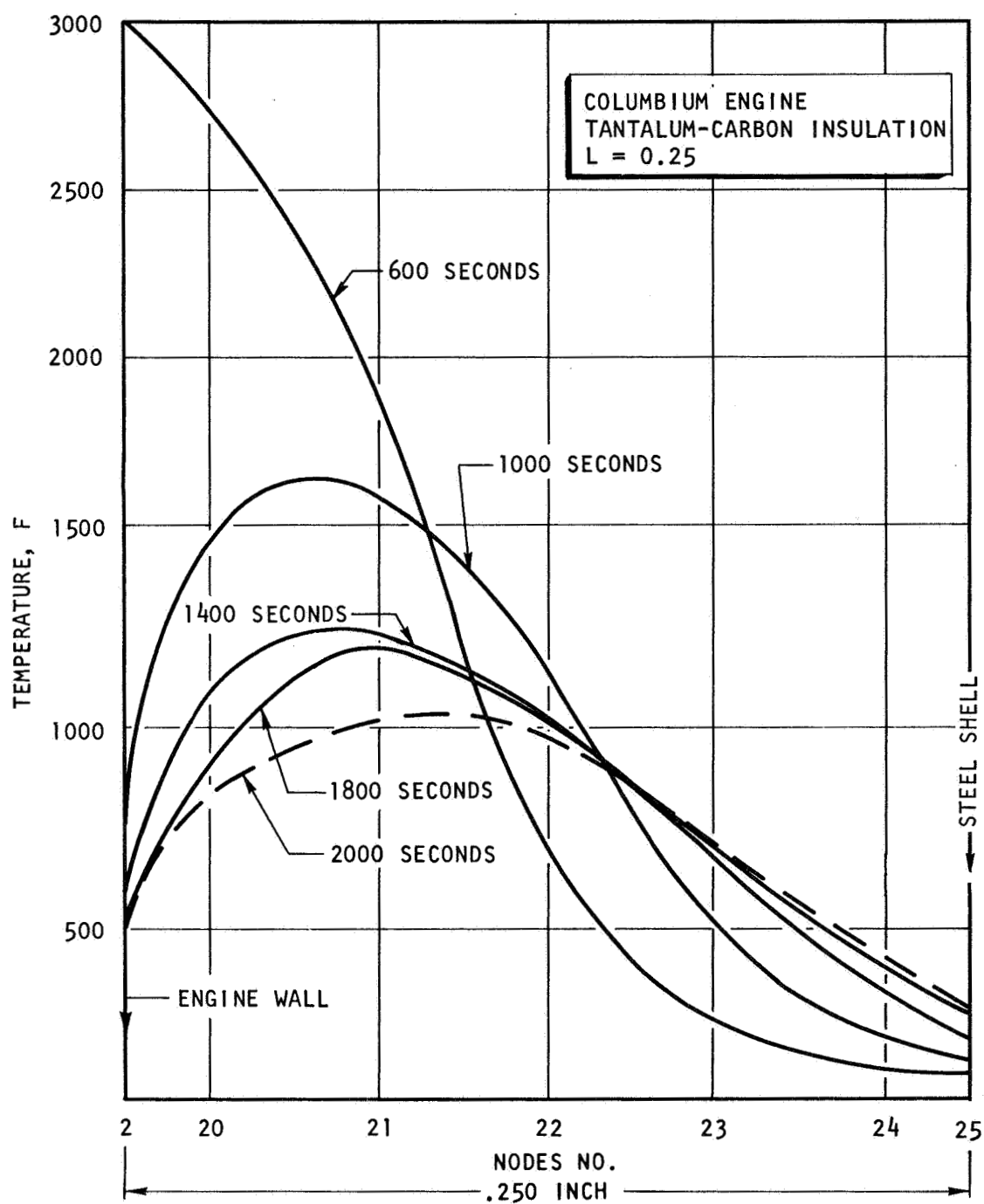


Figure 68. Temperature Distribution in the Nozzle Insulation of a ColumbiuM Engine

## Mariner '69 Description

Monopropellant: hydrazine

Catalyst: 1/8- by 1/8-inch cylindrical alumina pellets

Void fraction: 0.335

(Shell 405 spontaneous catalyst)

Thrust: 50 lb<sub>f</sub>; Chamber pressure 200 psi

Firing duration: 600 seconds

Design: See drawing (Fig. 69).

Throat diameter: 0.425 inch

(The throat diameter could not be obtained with precision from the drawing. It was scaled from the 100 lb<sub>f</sub> Rocket Research engine (Ref. 6)).

Catalyst bed diameter: 2.45 inches

Catalyst bed length: 2.01 inches

Engine walls: Haynes alloy 25

## Engine Operation

The catalyst bed is the site of exothermic decomposition of the hydrazine. The average temperature of the catalyst bed is about 2000 F (Ref. 7). The average gas temperature in the engine proper is somewhat lower. A steady temperature of 2000 F for the catalyst bed and of 1900 F for the engine walls was assumed throughout the firing period. After the firing, heat will radiate from the nozzle to space, and also from the catalyst-bed end plate to space. The heat stored in the catalyst pellets constituted a major portion of the total heat contained in the system at the end of firing. Radiation from the end plate to space was therefore taken into account even though the view angle from plate to space through the throat opening and nozzle is not large.

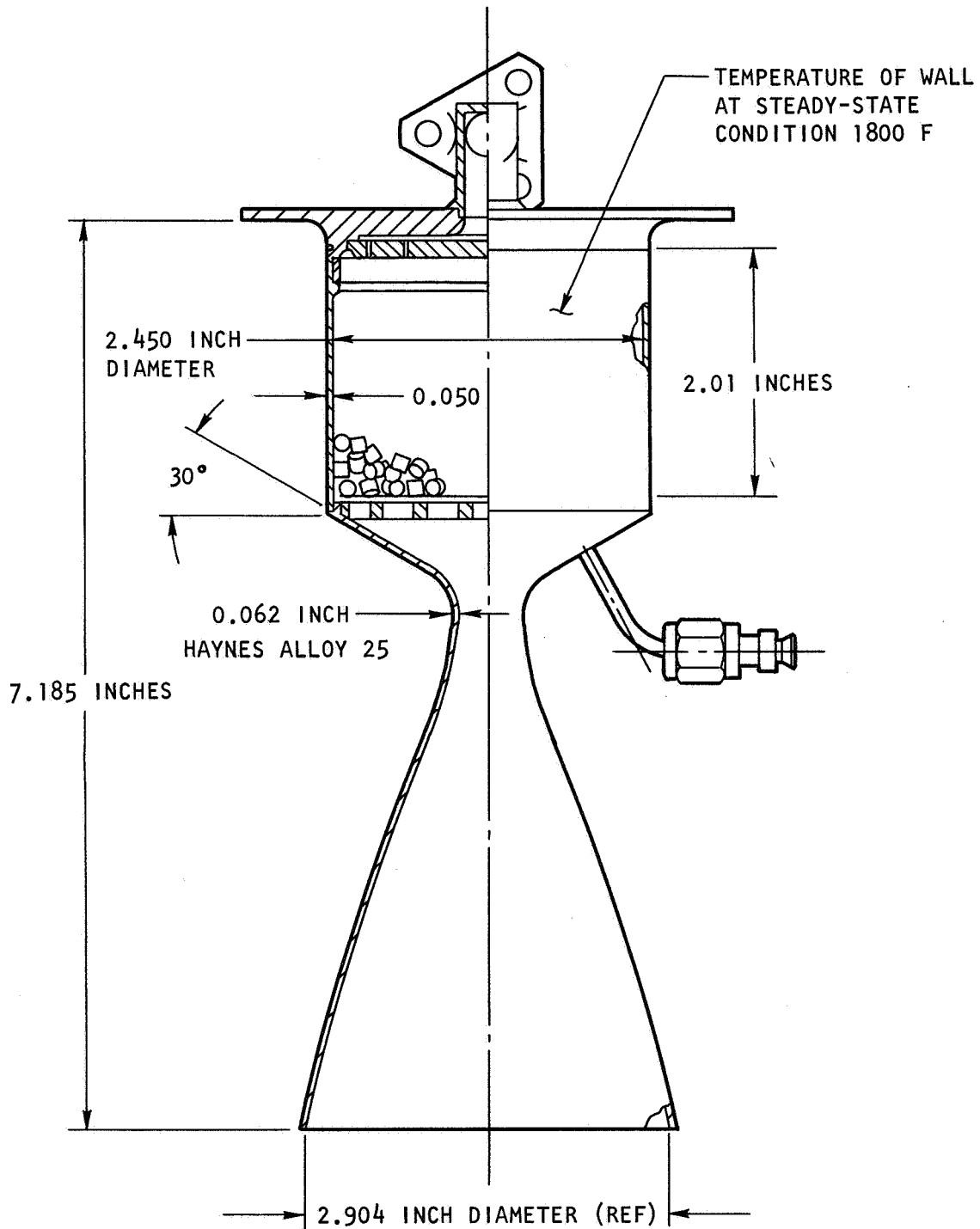


Figure 69. Mariner 69 Engine (Ref. 7)



## Insulation

The molybdenum-silica insulation was chosen since the engine wall temperature does not exceed 2000 F.

## Analog Network

The analog network is shown in Fig. 70. Node 1 contains the heat capacity of the whole catalyst bed. Node 2 represents the heat capacity of the Haynes alloy chamber walls; node 3 the heat capacity of the throat sector and node 4 that of the nozzle walls. Nodes 9 through 14 contain the heat capacity of the insulation enclosing the chamber and throat, while nodes 19 through 24 represent the insulation enclosing the nozzle. The mean diameter of the nozzle insulation is larger than the mean diameter of the chamber and throat insulation. Nodes 2 and 3 were not combined into one node, as was done for the columbium engine, to show that temperature variations in the engine walls can be taken into account without going to three insulation sections, as was done in the thick-walled beryllium engine. As catalyst rather than gas occupies the combustion chamber, the following calculations had to be performed to obtain the information needed for the data input to TAP II:

The radiative conductance from the catalyst and plate to space

$$R_{1,5} = \sigma \epsilon (AF)_{1,5}$$

was calculated assuming  $\epsilon = 0.8$  (a metal mesh at high temperature has a high emissivity) and using the view factor for two parallel disks separated by a distance  $h$

$$AF_{1,5} = \frac{\pi r^2}{2} \left\{ \frac{h^2 + 1}{r^2} + 1 - \left[ \left( \frac{h^2 + 1}{r^2} + 1 \right)^2 - \frac{4}{r^2} \right]^{1/2} \right\}$$

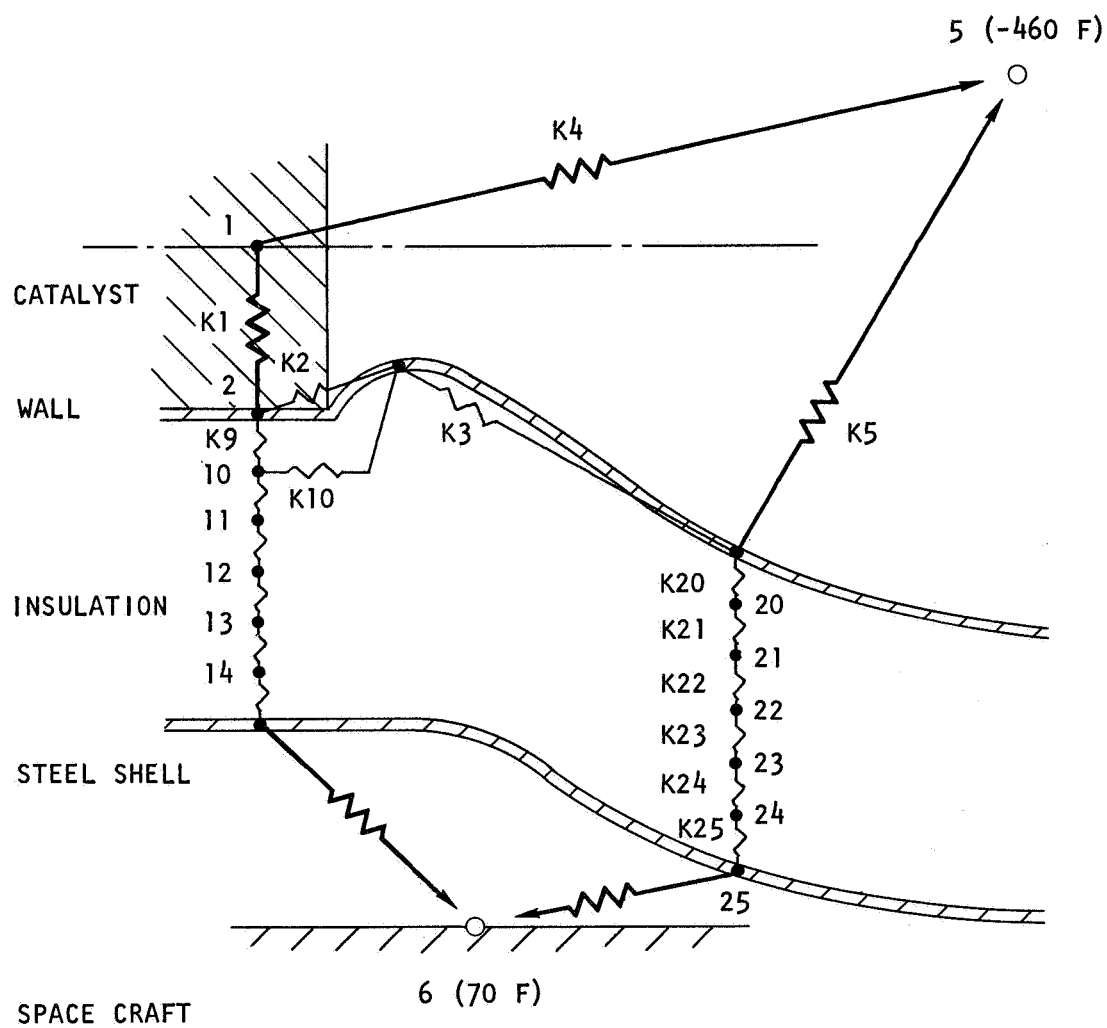


Figure 70. Analog Network for the Mariner Engine

where  $r$  is the throat radius (Ref. 8).

The resultant conductance was rather low:  $R_{1,5} = .3 \times 10^{-15} \text{ Btu/sec-R}^4$ .

The equivalent thermal conductivity of the catalyst bed during soakback was calculated by the method given by J. M. Smith (Ref. 9). The equivalent conductivity includes conduction inside a pellet, radiation between pellets, and conduction through points of contact and through stagnant gas. The equations developed in Appendix B of Ref. 9 were applied with the thermal properties of aluminum oxide taken from Ref. 1. The equivalent conductivity was found to be rather low, about  $0.2 \times 10^{-4} \text{ Btu/in.-sec-F}$ , and its variations with temperature were not taken into account because it was believed that such a refinement is out of proportion relative to the accuracy of the equivalent conductivity calculation. However, the variations of the specific heat capacity with temperature were taken into account.

#### Results of Computations

Three insulation thicknesses were investigated:  $1/2$ ,  $3/8$ , and  $1/4$  inch. Figure 71 shows the temperatures of the steel shell enclosing the insulation at the chamber and nozzle, while heat flux and total heat input to the spacecraft are given in Fig. 72. The temperature profiles in the chamber and nozzle insulations for a  $1/2$ -inch-thick insulation are given in Fig. 73 and 74. Radiation from the nozzle to space cools the nozzle insulation in a reasonable time. The chamber insulation, however, stays hot for a long time. The two paths for heat flow from chamber insulation to space have low conductance, inasmuch as the engine walls are made of thin, low-conductivity material, and the view factor for catalyst-bed to space is small.

Most of the heat stored in the system at the end of firing is stored in the catalyst bed. Thus, the chamber insulation keeps receiving heat from the catalyst bed slowly transmitting it to the spacecraft long after

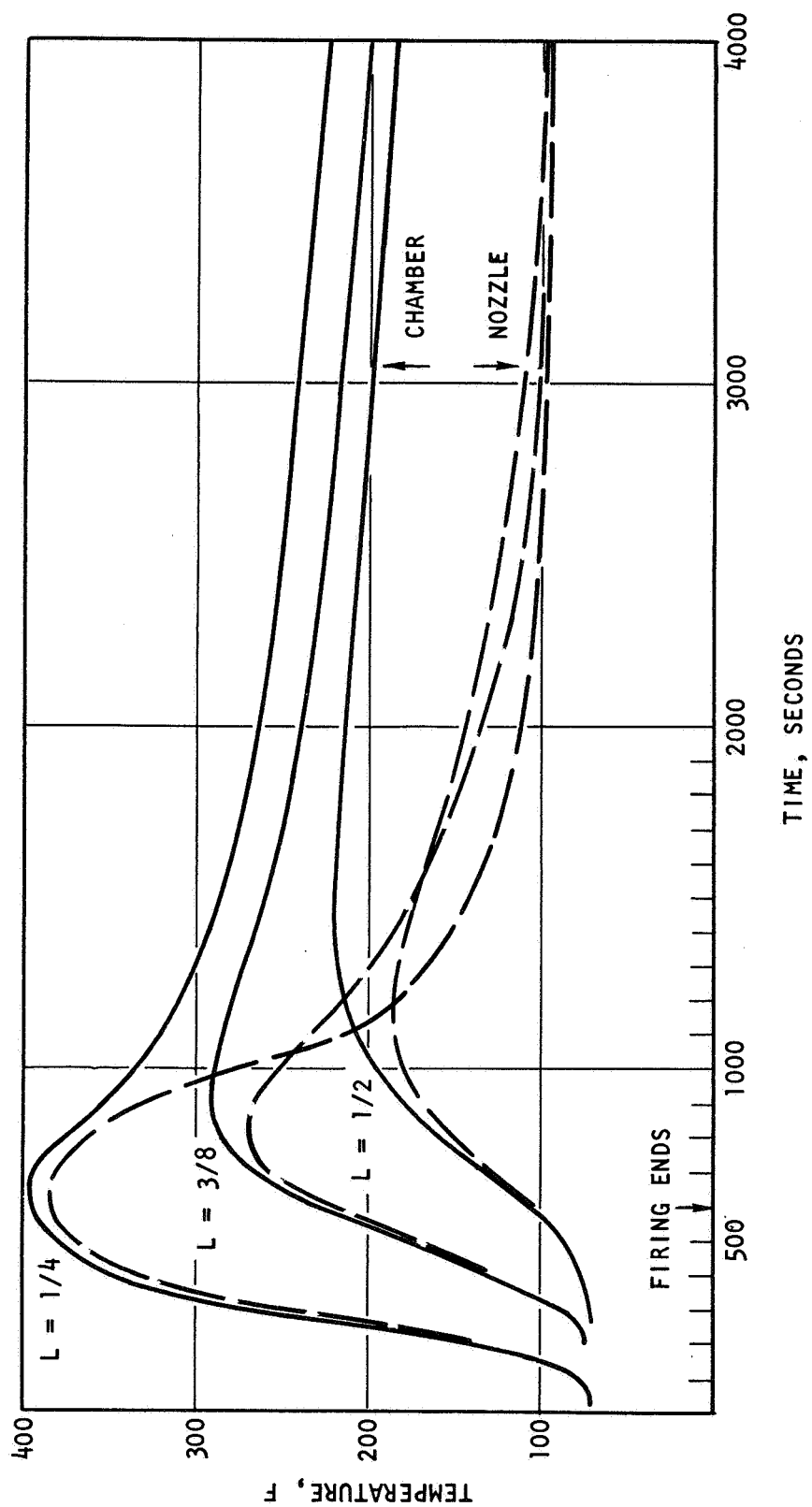


Figure 71. Steel Shell Temperatures at Various Insulation Thicknesses  
(Mariner Engine)

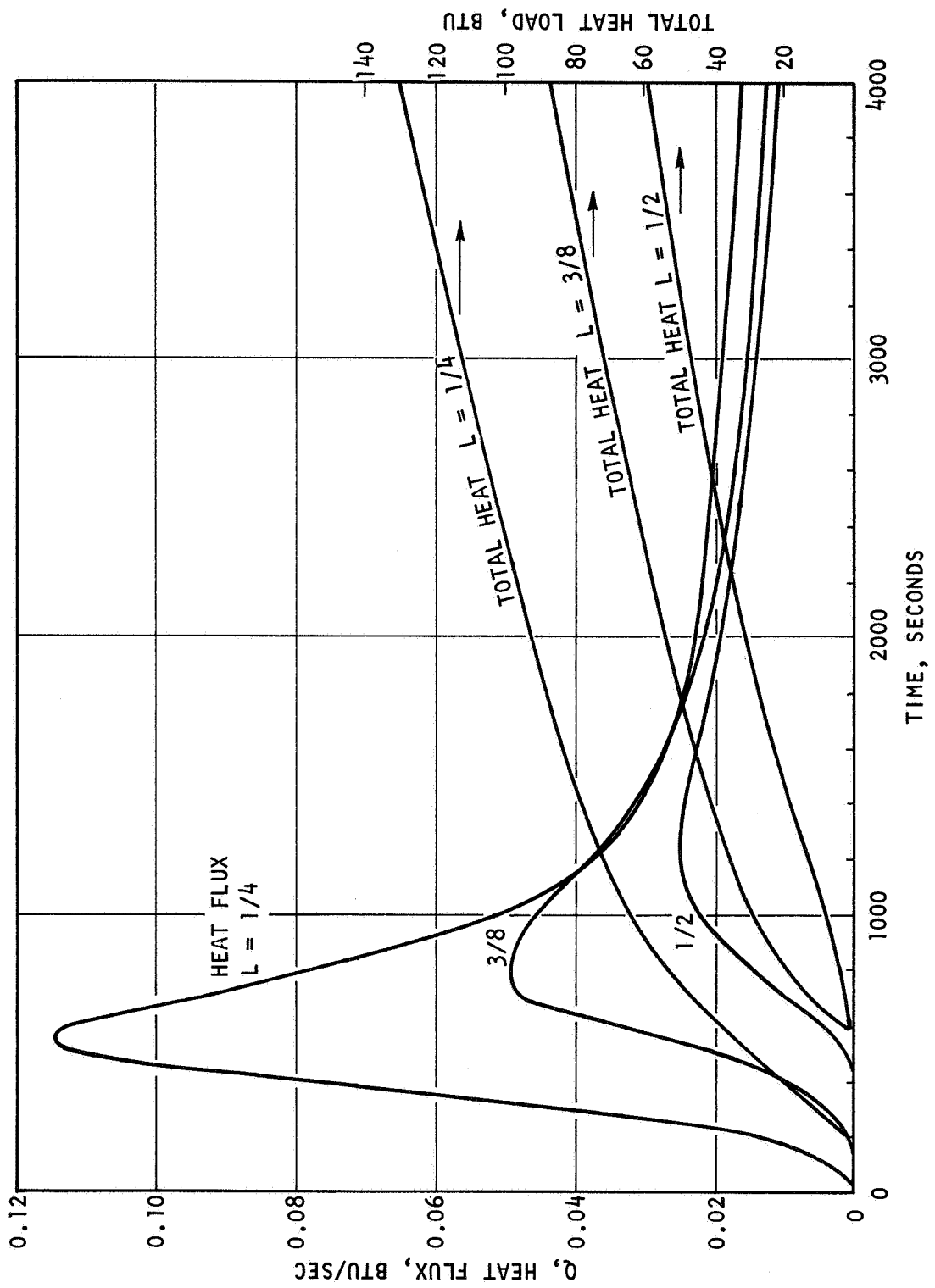


Figure 72. Mariner Engine Heat Flux and Total Heat Load to Spacecraft

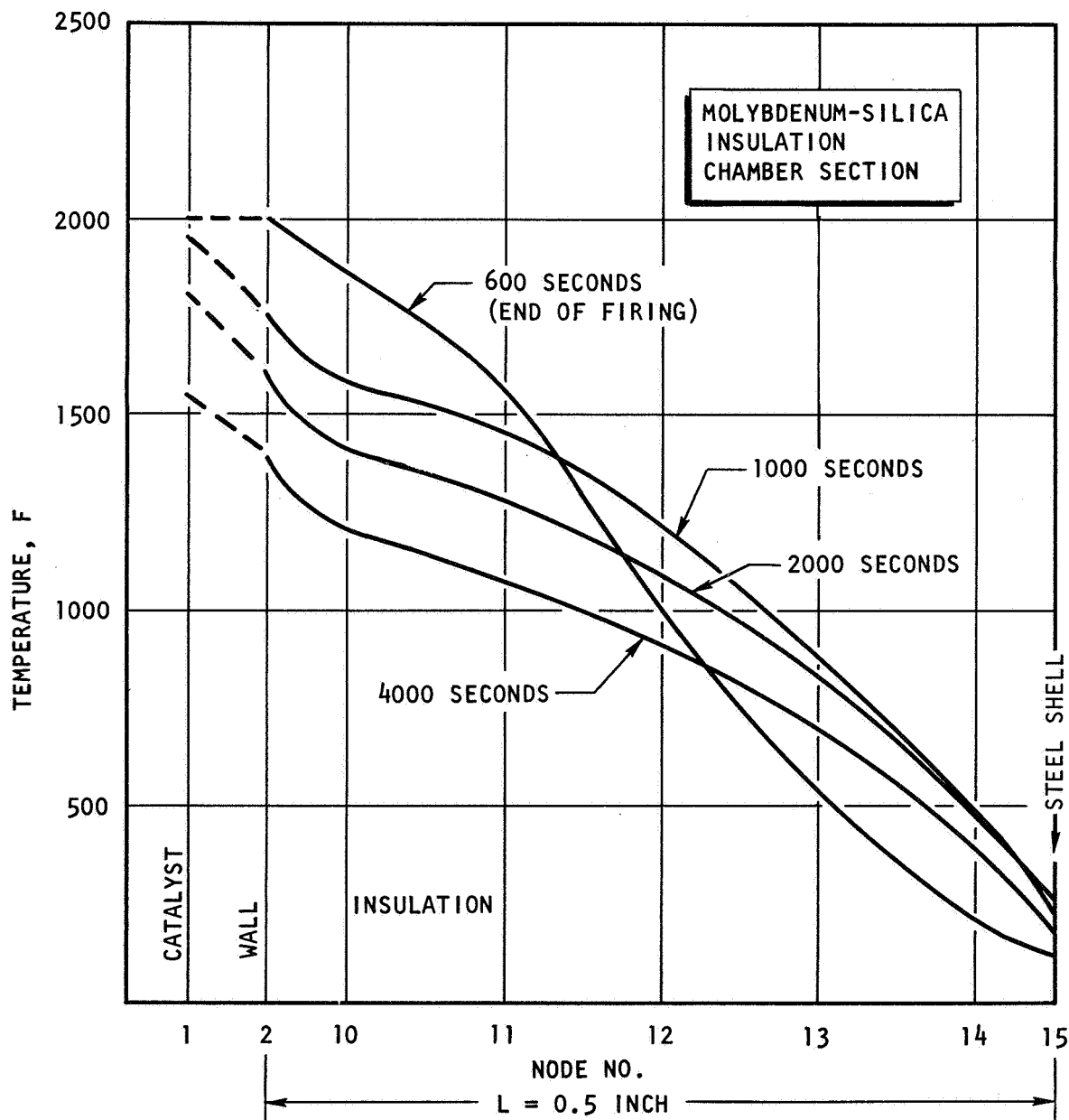


Figure 73. Temperatures in the Chamber Insulation During Soakback (Mariner Engine)

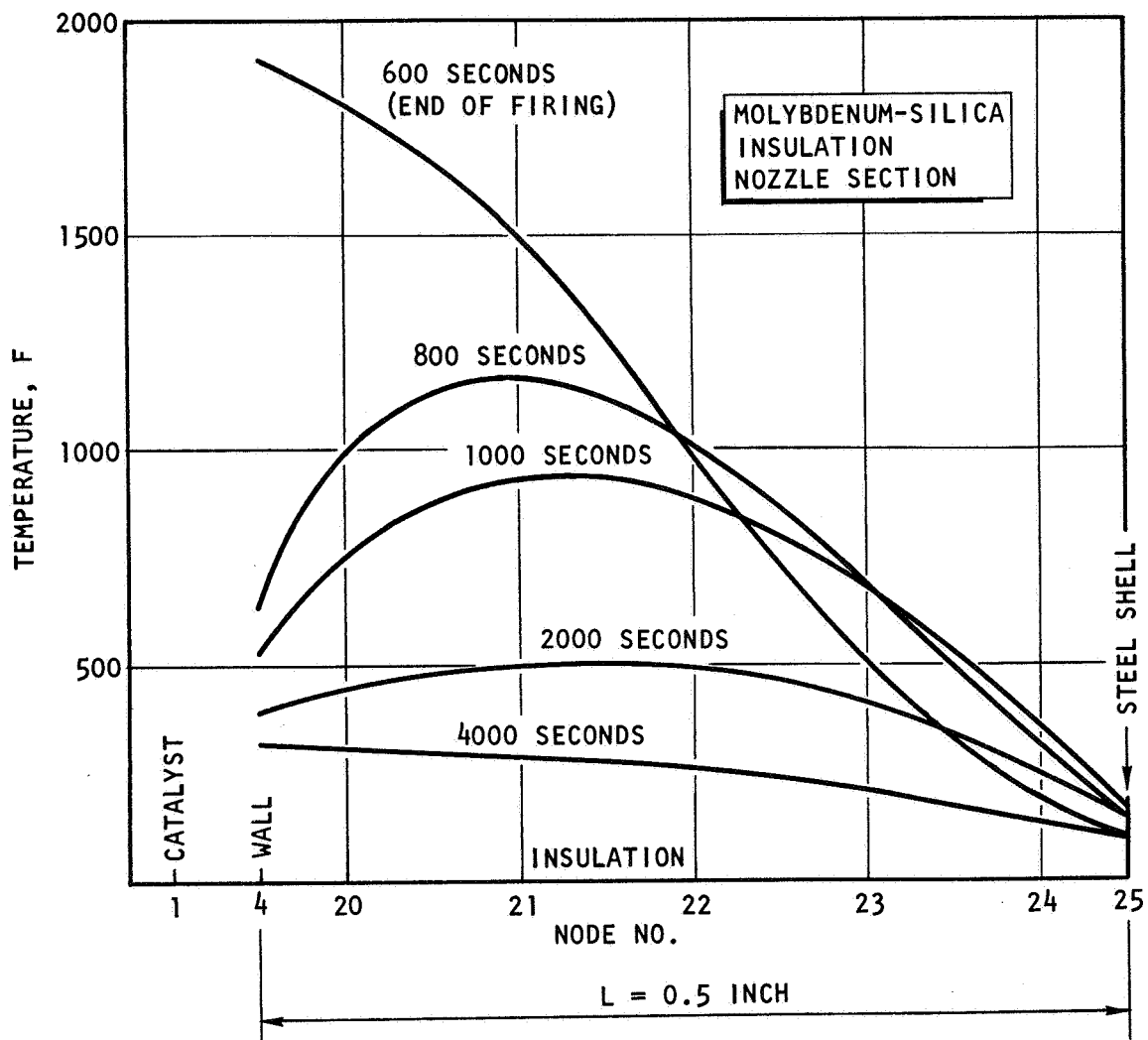


Figure 74. Temperature in the Nozzle Insulation During Soakback (Mariner Engine)

the nozzle insulation has cooled by radiation to space. The heat load to the spacecraft could be reduced by providing a better heat path from the catalyst to the nozzle, e.g., by using thicker or more conductive engine walls.

#### Graphite Engine Description

Propellants:  $\text{OF}_2\text{-B}_2\text{H}_6$

Chamber walls: pyrolytic graphite 1/10-inch thick capable of operating at 4500 to 5000 F

$L^* = 20$

Thrust 2000  $\text{lb}_f$ ; Chamber pressure: 150 psia

Firing duration: 600 seconds

Standoff or gap between engine liner and insulation permitted.

#### Engine Design and Operation

No design corresponding to the above specification was available. Engine dimensions were obtained by scaling a 1500  $\text{lb}_f$  ATJ graphite engine with a 2.54 throat diameter and  $L^* = 19.84$ , burning  $\text{OF}_2\text{-B}_2\text{H}_6$  at 100 psia. The throat diameter needed to obtain 2000  $\text{lb}_f$  thrust at 150 psia was calculated to be 2.80 inches, i.e., a geometric scaling factor of 1.1. A schematic of the engine is given in Fig. 75. The nozzle configuration was the 80 percent optimum bell shape with an expansion ratio of 40. The engine operation details (mixture ratio or injector configuration) are not needed for the analysis of the insulation behavior of a thin walled engine such as this. The assumption that the graphite liner temperature is at 4500 F for the firing duration is sufficient for the purpose of demonstrating insulation system design.



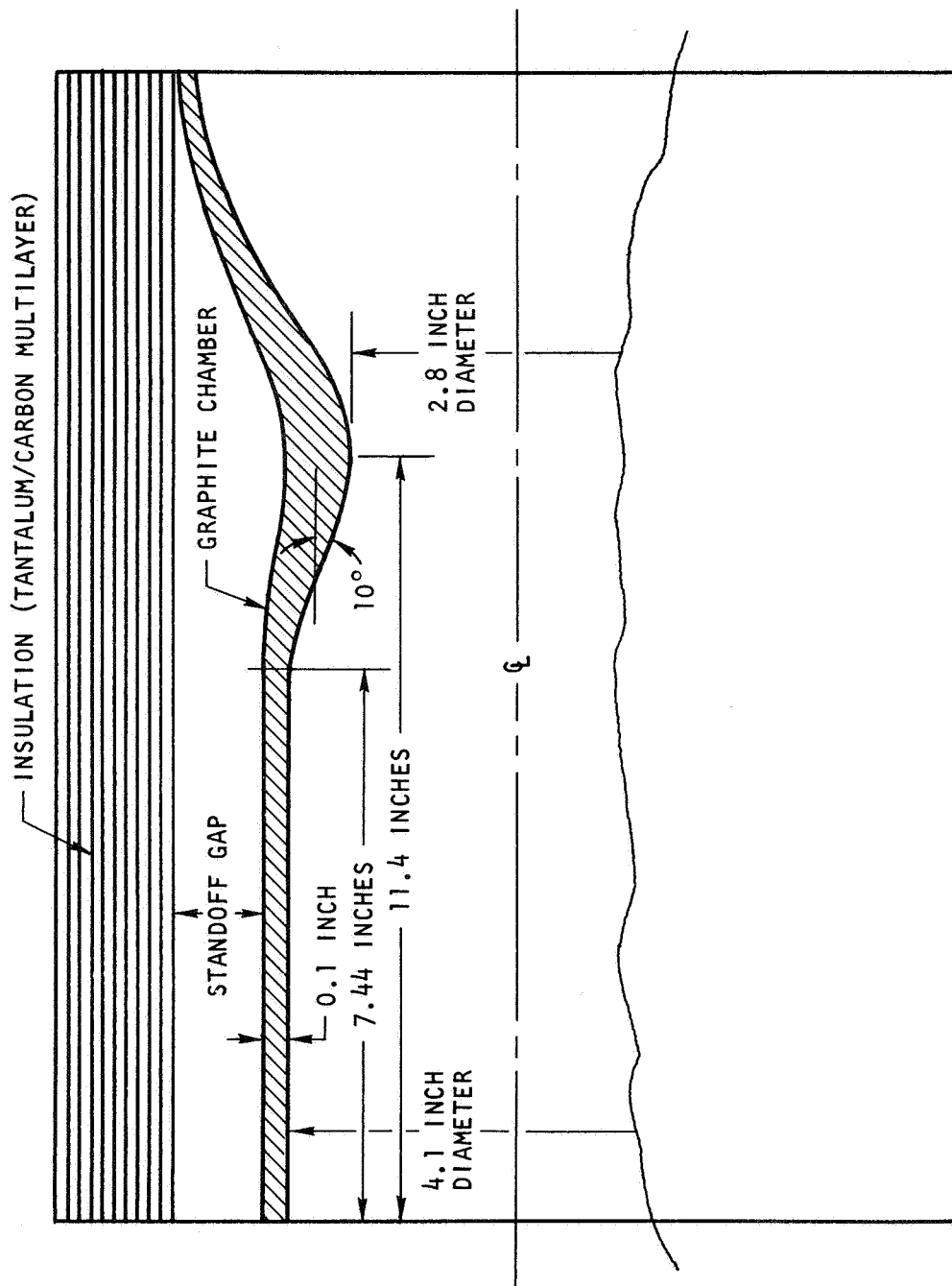


Figure 75. Schematic of Graphite Chamber Assembly

## Insulation

Tantalum-carbon insulation was assumed to be formed into a cylinder not touching the engine walls at any point. The logic of such a design is ease of construction and reduced insulation temperatures. It was found, however, that the gap did not appreciably reduce the insulating temperature even when a radiation shield was introduced into the gap. A radiation gap having a high-temperature, high-emissivity wall (graphite) facing the insulation is not an effective heat barrier. The inside surface of the insulation will rapidly approach the chamber wall temperature because of the high radiative flux. Radiation shields are impractical at temperatures near 4000 F because emissivities of all metals increase with temperature.

## Analog Network and Data Input

The distinguishing features of the analog network (Fig. 76), are the radiative conductances K9 and K19 between the chamber wall and the insulation, and the nozzle wall and the insulation, respectively. To permit radiation conductances to correctly represent engine wall-to-insulation surface radiation, surface nodes 9 and 19 were added to the usual internal insulation nodes. The heat capacity usually attributed to node 10 (or 20) was evenly divided between 9 and 10 (or 19 and 20).

The very high temperatures of the engine walls during firing indicate that thick insulation will be required. The mean insulation diameter (the same for the nozzle and the chamber insulation sections) was calculated for a 1-inch-thick insulation. The mean diameter correction for conductivity and heat capacity was introduced in the tables of  $\rho C_p L$  and  $k/L$ .

The radiative conductance K9 and K19 were calculated as (Ref. 8 )

$$R_{i,j} = \sigma A_i \left[ \frac{1}{\epsilon_i} + \frac{A_i}{A_j} \left[ \frac{1}{\epsilon_j} - 1 \right] \right]^{-1}$$

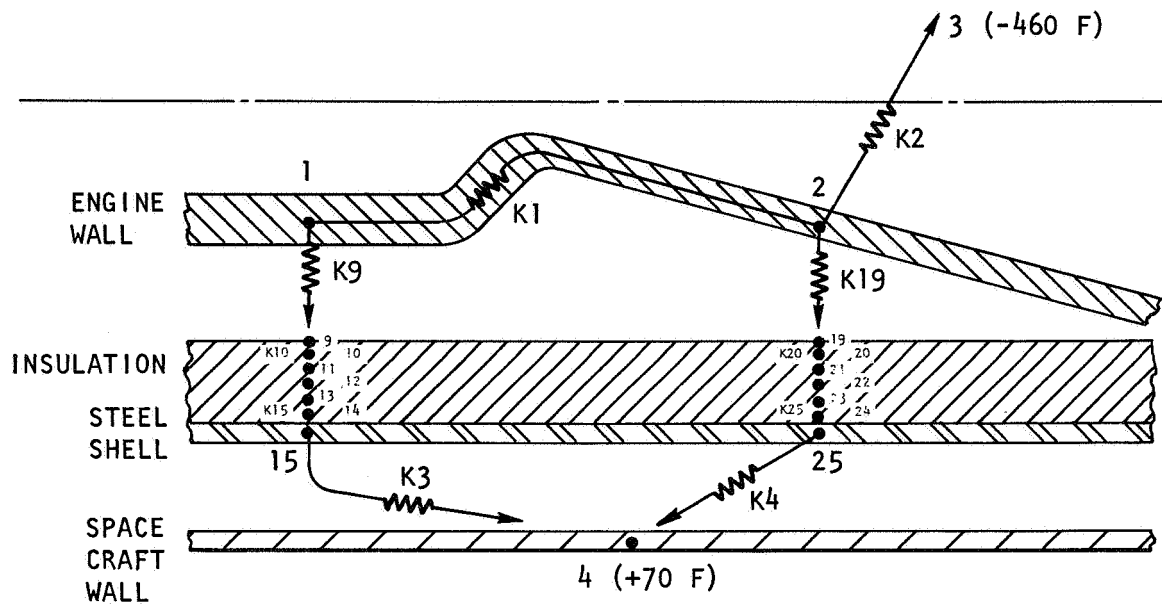


Figure 76. Analog Network for the Graphite Engine

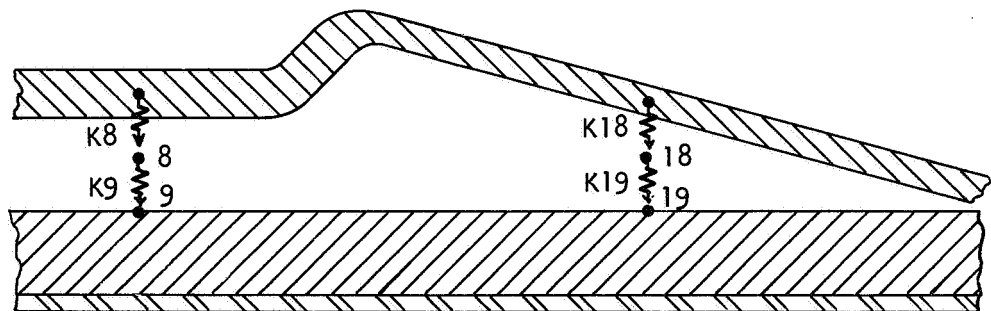


Figure 77. Analog Network for the Graphite Engine, Including a Radiation Shield in the Gap Between Engine Wall and Inlet

where:  $A_i$  = chamber wall area (or nozzle wall area),  $\epsilon_i$  = graphite emissivity (= 0.85),  $\epsilon_j$  = insulation emissivity (= 0.4; A high value of insulation emissivity was used because the inner surface of insulation is very hot, despite the radiation gap) and  $A_j$  = insulation area.

An attempt was made to reduce the heat flow to the insulation by introducing a thin radiation shield between the engine walls and the insulation. The network was modified as shown in Fig. 77. The radiative conductances K8, K9, K18 and K19 were calculated by the procedure used for K9 and K19. The radiation shield emissivity was set at 0.4 after it became clear that the shield would get very hot.

A radiation shield can be made very thin (0.001 inches thick) so that its heat capacity is very small. Introducing a low heat capacity node into the network leads to a very small, minimum time step in the calculations, resulting in excessive computer time expenditures. Therefore, a thick shield was arbitrarily used because an error in the response time of the shield, which would be small in any case, would not sensibly affect the overall response of the system.

One typical listing of the computer program input data for 1-1/2-inch-thick tantalum/carbon insulation considering soakabck for 10,000 seconds is given in Appendix D as a guide to programming a thermal analyzer computer program such as TAP II. The computer output listing of the results is also included.

### Results of Computation

The temperatures of the steel shell enclosing the insulation are shown in Fig. 78. An insulation thickness of 1 inch is clearly insufficient, since temperatures of nearly 1100 F are encountered. On the other hand, 3 inches of insulation is excessive for most applications. Heat flux and total heat received by the spacecraft from the engine with 1, 1-1/2, and 2 inches of insulation are given in Fig. 79 for 5000 seconds after firing starts. For the 1-inch insulation, the heat flux reaches a

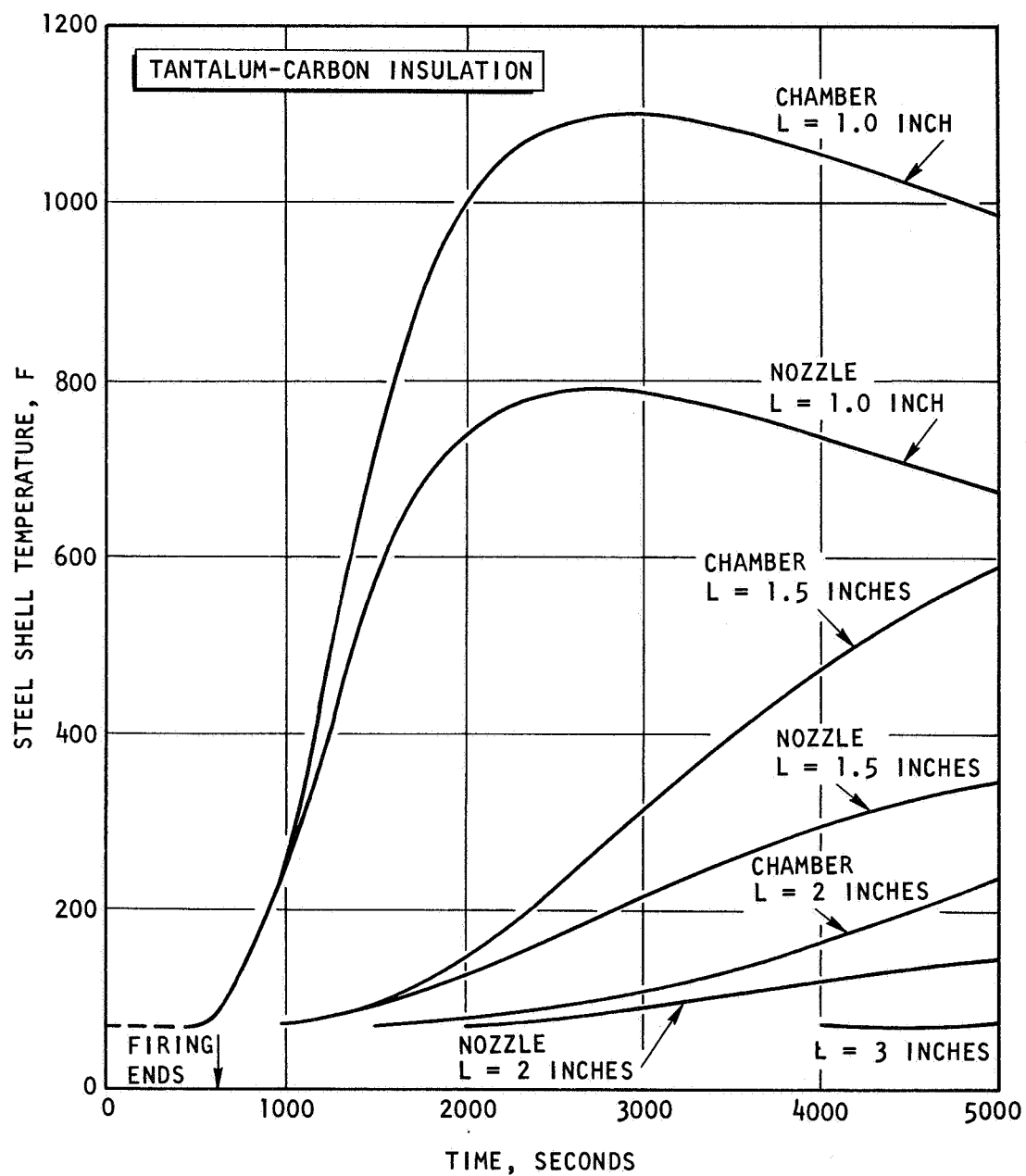


Figure 7E. Steel Shell Temperatures for Varying Insulation Thickness (Graphite Engine)

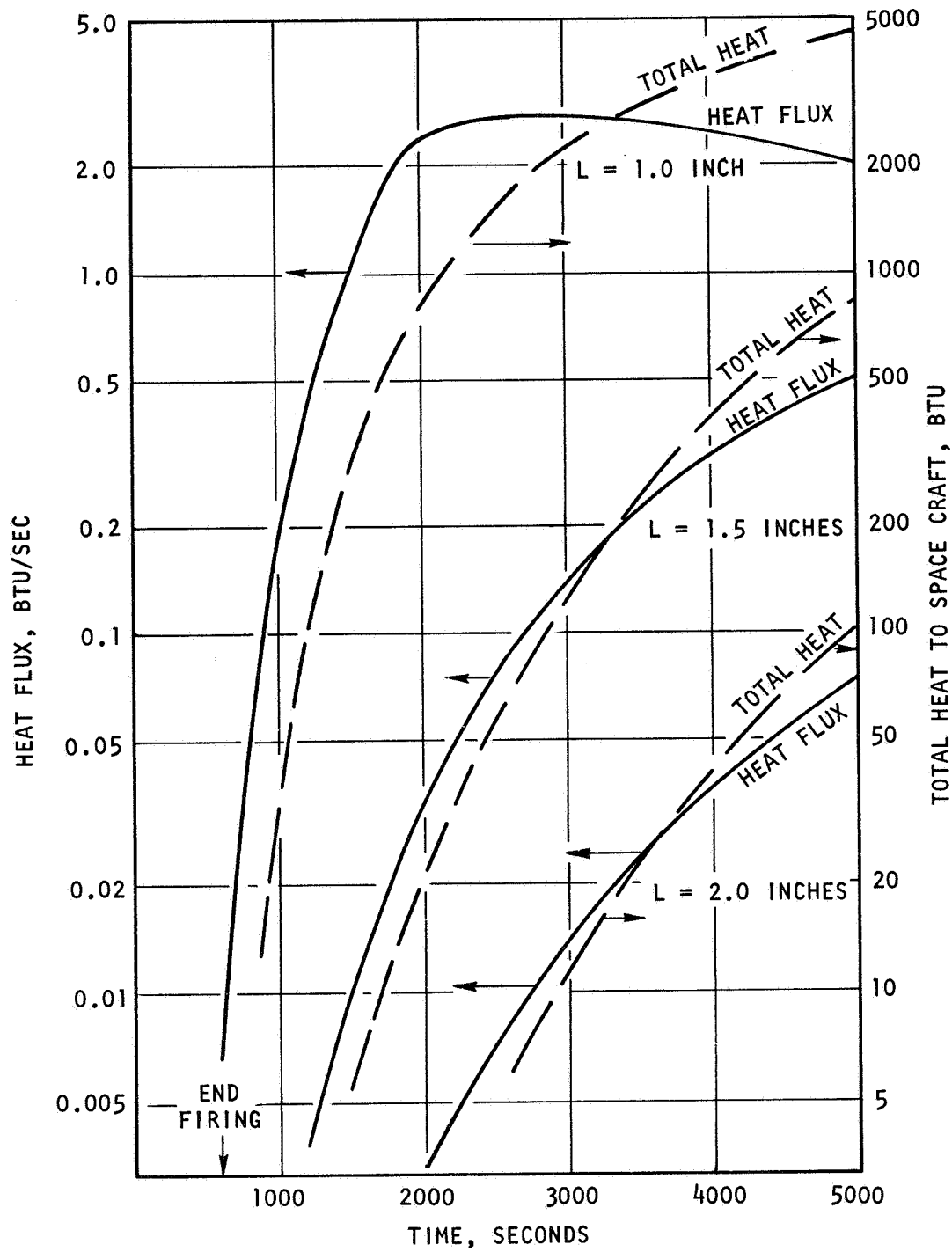


Figure 79. Heat Flux and Total Heat to Spacecraft (L = 1.0, 1.5, and 2.0 Inch) (Graphite Engine)

maximum after about 3000 seconds; for the thicker insulations the heat flux was still increasing at 5000 seconds. The calculations were repeated and extended to 10,000 seconds and 18,000 seconds for  $L = 1.5$  and  $2.0$  inches respectively, to attain maximum heat flux in each case (Fig. 80). The maximum heat flux is  $2.72 \text{ Btu/sec}$  for  $L = 1.0$  inch;  $0.76 \text{ Btu/sec}$  for  $L = 1.5$  inches, and  $0.42 \text{ Btu/sec}$  for  $L = 2.0$  inches. Figure 81 shows the temperature distribution in the chamber insulation with and without a radiation shield. At the end of firing, the surface temperature of the insulation is only  $50 \text{ F}$  lower than without the shield. Temperature distributions in the 1.5-inch insulation are shown in Fig. 82 and 83.

The nozzle insulation cools faster than the chamber insulation, the radiation of the nozzle wall to space having a direct path. The heat from the chamber section must first radiate to the engine chamber wall, be conducted to the nozzle wall, and then radiated to space. Radiation, which was quite effective in conducting heat from the high-temperature wall to the insulation during firing, became very ineffective when heat was to be rejected from the insulation to the engine wall. The reason is, of course, the relatively low temperatures of the insulation during soakback. Therefore, the stand-off gap concept of insulation design, is not effective as a heat barrier. Moreover, it results in an increase of insulation weight because of the increase of insulation mean diameter. Insulation wrapped directly on the graphite liner would weigh less for a given maximum heat load on the spacecraft.

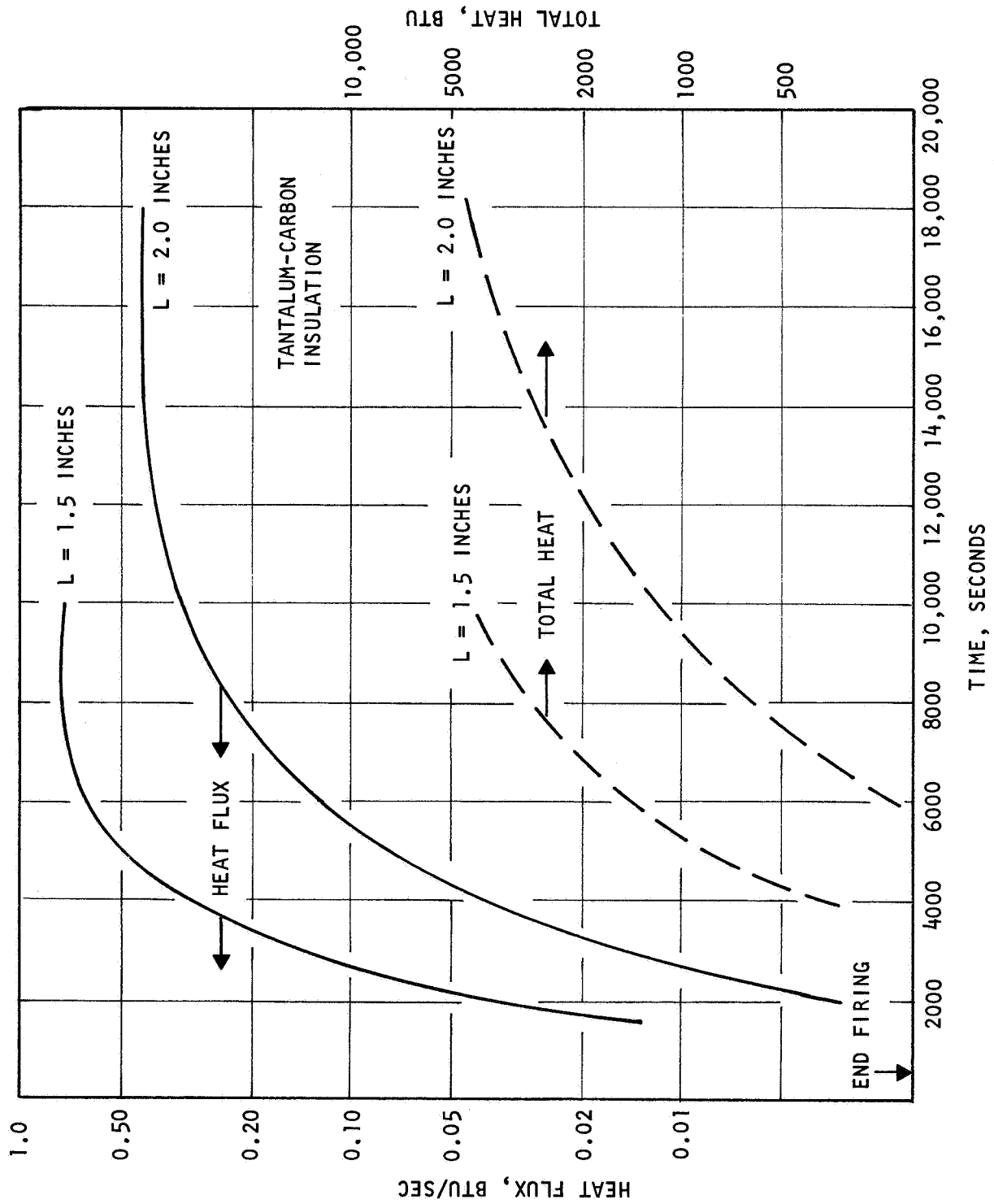


Figure 80. Heat Flux and Total Heat Input to Spacecraft ( $L = 1.5$  and 2.0 Inch Graphite Engine)



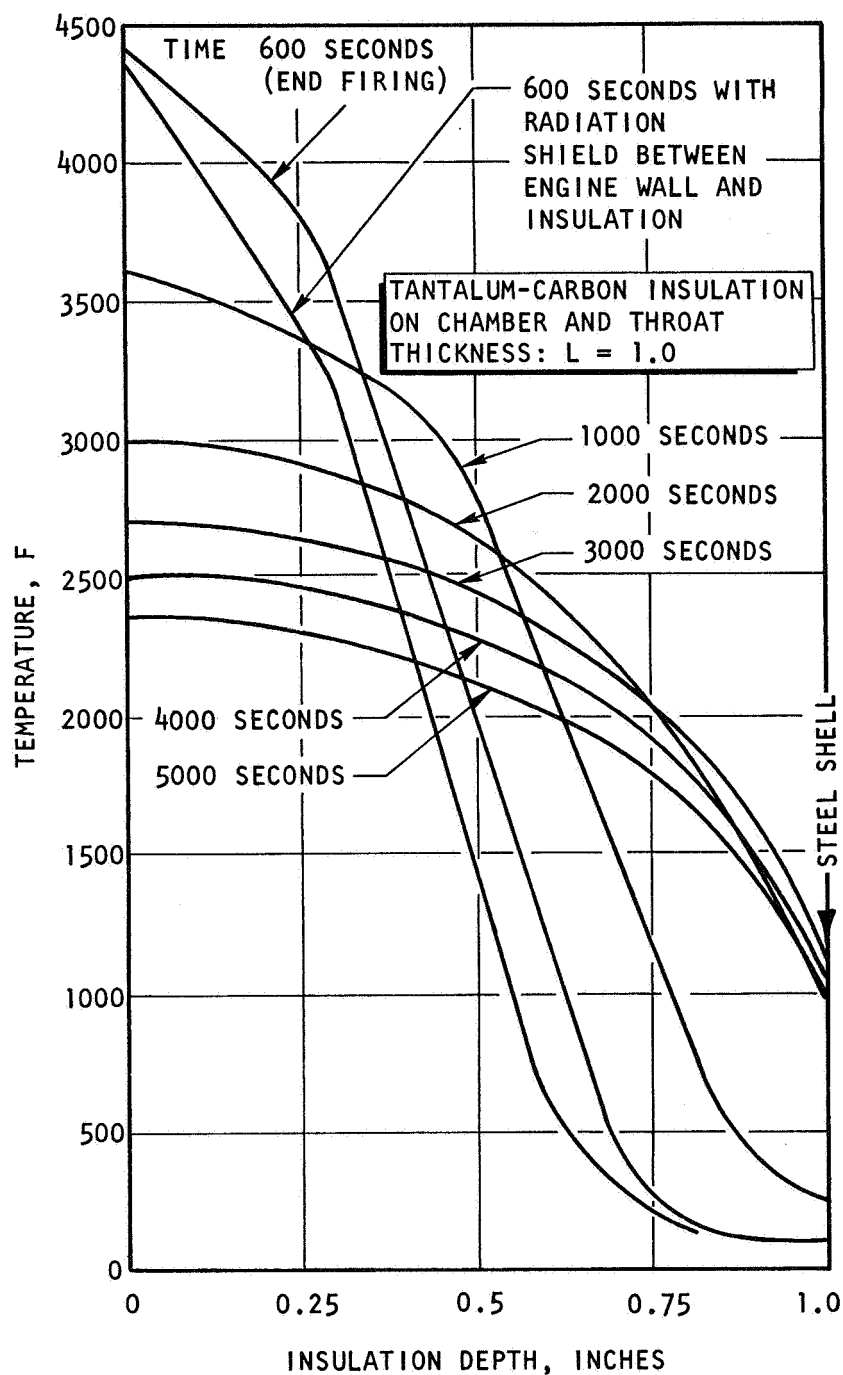


Figure 81. Temperature Profiles in the Insulation ;  $L = 1.0$  (Graphite Engine)

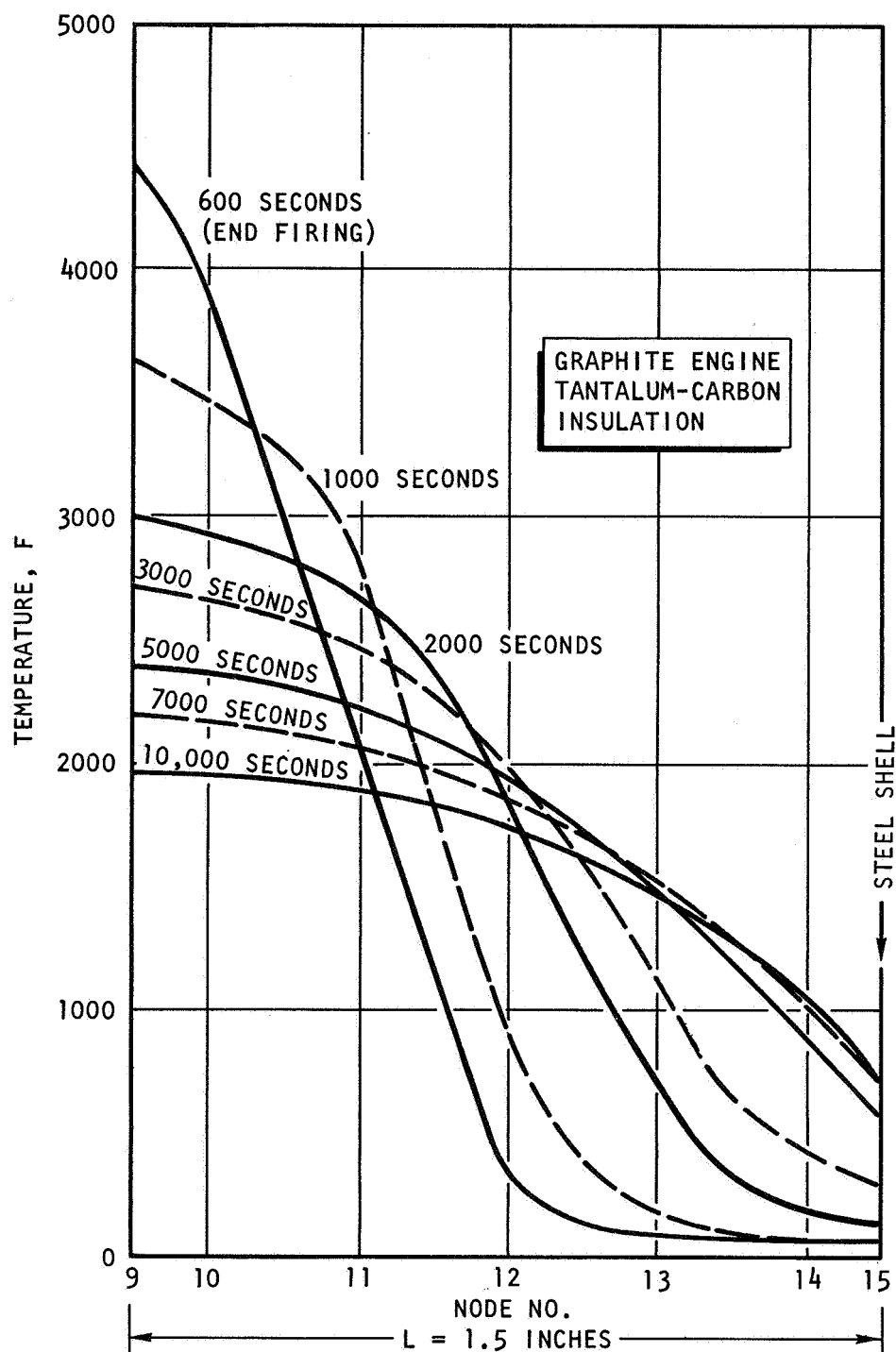


Figure 82. Temperature Distribution in the Insulation;  
L = 1.5 Inch; Chamber Section  
(Graphite Engine)

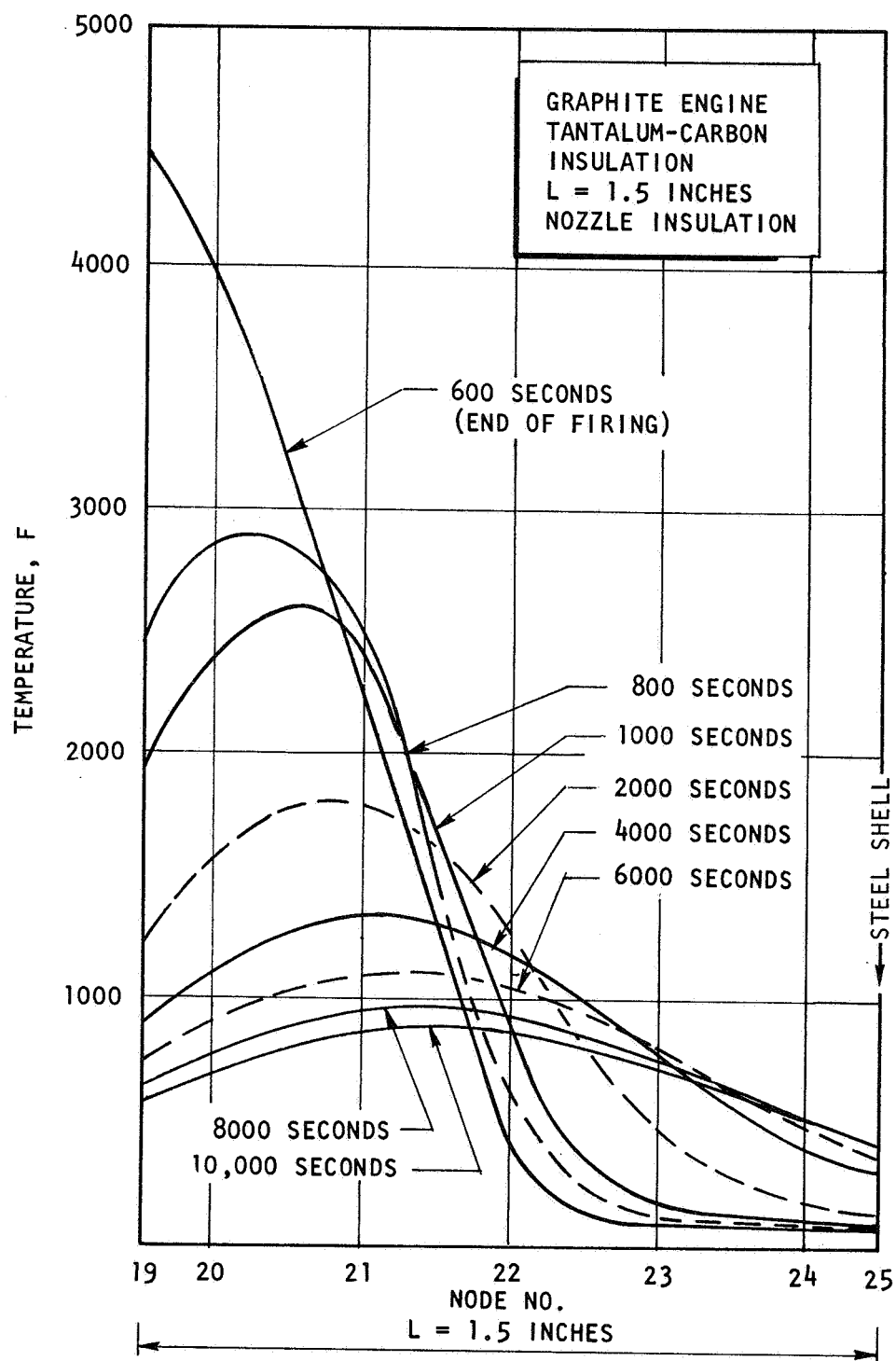


Figure 83. Temperature Distribution in the Insulation;  
L = 1.5 inch; Nozzle Section  
(Graphite Engine)

## REFERENCES

1. Touloukian, Y. S., Editor, Thermophysical Properties of High Temperature Solid Materials, Vols. 1 through 6, Thermophysical Properties Research Center, Purdue University, the Macmillan Company, New York (1967).
2. R-7121, Spacecraft Rocket Engine Chamber Insulation Materials, by A. L. Huebner, L. W. Carlson, H. Carpenter, Rocketdyne, a Division of North American Aviation, Inc., Canoga Park, California, Contract #NAS7-474, 26 July 1967.
3. R-7251-1, Spacecraft Rocket Engine Chamber Insulation Materials: Fifth Quarterly Progress Report, by A. L. Huebner, L. W. Carlson, H. Carpenter, Rocketdyne, a Division of North American Rockwell Corporation, Canoga Park, California, Contract #NAS7-474, October 1967.
4. Jakob, Max, Heat Transfer, Vol. I, John Wiley, p. 409-420 (1959).
5. Hummel, F. A. and C. A. Laren, Thermal Analyzer Program, Rocketdyne IL 4114-131, Rocketdyne, a Division of North American Aviation, Inc., Canoga Park, California, 17 November 1964.
6. RRC-66-R-76, Development of Design and Scaling Criteria for Monopropellant Hydrazine Reactors Employing Shell 405 Spontaneous Catalyst, Vol. I, Rocket Research Corp., Seattle, Washington, 19 January 1967.
7. Price, T. W. and D. D. Evans, The Status of Monopropellant Hydrazine Technology, JPL Technical Report 32-1227, p. 7, 15 February 1968.
8. Eckert and Drake, Heat and Mass Transfer, McGraw Hill, p. 398 (1959).
9. Smith, J. M., Chemical Engineering Kinetics, McGraw Hill, p. 384 (1956).

## NOMENCLATURE

$\bar{A}_c$	=	average conduction area (ft <sup>2</sup> ) for heat flow
$C_p$	=	specific heat (Btu/lb . F)
$e$	=	specific weight (lb/ft <sup>3</sup> )
$F$	=	view factor
$k_e$	=	effective thermal conductivity (Btu/lb ft F)
$K_{loss}$	=	thermal conductivity (Btu/lb ft F) in heat loss direction
$L$	=	calorimeter axial length (feet)
$q_c$	=	heat flow rate (Btu/hr)
$q_{loss}$	=	heat loss rate (Btu/hr)
$q(R_{No})$	=	calorimeter heat load (Btu/hr) at a given time
$R$	=	Radial location (feet)
$T$	=	temperature (F)
$2A_{loss}$	=	axial conduction area (ft <sup>2</sup> )
$\Delta R$	=	radial conduction length (feet) between thermocouple stations
$\Delta T$	=	temperature difference (F) between thermocouple stations
$\Delta Y$	=	axial distance (feet) between thermocouples measuring heat loss
$\epsilon$	=	emissivity
$\theta$	=	time (hours)
$w/o$	=	weight percent

## SUBSCRIPTS

$i$	=	indexing parameter denoting thermocouple position
$N$	=	Number of radial thermocouple locations
$e$	=	effective

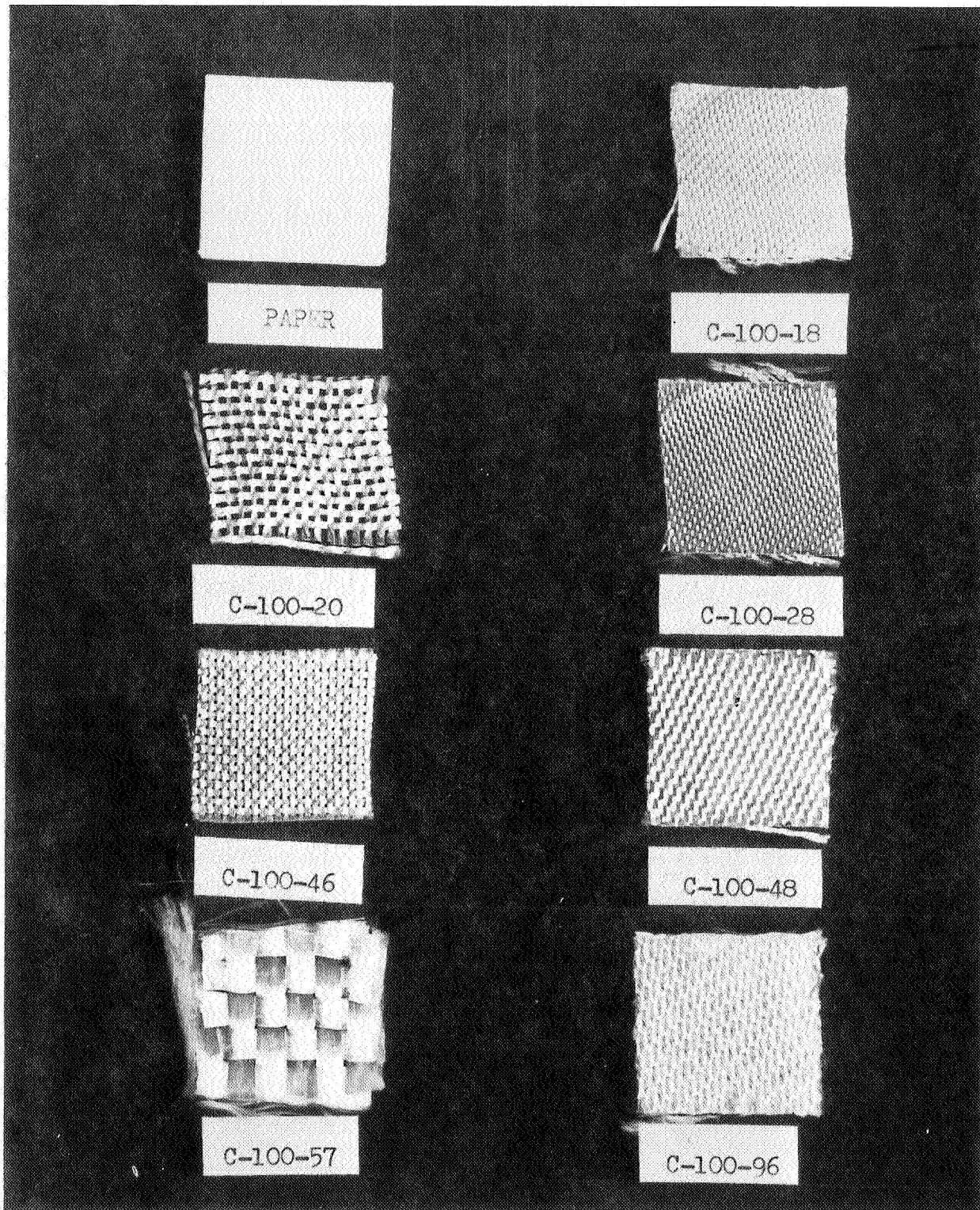
## APPENDIX A

### SELECTION OF A SILICA FABRIC

The purpose of the screening tests was to evaluate improved silica insulative separators for the multi-layer system that would not have the shortcomings of papers. High-purity silica fabrics showed the most promise as a substitute for the high-purity silica papers. Advantages of these fabrics are that they: (1) are more than 99 weight percent silica, (2) are stronger than the papers, (3) do not contain, or need, a binder to achieve this strength, (4) are economical, and (5) are available in a variety of weaves and thicknesses (Fig. A-1 and A-2).

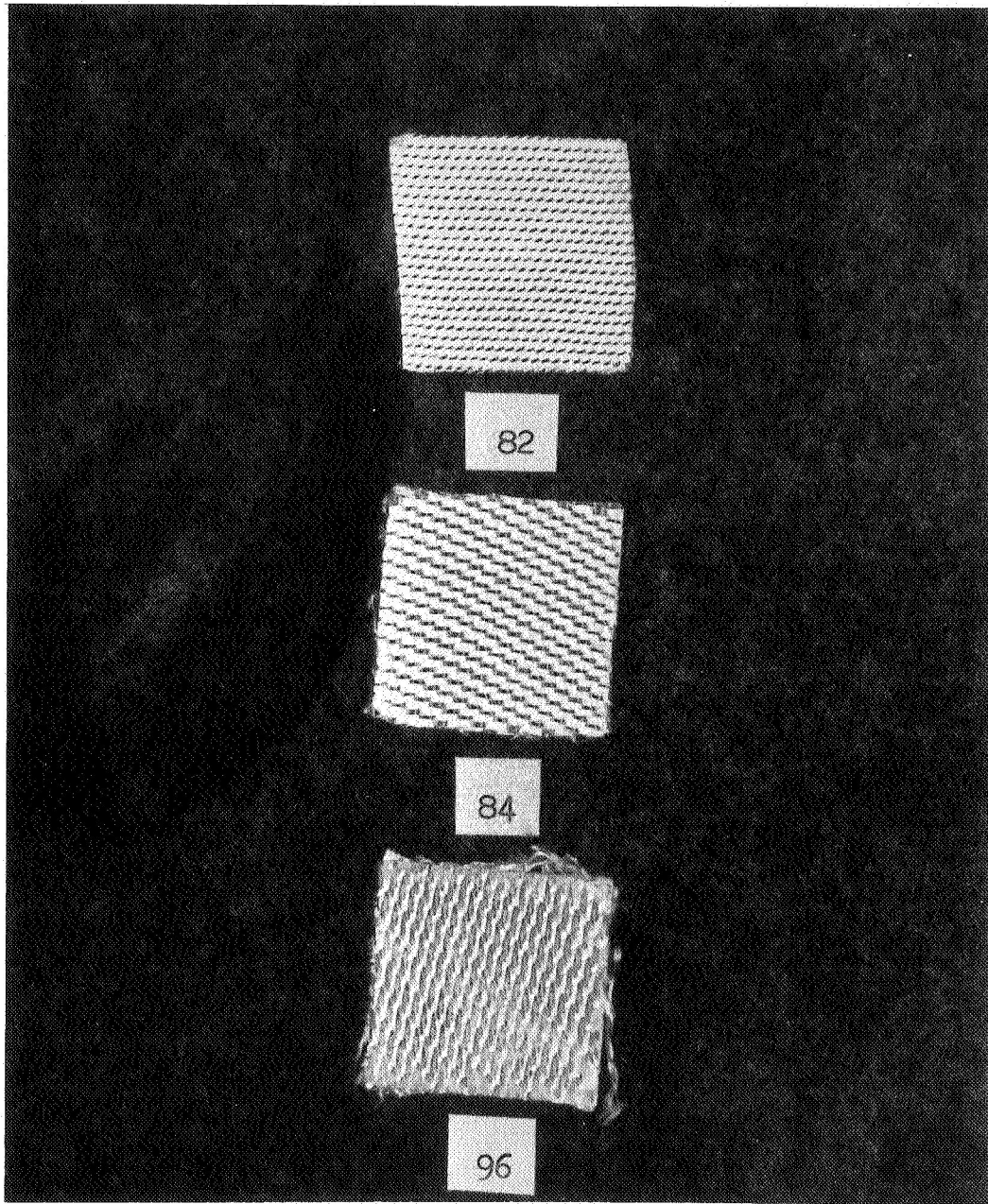
The character of the silica fibers in these fabrics is different from those in the papers because the fibers are made by different processes. These processes are proprietary with the vendors, and their exact nature is unknown. However, the following basic steps are probably followed.

A commercial silicate glass is drawn into appropriate fibers and all of the constituents except silica are chemically leached out. The fibers are annealed to reduce the excessive porosity and to reduce shrinkage when reheated ("sanforizing"). Although much of original porosity is eliminated, the fibers still remain highly porous. Because of the high surface of these porous fibers, they can absorb large quantities of gases. These fibers are reported by the vendor to adsorb as much as 50 weight percent of gases under certain conditions. However, special care can be used to reduce the adsorbed gas content of this material. Fabrics that are packaged immediately after manufacture can be stored indefinitely without adsorbing large amounts (over 3 weight percent) of gas. Also, when these fabrics are rolled tightly into the multilayer insulation configurations, only the edges are exposed to ambient gases. Under ordinary conditions, adsorption of gas on the fibers located inside the insulation system should be very slow due to the short mean free path of the gas passing through the bundles of woven fibers. Even if a small amount



5AG13-10/4/67-C1B

Figure A-1. Refrasil Paper and Fabrics



5AG13-10/4/67-C1A

Figure A-2. Astrosil Fabrics



of gas is adsorbed on the fibers, this adsorbed gas is not necessarily detrimental to thermal conductance properties of the composite. The gas will be removed rapidly at low temperatures by the pressure differential caused by exposure to a high vacuum, and, most importantly, because it is not an organic compound, it will not condense in cooler regions of the insulation system.

## PROCEDURE

The testing procedure of previous screening tests\* and of the thermal stability tests was used to evaluate a variety of selected silica fabrics. The fabrics were carefully cut into 1-inch squares using a razor blade. (Cutting small pieces of woven fabrics with scissors results in uneven cuts due to the "stretchability" of the weave when the fabric is cut into small sizes.) These 1-inch squares were weighed and measured for thickness, then sandwiched between 2-mil-thick molybdenum foils. Each stack, or sandwich, was weighted with a load of 1/2 pound of tungsten (1/2-psi loading pressure). Specimens were then annealed in a vacuum of  $10^{-5}$  torr at 2000 F for 1 hour. After cooling, all measurements were repeated.

## RESULTS AND DISCUSSION

### Silica Fabrics

Results of screening tests are listed in Table A-1. As expected, the silica fabrics appear to be superior to silica papers.

The strength of the fabric appeared to be unaffected by annealing at 2000 F. The fabric was still many times stronger than the paper. Vendor literature reports that the strength of Refrasil (trademark of H. I. Thompson Co.) fabric is 50 lb/in., whereas the strength of a paper of equivalent thickness (about 26 mils) was estimated at less than 1 lb/in.

\*R-7121, Spacecraft Rocket Engine Chamber Insulation Materials, A. L. Huebner, L. W. Carlson, and H. W. Carpenter, Rocketdyne, a Division of North American Aviation, Inc., Canoga Park, California, Contract #NAS7-474, July 1967.

TABLE A-1

## COMPARISON OF SILICA FABRICS

Vendor	Type	Specified Thickness, mils	Percent Linear Shrinkage		Weight Loss, percent	Fabric* Weave
			Parallel to Foils	Perpendicular to Foils		
H. I. Thompson Company	Refrasil paper	--	4	30	12	Paper
	Refrasil fabrics:					
	C-100-18	11	6	0	12	Closed
	C-100-20	21	0	0	10	Large opening
	C-100-28	14	3	0	8	Closed
	C-100-46	20	3	25		Small opening
	C-100-48	26	3	0	4	Closed
	C-100-57	--	0	--	10	Checkerboard
J. P. Stevens and Company	C-100-96	56	0	9	1	Closed
	Astrosil Fabrics:					
	96	52	3	4	9	Closed
	82	16	3	6	9	Closed
	84	26	3	0	6	Closed

NOTES: Purity of HHTCO and J. P. Stevens and Company silica fabrics is greater than 99 percent.  
 Strength of fabrics before and after annealing is much higher than paper (an estimated 50 times higher)

\*See Fig. A-1 and A-2

Weight loss of the fabrics varied from 1 to 12 percent as compared to 12 percent for the control specimen of silica paper. As stated, this weight loss is due to adsorbed gases rather than the pyrolyzation of organic binders. Therefore, weight loss can be reduced by quality control of the fabric, and the vapor should not affect thermal conductance properties because it will not condense in cooler regions.

Linear shrinkage parallel to the metal foils varied from 0 to 6 percent, as compared to the 4 percent shrinkage of the control paper specimen. A 6-percent shrinkage could result in tearing in large specimens because it occurred in the thinnest and, hence, the weakest fabric. However, in the case of all other fabrics, a nominal 3 percent shrinkage in a material that is more than 50 times stronger than the paper should not cause tearing.

Shrinkage perpendicular to the metal foil (in the direction of fabric thickness) varied from 0 to 9 percent with one exception. A loosely woven fabric shrank 25 percent, but this was most likely the result of the shifting of fibers due to the loose weave rather than sintering of the fibers. Even a shrinkage of 9 percent is small compared to the paper control specimen that shrank 30 percent. Although compressibility of the fabrics at room temperature was not measured in these tests, it appeared to be considerably less for the candidate fabrics than for the reference paper.

The density of silica fabrics and papers is apparently similar. Exact comparison of a parent density value was not made, but an approximate calculation of apparent density was made using vendor data and estimated thickness values. Surprisingly, the calculated density of the fabric was less than that of the paper,  $3 \text{ lb/ft}^3$  compared to  $8 \text{ lb/ft}^3$ . However, these densities are arbitrary and low, and such a small difference is unimportant compared to other properties.

### Wool Materials

Another insulative material was evaluated in these screening tests. This material was Kaowool (Babcock and Wilcox Co.), an aluminum silicate fibrous wool, or batting product, that is reported to be useful in service to temperatures above 2000 F. The particular material tested had a thickness of 15 mils and was of two types; with and without a binder. Results of tests showed that the batting lost 10 and 6 weight percent, respectively, for the materials with and without a binder. Linear shrinkage parallel to the metal foils was 3 percent and shrinkage perpendicular to the foils was 6 and 23 percent, respectively. This material was not selected for further evaluation because of the high shrinkage of the material without a binder. The material with the binder would offer no significant advantage over the silica paper previously used in this program.

### CONCLUSION

Based on the results of the above screening tests, silica fabric was selected for evaluation in silica/molybdenum multilayer insulation systems. The final selection, H. I. Thompson Co. Type C-100-48 cloth, was based on such items as weave and thickness, cost, and availability.

## APPENDIX B

### SELECTION OF A MATERIALS SYSTEM FOR DETAILED INVESTIGATION

An additional insulation materials system was selected for detailed evaluation during the second year of this program. Thermal conductivity, stability, and compatibility of this materials system were determined under simulated rocket engine environmental conditions. Requirements of the new materials system included those of existing systems, i.e., have a low effective thermal conductivity, be chemically and physically stable for at least 1 hour at 3500 F at a pressure of  $10^{-4}$  torr or less, be available in the desired form because material development and fabrication were beyond the scope of the effort, and be light weight and inexpensive. It was also desirable that it possessed advantages compared to systems already investigated.

Any effective high-temperature insulation system must contain means of dispersing and back-reflecting radiation. Reflective surfaces within the matrix are necessary to reduce heat conduction by radiation because the radiation heat transfer mode is dominant at the higher temperatures, particularly above 2000 F.

There are essentially two ways of forming a system with a high proportion of reflective surfaces. One is to use multi-layer systems like those used in this program, e.g., alternating thin layers of carbon fabric and tantalum foil, and of silica fabric and molybdenum foil. However, the composition of the solid material is relatively unimportant with respect to thermal conductivity (Ref. B-1). Therefore, selecting new insulative systems based on multi-layers of a new ceramic material and refractory metal foil would not have constituted a significant improvement in thermal protection. The major potential improvements can come from better system design (e.g., thicknesses of layers, number of total layers, and physical nature of the materials, such as fabric weave of the ceramic or degree of polish of the foil), and the use of more chemically and physically stable materials.

Changes in system design of multilayer materials systems have been studied in this program, and these systems are made of the most stable materials available.

Another way of forming a system with a high proportion of reflective surfaces is suspension of reflective particles in a stable matrix. Because suitable materials systems were not available commercially, these materials systems had to be developed and fabricated for this program. However, because development of a new materials composite was beyond the scope of the program, a way had to be found for testing this type of insulative material system without requiring a materials developmental program.

Refractory metal powder was mixed with the refractory ceramic particles (grains, fibers, or hollow microspheres) that formed the low-density matrix of the composite. The composite was housed in a molybdenum container of the appropriate shape for determining thermal conductivity and diffusivity. The matrix possessed a low effective thermal conductivity compared to previous insulating materials because of the increased path length for solid thermal conduction. It was composed of small particles so that solid conduction must take place across contact points between particles. Contact points represent a small portion of total surface area of the composite. Thus, by itself, the loosely packed matrix was an improvement over the Type IV material tested previously (Ref. B-1). The Type IV material was cementitiously bonded zirconia powder in which there was little contact resistance between zirconia grains.

Other methods of suspending or forming reflective surfaces in a refractory powder matrix are vapor deposition, precipitation, or decomposition. The most promising method would be to coat the particles in a way similar to that used to apply decorative films on ceramic pottery and dinnerware. The metal phase, a refractory or precious metal, would be dissolved in an appropriate organic liquid. The solution would then be mixed with the ceramic particles and the excess solution would be poured off for reuse. The film that would remain on each particle would be converted to the

pure metal phase by thermal treatment. Use of refractory metals would require a second heat treatment in hydrogen to reduce the oxide in the metal phase. Thickness would be very small so that relatively little material would be required.

Another method would be to suspend a refractory metal powder in a phenolic resin that could be molded or extruded into various shapes. The phenolic would be pyrolyzed to form a strong, yet porous, structure. Or, for example, an organic-based paint containing suspended refractory or precious metal powder could be successively applied as discrete layers on a fugitive mandrel. More metal powder could be attached on the wet surface after each coating. The multilayered composite would then be pyrolyzed to form poorly bonded multilayers of a low-density carbon structure impregnated with refractory metal-oxide powder. A reduction reaction would be required provided that the refractory metal oxidized during the pyrolyzation operations. Although both molybdenum and tantalum will carburize, the refractory metal carbide particles would still have a reflectance value of about 50 percent or more.

## SCREENING TESTS

### Description

The purpose of the screening tests was to compare the merits of candidate materials systems with respect to ease of preparation, degree of developmental effort required to perfect the material to the extent that it is satisfactory for this program, and physical and chemical stability. All materials systems were tested at 3500 F for 1 hour at a pressure of approximately  $10^{-5}$  torr. The candidate systems tested are listed in Table B-1. Basically, the systems include three matrices: zirconia, thoria, and graphite, and five reflective phases: tungsten, tantalum, molybdenum, rhenium, and rhodium. Reflective phases were added in two ways. Either the reflective powder was mixed with the ceramic matrix particles, or a solution of the reflective metal was mixed with the ceramic matrix particles.

TABLE B-1

## LIST OF CANDIDATE MATERIALS SYSTEMS

Specimen Number	Ceramic Matrix		Reflective Phase			
	Composition	Powder Character	Size (mesh)	Volume Percent	Composition	Form Powder Size (mesh)
6-1	Zirconia	Sintered Grains	-325	50	Tungsten	Powder -325
6-2	Zirconia	Sintered Grains	-100, +200	--	Tungsten	Film* --
23-1	Zirconia	Sintered Grains	-325	11	Tungsten	Powder -325
23-3	Zirconia	Sintered Grains	-200, +325	11	Tungsten	Powder -325
23-2	Zirconia	Sintered Grains	-100, +200	11	Tungsten	Powder -325
24-7	Zirconia	Microspheres	-36, +48	--	Tungsten	Film --
24-6	Zirconia	Microspheres	-36, +48	--	Rhenium	Film --
7-5	Zirconia	Sintered	-325	30	Molybdenum	Powder -325
8-6	Thoria**	Sintered	-325	50	Tungsten	Powder -325
8-7	Thoria**	Sintered	-325	30	Tantalum	Powder -200, +325
8-21	Thoria**	Sintered	-325	--	Tungsten	Film --
7-10	Graphite	Sintered	-200	50	Tantalum	Powder -200, +325
7-11	Graphite	Sintered	-200	--	Rhenium	Film --
7-12	Graphite	Sintered	-200	--	Rhodium	Film --
7-3	Zirconia	Sintered	-325	--	--	--
7-4	Zirconia	Sintered	-100, +200	--	--	--
21-5	Zirconia	Sintered	-100, +200	--	--	--
22-4	Zirconia	Microspheres	-36, +48	--	--	--
8-8	Thoria	Sintered	-325	--	--	--
8-9	Thoria	Sintered	-325	--	--	--
8-13	Tungsten	Sintered	-325	--	--	--

\*A very thin film of metal was deposited from a metal resinate solution and heat treated in air to remove the organic material.

\*\*Calcined at 2200 F for 2 hours to reduce subsequent shrinkage.



Because the solution was an organic material in the latter case, it had to be heat treated in air to pyrolyze the organic constituents. However, because the oxides (tungsten oxide at least) are volatile, pyrolyzation temperature was kept low. Thus, some organic material may have remained in the film and, subsequently, charred during testing in the vacuum environment. Consequently, the exact nature of the film before and after testing was not known.

Tungsten and rhenium films would have been in the form of oxides after heating in air. When heated to 3500 F in vacuum these oxides may have been volatilized, or they may have been reduced to a metal or a carbide. X-ray diffraction analysis was not attempted because of the very small thickness of the film. Chemical analysis was not pursued when evaluation of test results and the scope of the program suggested that this method of preparing insulation materials would not be employed.

#### Procedure

Zirconia- and Thoria-based mixtures were prepared as small batches, just enough for a particular test. Materials were mixed by gentle stirring in glass beakers. Zirconia and thoria composites were contained during testing in 1/2 by 1/2 by 2 inch cans that were made of molybdenum foil and open at one of the small ends. Graphite composites were contained in molybdenum cans that were lined with tantalum foil. Powders were initially compacted by lightly tamping the can on a table 20 times. Shrinkage of the powder composite was determined by measuring the decrease in height of the powder in the container. Starting height was 1 inch or more. Annealed powders were observed with the unaided eye, the low-power stereomicroscope, and high-power microscope when necessary. Powder composites were prepared for microscopic study by vacuum infiltrating with low-viscosity epoxy and standard ceramographic polishing procedures. Bulk density was determined by dividing weight by volume, which was measured by pouring the powder into a 10 cc graduated cylinder.

## Results

A summary of results is presented in Table B-2. Graphite-based powders did not shrink appreciably, but they outgassed considerably and reacted extensively with the tantalum containers. Containers carburized became brittle and disintegrated except in some areas where the tantalum had welded to and was supported by the molybdenum backing. Containment and outgassing of graphite (or carbon) powder was a problem.

Thoria-based powders also reacted with the containers, but in this case the containers were molybdenum. The nature of this reaction is not clear because tungsten, thoria, and molybdenum do not react appreciably at 3500 F (Ref. B-2). Thoria-based powders that were tested shrank as much as 23 percent, which is not acceptable for this application. However, raw material in the form of coarse fused grains, which is commercially available at a high cost, would eliminate excessive shrinkage due to sintering. Fused thoria was not available for testing.

Zirconia-based mixtures represented the most attractive materials system tested. The data are summarized in Table B-3. Linear shrinkage in the vertical direction varied between 6 and 5 percent, depending on particle size. One zirconia specimen shrank 8 percent, but that data point is not realistic compared to the other data; mixtures of even finer powders did not shrink that much. It is possible that the high shrinkage value was due to some of the powder being lost during handling rather than from sintering. Zirconia-based mixtures did not react with the molybdenum containers. The inside surface of the molybdenum was still clean and shiny after testing. Other advantages were the ease in handling these free-flowing powders and the wide selection of economically-priced forms of zirconia, e.g., sintered or fused powder and hollow microspheres. (Zirconia fibers are no longer commercially available.)

One potential problem in using these mixtures is segregation of the coarse zirconia powder and the fine tungsten powder. This phenomenon was not

TABLE B-2  
SUMMARY OF TEST RESULTS

Specimen Number	Materials System		Linear Shrinkage (percent)	Relative Strength as a Result of Sintering*	Reaction With Container	Comments
	Matrix	Reflective Phase				
6-1	Zirconia	Tungsten Powder	5	Moderate	None	No apparent problems; inexpensive materials easy to prepare.
6-2	Zirconia	Tungsten Powder	0	None		
23-1	Zirconia	Tungsten Powder	5	Hard	None	
23-2	Zirconia	Tungsten Powder	1	Intermediate		
23-3	Zirconia	Tungsten Powder	Expanded****	Intermediate		
24-7	Zirconia	Tungsten Film	10.5	None		
24-6	Zirconia	Rhenium Film	2.5	None		
7-3	Zirconia	--	0	Intermediate		
7-4	Zirconia	--	8	Weak		
21-5	Zirconia	--	0	Intermediate		
22-4	Zirconia	--	Expanded**	None		
7-5	Zirconia	Molybdenum	6	Strong		
8-6	Thoria**	Tungsten Powder	15	Weak	None	Corrosion may be a problem. This particular thoria powder shrinks too much even though it was calcined.
8-7	Thoria**	Tantalum	9	Weak		
8-8	Thoria**	--	23	Weak		
8-9	Thoria	--	***	Weak		
8-21	Thoria**	Tungsten Film	***	None		
7-10	Graphite	Tantalum Powder	****	Weak		
7-11	Graphite	Rhenium Film	****	None		Severe containment and outgassing problem.
7-12	Graphite	Rhenium Film	****	None		
13	--	Tungsten Powder	Not measured	Strong	Stuck slightly in some areas.	

\*"None" means that the powder remained loosely packed.

"Weak" means that the powder compact adhered slightly such that the compact could be handled carefully as one unit.

"Intermediate" means that the powder compact was intermediate between "weak" and "strong".

"Strong" means that the powder compact adhered such that the compact was difficult to break with a scalpel.

\*\*Calcined at 2200 F for 2 hours to reduce sintering.

\*\*\*Bottom of container corroded such that the powder spilled during removal from furnace.

\*\*\*\*The container corroded so badly that shrinkage measurements of the powder was not possible.

TABLE B-3

## SUMMARY OF TEST DATA ON ZIRCONIA MIXTURES

Specimen Number	Form	Mesh Size	Weight Percent Tungsten Powder	Percent Vertical Linear Shrinkage	Relative Sintered Strength
7-3	Sintered Powder	-325	0	0	Intermediate
23-1	Sintered Powder	-325	11	5	Strong
6-1	Sintered Powder	-325	50	5	Intermediate
7-4	Sintered Powder	-100, +200	0	8(?)	Weak
21-5	Sintered Powder	-100, +200	0	0	Intermediate
23-2	Sintered Powder	-100, +200	11	1	Intermediate
23-3	Sintered Powder	-200, +325	11	+4 (Expanded)	Intermediate
22-4	Fused Powder (Hollow Microspheres)	-36, +48	10	+2 (Expanded)	None
22-4	Fused Powder (Hollow Microspheres)	-36, +65	10	nil	None
22-4	Fused Powder (Hollow Microspheres)	-36, +100	10	nil	None
22-4	Fused Powder (Hollow Microspheres)	-36	10	6	None

observed, however, in these small samples. The zirconia powder has to be coarse so that it does not sinter, whereas the tungsten powder has to be fine to disperse radiation optimally. Thus, a tradeoff exists in selection of particle sizes. Finer zirconia can be used if it is derived from fused rather than sintered powder. Powder derived from fusion processes sinters less readily than equivalent powder derived from sintering processes under the same conditions.

Tungsten as a fine powder was the best additive having a reflective surface. Tungsten is less reactive with oxides than other metals (Ref. B-2 and B-3), and the powder form is most convenient for incorporation in the matrix. Addition as a resinate requires special heat treating operations in air and in hydrogen to convert it to the metallic form. The advantage of adding it as a resinate is that it would be in the form of a very thin film. Thus, the apparent density of the mixture would be reduced. However, low apparent density was not essential for evaluating this concept as an effective high-temperature insulation system.

#### CONCLUSIONS

Based on the preceding results, the materials system selected for detailed testing consisted of 2 and 10 weight percent of fine tungsten powder dispersed in -36, +100 mesh, fused zirconia particles. The mixture was housed in a single-walled molybdenum foil container fabricated to the shape of the thermal conductivity specimens, e.g., a hollow cylinder 10 or 16 inches long, 6 inches outside diameter and 4 inches inside diameter.

#### APPENDIX B REFERENCES

- B-1. R-7121, Spacecraft Rocket Engine Chamber Insulation Materials, A. L. Huebner, L. W. Carlson, and H. Carpenter, Rocketdyne, a Division of North American Aviation, Inc., Canoga Park, California, Contract #NAS7-474, 26 July 1967.

- B-2. Johnson, P. D., "Behavior of Refractory Oxides and Metals, Alone and in Combination, in Vacuo at High Temperatures," J. Amer. Ceram. Soc., 33, (5), 168-71, 1950.
- B-3. Gartland, J. W., "A High-Temperature Electric Tube Furnace," Trans. Electro-chem. Soc., 88, 121, 1945.

# APPENDIX C

## CURVE FITTING MOLYBDENUM/SILICA EFFECTIVE THERMAL CONDUCTIVITY RESULTS FOR ARGON PRESSURIZATION OF 1-, 400-, 800-, AND 1600 MICRONS

The results of Fig. C-1 were curve fitted with eighth-order polynomials to within 1 percent using a least-squares curve fitting computer program called Polyfit on the General Electric time-sharing computer. The polynomial expression in temperature is of the form:

$$K = A + BT + CT^2 + DT^3 + ET^4 + FT^5 + GT^6 + HT^7 + IT^8$$

where

$$K = \text{Btu/hr-ft F}$$

$$T = \text{Temperature, F}$$

A tabulation of the alphabetic coefficients is given below for each argon pressure level.

Pressure Level, $\mu$	A	B	C	D	E	F	G	H	I
0	6.04669 $\times 10^{-3}$	-5.45866 $\times 10^{-5}$	3.47849 $\times 10^{-7}$	-1.01619 $\times 10^{-9}$	1.65284 $\times 10^{-12}$	-1.56839 $\times 10^{-15}$	8.65755 $\times 10^{-19}$	-2.57630 $\times 10^{-22}$	3.20219 $\times 10^{-26}$
400	5.41095 $\times 10^{-3}$	-1.39732 $\times 10^{-5}$	1.25999 $\times 10^{-7}$	-4.52236 $\times 10^{-10}$	8.75924 $\times 10^{-13}$	-9.65048 $\times 10^{-16}$	6.08006 $\times 10^{-19}$	-2.03093 $\times 10^{-22}$	2.78918 $\times 10^{-26}$
800	1.03663 $\times 10^{-2}$	-7.02132 $\times 10^{-5}$	4.68908 $\times 10^{-7}$	-1.45735 $\times 10^{-9}$	2.49084 $\times 10^{-12}$	-2.46466 $\times 10^{-15}$	1.41235 $\times 10^{-18}$	-4.34701 $\times 10^{-22}$	5.56304 $\times 10^{-26}$
1600	1.40044 $\times 10^{-2}$	-9.80218 $\times 10^{-5}$	6.54448 $\times 10^{-7}$	-2.06940 $\times 10^{-9}$	3.59660 $\times 10^{-12}$	-3.60636 $\times 10^{-15}$	2.08410 $\times 10^{-18}$	-6.44268 $\times 10^{-22}$	8.25532 $\times 10^{-26}$

APPENDIX D

TYPICAL TAP II DATA INPUT AND RESULTS OUTPUT LISTING  
 FOR THE GRAPHITE CHAMBER, INSULATION THICKNESS EQUALS  
 1.5 INCHES OF TANTALUM/CARBON, FIRING TIME EQUALS  
 600 SECONDS, SOAKBACK EQUALS 10,000 SECONDS

TAP 2		10/62				DIBORANE FIRING CONDUCTORS LINER AXI. RADIATE SPACE WALL WALL	
3	1	0	0.0	0.0	0.0		
1	1	2	0	0.10000E 01	0.0		
2	2	3	0	0.10000E 01	0.0		
3	4	15	0	0.10000E 01	0.0		
4	4	25	0	0.10000E 01	0.0		
9	1	9	0	0.10000E 01	0.0		
19	2	19	0	0.10000E 01	0.0		



[illegible]

R-7548

RHD\*C\*L

VOL. STEEL CASE TABLE  
3 IS STEEL RHO\*C.  
AREA/DIST. TABLE 4 K C  
INSULATION AREA/DIST.  
TABLE 5 IS INSULATION  
K/L

PRINTOUT SPEC.

CONDUCTION TO SPACE

11	11	2	5	0.12000E 03	0.0
12	12	2	6	0.12000E 03	0.0
13	13	2	7	0.12000E 03	0.0
14	14	2	8	0.12000E 03	0.0
19	19	2	9	0.90000E 02	0.0
20	20	2	10	0.90000E 02	0.0
21	21	2	11	0.18000E 03	0.0
22	22	2	12	0.18000E 03	0.0
23	23	2	13	0.18000E 03	0.0
24	24	2	14	0.18000E 03	0.0
15	15	3	15	0.61000E 01	0.0
25	25	3	16	0.91500E 01	0.0
1	-1	4	17	0.20500E 00	0.0
10	-1	5	19	0.61000E 04	0.0
11	-1	5	20	0.30500E 04	0.0
12	-1	5	21	0.30500E 04	0.0
13	-1	5	22	0.30500E 04	0.0
14	-1	5	23	0.30500E 04	0.0
15	-1	5	24	0.61000E 04	0.0
20	-1	5	26	0.90000E 04	0.0
21	-1	5	27	0.45000E 04	0.0
22	-1	5	28	0.45000E 04	0.0
23	-1	5	29	0.45000E 04	0.0
24	-1	5	30	0.45000E 04	0.0
25	-1	5	31	0.90000E 04	0.0
-1	0	0	0	0.0	0.0
8	2	1	1	0.0	0.0
0	2	2	2	0.0	0.0
0	2	9	3	0.0	0.0
0	2	10	4	0.0	0.0
0	2	11	5	0.0	0.0
0	2	12	6	0.0	0.0
0	2	13	7	0.0	0.0
0	2	14	8	0.0	0.0
0	2	15	9	0.0	0.0
0	2	19	10	0.0	0.0
0	2	20	11	0.0	0.0
0	2	21	12	0.0	0.0
0	2	22	13	0.0	0.0
0	2	23	14	0.0	0.0
0	2	24	15	0.0	0.0
0	2	25	16	0.0	0.0
0	1	2	17	0.0	0.0

□ □ □ □

0.6660E-07  
0.11220E-06  
0.15750E-06  
0.22200E-06  
0.28500E-06  
0.46800E-06  
0.76700E-06  
0.12660E-05

0 0 0 0 0.35000E 04 0.34900F-05  
 0 0 0 0 0.45000E 04 0.45000E-05  
 -1 0 0 0 0.0 0.0  
 -1 0 0 0 0.0 0.0  
 9999 0 0 0 0.0 0.0

END TABLES  
 END FIRING.

COMPUTER TIME 0.0 MINUTES

R-7548

0.0	0.0	0	0	0.0	0.0	0.0
T( 1)	T( 2)	T( 9)	T( 10)	T( 11)	T( 12)	T( 13)
0.45000E 04	0.45000E 04	0.70000E 02	0.70000E 02	0.70000E 02	0.70000E 02	0.70000E 02
T( 14)	T( 15)	T( 19)	T( 20)	T( 21)	T( 22)	T( 23)
0.70000E 02	0.70000E 02	0.70000E 02	0.70000E 02	0.70000E 02	0.70000E 02	0.70000E 02
T( 24)	T( 25)	K( 2)	K( 3)	K( 4)	K( 9)	K( 19)
0.70000E 02	0.70000E 02	0.60997E-01	0.17834E-03	0.26751E-03	0.47800E-01	0.10652E 00
100.0000000	9.9730406	19	20	6.2142677	0.0	
T( 1)	T( 2)	T( 9)	T( 10)	T( 11)	T( 12)	T( 13)
0.45000E 04	0.45000E 04	0.42695E 04	0.21660E 04	0.13381E 03	0.70531E 02	0.70003E 02
T( 14)	T( 15)	T( 19)	T( 20)	T( 21)	T( 22)	T( 23)
0.70000E 02	0.70000E 02	0.43436E 04	0.24915E 04	0.16244E 03	0.70817E 02	0.70005E 02
T( 24)	T( 25)	K( 2)	K( 3)	K( 4)	K( 9)	K( 19)
0.70000E 02	0.70000E 02	0.60997E-01	0.17834E-03	0.26751E-03	0.15926E 00	0.36302E 00
199.9999695	9.7473688	19	21	6.2142677	0.0	
T( 1)	T( 2)	T( 9)	T( 10)	T( 11)	T( 12)	T( 13)
0.45000E 04	0.45000E 04	0.43582E 04	0.34835E 04	0.45927E 03	0.79286E 02	0.70133E 02
T( 14)	T( 15)	T( 19)	T( 20)	T( 21)	T( 22)	T( 23)
0.70000E 02	0.70000E 02	0.44175E 04	0.36215E 04	0.52195E 03	0.81669E 02	0.70175E 02
T( 24)	T( 25)	K( 2)	K( 3)	K( 4)	K( 9)	K( 19)

0.70002E 02	0.70000E 02	0.60997E-01	0.17834E-03	0.26751E-03	0.16361E 00	0.37125E 00
259.9987793 9.6927948 19 21 6.2142677 0.0						
T( 1)	T( 2)	T( 9)	T( 10)	T( 11)	T( 12)	T( 13)
0.45000E 04	0.45000E 04	0.44105E 04	0.38462E 04	0.89129E 03	0.10802E 03	0.70913E 02
T( 14)	T( 15)	T( 19)	T( 20)	T( 21)	T( 22)	T( 23)
0.70016E 02	0.70002E 02	0.44444E 04	0.39036E 04	0.96711E 03	0.11431E 03	0.71094E 02
T( 24)	T( 25)	K( 2)	K( 3)	K( 4)	K( 9)	K( 19)
0.70020E 02	0.70002E 02	0.60997E-01	0.17834E-03	0.26751E-03	0.16623E 00	0.37430E 00
359.9963379 9.6820345 19 21 6.2142677 0.0						
T( 1)	T( 2)	T( 9)	T( 10)	T( 11)	T( 12)	T( 13)
0.45000E 04	0.45000E 04	0.44242E 04	0.39309E 04	0.13300E 04	0.16509E 03	0.73271E 02
T( 14)	T( 15)	T( 19)	T( 20)	T( 21)	T( 22)	T( 23)
0.70083E 02	0.70014E 02	0.44500E 04	0.39532E 04	0.14126E 04	0.17611E 03	0.73735E 02
T( 24)	T( 25)	K( 2)	K( 3)	K( 4)	K( 9)	K( 19)
0.70097E 02	0.70016E 02	0.60997E-01	0.17835E-03	0.26752E-03	0.16693E 00	0.37492E 00
499.9938965 9.6853285 19 21 6.2142677 0.0						
T( 1)	T( 2)	T( 9)	T( 10)	T( 11)	T( 12)	T( 13)
0.45000E 04	0.45000E 04	0.44235E 04	0.39185E 04	0.17659E 04	0.25489E 03	0.78437E 02
T( 14)	T( 15)	T( 19)	T( 20)	T( 21)	T( 22)	T( 23)
0.70277E 02	0.70058E 02	0.44484E 04	0.39340E 04	0.18435E 04	0.27084E 03	0.79364E 02
T( 24)	T( 25)	K( 2)	K( 3)	K( 4)	K( 9)	K( 19)
0.70310E 02	0.70065E 02	0.60997E-01	0.17837E-03	0.26756E-03	0.16689E 00	0.37475E 00
599.9919434 9.6870775 19 21 6.2142677 0.0						
T( 1)	T( 2)	T( 9)	T( 10)	T( 11)	T( 12)	T( 13)
0.45000E 04	0.45000E 04	0.44217E 04	0.39069E 04	0.21466E 04	0.36552E 03	0.87707E 02

T( 14)	T( 15)	T( 19)	T( 20)	T( 21)	T( 22)	T( 23)
0.70714E 02	0.70176E 02	0.44475E 04	0.39258E 04	0.22132E 04	0.38417E 03	0.89194E 02
T( 24)	T( 25)	K( 2)	K( 3)	K( 4)	K( 9)	K( 19)
0.70782E 02	0.70193E 02	0.60997E-01	0.17843E-03	0.26765E-03	0.16680E 00	0.37465E 00

COMPUTER TIME 0.0 MINUTES

R-7548

TAP 2 10/62

3	2	0	0	0.0	0.0
-1	0	0	0	0.0	0.0
-1	0	0	0	0.0	0.0
7	0	0	0	0.0	0.0
1	1	1	1	0.20000E 02	0.0
2	2	1	2	0.71000E 02	0.0
-1	0	0	0	0.0	0.0
9	0	1	0	0.20000E 03	0.0
0	0	3	0	0.50000E 00	0.0
0	0	4	0	0.10000E 05	0.0
-1	0	0	0	0.0	0.0
-1	0	0	0	0.0	0.0
-1	0	0	0	0.0	0.0
9999	0	0	0	0.0	0.0

SOAKBACK

VOL.OF LINER.CORRECT  
 VALUE USED IN SOAKBACK  
 END FUNCTION 7  
 PRINT INTERVAL

TOTAL TIME  
 END 9

END FUNCS.  
 END TABLES  
 END CASE

COMPUTER TIME 0.0 MINUTES

759.9907227	6.0556841	1	78	4.3158360	600.0000000
T( 1)	T( 2)	T( 9)	T( 10)	T( 11)	T( 12)
0.39360E 04	0.21939E 04	0.39252E 04	0.36782E 04	0.26522E 04	0.66010E 03
T( 14)	T( 15)	T( 19)	T( 20)	T( 21)	T( 22)
0.73071E 02	0.70964E 02	0.24356E 04	0.28915E 04	0.24798E 04	0.66109E 03
T( 24)	T( 25)	K( 2)	K( 3)	K( 4)	K( 9)
0.73244E 02	0.71021E 02	0.93413E-02	0.17883E-03	0.26828E-03	0.11847E 00

R-7548

999.9846191	7.4888668	1	60	4.3158360	600.0000000
T( 1)	T( 2)	T( 9)	T( 10)	T( 11)	T( 12)
0.36386E 04	0.17393E 04	0.36303E 04	0.34697E 04	0.28201E 04	0.97914E 03
T( 14)	T( 15)	T( 19)	T( 20)	T( 21)	T( 22)
0.78736E 02	0.73216E 02	0.19435E 04	0.24203E 04	0.23749E 04	0.88415E 03

T( 13)  
 0.18791E 03  
 T( 23)  
 0.18335E 03

T( 24)	T( 25)	K( 2)	K( 3)	K( 4)	K( 9)	K( 19)
0.78786E 02	0.73281E 02	0.53161E-02	0.17997E-03	0.27000E-03	0.96078E-01	0.38090E-01
R 1199.9792480 8.6702080 1 50 4.3158360 600.0000000						
T( 1)	T( 2)	T( 9)	T( 10)	T( 11)	T( 12)	T( 13)
0.34411E 04	0.15044E 04	0.34347E 04	0.33182E 04	0.28456E 04	0.12613E 04	0.27670E 03
T( 14)	T( 15)	T( 19)	T( 20)	T( 21)	T( 22)	T( 23)
0.89685E 02	0.78207E 02	0.16902E 04	0.21516E 04	0.22365E 04	0.10394E 04	0.25221E 03
T( 24)	T( 25)	K( 2)	K( 3)	K( 4)	K( 9)	K( 19)
0.88454E 02	0.77910E 02	0.37875E-02	0.18253E-03	0.27356E-03	0.82895E-01	0.27210E-01
R 1399.9738770 9.6981859 1 44 4.3158360 600.0000000						
T( 1)	T( 2)	T( 9)	T( 10)	T( 11)	T( 12)	T( 13)
0.32977E 04	0.13544E 04	0.32924E 04	0.31973E 04	0.28112E 04	0.14954E 04	0.37169E 03
T( 14)	T( 15)	T( 19)	T( 20)	T( 21)	T( 22)	T( 23)
0.10676E 03	0.87170E 02	0.15295E 04	0.19621E 04	0.21072E 04	0.11445E 04	0.31772E 03
T( 24)	T( 25)	K( 2)	K( 3)	K( 4)	K( 9)	K( 19)
0.10226E 03	0.85531E 02	0.29844E-02	0.18720E-03	0.27951E-03	0.74107E-01	0.21500E-01
R 1599.9699707 10.6441460 1 40 4.3158360 600.0000000						
T( 1)	T( 2)	T( 9)	T( 10)	T( 11)	T( 12)	T( 13)
0.31832E 04	0.12465E 04	0.31787E 04	0.30962E 04	0.27595E 04	0.16732E 04	0.47818E 03
T( 14)	T( 15)	T( 19)	T( 20)	T( 21)	T( 22)	T( 23)
0.13017E 03	0.10076E 03	0.14124E 04	0.18178E 04	0.19940E 04	0.12127E 04	0.37719E 03
T( 24)	T( 25)	K( 2)	K( 3)	K( 4)	K( 9)	K( 19)
0.11933E 03	0.96120E 02	0.24830E-02	0.19448E-03	0.28795E-03	0.67555E-01	0.17906E-01
R 1799.9658203 11.5351944 1 37 4.3158360 600.0000000						
T( 1)	T( 2)	T( 9)	T( 10)	T( 11)	T( 12)	T( 13)



0.30872E 04	0.11626E 04	0.30833E 04	0.30095E 04	0.27069E 04	0.17990E 04	0.59444E 03
T( 14)	T( 15)	T( 19)	T( 20)	T( 21)	T( 22)	T( 23)
0.16048E 03	0.11948E 03	0.13206E 04	0.17045E 04	0.18962E 04	0.12540E 04	0.43507E 03
T( 24)	T( 25)	K( 2)	K( 3)	K( 4)	K( 9)	K( 19)
0.13912E 03	0.10929E 03	0.21344E-02	0.20492E-03	0.29877E-03	0.62366E-01	0.15398E-01
1999.9614258	12.3653307	1	34	4.3158360	600.0000000	
T( 1)	T( 2)	T( 9)	T( 10)	T( 11)	T( 12)	T( 13)
0.30048E 04	0.10948E 04	0.30013E 04	0.29342E 04	0.26583E 04	0.18847E 04	0.71099E 03
T( 14)	T( 15)	T( 19)	T( 20)	T( 21)	T( 22)	T( 23)
0.19770E 03	0.14361E 03	0.12471E 04	0.16108E 04	0.18117E 04	0.12765E 04	0.48951E 03
T( 24)	T( 25)	K( 2)	K( 3)	K( 4)	K( 9)	K( 19)
0.16117E 03	0.12464E 03	0.18776E-02	0.21908E-03	0.31182E-03	0.58129E-01	0.13557E-01
2199.9572754	13.1701479	1	32	4.3158360	600.0000000	
T( 1)	T( 2)	T( 9)	T( 10)	T( 11)	T( 12)	T( 13)
0.29329E 04	0.10391E 04	0.29299E 04	0.28683E 04	0.26142E 04	0.19418E 04	0.82113E 03
T( 14)	T( 15)	T( 19)	T( 20)	T( 21)	T( 22)	T( 23)
0.24136E 03	0.17302E 03	0.11868E 04	0.15297E 04	0.17383E 04	0.12861E 04	0.53924E 03
T( 24)	T( 25)	K( 2)	K( 3)	K( 4)	K( 9)	K( 19)
0.18488E 03	0.14169E 03	0.16829E-02	0.23744E-03	0.32688E-03	0.54592E-01	0.12161E-01
2399.9543457	13.9307814	1	30	4.3158360	600.0000000	
T( 1)	T( 2)	T( 9)	T( 10)	T( 11)	T( 12)	T( 13)
0.28694E 04	0.99190E 03	0.28667E 04	0.28098E 04	0.25740E 04	0.19787E 04	0.92164E 03
T( 14)	T( 15)	T( 19)	T( 20)	T( 21)	T( 22)	T( 23)
0.28742E 03	0.20627E 03	0.11352E 04	0.14592E 04	0.16738E 04	0.12868E 04	0.58378E 03
T( 24)	T( 25)	K( 2)	K( 3)	K( 4)	K( 9)	K( 19)
0.20965E 03	0.15990E 03	0.15290E-02	0.25972E-03	0.34364E-03	0.51591E-01	0.11052E-01

2599.9514160	14.6520557	1	28	4.3158360	600.0000000	
T( 1)	T( 2)	T( 9)	T( 10)	T( 11)	T( 12)	T( 13)
0.28128E 04	0.95102E 03	0.28105E 04	0.27576E 04	0.25370E 04	0.20017E 04	0.10117E 04
T( 14)	T( 15)	T( 19)	T( 20)	T( 21)	T( 22)	T( 23)
0.33288E 03	0.24024E 03	0.10903E 04	0.13975E 04	0.16161E 04	0.12820E 04	0.62307E 03
T( 24)	T( 25)	K( 2)	K( 3)	K( 4)	K( 9)	K( 19)
0.23499E 03	0.17874E 03	0.14034E-02	0.28422E-03	0.36173E-03	0.49011E-01	0.10144E-01
2799.9479980	15.3648682	1	27	4.3158360	600.0000000	
T( 1)	T( 2)	T( 9)	T( 10)	T( 11)	T( 12)	T( 13)
0.27619E 04	0.91498E 03	0.27599E 04	0.27104E 04	0.25027E 04	0.20141E 04	0.10933E 04
T( 14)	T( 15)	T( 19)	T( 20)	T( 21)	T( 22)	T( 23)
0.37875E 03	0.27357E 03	0.10505E 04	0.13431E 04	0.15642E 04	0.12734E 04	0.65732E 03
T( 24)	T( 25)	K( 2)	K( 3)	K( 4)	K( 9)	K( 19)
0.26009E 03	0.19773E 03	0.12986E-02	0.31002E-03	0.38076E-03	0.46765E-01	0.93842E-02
2999.9448242	16.0470428	1	26	4.3158360	600.0000000	
T( 1)	T( 2)	T( 9)	T( 10)	T( 11)	T( 12)	T( 13)
0.27157E 04	0.88287E 03	0.27140E 04	0.26675E 04	0.24704E 04	0.20190E 04	0.11662E 04
T( 14)	T( 15)	T( 19)	T( 20)	T( 21)	T( 22)	T( 23)
0.42692E 03	0.30700E 03	0.10151E 04	0.12953E 04	0.15167E 04	0.12622E 04	0.68690E 03
T( 24)	T( 25)	K( 2)	K( 3)	K( 4)	K( 9)	K( 19)
0.28380E 03	0.21601E 03	0.12097E-02	0.33773E-03	0.39985E-03	0.44789E-01	0.87402E-02
3199.9416504	16.7024078	1	25	4.3158360	600.0000000	
T( 1)	T( 2)	T( 9)	T( 10)	T( 11)	T( 12)	T( 13)
0.26735E 04	0.85402E 03	0.26721E 04	0.26281E 04	0.24399E 04	0.20190E 04	0.12298E 04
T( 14)	T( 15)	T( 19)	T( 20)	T( 21)	T( 22)	T( 23)
0.47679E 03	0.34087E 03	0.98320E 03	0.12526E 04	0.14733E 04	0.12492E 04	0.71225E 03

T( 24)	T( 25)	K( 2)	K( 3)	K( 4)	K( 9)	K( 19)
0.30614E 03	0.23316E 03	0.11334E-02	0.36773E-03	0.41844E-03	0.43032E-01	0.81873E-02
3399.9389648 17.3341980 1 24 4.3158360 600.0000000						
T( 1)	T( 2)	T( 9)	T( 10)	T( 11)	T( 12)	T( 13)
0.26347E 04	0.82793E 03	0.26335E 04	0.25917E 04	0.24108E 04	0.20160E 04	0.12846E 04
T( 14)	T( 15)	T( 19)	T( 20)	T( 21)	T( 22)	T( 23)
0.52694E 03	0.37521E 03	0.95435E 03	0.12142E 04	0.14334E 04	0.12352E 04	0.73381E 03
T( 24)	T( 25)	K( 2)	K( 3)	K( 4)	K( 9)	K( 19)
0.32712E 03	0.24908E 03	0.10672E-02	0.40022E-03	0.43633E-03	0.41458E-01	0.77074E-02
3599.9357910 17.9471741 1 23 4.3158360 600.0000000						
T( 1)	T( 2)	T( 9)	T( 10)	T( 11)	T( 12)	T( 13)
0.25987E 04	0.80417E 03	0.25977E 04	0.25573E 04	0.23836E 04	0.20111E 04	0.13313E 04
T( 14)	T( 15)	T( 19)	T( 20)	T( 21)	T( 22)	T( 23)
0.57627E 03	0.40887E 03	0.92804E 03	0.11793E 04	0.13966E 04	0.12205E 04	0.75199E 03
T( 24)	T( 25)	K( 2)	K( 3)	K( 4)	K( 9)	K( 19)
0.34681E 03	0.26381E 03	0.10092E-02	0.43414E-03	0.45341E-03	0.40030E-01	0.72867E-02
3799.9331055 18.5500793 1 22 4.3158360 600.0000000						
T( 1)	T( 2)	T( 9)	T( 10)	T( 11)	T( 12)	T( 13)
0.25647E 04	0.78240E 03	0.25638E 04	0.25244E 04	0.23584E 04	0.20050E 04	0.13711E 04
T( 14)	T( 15)	T( 19)	T( 20)	T( 21)	T( 22)	T( 23)
0.62391E 03	0.44091E 03	0.90384E 03	0.11473E 04	0.13624E 04	0.12055E 04	0.76721E 03
T( 24)	T( 25)	K( 2)	K( 3)	K( 4)	K( 9)	K( 19)
0.36568E 03	0.27754E 03	0.95789E-03	0.46842E-03	0.46982E-03	0.38713E-01	0.69142E-02
3999.9304199 19.1735382 1 22 4.3158360 600.0000000						
T( 1)	T( 2)	T( 9)	T( 10)	T( 11)	T( 12)	T( 13)

0.25325E 04	0.76231E 03	0.25318E 04	0.24932E 04	0.23345E 04	0.19982E 04	0.14044E 04
T( 14)	T( 15)	T( 19)	T( 20)	T( 21)	T( 22)	T( 23)
0.66963E 03	0.47096E 03	0.88149E 03	0.11180E 04	0.13306E 04	0.11904E 04	0.77984E 03
T( 24)	T( 25)	K( 2)	K( 3)	K( 4)	K( 9)	K( 19)
0.38374E 03	0.29050E 03	0.91217E-03	0.50237E-03	0.48573E-03	0.37493E-01	0.65818E-02
4199.8984375	19.7618103	1	21	4.3158360	600.0000000	
T( 1)	T( 2)	T( 9)	T( 10)	T( 11)	T( 12)	T( 13)
0.25019E 04	0.74375E 03	0.25013E 04	0.24637E 04	0.23120E 04	0.19910E 04	0.14320E 04
T( 14)	T( 15)	T( 19)	T( 20)	T( 21)	T( 22)	T( 23)
0.71331E 03	0.49908E 03	0.86099E 03	0.10906E 04	0.13010E 04	0.11754E 04	0.79023E 03
T( 24)	T( 25)	K( 2)	K( 3)	K( 4)	K( 9)	K( 19)
0.40085E 03	0.30269E 03	0.87123E-03	0.53577E-03	0.50107E-03	0.36356E-01	0.62854E-02
4399.8554687	20.3472748	1	20	4.3158360	600.0000000	
T( 1)	T( 2)	T( 9)	T( 10)	T( 11)	T( 12)	T( 13)
0.24726E 04	0.72662E 03	0.24721E 04	0.24361E 04	0.22905E 04	0.19834E 04	0.14548E 04
T( 14)	T( 15)	T( 19)	T( 20)	T( 21)	T( 22)	T( 23)
0.75439E 03	0.52511E 03	0.84210E 03	0.10648E 04	0.12732E 04	0.11605E 04	0.79867E 03
T( 24)	T( 25)	K( 2)	K( 3)	K( 4)	K( 9)	K( 19)
0.41693E 03	0.31407E 03	0.83454E-03	0.56812E-03	0.51575E-03	0.35288E-01	0.60201E-02
4599.8085937	20.9578857	1	20	4.3158360	600.0000000	
T( 1)	T( 2)	T( 9)	T( 10)	T( 11)	T( 12)	T( 13)
0.24445E 04	0.71072E 03	0.24441E 04	0.24098E 04	0.22701E 04	0.19755E 04	0.14736E 04
T( 14)	T( 15)	T( 19)	T( 20)	T( 21)	T( 22)	T( 23)
0.79252E 03	0.54890E 03	0.82451E 03	0.10405E 04	0.12471E 04	0.11459E 04	0.80542E 03
T( 24)	T( 25)	K( 2)	K( 3)	K( 4)	K( 9)	K( 19)
0.43195E 03	0.32464E 03	0.80144E-03	0.59892E-03	0.52966E-03	0.34287E-01	0.57802E-02

4799.7500000	21.5312653	1	19	4.3158360	600.0000000	
T( 1)	T( 2)	T( 9)	T( 10)	T( 11)	T( 12)	T( 13)
0.24178E 04	0.69590E 03	0.24175E 04	0.23847E 04	0.22505E 04	0.19674E 04	0.14892E 04
T( 14)	T( 15)	T( 19)	T( 20)	T( 21)	T( 22)	T( 23)
0.82754E 03	0.57043E 03	0.80803E 03	0.10178E 04	0.12225E 04	0.11315E 04	0.81071E 03
T( 24)	T( 25)	K( 2)	K( 3)	K( 4)	K( 9)	K( 19)
0.44588E 03	0.33438E 03	0.77137E-03	0.62784E-03	0.54274E-03	0.33350E-01	0.55618E-02

202

4999.7148437	22.1296387	1	19	4.3158360	600.0000000	
T( 1)	T( 2)	T( 9)	T( 10)	T( 11)	T( 12)	T( 13)
0.23922E 04	0.68201E 03	0.23920E 04	0.23607E 04	0.22318E 04	0.19591E 04	0.15020E 04
T( 14)	T( 15)	T( 19)	T( 20)	T( 21)	T( 22)	T( 23)
0.85943E 03	0.58976E 03	0.79254E 03	0.99632E 03	0.11993E 04	0.11175E 04	0.81472E 03
T( 24)	T( 25)	K( 2)	K( 3)	K( 4)	K( 9)	K( 19)
0.45872E 03	0.34330E 03	0.74389E-03	0.65467E-03	0.55495E-03	0.32471E-01	0.53619E-02

5199.6835938	22.6894531	1	18	4.3158360	600.0000000	
T( 1)	T( 2)	T( 9)	T( 10)	T( 11)	T( 12)	T( 13)
0.23677E 04	0.66895E 03	0.23677E 04	0.23378E 04	0.22138E 04	0.19507E 04	0.15126E 04
T( 14)	T( 15)	T( 19)	T( 20)	T( 21)	T( 22)	T( 23)
0.88825E 03	0.60701E 03	0.77792E 03	0.97611E 03	0.11773E 04	0.11038E 04	0.81762E 03
T( 24)	T( 25)	K( 2)	K( 3)	K( 4)	K( 9)	K( 19)
0.47047E 03	0.35157E 03	0.71865E-03	0.67930E-03	0.56644E-03	0.31644E-01	0.51781E-02

5399.6484375	23.2755127	1	18	4.3158360	600.0000000	
T( 1)	T( 2)	T( 9)	T( 10)	T( 11)	T( 12)	T( 13)
0.23443E 04	0.65663E 03	0.23444E 04	0.23158E 04	0.21964E 04	0.19422E 04	0.15211E 04
T( 14)	T( 15)	T( 19)	T( 20)	T( 21)	T( 22)	T( 23)
0.91404E 03	0.62281E 03	0.76411E 03	0.95701E 03	0.11564E 04	0.10905E 04	0.81956E 03

R-7548

T( 24)	T( 25)	K( 2)	K( 3)	K( 4)	K( 9)	K( 19)
0.48116E 03	0.35913E 03	0.69536E-03	0.70246E-03	0.57712E-03	0.30866E-01	0.50083E-02
5599.6093750	23.8223267	1	17	4.3158360	600.0000000	
T( 1)	T( 2)	T( 9)	T( 10)	T( 11)	T( 12)	T( 13)
0.23218E 04	0.64497E 03	0.23220E 04	0.22947E 04	0.21796E 04	0.19335E 04	0.15280E 04
T( 14)	T( 15)	T( 19)	T( 20)	T( 21)	T( 22)	T( 23)
0.93694E 03	0.63710E 03	0.75101E 03	0.93893E 03	0.11366E 04	0.10776E 04	0.82065E 03
T( 24)	T( 25)	K( 2)	K( 3)	K( 4)	K( 9)	K( 19)
0.49084E 03	0.36597E 03	0.67380E-03	0.72387E-03	0.58691E-03	0.30131E-01	0.48509E-02
5799.5820312	24.3968353	1	17	4.3158360	600.0000000	
T( 1)	T( 2)	T( 9)	T( 10)	T( 11)	T( 12)	T( 13)
0.23002E 04	0.63391E 03	0.23005E 04	0.22744E 04	0.21633E 04	0.19248E 04	0.15334E 04
T( 14)	T( 15)	T( 19)	T( 20)	T( 21)	T( 22)	T( 23)
0.95717E 03	0.64963E 03	0.73856E 03	0.92176E 03	0.11177E 04	0.10649E 04	0.82099E 03
T( 24)	T( 25)	K( 2)	K( 3)	K( 4)	K( 9)	K( 19)
0.49955E 03	0.37211E 03	0.65377E-03	0.74304E-03	0.59580E-03	0.29437E-01	0.47047E-02
5999.5507812	24.9662323	1	17	4.3158360	600.0000000	
T( 1)	T( 2)	T( 9)	T( 10)	T( 11)	T( 12)	T( 13)
0.22795E 04	0.62340E 03	0.22799E 04	0.22549E 04	0.21476E 04	0.19160E 04	0.15374E 04
T( 14)	T( 15)	T( 19)	T( 20)	T( 21)	T( 22)	T( 23)
0.97498E 03	0.66058E 03	0.72671E 03	0.90541E 03	0.10997E 04	0.10527E 04	0.82069E 03
T( 24)	T( 25)	K( 2)	K( 3)	K( 4)	K( 9)	K( 19)
0.50734E 03	0.37760E 03	0.63510E-03	0.76009E-03	0.60383E-03	0.28779E-01	0.45682E-02
6199.5234375	25.4956970	1	16	4.3158360	600.0000000	
T( 1)	T( 2)	T( 9)	T( 10)	T( 11)	T( 12)	T( 13)

0.22595E 04	0.61339E 03	0.22600E 04	0.22361E 04	0.21323E 04	0.19072E 04	0.15404E 04
T( 14)	T( 15)	T( 19)	T( 20)	T( 21)	T( 22)	T( 23)
0.99054E 03	0.67010E 03	0.71540E 03	0.88988E 03	0.10825E 04	0.10407E 04	0.81982E 03
T( 24)	T( 25)	K( 2)	K( 3)	K( 4)	K( 9)	K( 19)
0.51426E 03	0.38246E 03	0.61765E-03	0.77515E-03	0.61103E-03	0.28155E-01	0.44406E-02
6399.4882812	26.0551910	1	16	4.3158360	600.0000000	
T( 1)	T( 2)	T( 9)	T( 10)	T( 11)	T( 12)	T( 13)
0.22402E 04	0.60385E 03	0.22408E 04	0.22179E 04	0.21175E 04	0.18984E 04	0.15423E 04
T( 14)	T( 15)	T( 19)	T( 20)	T( 21)	T( 22)	T( 23)
0.10040E 04	0.67833E 03	0.70461E 03	0.87520E 03	0.10659E 04	0.10291E 04	0.81845E 03
T( 24)	T( 25)	K( 2)	K( 3)	K( 4)	K( 9)	K( 19)
0.52037E 03	0.38676E 03	0.60131E-03	0.78832E-03	0.61743E-03	0.27562E-01	0.43212E-02
6599.4531250	26.6103973	1	16	4.3158360	600.0000000	
T( 1)	T( 2)	T( 9)	T( 10)	T( 11)	T( 12)	T( 13)
0.22216E 04	0.59473E 03	0.22223E 04	0.22004E 04	0.21031E 04	0.18895E 04	0.15433E 04
T( 14)	T( 15)	T( 19)	T( 20)	T( 21)	T( 22)	T( 23)
0.10157E 04	0.68539E 03	0.69432E 03	0.86125E 03	0.10500E 04	0.10178E 04	0.81663E 03
T( 24)	T( 25)	K( 2)	K( 3)	K( 4)	K( 9)	K( 19)
0.52571E 03	0.39052E 03	0.58599E-03	0.79976E-03	0.62308E-03	0.26998E-01	0.42092E-02
6799.4296875	27.1252136	1	15	4.3158360	600.0000000	
T( 1)	T( 2)	T( 9)	T( 10)	T( 11)	T( 12)	T( 13)
0.22036E 04	0.58603E 03	0.22044E 04	0.21834E 04	0.20889E 04	0.18807E 04	0.15435E 04
T( 14)	T( 15)	T( 19)	T( 20)	T( 21)	T( 22)	T( 23)
0.10256E 04	0.69141E 03	0.68448E 03	0.84797E 03	0.10348E 04	0.10067E 04	0.81443E 03
T( 24)	T( 25)	K( 2)	K( 3)	K( 4)	K( 9)	K( 19)
0.53035E 03	0.39379E 03	0.57159E-03	0.80960E-03	0.62803E-03	0.26459E-01	0.41040E-02

6959.4023437	27.6726379	1	15	4.3158360	600.0000000	
T( 1)	T( 2)	T( 9)	T( 10)	T( 11)	T( 12)	T( 13)
0.21862E 04	0.57770E 03	0.21871E 04	0.21669E 04	0.20750E 04	0.18720E 04	0.15430E 04
T( 14)	T( 15)	T( 19)	T( 20)	T( 21)	T( 22)	T( 23)
0.10340E 04	0.69648E 03	0.67508E 03	0.83529E 03	0.10200E 04	0.99597E 03	0.81187E 03
T( 24)	T( 25)	K( 2)	K( 3)	K( 4)	K( 9)	K( 19)
0.53432E 03	0.39660E 03	0.55804E-03	0.81797E-03	0.63230E-03	0.25945E-01	0.40051E-02

R-7548

7199.3750000	28.2173157	1	15	4.3158360	600.0000000	
T( 1)	T( 2)	T( 9)	T( 10)	T( 11)	T( 12)	T( 13)
0.21693E 04	0.56973E 03	0.21703E 04	0.21508E 04	0.20613E 04	0.18634E 04	0.15418E 04
T( 14)	T( 15)	T( 19)	T( 20)	T( 21)	T( 22)	T( 23)
0.10410E 04	0.70072E 03	0.66607E 03	0.82315E 03	0.10059E 04	0.98548E 03	0.80901E 03
T( 24)	T( 25)	K( 2)	K( 3)	K( 4)	K( 9)	K( 19)
0.53768E 03	0.39899E 03	0.54527E-03	0.82500E-03	0.63595E-03	0.25452E-01	0.39118E-02

7399.3476562	28.7596893	1	15	4.3158360	600.0000000	
T( 1)	T( 2)	T( 9)	T( 10)	T( 11)	T( 12)	T( 13)
0.21529E 04	0.56210E 03	0.21539E 04	0.21352E 04	0.20480E 04	0.18548E 04	0.15400E 04
T( 14)	T( 15)	T( 19)	T( 20)	T( 21)	T( 22)	T( 23)
0.10467E 04	0.70421E 03	0.65750E 03	0.81143E 03	0.99222E 03	0.97524E 03	0.80588E 03
T( 24)	T( 25)	K( 2)	K( 3)	K( 4)	K( 9)	K( 19)
0.54047E 03	0.40099E 03	0.53324E-03	0.83082E-03	0.63902E-03	0.24980E-01	0.38243E-02

7599.3164062	29.2614288	1	14	4.3158360	600.0000000	
T( 1)	T( 2)	T( 9)	T( 10)	T( 11)	T( 12)	T( 13)
0.21369E 04	0.55480E 03	0.21381E 04	0.21200E 04	0.20349E 04	0.18462E 04	0.15378E 04
T( 14)	T( 15)	T( 19)	T( 20)	T( 21)	T( 22)	T( 23)
0.10513E 04	0.70703E 03	0.64929E 03	0.80012E 03	0.97903E 03	0.96525E 03	0.80250E 03

205



T( 24)	T( 25)	K( 2)	K( 3)	K( 4)	K( 9)	K( 19)
0.54274E 03	0.40264E 03	0.52189E-03	0.83555E-03	0.64156E-03	0.24526E-01	0.37416E-02
7799.3007812	29.7997284	1	14	4.3158360	600.0000000	
T( 1)	T( 2)	T( 9)	T( 10)	T( 11)	T( 12)	T( 13)
0.21214E 04	0.54780E 03	0.21226E 04	0.21052E 04	0.20220E 04	0.18376E 04	0.15350E 04
T( 14)	T( 15)	T( 19)	T( 20)	T( 21)	T( 22)	T( 23)
0.10550E 04	0.70925E 03	0.64140E 03	0.78923E 03	0.96628E 03	0.95549E 03	0.79891E 03
T( 24)	T( 25)	K( 2)	K( 3)	K( 4)	K( 9)	K( 19)
0.54453E 03	0.40396E 03	0.51116E-03	0.83930E-03	0.64359E-03	0.24090E-01	0.36634E-02
7999.2734375	30.3367004	1	14	4.3158360	600.0000000	
T( 1)	T( 2)	T( 9)	T( 10)	T( 11)	T( 12)	T( 13)
0.21062E 04	0.54108E 03	0.21076E 04	0.20908E 04	0.20094E 04	0.18290E 04	0.15319E 04
T( 14)	T( 15)	T( 19)	T( 20)	T( 21)	T( 22)	T( 23)
0.10577E 04	0.71095E 03	0.63380E 03	0.77872E 03	0.95396E 03	0.94596E 03	0.79514E 03
T( 24)	T( 25)	K( 2)	K( 3)	K( 4)	K( 9)	K( 19)
0.54587E 03	0.40497E 03	0.50100E-03	0.84216E-03	0.64516E-03	0.23670E-01	0.35893E-02
8199.2460937	30.8726044	1	14	4.3158360	600.0000000	
T( 1)	T( 2)	T( 9)	T( 10)	T( 11)	T( 12)	T( 13)
0.20915E 04	0.53462E 03	0.20929E 04	0.20767E 04	0.19971E 04	0.18205E 04	0.15283E 04
T( 14)	T( 15)	T( 19)	T( 20)	T( 21)	T( 22)	T( 23)
0.10596E 04	0.71217E 03	0.62647E 03	0.76859E 03	0.94203E 03	0.93662E 03	0.79119E 03
T( 24)	T( 25)	K( 2)	K( 3)	K( 4)	K( 9)	K( 19)
0.54680E 03	0.40571E 03	0.49136E-03	0.84423E-03	0.64631E-03	0.23265E-01	0.35188E-02
8399.2226562	31.3664856	1	13	4.3158360	600.0000000	
T( 1)	T( 2)	T( 9)	T( 10)	T( 11)	T( 12)	T( 13)

0.2C771E 04	0.52839E 03	0.20785E 04	0.20629E 04	0.19849E 04	0.18119E 04	0.15244E 04
T( 14)	T( 15)	T( 19)	T( 20)	T( 21)	T( 22)	T( 23)
0.10608E 04	0.71298E 03	0.61940E 03	0.75880E 03	0.93047E 03	0.92748E 03	0.78709E 03
T( 24)	T( 25)	K( 2)	K( 3)	K( 4)	K( 9)	K( 19)
0.54735E 03	0.40620E 03	0.48218E-03	0.84558E-03	0.64706E-03	0.22874E-01	0.34517E-02
8599.1914063	31.9002838	1	13	4.3158360	600.0000000	
T( 1)	T( 2)	T( 9)	T( 10)	T( 11)	T( 12)	T( 13)
0.20630E 04	0.52239E 03	0.20645E 04	0.20494E 04	0.19730E 04	0.18033E 04	0.15201E 04
T( 14)	T( 15)	T( 19)	T( 20)	T( 21)	T( 22)	T( 23)
0.10614E 04	0.71340E 03	0.61256E 03	0.74935E 03	0.91925E 03	0.91851E 03	0.78287E 03
T( 24)	T( 25)	K( 2)	K( 3)	K( 4)	K( 9)	K( 19)
0.54756E 03	0.40646E 03	0.47344E-03	0.84630E-03	0.64746E-03	0.22497E-01	0.33877E-02
8799.1679687	32.4337006	1	13	4.3158360	600.0000000	
T( 1)	T( 2)	T( 9)	T( 10)	T( 11)	T( 12)	T( 13)
0.20492E 04	0.51658E 03	0.20508E 04	0.20363E 04	0.19613E 04	0.17948E 04	0.15156E 04
T( 14)	T( 15)	T( 19)	T( 20)	T( 21)	T( 22)	T( 23)
0.10614E 04	0.71349E 03	0.60594E 03	0.74020E 03	0.90835E 03	0.90971E 03	0.77852E 03
T( 24)	T( 25)	K( 2)	K( 3)	K( 4)	K( 9)	K( 19)
0.54745E 03	0.40650E 03	0.46510E-03	0.84645E-03	0.64752E-03	0.22132E-01	0.33266E-02
8999.1445312	32.9671478	1	13	4.3158360	600.0000000	
T( 1)	T( 2)	T( 9)	T( 10)	T( 11)	T( 12)	T( 13)
0.20358E 04	0.51098E 03	0.20374E 04	0.20233E 04	0.19498E 04	0.17863E 04	0.15108E 04
T( 14)	T( 15)	T( 19)	T( 20)	T( 21)	T( 22)	T( 23)
0.10609E 04	0.71327E 03	0.59953E 03	0.73135E 03	0.89776E 03	0.90107E 03	0.77407E 03
T( 24)	T( 25)	K( 2)	K( 3)	K( 4)	K( 9)	K( 19)
0.54706E 03	0.40635E 03	0.45713E-03	0.84609E-03	0.64729E-03	0.21778E-01	0.32682E-02

9199.1171875	33.5016937	1	13	4.3158360	600.0000000	
T( 1)	T( 2)	T( 9)	T( 10)	T( 11)	T( 12)	T( 13)
0.20226E 04	0.50555E 03	0.20243E 04	0.20105E 04	0.19385E 04	0.17777E 04	0.15058E 04
T( 14)	T( 15)	T( 19)	T( 20)	T( 21)	T( 22)	T( 23)
0.10599E 04	0.71279E 03	0.59332E 03	0.72278E 03	0.88746E 03	0.89259E 03	0.76953E 03
T( 24)	T( 25)	K( 2)	K( 3)	K( 4)	K( 9)	K( 19)
0.54640E 03	0.40602E 03	0.44950E-03	0.84527E-03	0.64678E-03	0.21435E-01	0.32122E-02

9399.0937500	33.9928741	1	12	4.3158360	600.0000000	
T( 1)	T( 2)	T( 9)	T( 10)	T( 11)	T( 12)	T( 13)
0.20096E 04	0.50029E 03	0.20114E 04	0.19980E 04	0.19275E 04	0.17692E 04	0.15005E 04
T( 14)	T( 15)	T( 19)	T( 20)	T( 21)	T( 22)	T( 23)
0.10585E 04	0.71207E 03	0.58729E 03	0.71446E 03	0.87743E 03	0.88425E 03	0.76490E 03
T( 24)	T( 25)	K( 2)	K( 3)	K( 4)	K( 9)	K( 19)
0.54549E 03	0.40552E 03	0.44219E-03	0.84404E-03	0.64601E-03	0.21102E-01	0.31586E-02

9599.0664062	34.5298767	1	12	4.3158360	600.0000000	
T( 1)	T( 2)	T( 9)	T( 10)	T( 11)	T( 12)	T( 13)
0.19969E 04	0.49519E 03	0.19987E 04	0.19857E 04	0.19166E 04	0.17608E 04	0.14951E 04
T( 14)	T( 15)	T( 19)	T( 20)	T( 21)	T( 22)	T( 23)
0.10567E 04	0.71113E 03	0.58143E 03	0.70640E 03	0.86768E 03	0.87606E 03	0.76021E 03
T( 24)	T( 25)	K( 2)	K( 3)	K( 4)	K( 9)	K( 19)
0.54437E 03	0.40488E 03	0.43518E-03	0.84245E-03	0.64502E-03	0.20777E-01	0.31071E-02

9799.0429687	35.0692749	1	12	4.3158360	600.0000000	
T( 1)	T( 2)	T( 9)	T( 10)	T( 11)	T( 12)	T( 13)
0.19843E 04	0.49024E 03	0.19862E 04	0.19736E 04	0.19058E 04	0.17523E 04	0.14895E 04
T( 14)	T( 15)	T( 19)	T( 20)	T( 21)	T( 22)	T( 23)
0.10546E 04	0.70999E 03	0.57574E 03	0.69856E 03	0.85818E 03	0.86801E 03	0.75545E 03

T( 24)	T( 25)	K( 2)	K( 3)	K( 4)	K( 9)	K( 19)
0.54305E 03	0.40411E 03	0.42845E-03	0.84054E-03	0.64382E-03	0.20461E-01	0.30576E-02
R 9999.0117187	35.6107788	1	12	4.3158360	600.0000000	
T( 1)	T( 2)	T( 9)	T( 10)	T( 11)	T( 12)	T( 13)
0.19720E 04	0.48543E 03	0.19739E 04	0.19617E 04	0.18953E 04	0.17439E 04	0.14837E 04
T( 14)	T( 15)	T( 19)	T( 20)	T( 21)	T( 22)	T( 23)
0.10522E 04	0.70868E 03	0.57021E 03	0.69095E 03	0.84892E 03	0.86009E 03	0.75065E 03
T( 24)	T( 25)	K( 2)	K( 3)	K( 4)	K( 9)	K( 19)
0.54154E 03	0.40320E 03	0.42198E-03	0.83833E-03	0.64243E-03	0.20154E-01	0.30101E-02

R-7548

COMPUTER TIME 0.0 MINUTES

APPENDIX E

DISTRIBUTION LIST

<u>Copies</u>	<u>Recipient</u>	<u>Designee</u>
4	Chief, Liq. Prop. Technology, RPL NASA Washington, D. C. 20546	(X)
1	Director, Launch Vehicles and Propulsion, SV NASA Washington, D. C. 25046	(X)
1	Director, Advanced Manner Missions, MT NASA Washington, D. C. 20546	(X)
1	Director, Mission Analysis Division NASA Ames Research Center Moffett Field, California 24035	(X)
2	Jet Propulsion Laboratory 4800 Oak Grove Dr. Pasadena, California 91103 Mr. Robert W. Riebling	(X)
1	NASA Pasadena Office 4800 Oak Grove Drive Pasadena, California 91103	(X)
1	Contracting Officer	(X)
1	Office of Technical Information and Patent Matters	(X)
25	NASA Scientific + Technical Information Facility P. O. Box 33 College Park, Maryland 20740	(X)
1	Marshall Space Flight Center Huntsville, Alabama 35812 Mr. Keith Chandler	(X)

NASA FIELD CENTERS

2	AMES Research Center Moffett Field, California 94035	Harold Hornby
2	Goddard Space Flight Center Greenbelt, Maryland 20771	Merland L. Moseson Code 620
2	Jet Propulsion Laboratory California Institute of Technology 4800 Oak Grove Drive Pasadena, California 91103	Henry Burlage, Jr. Propulsion Div.

<u>Copies</u>	<u>Recipient</u>	<u>Designee</u>
2	Langley Research Center Langley Station Hampton, Virginia 23365	Dr. Floyd L. Thompson Director
2	Lewis Research Center 21000 Brookpark Road Cleveland, Ohio 44135	Dr. Abe Silverstein Director
2	Marshall Space Flight Center Huntsville, Alabama 35812	Hans G. Paul Code R-P+VED Werner Voss R-P and VE-PM
2	Manned Spacecraft Center Houston, Texas 77001	Dr. Robert R. Gilruth Director G. Thibodaux
2	John F. Kennedy Space Center, NASA Cocoa Beach, Florida 32931	Dr. Kurt H. Debus
1	NASA Test Facility Propulsion Engineering Office White Sands, New Mexico	I. D. Smith Staff Chemist

GOVERNMENT INSTALLATION

1	Aeronautical Systems Division Air Force Systems Command Wright-Patterson Air Force Base Dayton, Ohio 45433	D. L. Schmidt Code ASRCNC-2
1	Air Force Missile Development Center Holloman Air Force Base New Mexico 88330	Maj. R. E. Bracken Code MDGRT
1	Air Force Missile Test Center Patrick Air Force Base, Florida	L. J. Ullian
1	Air Force Systems Division Air Force Unit Post Office Los Angeles 45, California 90045	Col. Clark Technical Data Center
2	AFFTC (FTBPP-21) Edwards AFB, California 93523	Myrtle C. Jones
1	Arnold Engineering Development Center Arnold Air Force Station Tullahoma, Tennessee 37388	Dr. H. K. Doetsch

<u>Copies</u>	<u>Recipient</u>	<u>Designee</u>
1	Bureau of Naval Weapons Department of the Navy Washington, D. C. 20546	J. Kay RTMS-41
1	Defense Documentation Center Headquarters Cameron Station, Building 5 5010 Duke Street Alexandria, Virginia 22314 Attn- TISIA	
1	Headquarters, U. S. Air Force Washington 25, D. C. 20546	Col. C. K. Stambaugh AFRST
1	Picatinny Arsenal Dover, New Jersey 07801	I. Forsten, Chief Liquid Propulsion Laboratory, SMUPA-DL
2	Air Force Rocket Propulsion Laboratory Research and Technology Division Air Force Systems Command Edwards, California 93523	RPRR/Mr. H. Main
1	U.S. Atomic Energy Commission Technical Information Services Box 62 Oak Ridge, Tennessee 37830	A. P. Huber Oak Ridge Gaseous Diffusion Plant (ORGDG) P.O. Box P
1	U.S. Army Missile Command Redstone Arsenal Alabama 35809	Dr. Walter Wharton
1	U.S. Naval Ordnance Test Station China Lake California 93557	Code 4562 Chief, Missile Propulsion Div.
	CPIA	
1	Chemical Propulsion Information Agency Applied Physics Laboratory 8621 Georgia Avenue Silver Spring, Maryland 20910	P. Martin

CopiesRecipientDesignee

## INDUSTRY CONTRACTORS

1	Aerojet-General Corporation P.O. Box 296 Azusa, California 91703	L. F. Kohrs
1	Aerojet-General Corporation P.O. Box 1947 Technical Library, Bldg. 2015, Dept. 2410 Sacramento, California 95809	R. Stiff
1	Aeronutronic Division Philco Corporation Ford Road Newport Beach, California 92663	N. Stern
1	Aerospace Corporation 2400 East El Segundo Boulevard P. O. Box 95085 Los Angeles, California 90045	M. J. Russi
1	Air Research Mfg. Co. 9851 Sepulveda Blvd. Los Angeles, California 90045	C. S. Coe
1	Arthur D. Little, Inc. 20 Acorn Park Cambridge, Massachusetts 02140	E. Karl Bastress
1	Astropower Laboratory Douglas Aircraft Company 2121 Paularino Newport Beach, California 92663	Dr. George MOC Director, Research
1	Astrosystems International, Inc. 1275 Bloomfield Avenue Fairfield, New Jersey 07007	A. Mendenhall
1	Atlantic Research Corporation Edsall Road and Shirley Highway Alexandria, Virginia 22314	A. Scurlock
1	Beech Aircraft Corporation Boulder Division Box 631 Boulder, Colorado 80302	J. H. Rodgers
1	Bell Aerosystems Company P.O. Box 1 Buffalo, New York 14240	J. Flanagan



<u>Copies</u>	<u>Recipient</u>	<u>Designee</u>
1	Bendix Systems Division Bendix Corporation 3300 Plymouth Road Ann Arbor, Michigan 48105	John M. Brueger
1	Boeing Company P.O. Box 3707 Seattle, Washington 98124	J. D. Alexander
1	Brown Engineering Co., MS-190 Research Park Huntsville, Alabama 35807	W. J. Tomme
1	Missile Division Chrysler Corporation P.O. Box 2628 Detroit, Michigan 48231	John Gates
1	Wright Aeronautical Division Curtiss-Wright Corporation Wood-Ridge, New Jersey 07075	G. Kelley
1	Missile and Space Systems Division Douglas Aircraft Company, Inc. 3000 Ocean Park Boulevard Santa Monica, California 90406	R. W. Hallet Chief Engineer Advanced Space Tech.
1	Aircraft Missiles Division Fairchild Hiller Corporation Hagerstown, Maryland 21740	J. S. Kerr
1	General Dynamics Convair Division 5001 Kearny Villa Road P.O. Box 1628 San Diego, California 92112	E. R. Peterson V.P., Research and Eng.
1	Missile and Space Systems Center General Electric Company Valley Forge Space Technology Center P.O. Box 8555 Philadelphia, Pa.	F. Mezger
1	Advanced Engine + Technology Dept. General Electric Company Cincinnati, Ohio 45215	D. Suichu
1	Grumman Aircraft Engineering Corp. Bethpage, Long Island New York 11714	Joseph Gavin

<u>Copies</u>	<u>Recipient</u>	<u>Designee</u>
1	Honeywell, Inc. Aerospace Div. 2600 Ridgway Rd. Minneapolis, Minn.	Mr. Gordon Harms
1	Hughes Aircraft Co. Aerospace Group Centinela and Teale Streets Culver City, California	E. H. Meier V.P. and Div. Mgr., Research and Dev. Div.
1	Walter Kidde and Company, Inc. Aerospace Operations 567 Main Street Belleville, New Jersey	Mr. R. J. Hanville Dir. of Research Engr.
1	Ling-Temco-Vought Corporation Astronautics P.O. Box 5907 Dallas, Texas 75222	Garland Whisenhunt
1	Lockheed Missiles and Space Co. Attn-Technical Information Center P.O. Box 504 Sunnyvale, California 94088	Y. C. Lee
1	Lockheed Propulsion Company P.O. Box 111 Redlands, California 92374	H. L. Thackwell
1	The Marquardt Corporation 16555 Saticoy Street Van Nuys, California 91409	Warren P. Boardman, Jr.
1	Baltimore Division Martin Marietta Corporation Baltimore, Maryland 21203	John Calathes (3214)
1	Denver Division Martin Marietta Corporation P.O. Box 179 Denver, Colorado 80201	J. D. Goodlette (A-241) A. J. Kullas
1	Orlando Division Martin Marietta Corp. Box 5837 Orlando, Florida	Mr. J. Ferm
1	Rocket Research Corporation 520 South Portland Street Seattle, Washington 98108	Foy McCullough, Jr.

<u>Copies</u>	<u>Recipient</u>	<u>Designee</u>
1	Space + Information Systems Division North American Aviation, Inc. 12214 Lakewood Blvd. Downey, California 90241	H. Storms
1	Rocketdyne (Library 586-306) North American Rockwell Corporation 6633 Canoga Avenue Canoga Park, California 91304	E. B. Monteath
1	Northrop Space Laboratories 3401 West Broadway Hawthorne, California 90250	Dr. William Howard
1	Reaction Motors Division Thiokol Chemical Corporation Denville, New Jersey 07832	Arthur Sherman Mr. Robert Gere
1	Republic Aviation Corporation Farmingdale Long Island, New York	Dr. William O'Donnell
1	Space General Corporation 9200 East Flair Avenue El Monte, California 91734	C. E. Roth
1	Stanford Research Institute 333 Ravenswood Avenue Menlo Park, California 94025	Lionel Dickinson
1	TRW Systems One Space Park Redondo Beach, California 90278	Mr. D. Lee
1	Tapco Division TRW, Incorporated 23555 Euclid Avenue Cleveland, Ohio 44117	P. T. Angell
1	Thiokol Chemical Corporation Huntsville Division Huntsville, Alabama 35807	John Goodloe
1	United Technology Center 587 Methilda Avenue P. O. Box 358 Sunnyvale, California 94088	B. Adelman

<u>Copies</u>	<u>Recipient</u>	<u>Designee</u>
1	Florida Research and Development Pratt and Whitney Aircraft United Aircraft Corporation P.O. Box 2691 West Palm Beach, Florida 33402	R. J. Coar
1	Vickers Inc. Box 302 Troy, Michigan	
1	Sunstrand Aviation 2421 11th Street Rockford, Illinois 61101	R. W. Reynolds
1	Hamilton Standard Division United Aircraft Corp. Windsor Locks, Conn. 06096	R. Hatch
1	Astro-Electronics Division Radio Corporation of America Princeton, New Jersey 08540	Y. Brill

UNCLASSIFIED

Security Classification

## DOCUMENT CONTROL DATA - R &amp; D

(Security classification of title, body of abstract and indexing annotation must be entered when the overall report is classified)

1. ORIGINATING ACTIVITY (Corporate author) Rocketdyne, a Division of North American Rockwell Corporation, 6633 Canoga Avenue, Canoga Park, California 91304		2a. REPORT SECURITY CLASSIFICATION UNCLASSIFIED	
		2b. GROUP	
3. REPORT TITLE SPACECRAFT ROCKET ENGINE CHAMBER INSULATION MATERIALS (Second Interim Report)			
4. DESCRIPTIVE NOTES (Type of report and inclusive dates) Second Interim Report, 1 July 1967 through 30 June 1968			
5. AUTHOR(S) (First name, middle initial, last name) Carlson, L. W.; Carpenter, H.; Huebner, A. L.; Manson, L.; Talmor, E.			
6. REPORT DATE 30 July 1968	7a. TOTAL NO. OF PAGES 218 & xvi	7b. NO. OF REFS 9	
8a. CONTRACT OR GRANT NO. NAS7-474	9a. ORIGINATOR'S REPORT NUMBER(S) R-7548		
b. PROJECT NO.			
c.	9b. OTHER REPORT NO(S) (Any other numbers that may be assigned this report)		
d.			
10. DISTRIBUTION STATEMENT			
11. SUPPLEMENTARY NOTES		12. SPONSORING MILITARY ACTIVITY JPL, Pasadena	
13. ABSTRACT <p>Three insulation systems were evaluated in an extensive experimental program: multilayers of silica fabric/molybdenum foil, carbon fabric/tantalum foil and fine tungsten powder dispersed in a matrix of hollow zirconia microspheres.</p> <p>At temperatures below 2000 F, molybdenum/silica is clearly the superior insulation. Above 2000 F, tantalum/carbon is clearly superior. The tungsten/zirconia insulation system has an order of magnitude higher conductivity than the other material systems at the low temperatures, but is only 30 percent higher at the higher temperature. Means of maintaining tungsten/zirconia homogeneity under vibration have to be provided.</p> <p>Measurements of effective thermal conductivity and thermal stability tests were conducted at temperatures up to and exceeding 3500 F. Compatibility studies were conducted with B-66 (a columbium alloy), Ta-10W, Mo-1/2 Ti, and Haynes 25 vs molybdenum and tantalum foils, and with Haynes 25 vs silica fabric. While no compatibility problems were encountered at 2000 F, diffusion barriers may be required to keep the materials from welding at temperatures exceeding 2000 F.</p> <p>The details of all phases of work are fully discussed in a four-section report: (1) Selection of Materials, (2) Thermal Properties, (3) Thermal Stability and Compatibility, and (4) Applications Analysis. The latter includes four design examples of insulation systems for "buried" rocket chambers having arbitrary duty cycles, geometrical features, propellants and thrust. Insulation temperature profiles for each case are graphically presented.</p>			

DD FORM 1473

1 NOV 65

UNCLASSIFIED

Security Classification

UNCLASSIFIED

Security Classification

14. KEY WORDS	LINK A		LINK B		LINK C	
	ROLE	WT	ROLE	WT	ROLE	WT
Rocket Insulation Thermal Properties Heat Transfer Thermal Stability Multilayer Insulation Compatibility Application Analysis						

UNCLASSIFIED

Security Classification